THE EFFECT OF STEAM TREATMENT AND PRECIPITATION HARDENING ON THE MECHANICAL PROPERTIES AND WEAR RESISTANCE OF SINTERED IRON AND IRON-COPPER ALLOYS.

A thesis submitted to Brunel University in fulfilment of the requirements for the degree of Doctor of Philosophy

by

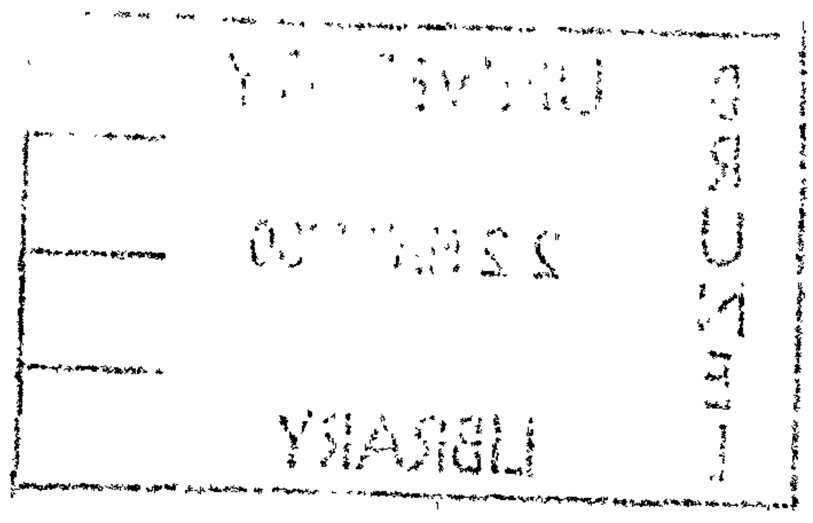

K. Razavizadeh, B.Sc.(Physics), M.Phil. (Metallurgy)

Department of Metallurgy, Brunel University

February 1980

TO: MAHSHID

ABSTRACT

Steam treatments reduce porosity[1] of sintered iron and sintered iron-base alloy products and provide them with increased compressive strength, hardness, resistance to wear and corrosion.

The aims of the present investigation were:

(a) to examine the influence of copper content and process variables on the response of sintered iron to steam treatment.

(b) to explore the possibility of combining steam treatment with precipitation hardening in sintered iron/copper alloys.

(c) to survey the influence of process parameters on the mechanical and wear properties of these materials.

Samples prepared from - 100# A.S.C. iron powder and - 100# pre-alloyed powder containing 2, 4, 6 and 8% copper, pressed to densities of 6.0, 6.4, 6.8 $^{g}/_{cc}$ and sintered for 1 hour at 1120°C were treated in superheated steam and inert gas at 525°C for periods ranging from 5 to 100 minutes and under vacuum for 500 hours.

The main results of the investigation were:

(i) Addition of copper in amounts of 2 to 8% slightly improves the resistance of iron to steam oxidation.

(ii) During ageing in steam, the hardness increased due to simultaneous precipitation of copper from solution and formation of and void filling by layers of iron oxide. The results indicated that maximum benefit is for Fe - 2% Cu alloy and steam ageing of higher copper content alloys reduces the effect of precipitation of copper.

(iii) Steam treatment of sintered pure iron improves the wear properties but the effect of this treatment on Fe-Cu alloys is not pronounced and sometimes disadvantageous.

(iv) Steam oxidation of sintered pure iron improved radial-crushing stress (R.C.S.) but this treatment reduced the R.C.S. of iron-copper alloys.

CONTENTS

ACKNOWLEDGEMENTS

I would like to thank Professor C. Bodsworth for the provision of laboratory facilities.

I am grateful to Dr T. S. Eyre for helpful discussion on wear properties.

My sincere thanks are due to Mr B.L. Davies for his supervision and continual encouragement with regard to this project and I am also grateful for his friendship.

I thank also the technical staff of the Metallurgy Department for all their valuable assistance.

My thanks, too, to Mrs V. Short for her accurate typing of the manuscript.

Finally, I acknowledge my special debt to my parents, my wife's parents and my wife (Mahshid). Without their help and loving support my studies would not have been possible.

INTRODUCTION

APPLICATIONS OF SINTERED IRON-COPPER ALLOYS

As in most other metals oriented fields powder metallurgy is strongly linked to the use and development of ferrous materials. The least expensive materials are those with low sintered density and with no alloying additions. Although the mechanical properties are low, many applications actually do not require high strength. For example, lightly loaded gears and structural components may be efficiently lubricated and do not necessitate high strength and hardness. By increasing the sintered density and by including alloy additions mechanical properties can be improved significantly. For example, medium density (6.2 - 6.6 ^{g}/cc) iron-carbon and iron-copper-carbon alloys in the as sintered condition are widely used. Almost every conceivable type of component has been made from these materials in applications ranging from toys to typewriters to industrial conveyor systems.

High density (greater than 6.6^{g}/cc) iron and iron alloy materials are also used in a broad range of applications. Although the costs are higher this can often be justified for applications requiring high strength, low porosity and high wear resistance.

The wear resisting characteristics can often be further improved by impregnating the pores with oil, somewhat in the manner of the porous bearing, or by some post-sintering treatment to produce a solid lubricant layer on the surface of the product.

It is a general characteristic of this group of materials that there is a virtually continuous transition in properties and performance

from high density, high-strength parts through parts needing strength but with propensity for impregnation and marginal bearing properties, to the high-porosity, low-strength oil-impregnated bearing.

The combination of wear resistance and good strength with bearing properties, together with the ability to produce components of complex form has allowed single sintered parts to replace assemblies previously built up from two or more materials.

Sintered iron parts are becoming more widely used, particularly for components requiring low friction and high wear resistance. Sintered plain bearings are being extensively used and sintered piston rings for internal combustion engines are now generally accepted, particularly for diesel engines[2].

It may be appropriate to start by defining the main function of a piston compression ring used in an internal-combustion engine. It is to provide a virtually gas-tight seal between piston and cylinder liner, allowing the combustion pressures developed to be efficiently transmitted from the piston to the crankshaft. Therefore the efficiency of the engine is directly related to the efficiency of the seal. In performing its function the ring must operate under high combustion pressures, high temperature, high sliding velocity with low coefficient of friction and very marginal lubrication.

Usually two or three compressive rings are used on each piston but the top ring nearest the combustion gases,(and in the worst position for cooling), at the top of the piston stroke operates under the most arduous conditions.

Anti-friction materials must possess a combination of certain fundamental physical and mechanical properties. According to Jaeger's [3] formula the temperature rise produced by frictional heating depends on the following factors: the sliding speed, the pressure at the contact spot which, in conditions of plastic deformation, equals the hardness of the material, thermal conductivity and diffusivity. Hence, an anti-friction material should have low hardness, high thermal conductivity and high thermal diffusivity.

In the majority of engines produced today the top compression ring material is an alloy cast iron, the peripheral rubbing surface of which is coated with a material to confer improved wear resistance or other properties.

The relevant physical properties of typical cast irons used were summarised by Hewitt et al.[2]

Cast irons have reasonable wear resistance and thermal conductivity and it is thought that the greater the quantity of free graphite present in cast irons, the better are their anti-friction properties, and wear resistance of a cast iron increases with pearlite content.[4]

Special alloying elements are often introduced into the above materials to improve the wear resistance and to reduce running in wear[5].

The problem encountered by many engine manufacturers is scuffing of the piston ring/cylinder liner pair.

During the early stages of rubbing under sliding, (adhesive), conditions the metal surfaces are relatively clean and wear is transient.

Wear is metallic and its extent and duration depend on the load/speed conditions. Under some conditions this running-in wear is normal, but under other conditions, (explained in the next paragraph), particularly at loads close to the mild/severe transition load a particular form of wear called "scuffing" occurs.

This is the condition where lubrication between the pair breaks down, allowing metal-to-metal contact to generate high local temperatures when metal transfer or welding takes place, thereby destroying the surface conditions. Invariably this process takes place in small areas where one or more of the following factors are operative.

(a) high surface temperature,

(b) high surface pressure,

(c) high acceleration,

(d) marginal lubrication.

This condition quickly spreads, destroying the piston ring, piston, and cylinder liner with consequential high blow-by past the piston rings, overheating of the piston and heavy oil consumption.

Sintered friction materials might give good service as rings because they have the ability to generate a non weldable film having consistent frictional properties over a wide range of conditions. Such films can be readily produced on sintered iron base materials, (for example, by steam treatment) and in piston ring applications these might resist scuffing and also retain the characteristic wear resistance and bearing properties of sintered parts.

Another important application of porous iron and iron-copper alloys lies in the field of bearings.

The friction loss of a bearing is largely dependent upon the presence of a lubricant, usually a liquid. In general, the nature of the bearing material exerts little influence upon the friction value of well lubricated systems. It is, however, usual for part or all of the load to be carried by sliding contact between the bearing and journal surfaces separated only by a thin film of lubricant. Thus with lubricant the performance of the bearing is dependent upon the ability of the lubricant to maintain a continuous film under load. Since direct bearing-journal contact does not normally occur the bearing material has only a minor influence upon friction losses.

A low friction loss is not, however, the only criterion for a good bearing and the bearing material does have an important influence on the overall bearing performance. The chief requirements of a good bearing material are that the rate of wear of both journal and bearing should be a minimum and distortion and mechanical failure should not occur under the chosen load/speed conditions. Some of these properties are needed as an insurance against inadequate lubrication. To avoid distortion and mechanical failure adequate compression and fatigue strength are needed, requirements which are best met by hard materials of high compressive strength. Unfortunately, hard materials do not conform well to journals and do not allow abrasive particles to become embedded in them. Soft materials are better able to accommodate hard particles by allowing them to embed, but are, of course, relatively weak. Thus the structure of an ideal bearing is a mixture of hard and soft phases.

In porous products the pores are the softer "structural element" and the basic metal the harder.

In some applications (for example in the pharmaceutical, textile and food processing fields), a liquid lubricant cannot be tolerated. Thus dry-lubricated bearings must be used.

Graphite was the earliest of the solid "self-lubricating" additions to be widely employed. It is frequently added to porous product bearings to coat the metal particles during mixing, thus reducing metal-to-metal contact.

Polytetrafluoroethylene, (P.T.F.E.) has[6]:

(a) a very low coefficient of friction,

(b) chemical stability in the presence of most corrosive agents,

(c) low shear strength,

(d) low thermal conductivity,

(e) high coefficient of thermal expansion.

Of these (d) and (e) are undesirable in a bearing material. In order to take advantage of its remarkably low coefficient of friction, metal/P.T.F.E. mixtures have been developed, the metal providing the strength and raising thermal conductivity.

Impregnation of metallic matrices with P.T.F.E. has been discussed by Blainely[7], who explains filling of pores by P.T.F.E. plastic.

Steam oxidation can be used to improve the bulk and surface properties of iron base bearing materials, by formation of oxide on the pore surface which increases the mechanical properties and may provide a solid self lubricating film on the surface.

EFFECTS OF COPPER ON OXIDATION AND MECHANICAL PROPERTIES OF SOLID Fe-Cu ALLOYS.

Addition of copper in amounts of 0.8 - 2.2% slightly improves the oxidation resistance of iron in air[8]. Such a result might have been expected since the affinity of copper for oxygen is less than that of iron.

One of the major reasons for using copper in wrought alloys is that when present in amounts above about 0.6% a useful strengthening effect can be obtained by ageing[9].

While methods of increasing the strength of steel are attractive from the point of strength/weight ratio, it is also important that the increase in strength should not adversely affect ductility. It has been reported[10] that precipitation in 1% Cu steel increases the tensile and yield strength by about 138 MN/m^2 and although the ductility is decreased at the same time, the decrease is less than when the increased strength is obtained in normalised steel by increasing the carbon content.

REASONS FOR THE USE OF COPPER IN SINTERED FERROUS PARTS.

Copper has been accepted as a major alloying element because of its suitability for the powder metallurgy process. The reasons for use of copper are well documented[11] and are discussed below.

1. Pre-Mixed sintered Fe-Cu alloys.

(i) The reducibility of copper is greater than that of iron[12]. Therefore complete reduction of traces of copper oxide to metallic copper is possible during sintering under conditions applicable to iron and no special measures in regard to sintering atmosphere are necessary.

(ii) The melting point of copper is below the common sintering temperatures for iron and the liquid copper wets iron efficiently.[13]

Therefore it is possible to alloy copper with iron rapidly by sintering at temperatures below 1150°C.

(iii) The high ductility of copper leads to good compressibility and high green strength.

(iv) Due to the small difference between the densities of iron and copper, copper powder can be mixed with iron without the danger of segregation.

(v) The systems Fe-Cu and Fe-Cu-C offer valuable physical and mechanical properties, as a result of solid solution strengthening and precipitation hardening[14].

(vi) In low concentration, (about 2½%) addition of copper produces a dimensionally stable compact by compensating the normal shrinkage of plain iron compacts.

2. Pre-alloyed sintered Fe-Cu alloys.

(i) Pre-alloyed powders are a more intimate mixture of base metal and alloying element, the diffusion paths required for saturation are shorter and the saturated condition is more closely approached during a conventional sinter[15].

(ii) Pre-alloyed compacts do not grow during sintering because no liquid copper phase is formed.

(iii) Pre-alloyed powders shrink on sintering, the shrinkage increasing with increasing copper content.

(iv) In the sintered state porosity is less than in the green state and this is an advantage for post-sintering treatment, (void filling).

STEAM TREATMENT OF SINTERED IRON AND IRON-COPPER ALLOYS

One of the post sintering operations is steam treatment. By this process the products are subjected to the action of superheated steam at temperatures of from 450°C - 650°C. The iron is then oxidised to blue-black oxide, Fe_3O_4, which forms an oxide film on the external surface and within the interconnected porosity of the parts[16] to improve:

(i) Hardness and compressive strength,

(ii) Corrosion resistance,

(iii) Wear resistance.

Therefore physical properties can be improved over a wide range and better opportunity is provided for retention of lubricants or rust preventative compared with those that can be developed in wrought steel counterparts. Consequently applications for powdered ferrous parts are being expanded continuously.

Another post-sintering treatment is precipitation hardening of iron-copper alloys to improve the resistance to plastic deformation and this is usually carried out at temperatures between 425°C - 550°C.[17]

Comparison of the operating temperature used for ageing and steam treatment suggests that it might be possible to obtain the benefits of both treatments by using a single post sintering operation.

CHAPTER 1

1. SINTERED PRODUCTS.

1.1. Porous Structures.

Residual porosity is an inherent feature of sintered metals in the majority of cases. There are some applications of metals where the presence of porosity is made deliberate use of and examples include filters, devices for transpiration cooling and self-lubricating bodies. In all of these instances rigorous procedures are employed to control the size and distribution of porosity.

However, in general engineering components produced by powder metallurgical routes, residual porosity is a major disadvantage and results in inferior mechanical properties compared with those obtainable in cast or wrought products. Furthermore, problems are encountered during subsequent heat treatment as a result of entrapment of solidified salts from salt baths or quenchants, diffusion type surface hardening treatments are difficult to control and the components are highly prone to attack when employed in corrosive environments because of differential aeration effects and crevice corrosion.

To overcome some of these problems components are often vacuum impregnated with oil or resin. Any treatment which fills the pores or seals the surface is likely to prove beneficial and steam treatment is such a process.

The final porosity in a sintered part is governed by:

(a) powder characteristics, (e.g. particle size, particle shape), which are determined by the method employed for powder production.

(b) the procedure used for lubrication of powders, (e.g. lubricant amount, mixing time).

(c) powder compaction, (e.g. pressure, die design).

(d) sintering practice, (e.g. temperature, time and atmosphere).

(e) post sintering practice.

The influence of these factors will be reviewed in the following sections of the thesis.

1.2. Production of pure powders and alloy powders.

The commonest methods for production of metals are:

1) Atomisation, 2) Electrolysis, and 3) Reduction of oxides.

The mentioned methods for production of pure metals were reviewed by the author[18], but generally:

Atomised powders are dense, in shape they are regular if water-atomised and spherical if gas atomised, uniformity of particle size distribution can be closely maintained and apparent densities are sufficiently high for all types of moulding work. The process is widely used for the manufacture of both elemental, (Fe, Cu, Al), and pre-alloyed, (steel, bronze), powders.

Electrolytic powders are of dendritic shape with low apparent density, they are very pure and by varying the conditions in the bath, a range of powder qualities may be produced which have good pressing and sintering properties.

Reduced powders are irregular in shape with poorer flow properties and lower apparent densities than those made by other processes.

The most common methods used for production of sintered alloys are: 1) Mixing of individual elemental powders, 2) Using completely homogeneous pre-alloyed powders, each particle having the desired composition, 3) Composite powder in which surface and core are of different compositions, and 4) Reduction of mixed oxides by hydrogen.

Case 1)

Mixing of elemental powders with different percentages of weight due to phase diagram for desired properties. For instance in sintering of elemental powders of Al - 4.5% Cu, Fe - 5% Cu - 0.4% C, and so on.

Case 2)

Pre-alloyed metal powders are those in which each individual particle is nominally the same as regards composition and microstructure. Considerable interest in the use of those powders for solid and porous stainless-steel parts, has long been shown. However, limitations in the supply grading, have restricted their applications. The usual method of pre-alloyed powder production is atomisation, which is defined as the disintegration into fine particles of a molten stream of metal by the action of high pressure water or air jets. Atomisation is the best means of obtaining a wide range of stainless-steel and other alloys in powder form without too severe a limitation on composition. Naturally there is a tendency for an oxide film to form on the surface of powder particles during production. Thus it is necessary to anneal the powder in hydrogen before use.

A wide range of alloys including Fe - Al, Fe-Al-Cr, Al-Ni-Co, low alloy steels and stainless steel is currently produced in powder form by this process. The general details about precautions necessary for

different alloys, furnaces, type of jet were reviewed by Watkinson[19], and modern atomizing techniques have been reviewed by Ulfgummson[20].

Production of iron-copper pre-alloyed powder by Davy Loewe Ltd[21] involves the melting of iron and copper, then stirring it in the molten stage for homogenization and atomisation of the molten stream by water jet.

Case 3)

Composite powders usually consist of so-called "coated" powder particles. Each individual particle consists of a core of one particular metal surrounded by a shell of another metal.

There are several methods of chemical replacement, but condensation and mechanical coating processes are also in use.

The last two methods are practical only when very thin coats are the objective.

Probably the best known example of the replacement method is copper-coated lead. Powders containing from 30% to 50% lead can be made by this method with each particle substantially spherical in shape and analagous to the initial atomized lead. The high proportion of copper in each particle permits complete closure of each shell. Other examples include copper-coated iron and steel powders with a copper content of 5 - 25%. The electrolytic method can be used to produce a variety of combinations.[22 - 23] For example, tin can be plated on copper particles by employing tin anodes and a tin plating bath or, conversely, copper can be plated on tin powder by using a copper anode and a copper plating bath[24].

Most of these powders pass through 200 mesh, with more than 80%

passing through a 325 mesh sieve. For example, the A.D of silver-coated nickel powder is 2.65, that of silver coated molybdenum 2.75 $^{g}/cc$.

The condensation method is suitable for the production of zinc-coated powders, but has been suggested for other low-melting point metals. The method is similar to the sherardising process. Zinc dust is intimately mixed with the metal powder to be coated, (e.g. iron), the mixture is heated in a closed chamber under controlled atmospheric conditions to a temperature above the melting point of zinc. This is followed by rapid cooling, whereupon the zinc condensate forms solid films around the iron particles.

Mechanical coating is commonly used in the manufacture of cemented carbides and steels. Cobalt coatings are applied to refractory metal particles and graphite films to iron particles by means of ball milling. This is often carried out in the presence of a liquid phase, e.g. carbon tetrachloride in some cases, at elevated temperatures and under controlled atmospheric conditions. The method is also practical for other combinations such as copper-coated tungsten, silver-coated molybdenum, etc. The proportion by weight between shell and case does not usually exceed 1:5.

Case 4)

Reduction of mixed oxides which can be used for production of pre-alloyed iron/copper powder involves reduction of a mixture[25] of Fe_2O_3 and Cuo by gas containing 98% hydrogen and 2% HCl by volume. For this purpose the materials are spread on a tray to a depth of about $\frac{1}{4}$ inch and the loaded tray is sealed in an electrically heated muffle furnace.

The gas is passed through the furnace over the surface of the mixture at about 1200°F and the sealed inner tube of the furnace is then removed and allowed to cool to a temperature below 200°F. The product forms as a semi-sintered, but easily frangible cake which is then ground to a particle size of - 100 mesh. The powder contains 15% copper and 85% iron. The process often yields powders with distinct Fe and Cu phases with little interdiffusion between them.

1.3. Properties of Alloy Powders.

Properties of alloy powder can be generalized by comparison between the different routes of manufacturing processes.

In pre-alloyed powder made by atomisation of liquid alloy in spite of shape due to applied jet, there are two possibilities.

(i) Solute element is in solution with solvent (e.g. Fe - 6% Cu). Due to solution strengthening, particles are very hard and their ability to deform under load is poor and some times impossible.

(ii) Solute element precipitates during cooling and thus particles are softer and have good compressibility.

Pre-alloyed[15] Fe - Cu powder produced from a melt has good compressibility from the softening accompanying the overageing of copper precipitates in the iron grains.

Thus case (i) has poorer compressibility than pre-mixed powders and case (ii) has better pressing characteristics.

The chemistry of the two or more components of a coated powder can obviously vary throughout such a wide range that it is not possible

to generalise upon the chemistry of these powders.

However, these powders do have some general physical characteristics [26] in common. In this context the term powder is used to denote particles lying between 5 mm and 1μ. The thickness of coating could cover this same range but usually lies between 1 - 100 μ with the coating material normally representing 5 - 90% of the total weight of the product. Lund et al [27] studied the compacting, sintering and homogenization of Ni - Cu composite and mixture of these alloys. They demonstrated that compressibility of pre-mixed powder in coarser powder (- 325 #) is higher than that of composite powder with the same size in core, but the reverse is true when the particle size is reduced to 1 - 2μ.

During the sintering of composite powder segregation is prevented at all stages of processing.

For a given core particle size, (and equivalent particle size in a mixture), the composite compacts sinter to substantially higher density in the time required for alloy equilibrium to be established by diffusion. In addition homogenization also progresses more rapidly in the composite material.

Sintered parts manufactured from powders produced by reduction of mixed oxides have a higher tensile strength and density when compared with alloys prepared by mixing of elemental powders [28].

1.4. Compaction.

Compressibility of a powder which is a measure of the influence of compaction pressure is expressed [29] in terms of densification parameter.

$$D.P. = \frac{\text{Green density - Apparent density}}{\text{Theoretical density - Apparent density}}$$

Thus compressibility is dependent upon green density and apparent density. Green density of a compacted powder is influenced by several factors, e.g. a) pressure, b) particle size and shape, c) strength and hardness of individual particles, d) speed of compaction, e) punch/die clearance, f) nature of lubricant.

For example, green density increases with:

(i) Increasing compaction pressure.
(ii) Increasing particle size.
(iii) Decreasing strength and hardness of individual particles.
(iv) Decreasing speed of compaction.

Apparent density which is ability of powder packing will generally:

(i) Decrease with decreasing particle size.
(ii) Decrease as the particle shape departs from spheroidal.
(iii) Decrease with increasing surface roughness.

Metal stearates, (zinc stearate), are added to powder before pressing to decrease die-wall friction and friction between particles, but there are some disadvantages because lubricants decompose at low temperatures with formation of undesirable products which can damage the furnace elements and reduce element life during sintering.

$$\text{Zn stearate} \xrightarrow{400^{\circ}C} H2O + CO_2 + Zno + \text{gummy residue}$$

These lubricants can decrease the rate of powder flow into the die and as a consequence of decomposition during sintering, staining of the parts can occur. They also decrease the apparent density of the powder.

Green strength of a powder component is increased by:

(i) Increase of particle surface roughness.
(ii) Increase of particle surface area.
(iii) Decrease of apparent density.
(iv) Increase of compaction pressure.
(v) Decrease in the per cent lubricant addition.

1.5. Sintering Process

Sintering is carried out normally at temperatures in excess of at least 0.6 Tm in ^{o}K, where Tm is the melting point. At this temperature atomic mobility is high, self-diffusion occurs fairly rapidly, and plastic flow occurs under relatively low stress. Thus, there should not be any residual porosity.

For this reason it is necessary to examine the sintering mechanisms.

At high homologous temperatures of a solid the surface energy may be assumed to be equal to the surface tension. High atomic mobility is necessary for this equivalence. The surface tension is the force acting to minimise the surface area and hence, surface energy, and it is generally accepted that sintering occurs as a result of excess free energy of the powder over that of the solid because of the different free surface area of the two states.

To illustrate this driving force it is necessary to consider an actual model. Fig. 1 shows the neck growth of an idealised two-sphere model. If the radius of neck r_c is much greater than the radius of the neck ρ then the stress acting in the neck is related to surface tension γ

and is equal to γ/ρ. This stress is directed outwards from the neck and is thus tensile in character. This stress at the neck produces a force which results in:

(i) The vapour pressure above the neck being greater than elsewhere.

(ii) An excess of vacancies in the neck area.

(iii) The possibility of plastic flow.

If the equilibrium vapour pressure remote from the neck is P then over the neck it is

$$(P + \Delta P) \text{ , So } \qquad \frac{\Delta P}{P} = \frac{\gamma Vo}{RT\rho}$$

where Vo is molar volume

R is gas constant

T is absolute temperature

This difference in vapour pressure constitutes a driving force for a material transport mechanism leading to neck growth and pore rounding. Thus the larger the surface area in the original material the greater the driving force for sintering.

This mechanism is expected to operate during sintering of particles made of material with high vapour pressure such as zinc[30] above 1050°C, cadmium and Na Cl[31] spheres.

A similar argument will show that a gradient exists in the concentration of vacancies between the neck and the adjacent solid. If C is the equilibrium concentration of vacancies in solid and ΔC the excess concentration in the neck

$$\frac{\Delta C}{C} = \frac{\gamma Vo}{RT\rho}$$

Thus there will be a vacancy concentration gradient between the neck and other locations on the particle surface which can result in a flow of material towards the neck. The mechanism for this flow may be either surface or volume diffusion.

Down this gradient the vacancies are migrating into the interior of the system and are replaced by atoms diffusing in the opposite direction. There are three important mechanisms[32] of material transport which depend upon this difference of vacancy concentration between various locations in the structure. These are shown in Fig. 2 and are:

(i) From the sphere surface to the neck surface by means of surface migration.

(ii) From the sphere surface to the neck surface by means of volume diffusion.

(iii) From the grain boundaries to the neck surface by grain boundary diffusion or volume diffusion.

There are also two other cases[33] where vacancies play a major role:

(iv) From the larger pores to the small rounded pores.

(v) From the grain boundaries to the small rounded pores.

Passavana[30] identified volume diffusion in polycrystalline TiO_2 (900 - 1550°C) V_2O_5 (560 - 650°C) and ZnO (600 - 1050°C). In the model experiments with single-crystal spheres[34] evidence was obtained that several mechanisms contribute to the sintering process. In tests on ZnS[35] above 600°C and γFe[36] sintering has been shown to occur by volume diffusion.

Surface diffusion is the mechanism of material transport to be expected when the ratio of surface area to volume of the system is relatively large,[37] (i.e. for particles within the size range 10 - 20μ). The mechanism is also most probable at low temperatures when the effect of volume diffusion becomes negligible because the mechanism requires the least activation energy of all types of diffusion. Seigle[38] sintered 3 - mil iron wire at 875°C, which is a rather low temperature for self-diffusion in iron. It is quite obvious that this type of flow can change the shape but not the volume of a system so the mechanism of material transport will be as in case 1. Experiments by Mullins[37] have shown that for each crystalline material studied, (Au, Ag, Cu, Ni, Al_2O_3, Pt, αFe[36] and ZnS[35] surface diffusion was clearly the dominant transport mechanism at temperatures less than 600°C.

1.5.1. Stages of Sintering

There are theoretically three stages during sintering:

1.5.1.1. The early stage of neck growth. Welding occurs at points of contact during the compacting process and sintering begins with transport of material under the influence of stresses and excess vacancies as described above and neck growth proceeds. In this stage there is no decrease in the amount of porosity, no shrinkage and no effect on the continuity of the porosity. However, it may lead to smoothing of the irregular channels of interconnected porosity. In this stage a natural consequence of neck growth is pore rounding. When material is transported to the neck regions from the pore surfaces the pores themselves become more rounded. The rounding process applies also to interconnected

porosity and with sufficient time at temperature it is possible to achieve almost perfectly spherical pores.

1.5.1.2. Densification. This stage represents a rather major change in the nature of the porosity in the sinter mass. Closing of the channels between interconnected porosity leads to development of isolated or closed porosity. One of the causes of pore channel closure is neck growth. Pore shrinkage and eventual elimination is often considered the most important stage of sintering. Although it is a fundamental aspect of sintering, it does not have to occur. Only after sufficient time at temperature may it evidence itself by densification of the sinter mass. Pore shrinkage leading to a decrease in the volume of the sinter mass must involve diffusion of the solid into the porosity and movement of any gas in the porosity to the external surfaces.

1.5.1.3. Closed Pore Spaces. Usually takes place after most of the other stages of sintering have occurred. In the majority of commercial operations it is of no consequence. The process simply consists of the shrinkage and elimination of small isolated, (and usually quite spherical at this stage), pores and the growth of larger ones.

1.5.2. Sintering Conditions

The important variables during the sintering process are:

1) Temperature, 2) Time, 3) Environment.

1.5.2.1. Temperature. By increasing the temperature residual porosity will decrease but if the metal undergoes allotropic transformation or recrystallisation and grain growth effects like iron near the (α - γ)

transformation temperature the rate of sintering is greater in the α range than in the γ range[39]. Cohen et al[40] have established that the influence of allotropic changes may be explained on the basis of differences in the rate of self-diffusion and vacancy diffusion in the crystallographic structure involved. It is supposed that increased densification above the recrystallisation temperature is a consequence of the new grain-boundary area which is created and which is available for the absorption of diffusing vacancies. Jenkins[41] claims that with increasing temperature the equilibrium concentration of vacancies in a metal crystal rises sharply, (for example at 500°K the fraction of lattice sites that are vacant is of the order 1×10^{-10}, at 1000°K it is increased to 1×10^{-5} and at 1500°K to 1×10^{-4}).

1.5.2.2. Time. Both time and temperature have a bearing upon the shape and distribution of residual porosity in that an increase in either will tend to spheroidisation and disappearance of the smaller pores and a growth of the larger ones with an increase in spacing between adjacent pores.

1.5.2.3. Environment. Sintering environment has an influence on densification and hence the nature of residual porosity. Atmospheres that lead to the clean up of internal surfaces can clearly have an important effect on removing the gaseous products of any surface reaction. Inert gases may be harmful because of their inability to clean up contaminated surfaces and if trapped in closed pores will eventually slow down and inhibit pore closure.

1.6. Liquid Phase Sintering.

This field occupies a special position compared with sintering without the formation of a liquid phase. This is attributable to the ease of diffusion in melts, and to the possibilities of re-ordering of the phase remaining solid in the melt and of rapid dissolution and re-precipitation.

One of the important applications of liquid phase sintering is the production of bronze materials from compacts of copper and tin powder. At the sintering temperature the tin particles quickly melt and diffuse into the copper particles forming α bronze.

Another application is tungsten carbide-cobalt in which, during sintering, the metal component becomes the liquid phase while the carbide component remains solid. Unlike the situation during the sintering of Fe-Cu and Cu-Sn alloys the liquid phase is present through most of the sintering cycle.

The fundamental aspects of liquid phase sintering are usually discussed in terms of three distinct stages[6].

1.6.1. Rearrangement

Liquid flow is important in this stage of liquid phase sintering when rapid densification occurs. The solid particles are considered in suspension in the liquid, the liquid moves towards the centre of the compact carrying solid particles with it, the compact shrinks and density increases. Complete densification should result if enough liquid is present but if there is less than the critical amount then the limit of densification is reached when the majority of solid particles touch. If

this is the case then:

(i) Liquid flow densification is favoured by low compacting pressure since a high pressure would force more particles into contact.

(ii) Initial densification is more rapid in vacuum than in H_2 since gases in pores must be removed before liquid flow can occur.

The driving force for this stage may be described in terms of surface energies or tensions and the concept of wetting. Wetting of the solid by the liquid phase is necessary. This may be expressed in terms of the free energy change associated with the change in the kinds of interface present in the system.

$$\Delta F = \gamma_{sl} - (\gamma_s + \gamma_l)$$

where ΔF = the free energy change, which should be negative for a wetting condition

γ_{sl} = the solid-liquid interfacial energy

γ_s = the solid (or solid - gas) interfacial energy

γ_l = the liquid (or liquid - gas) interfacial energy

The greater the decrease in free energy, the greater the driving force for densification (or the greater the tendency for the liquid to wet the solid).

A liquid drop on a solid substrate is a convenient geometry to use in order to study the wetting of solids by liquids. A non wetting configuration is one in which the contact angle is 90° or greater, and in this situation liquid phase sintering cannot be carried out normally and the liquid will exude from the sintered material. If the contact angle is less than 90° the possibility of liquid phase sintering can be predicted.

The degree of wetting can be found from the surface forces acting on the system to reduce the surface free energy, and thus minimizing

the total free energy of the system.

The degree of wetting can be found from this expression

$$\cos \theta = \frac{\gamma_s - \gamma_{sl}}{\gamma_l}$$

1.6.2. Solution and Re-precipitation

During liquid phase sintering fine particles dissolve in liquid but large particles have a lower solubility limit and hence material may be re-deposited on them. Thus small particles shrink and large particles grow. Basic requirements for this stage are:

(i) Appreciable solubility of solid phase in liquid phase.

(ii) Presence of an appreciable amount of liquid, (not less than 5 volume % liquid phase).

In iron-copper alloys of 2, 4, 6 and 8% copper, the volume of liquid phase is 1.7%, 3.6%, 5.3%, and 7.1% respectively. This means that only very limited liquid phase sintering may take place in alloys with 8% copper and may be totally absent in 2% and 4% copper alloys.

1.6.3. Coalescence

If wetting of the solid by the liquid is incomplete, then there is some contact between solid particles rather than complete separation of the particles by the liquid. If enough bonds are formed the solid phase may become a rigid skeleton. Densification would then be slow and similar in character to solid state sintering.

1.7. Sintering of iron-copper (Pre-mixed and Pre-alloyed)

1.7.1. Sintering mechanisms

During the sintering of pre-mixed Fe/Cu powders containing less than 8.4% Cu (the limit of solubility of Cu in Fe), liquid phase forms when the temperature exceeds the melting point of copper, (1083^{o}C). However, this liquid phase has a relatively brief existence because it wets the surfaces of iron particles and diffusion of copper into these particles then occurs rapidly. Trudel et al[42] did not find any shrinkage during isothermal sintering of pure iron and alloys of 2.4%, 5.4% and 8.1% Cu for 30 minutes. For copper contents higher than 8.4% a permanent liquid phase will be present during isothermal sintering. In alloys containing more than 8.5% Cu[42] isothermal sintering at 1120^{o}C causes a relatively important shrinkage which can be attributed to the presence of liquid.

In the sintering of pre-alloyed powder up to the maximum solubility of copper in iron (8.4%) solid state sintering applies as in pure iron[42] but if the limit of solid solubility is exceeded a liquid phase can form and liquid phase sintering is dominant.

1.7.2. Dimensional changes.

Two main theories have been proposed to account for the above features.

(i) Expansion of the iron lattice due to solid solution of copper by diffusion - diffusion theory.

(ii) Grain boundary penetration and spreading apart of iron particles by liquid copper - penetration theory.

1.7.2.1. Diffusion mechanism. The presence of copper in iron compacts, (pre-mixed), leads to the formation of liquid copper during conventional sintering. Although copper wets iron well it also dissolves rather quickly in the iron. Hence for relatively small amounts of copper expansion rather than the usual shrinkage can result. Maximum growth is to be expected at the maximum solubility of copper in austenite, (about 8.4%).[43]

Berner et al[44] investigated the expansion of Fe - 8% Cu as a function of sintering temperature for 14 minutes. The results showed a pronounced maximum at around 1150°C and a minimum dihedral angle of about 9° at 1150°C. Trudel et al[45] found that diffusion of copper partially balanced the shrinkage which occurred during sintering for 30 minutes at 1120°C. Krantz[46] observed growth after 10 minutes. This high rate of growth has been explained by assuming that grain boundary diffusion is the rate controlling process. It may be noted that although grain boundaries act as channels for rapid distribution of solute the final rate of homogenization is controlled by volume diffusion. The diffusion model was presented by Berner et al[44] and they have shown that even under ideal conditions of complete wetting by liquid copper, solid solution of copper cannot account for the observed rates and magnitude of growth.

1.7.2.2. Penetration mechanism. Smith[47] showed first that if γ_{sl}, the solid-liquid interfacial energy, is less than half the grain boundary energy, (Fig. 3), then a liquid phase penetrates the grain boundary. The dihedral angle of copper-rich phase, at the γ grain boundaries was measured [13] to assess the effect of temperature on the penetration of the grain boundary by the copper-rich phase. The grain boundary penetration is inversely proportional to the dihedral angle. It was found that dihedral

angle values vary from 0 to 34° over the temperature range 1100 to 1200°C[48]. Thus when the condition $2\gamma_{sl}<\gamma_{gb}$ is satisfied, the grain boundaries of iron are separated by a liquid film of finite thickness and, therefore, the green dimensions increase. This theory accounts satisfactorily for the rapid rate of growth observed at temperatures just above the melting point of copper and the magnitude of growth can be explained in terms of the degree of penetration, (i.e. the dihedral angle), and the amount of the liquid phase.

In addition, the penetration theory is capable of accounting for the following features of growth which cannot be accounted for by the diffusion theory.

(i) Maximum growth occurs at about 1150°C because the dihedral angle is a minimum at this temperature.

(ii) Presintering reduces growth because the extent of penetration decreases due to formation of rigid necks.

From the comparison of the two theories, it may be concluded that the rate controlling growth mechanism is penetration by liquid copper.

Phadke and Davies[49] demonstrated the effects of sintering time and temperature on Fe - 6% Cu alloy for two density levels. Again maximum growth was found between 1140 and 1160°C confirming the conclusions of Berner et al. However, compared with their results, the difference between maximum and minimum values was less pronounced. This observation tends to suggest that the conditions responsible for growth due to penetration are also favourable for solid solution of copper.

In pre-alloyed specimens containing 2.4 and 5.4% Cu[42], copper growth does not occur because no liquid phase should form during sintering. The absence of growth in pre-alloyed samples containing 8.1 and 12.8% Cu can be explained by the fact that liquid copper penetrates in smaller amounts and more slowly in grain boundaries of Fe-Cu alloys than in those of pure iron. Trudel[42] et al by ancillary experiments showed that the diffusion of copper in grain boundaries of Fe-Cu alloys at 1120°C decreases considerably as the copper concentration of alloys increases towards the solubility limit of copper in γ-iron.

Addition of carbon (1%) to iron-copper mixes reduces greatly the swelling of compacts[46]. The following explanations for this effect have been given.

Originally[50] it was believed that carbon reduced the solubility of copper in iron but subsequently it has been found[51] that carbon has no effect on the solubility of copper. Elliot[43] found that in alloy of 5% Cu and up to 1.5% carbon a substantial reduction in growth occurred.

The dimensional change of pure iron - 1.5% graphite mix is exactly nil, and it would appear that the reduction in growth of iron-copper mix cannot be due to any real change in the shrinkage factor, but must be associated with the growth factor. It is suggested, therefore, that the influence of graphite upon growth is due to the effect of carbon in reducing the intersolubility of copper and iron.

In addition it may be said that rapid solution of carbon in premixes decreases the rate of grain boundary penetration of the liquid

copper and hence its solution in the iron lattice.

In pre-alloyed powder the carbon dissolves as rapidly but cannot retard solution of the copper already within the iron grains.

Carbon expands the alloy lattice but on the other hand pre-alloyed Fe/Cu shrinks during sintering. Thus shrinkage of the lattice can be decreased by addition of carbon.

Holcomb[15] demonstrated the effect of copper content versus dimensional change in pre-alloyed powders up to 12% Cu at two different carbon contents. He found that minimum shrinkage can be achieved in 8% Cu with 0.09% C and in 2.4% Cu with 0.79% C. At 12% Cu, (Liquid Phase), and at both carbon levels the above explanation would be swamped by solution reprecipitation[52] mechanisms.

1.7.3. Sintered Strength

The difference between prealloyed and pre-mixed powders in this respect can be accounted for by the fact that in the former there is a more intimate mixture of base metal and alloying element, the diffusion paths required for saturation are shorter and the saturated condition is more closely approached during a conventional sinter.

Trudel et al[45] reported a relatively sharp increase of U.T.S. in premixed alloys with copper contents up to about 6% Cu. This increase is due to solid solution strengthening. Above 6% Cu, the U.T.S. decreases with increasing copper content, because of the formation of large pores due to the displacement of molten copper during sintering. The U.T.S. of specimens made from pre-alloyed powders increases by solution strengthening up to about 8%. The slower increase in strength above 8% Cu is thought to be due to increasing densification and to the

elimination of some porosity.

Holcomb[15] reported.

(i) The sintered strength and microhardness of prealloyed compacts increases with increasing copper content up to 8% Cu. In a conventional sintering treatment the material is copper-saturated, whereas the strength of premixed compacts does not increase above 4% cu because the time available for diffusion of copper is limited.

(ii) Prior solution of copper does not limit the solution of carbon in prealloyed powders and, as a result, additive copper-carbon strengthening occurs up to a composition of 8% Cu - 0.8% C. The rapid diffusion of carbon in premixes retards grain boundary diffusion of copper so that addition strengthening is not found at 6% Cu - 0.8% C.

1.8. Residual Porosity.

The term residual porosity refers to the total pore volume remaining in the specimen at the completion of the sintering stage of production, or after post sintering operations, (e.g. coining, heat treatment or surface treatment), have been completed.

It is important to distinguish between closed and open or interconnected porosity. Closed pores are isolated from each other and from grain boundaries and free surfaces. In contrast, open pores are connected to each other via distinct channels or grain boundaries and the network is connected to the free surface.

Normally a sintered component produced commercially will contain both types of porosity but, for reasons explained later, interconnected porosity is predominant.

In terms of mechanical, chemical and physical properties closed pores because they tend to be spheroidal in shape, possess a small surface area per unit volume and will not have as pronounced a notch effect. Open pores, because of their irregular shape, possess a large surface area per unit volume, exert a notch effect on the surrounding metal and provide a route whereby liquids or gases can permeate through the structure from the free surface and give rise to corrosion problems or difficulties during heat treatment.

Residual porosity has its origins in the fact that, unless all particles are rectilinear, (e.g. cubes), and packed in a perfectly systematic manner, it is impossible to fill 3-dimensional space completely.

The actual prosity which remains in a sintered product is intimately dependent upon the route employed for powder production, the influence which this has on particle shape, particle size distribution, purity and surface condition and the pressing and sintering conditions employed.

As mentioned in 1.4 section, apparent density depends on particle size, shape, surface area and P.S.D. Decrease in particle size or a departure of particle shape from the spherical will lead to an increase in surface area. The importance of these parameters arises from the influence which they have on the basic operations of compacting and sintering. Very fine particles and irregular shapes are desirable

for sintering, because they have high surface area and driving force for bonding during sintering is the excess energy due to high surface area. However, fine powders have low apparent density, which means poor compressibility.

Another important powder characteristic is flow time. The shorter the time the smaller are the frictional forces between particles. Fine powders tend to have poor flow properties and low apparent density, two factors which are of great importance when compacting on automatic presses. Particle shape also affects flow properties and apparent density, spherical particles giving the best properties in both cases. Spherical particles, however, also have the poorest compacting properties since they provide no mechanical interlocking and have the smallest number of point contacts.

From the above it can be concluded that for a reasonable powder flow, compressibility and sintering process a compromise between A.D and flow rate is necessary.

Table 1[53] shows the relationship between shape of powders and flow, packing, pressing and sintering. The other factor is apparent density, which is a measure of the packing ability of particles and defined as the weight of uncompacted powder occupying a unit volume of container space.

If one considers an ideal system of uniform size spheres, the closest packing possible is a F.C.C. arrangement which would give 26% void space between spheres. The simple cubic and B.C.C. arrangements have 47% and 41% porosity respectively. The void space can be reduced by

introducing smaller spheres[54]. For example, in the simple cubic arrangement by introducing a spherical powder with ratio of $\frac{r}{R}$ = 0.41, the porosity reduces from 47% to 24-25%. In the F.C.C. arrangement with a ratio of $\frac{r}{R}$ = 0.15 porosity reduces to 18% - 14%. Because powders consist of particles of varying shapes and sizes, considerable variation in packing and, therefore, A.D. will be experienced.

There are some published data on the effect of the powder manufacturing process, particle shape, and P.S.D. on densification. Leadbetter et al[55] investigated the properties of a variety of iron powders on the properties of sintered specimens. The residual porosity varied widely from 10 to 42% but averaging the results for all types of powder which included electrolytic, carbonyl, abrasion and oxide reduced material, the spread in porosity was only from 26 to 30%. Zoff[56] has reported on sintering properties of reduced, atomised and electrolytic powders, but no specific qualitative data are provided to indicate the dependence of residual porosity on the powder characteristics. To this observation Jenkins[41] comments that particle shape and the chemical state of the surfaces of the particles are important. He says that finer powder may yield lower sintered density but a more widely dispersed porosity than the coarser grades, that particles of irregular shape and which may be micro-porous, such as oxide-reduced and annealed electrolytic varieties, will sinter to higher densities than those produced by atomisation. Particle composition has an effect on the sintering mechanism because the presence of alloying constituents or impurities may retard diffusion processes and oxide films on the surface are effective barriers for slowing down the various mechanisms associated with the

processes of shrinkage and pore closure. Even if such films are dispersed they may act as anchoring points for stabilising closed pores.

The work of Arthur[57] has shown that open porosity persists even beyond 90% densification. The A.S.T.M. standard[58] for metal products quotes values of interconnected porosity of from 7 to 18% for bronze, less than 7% for brass and less than 18% for low and medium density iron. Even for high density sintered iron a total porosity that may range from 8 to 13% is normal. Thus in industry it is impossible to produce a sinter mass free from porosity because usually the maximum sintering time is 1 hour and in this period the probability of complete densification and porecoarsening is very low. Extension of sintering time to effect further densification would be uneconomic.

The fact that closed pores remain practically constant for most of the sintering time, while the open pores decrease, may be explained by one of two processes.

(a) Closed pores are being formed from open pores and being removed at approximately the same rate, so that at any given time the amount of closed pores is constant.

(b) The increase in density during sintering is due to the reduction in volume of the open pores. Most probably the two processes are taking place simultaneously to a greater or lesser extent (i.e. both closed and open pores are shrinking and some closed pores are being formed from open pores).

The fact that most of the pores are surface connected during the major portion of the sintering time means, however, that it is unnecessary for material to move between pores separated by solid metal,

and it is possible for surface diffusion to be operative. Investigations on copper[59] have shown that the value of D_o for surface diffusion is approximately 10^5 times that for volume diffusion. Thus surface diffusion could be operative for closing the pores.

In practice, the process of spheroidisation of pores is slow, even at sintering temperature close to the melting point of the metal, and in commercial products most of the pores present retain an irregular form.

Flow	Properties
Spherical	Maximum flow
Dendritic	Poor flow
Irregular	Reduced flow
Packing or A.D.	Properties
Spherical	Maximum density
Dendritic	Reduced density
Irregular	Reduced density
Pressing	Properties
Spherical	Reduced
Dendritic	Good
Irregular	Good
Sintering	Properties
Spherical	Good
Dendritic	Good
Irregular	Good

Table 1[53] Relationship between shape of powders and flow, packing, pressing and sintering.

CHAPTER 2

2. OXIDATION

2.1. Diffusion.

A concentration gradient within a homogeneous solid phase causes diffusion of atoms or ions via interstitial or vacant lattice sites.

According to Fick's[60] first law the amount of solute, J_1, diffusing through a certain cross-section A per second is proportional to the concentration gradient $\frac{dc}{dx}$ at this plane

$$J_1 = -D_1 \frac{dc}{dx} \cdot A$$

where D_1 is diffusion coefficient and c is volume concentration of component.

The first Fick equation applies to the case in which the concentration gradient does not change with time over the region of flow. This situation is represented by the flow of gases through metals where a constant pressure of gas is maintained on one side of a metal specimen, the gas being removed on the other. Hydrogen, nitrogen, and oxygen, for example, diffuse rapidly through many metals at elevated temperature.

2.1.1. Effect of other elements on diffusion rate.

Defect concentrations in oxides may be changed by addition of foreign ions with a valence different from that of the ions of the parent oxide.

In ideal cases it is assumed that the foreign ion additions are homogeneously distributed through the scale, which means parent and foreign ions are oxidised at the same rate and that the rates of diffusion of the parent and foreign ions are equal. In practice this probably never occurs,

because the concentration of foreign ions at the interfaces will change with time. Such consideration leads to the following rules:-

(i) The oxidation rates of metals forming oxidation layers consisting of P-type semiconductors can be decreased, (but electron hole concentration is increased), by adding metals of lower valency than the basis metal and oxidation rate can be increased, (vacancy concentration is increased), by adding metals of higher valency than the parent metal.

For example: Nickel oxide, is a metal-deficit, (P.type), semiconductor. Its defect structure is characterized by the existence of Ni^{++} deficits and electron deficits according to this equation

$$\tfrac{1}{2}\ O_2 \ = \ NiO + \square Ni^{++} + 2\ \oplus \bar{e}$$

If Lithium oxide is added to the nickel oxide

$$Li_2O \ = \ 2\ Li_{\bullet}^{+}(Ni) + \ \square Ni^{++} + NiO$$

The concentration of $\square Ni^{++}$, i.e. cation deficits, is reduced by the Lithium ions which have only one charge in place of two, as illustrated by Figure 4a where the number of Ni++ vacancies is smaller than that of the electron defects represented by Ni^{3+}. Hauffe[61] has indeed shown that nickel oxidizes more slowly in oxygen when Li_2O vapour is added to the gas. When the number of electron defects is small compared with the number of Li^{+} ions on Ni^{++} sites, $Li^{+}_{\bullet}$ (Ni), then, at constant pressure of oxygen

$$K/K^{o} \approx 2C\ (\square Ni^{++})/C(Li^{+}_{\bullet}\ (Ni))$$

where K^{o} is the rate constant for the formation of pure NiO

scale and K that for the formation of an $NiO - Li_2O$ phase. The higher the defect concentration in an oxide, the smaller the effect of an added ion of different valency upon oxidation rate is likely to be. This is obviously the reason for the smallness of the reduction in oxidation rate of iron when Li_2O is evaporated on to its surface[62], the concentration of cation vacancies in wustite being exceptionally high. The other example is oxidation of iron when a small amount of copper is added in it.

When ions of higher valency are added to growing P-type oxides, the effect, according to the Wagner mechanism, is to increase the number of vacancies and the oxidation rate, as illustrated in Figure 4b, for the addition of tungstic oxide to nickel oxide. In contrast to Fig. 4a the number of Ni^{++} vacancies is larger than that of the electron defects represented by Ni^{3+}.

(ii) The oxidation rates of metals forming oxidation layers consisting of n-type semiconductors can be decreased, (but electron concentration is increased), by adding metals of higher valency than that of the basis metal.

For example: Embedded titanium in tungstic oxide[63]. On titanium the oxide that controls the overall oxidation rate is TiO_2 which is an n-type conductor with vacancies in O^{2-} lattice with a cation/anion ratio larger than $\frac{1}{2}$. The effect of W^{6+} ions is to reduce the number of vacant sites since $2W^{6+}$ ions replace 3 Ti^{4+} ions and thus decrease the cation/anion ratio.

2.2. Structure of Oxide

All atoms in a perfect crystal are at specific atomic sites. However, in real crystals a given atomic site may not be occupied, (vacancy), or may be present in an interstitial position. Impurity atoms in pure crystals can be considered as point defects and they play an important role in determining the electrical and mechanical properties of all materials. Impurity atoms may either occupy a normal atomic site in the parent lattice, (substitutional), or a non-regular atomic site, (interstitial).

All point defects produce a local distortion in the perfect lattice. The amount of distortion depends on the crystal structure, parent atom size, impurity atom size, and crystal bonding. These local distortions act as extra scattering centres to the flow of electrons through the crystal, thus increasing the resistance of the crystal. The other imperfections in solids are line and surface defects which include dislocations, grain boundaries and inner and outer surfaces.

Crystals of oxides, like metals, contain point defects at temperatures above absolute zero. However, oxides are made up of two or more different elements and the energy to form the different kinds of point defect will also be different. The defects which can be formed are anion vacancies or interstitials, and cation vacancies or interstitials. If the two defects have similar energies of formation then approximately equal concentrations of each defect will be formed, but if the energy to form one type of defect, say cation vacancy, is significantly smaller than the energy of formation of the other defect then the concentration of cation vacancies far outweighs the concentration of the other defect in

the crystal. When a large concentration of each type of defect is present in turn, a change in composition occurs leading to a deviation from stoichiometry.

These deviations are:

(i) Excess metal, due to anion vacancies like ZrO_2 [64]

(ii) Excess metal, due to interstitial cations like ZnO[12]

(iii) Excess metal, due to insterstitial anions

(iv) Excess non-metal, due to the cation vacancies like Cu_2O[65] and FeO[66].

The concept of Wagner's[65] model of semiconducting compounds is that they are of exactly stoichiometric composition, but are stable with an excess of either cations or anions, such as Cu_2O (P-types) or ZnO (N-type).

It is well known that FeO, for instance, is stable only with considerably less than the stoichiometric ratio of iron.With other compounds, such as Cu_2O and NiO, the metal deficit is not so obvious but can be detected. The formula of these oxides may be written $M_{b-m}O$ where m is a small fraction of b and they have an atomic disorder which is comprised predominantly of metal ion vacancies.

A P-type semiconductor is always positive and conduction is a consequence of vacancy migration.

A N-type semiconductor is always negative and conduction is a result of electron migration.

2.3. Initial oxide and Nucleation

The adsorption of gas on a solid surface is the accumulation of gas molecules on the surface. In the reaction between a metal and

a gas, this adsorption is the initial process.

On average there are about 10^{15} adsorption[67] sites per cm^2 of a clean metal surface. From the kinetic gas theory it may be estimated that, if all the molecules that impinge on a clean metal surface are adsorbed, a monolayer of adsorbed gas will be formed in about 2 sec at a pressure of 10^{-6} Torr at room temperature. As the rate of impingement of gas molecules is proportional to the gas pressure, pressures considerably lower than 10^{-6} Torr are required to prevent serious contamination of a clean surface.

The adsorption process results in a decrease of the surface free energy and also normally results in a decrease in entropy, because gas molecules or atoms lose some degree of freedom. A simultaneous decrease in both the free energy and the entropy also implies a decrease of enthalpy because $\Delta G = \Delta H - T\Delta S$. Thus adsorption is normally an exothermic process.

In considering adsorption on the surface it is customary to distinguish between physical and chemical adsorption.

Physical adsorption[68] proceeds without any activation energy and occurs as fast as molecules impinge on the surface. In chemisorption, the reaction may proceed slowly and may involve an activation energy. Chemisorption is more specific in nature than is physical adsorption[69]. Chemisorption is dependent on crystallographic orientation, edges, holes and defects in the surface, and is supposed to predominate at "active" spots or patches on the surface. Chemisorption is generally considered to proceed only until a monolayer of the adsorbed substance is formed on

the surface. Physical adsorption may take place on all surfaces and may also result in multimolecular layers.

When the surface layer becomes supersaturated with gas, oxide particles nucleate[70]. The nuclei often form at discrete heterogeneties such as dislocations and grain boundaries. They grow by diffusion of adsorbed oxygen along the metal surface to the edge of the island of oxide. This widening of the islands continues until the various islands of oxide impinge on one another and an oxide layer completely covers the metal. This film is then polycrystalline and has an initial size. During continued annealing this film undergoes grain growth.

As in any solid-solid nucleation, (to be discussed in chapter 3), the oxide-metal interfacial energy will be lower for the relative orientations of the two lattices that give good matching across the interface. For this special orientation the critical surface concentration of oxygen required for oxide nucleation is lower and the nucleation rate will be much higher. Thus nuclei of only a few orientations will be formed.

Using an optical microscope Bernard et al[71] made careful observations of the growth of nuclei under isothermal conditions and distinguished three successive stages. At the beginning of the oxidation the metal is covered by a film, the thickness of which increases to a critical value of several tens of Angstroms. Then the oxide which continues to form tends to accumulate at certain crystallisation centres, the average number of which corresponds, for a given crystallographic orientation, temperature and pressure to an equilibrium determined by the rate of surface diffusion of the metal and the oxygen. Formation of

the oxide layer is a three-stage process as follows:-

(i) The invisble film,

(ii) The nuclei, and

(iii) The continuous layer.

As mentioned above, the metal structure has an effect on nucleation. For instance, in the case of α-iron[71], the (100) face becomes covered with square nuclei of FeO, whilst the (111) and (110) faces become covered with triangular and acicular nuclei respectively.

With a given surface orientation and under a given pressure the number of nuclei per unit area becomes smaller as the temperature is increased. Over quite a wide range the number of nuclei formed on a given surface at a given temperature is proportional to the partial pressure of the oxygen or of the oxidising agent in the gas phase.

2.4. Parabolic Law (Wagner's Theory)

The mechanism is that of film thickening controlled by diffusion under the influence of a concentration gradient. Since the film is composed of cations and anions this diffusion across the film must be accompanied by a simultaneous diffusion of electrons in the same direction as the cations or in the opposite direction to the anions[72].

The driving force of the reaction is the free energy change associated with the formation of the oxide MO from the metal M and the oxygen gas and as a result concentration gradients of the components are established in the oxide. Such concentration gradients are illustrated schematically in Fig. 5a and 5b for oxide scales which contain mostly metal and oxygen vacancies, respectively. The partial pressure of oxygen

at the metal/oxide interface is equal to the equilibrium dissociation pressure of the oxide in contact with its metal $Po_2^{(d)}$, while at the oxide/oxygen interface it is equal to oxygen pressure in the gas phase, $Po_2^{(g)}$. For an oxide scale with metal ion vacancies, the metal ions diffuse outward from the M/MO to the MO/O_2 interface. The vacancies migrate in the opposite direction and their equilibrium concentrations at the interface are given by the defect equilibrium, (when the intrinsic electronic equilibrium is neglected).

$$\tfrac{1}{2}\ O_2 \ = \ MO + \square M^{p-} + P\oplus^{+}$$

As $Po_2^{(g)} > Po_2^{(d)}$ the metal ion vacancies are continuously produced at the MO/O_2 interface and consumed at the M/MO interface.

Oxygen ion vacancies migrate in the direction opposite to the metal ions vacancies and their equilibrium concentration at the interface is given by

$$O \ = \square O^{q+} + q\oplus^{-} + \tfrac{1}{2}O_2$$

Where $\oplus^-$ and $\oplus^+$ represent free electrons and electron-holes respectively, P and q are the number of ion charges. Oxygen ion vacancies are correspondingly created continuously at the M/MO interface and consumed at the MO/O_2 phase boundary.

The rate of growth is, in these terms, determined by the concentration gradients and the rate of diffusion of the components. These mechanisms lead to a parabolic rate of oxidation[73].

The diffusion coefficients for the cations, anions, and electrons are not equal, and because of this difference a separation of

charges take place in a growing oxide scale. However, the resulting space charge also creates an electric field which opposes a further separation of charges and a stationary state is reached for which no net electric current flows through the scale.

2.5. Oxidation of Iron.

Iron forms three stable oxides: wustite, FeO, magnetite, Fe_3O_4, and Hematite, Fe_2O_3.

Wustite, the lowest oxide, is a p-type conductor. It has a Na Cl type cubic lattice formed by close packing of the relatively larger oxygen ions with the smaller iron ions arranged in the interstices. The ionic radius[74] of oxygen is about 1.3Å while divalent iron has a radius of about 0.8Å and for trivalent iron the value is about 0.7Å. Its defects consist of vacant cation sites and an equivalent number of electron defects represented chemically by trivalent iron ions. Consequently diffusion is essentially cationic via vacant sites. The diffusion rate is relatively high.

Magnetite, Fe_3O_4, also exists with an excess of oxygen, but the excess is much smaller than with wustite, and the defect concentration correspondingly less. The diffusion is via cations and anions.

Hematite, Fe_2O_3, is an n-type conductor in which anions largely diffuse. Ionic transport in this phase is probably by oxide ions as compared with wustite where iron is almost certainly the mobile constituent. αFe_2O_3 is a rhombohedral crystal with the oxygen ion in a nearly close-packed hexagonal arrangement. The iron ions reside in the interstices.

During the oxidation of iron in pure oxygen these three oxides form under special conditions of temperature and pressure. The rate of growth of these oxides follows a parabolic law.

Below 570°C the overall rate is determined by the growth rate of Fe_3O_4. Above about 650°C the overall rate seems to be determined principally by the rate of FeO growth. Between 570°C and 620°C as the temperature increases the rate controlling layer changes from Fe_3O_4 to FeO. At 700°C the ratio $XFeO/XFe_3O_4/XFe_2O_3$ is about 100/5/1 according to Paeddisi[75].

Above 700°C the relative thickness of the three oxide layers is independent of time[76]. At temperatures below 900°C the mobility of cation vacancies in wustite becomes considerably lower owing to its high temperature coefficient, so that the outward diffusion of divalent iron ions becomes slower than the adsorption, thus giving the parabolic rate relationship. If at 900 - 1000°C the oxygen pressure exceeds 1 - 20mm Hg, a transition from linear to parabolic oxidation takes place. Under these conditions Fe_3O_4 and Fe_2O_3 are formed on top of wustite, and oxidation thus becomes diffusion-controlled. Fig. 6 shows the formation of different oxides of iron as a function of change of temperature and weight per cent oxygen.

The parabolic rate constant is a complex function of temperature in the growth of layers such as FeO, where the range of existence of the phase, as well as the diffusion coefficient for a given composition, depend strongly upon temperature. The rates of growth of iron oxide layers are rather insensitive to changes in the substrate. There seems to be a large change in the rate of growth of FeO when the substrate changes from

γFe to αFe and no great change in the growth of Fe_3O_4 when the substrate changes from αFe to FeO[74].

2.5.1. Transport Mechanism of Iron.

Study of the transport mechanism in oxides is possible[77] by studying the movement of inert markers in the diffusing system using radioactive silver as the inert marker.

Three series of these studies were carried out.[74]

(i) Iron metal was marked, then scaled in oxygen to give a multilayer scale.

(ii) Wustite was marked then reacted completely to magnetite in water vapour.

(iii) Magnetite was marked then partially reacted to hematite in oxygen.

From these measurements the following conclusions may be drawn about the transport mechanism:

(i) Wustite grows almost entirely by diffusion of iron ions. Oxide ions are added at the outer face of the phase and remain essentially fixed.

(ii) Magnetite grows largely by oxide ion diffusion.

(iii) Hematite grows by oxide ion diffusion with practically no iron participation.

2.6. Oxidation of alloys.

The purpose of the study of alloy oxidation is to improve the oxidation resistance of metals. The specific goal of such studies is to obtain compact scales with low rates of diffusion for the reacting atoms.

This approach may in principle be applied to metals which at high temperatures follow the Wagner oxidation mechanism. It is assumed that thermodynamic equilibria are established at the metal/scale and scale/gas interfaces, and that the driving force is equal to the chemical potential gradient across the scale. The rate of oxidation is thus dependent both on the concentration of the defects at the interfaces and on the rate of diffusion of the defects.

In the semiconductor valence approach the oxidation rate is changed by altering the defect concentration in the scale by appropriate addition of foreign ions, as mentioned in section 2.1.1.

The factors to be considered are many and include:

(i) The affinity of the component metals for each other and for the non-metal, in particular oxygen.

(ii) The diffusion rates of atoms in the alloy and of ions in the compounds.

(iii) The mutual solubility in the oxidation layer.

If the oxidation of an alloy follows, at least approximately, the parabolic time law, one may assume that the rate-determining reaction is a diffusion process. Larsen et al[7,8] have pointed out that no binary alloy can be expected to oxidise exactly in proportion to the square root

of the elapsed time at constant temperature, because the condition that the composition of the alloy immediately adjacent to the scale remains constant with time is not likely to hold, in view of differences in the rates of oxidation of the component metals and in the oxygen pressure of the oxide. This is correct when the first stages of oxidation are considered. However, after some time, when stationary equilibrium is established, the concentrations at the alloy-oxide interface may usually be taken to be constant.

In considering the oxidation of an alloy, it is useful to decide first, which of the components is likely to be attacked preferentially. This can be done by comparing the free energy of compounds (Appendix 2), that could possibly be formed at the temperature under consideration.

The valence approach to alloy oxidation is in practice limited to alloys with minor alloying additions, and it is confined to cases in which the oxide of the alloying constituent is soluble in the oxide of the parent metal. In more general cases of alloy oxidation, more than one oxide may be formed.

For example when Fe-Ni alloy, (N_{Ni} = 0.30), is oxidized a heterogeneous scale consisting of wustite and Ni-rich alloy is found underneath an outer layer of iron oxides[79]. It may be assumed that initially both iron oxide and nickel oxide nucleate at the surface of an Fe-Ni alloy. When the oxidation is continued, the faster growing iron oxide buries nickel oxide and it subsequently behaves as if it was an inert material. Buried nickel oxide, however, is not stable. Since the absolute value of the standard free energy of formation of nickel oxide is considerably less than that of wustite, the oxygen activity at the alloy-wustite interface

is so low that nickel rather than oxidized nickel is found at this location. Thus Ni in Fe-Ni alloys behaves in the same manner as a noble metal.

Also in the case of Fe-Ni alloys, the oxidation rate has been found to reduce only slightly with the Ni content up to 30 at: % Ni (80, 81, 82).

Likewise, oxidation of Fe-Cu alloys yields an outer scale consisting of iron oxides and an inner scale consisting of wustite and nearly pure Cu as a separate phase.

Addition of Cu in amounts of 0.8 - 2.2% slightly improves the oxidation resistance of iron in air[8], the oxidation rate being usually parabolic. Such a result might have been expected since the affinity of copper for oxygen is less than that of iron.

2.7. Summary.

When iron is exposed to an oxygen-containing atmosphere it is rapidly covered with an oxide layer. The oxide phases in this layer are Fe_2O_3, Fe_3O_4 and if the temperature exceeds 570°C, wustite FeO. Magnetite, wustite and probably also hematite are so-called p-type semiconductors, which permit internal transport of cations. Due to the outward diffusion of iron ions there is an inward diffusion of iron vacancies towards the oxide/metal boundary. These vacancies dissolve, to a limited extent, in the metal, but, if the concentration of vacancies becomes too large, they may be precipitated as cavities[83, 84]. Such cavities are often formed on discontinuities, such as grain boundaries or inclusions in the metal or in the oxide/metal interface. If the deformability of the phases is insufficient, the cavities may grow to such an extent that the active surface

of the iron phase is considerably reduced. As stated[85] the formation of such cavities leads to a decrease in the oxidation rate, followed by a change in the oxide phase composition.

If iron is alloyed with an element such as copper, it is likely to be found unoxidised in the oxide/metal interface. It is, therefore, very probable[86] that it affects the oxidation properties of iron by influencing the adherence between the oxide and the metal. The oxidation of the samples at 500°C[87] is as expected, little affected by the addition of small amounts of copper. At 650°C[87] the effect is more pronounced. The decrease in oxidation rate can be attributed to a weakening of the adherence forces between the oxide and the copper-rich iron.

The copper film in the metal close to the oxide phase prevents the formation of wustite in oxide films formed at 650°C if the copper content is one per cent or more.

In the outermost part of the hematite layer an enrichment of copper was found. The enrichment of copper at the oxide/metal interface causes a net diffusion of copper through the oxide. When diffusing copper reaches the hematite phase, it is oxidized and trapped in the outer zone.

2.8. Steam Oxidation.

Steam oxidation is being applied widely to a range of materials with the objective of increasing service life[88] through improved mechanical properties and wear and corrosion resistance.

2.8.1. Theoretical Aspects.

In the steam treatment of ferrous components there are usually

three types of oxide that form depending on temperature and surrounding gas.

At low temperature, ($25^{o}C$), $Fe(OH)_2$ is the main[89] oxidation product on iron when attacked by water vapour free from oxygen, but some Fe_3O_4 is formed. At higher temperatures, $60^{o}C$, $300^{o}C$ and even up to $450^{o}C$, Fe_3O_4 is formed.

Fig. 7 shows the formation of the different oxides according to change of temperature and steam equilibrium (Appendix 1).

Unlike oxidation in air, when three layers are normally formed, FeO is the main oxide formed by water vapour at temperatures above $700^{o}C$, but it is less predominant in the range 575 - $700^{o}C$ and it is unstable below $570^{o}C$. Larsen et al[78] have found a layer of only FeO above $700^{o}C$. Others[90] report a higher ferrous ion concentration in the scale formed in water vapour than in air. Since the standard free energy of the reaction

$$Fe_3O_4 + H_2 \longrightarrow 3FeO + H_2O$$

becomes negative at $700^{o}C$, the formation of magnetite at higher temperatures will depend largely on external conditions, in particular on the flow rate of the water vapour.

The oxidation layers formed in water vapour have less tendency than those formed in air to develop mechanical defects such as cracks and blisters. When several oxides are formed, as in air, the stresses set up as a result of differences in density and coefficient of expansion between the metal and the oxides might be expected to cause more extensive cracking than when, as in water vapour, the oxide FeO is the main product. It should be noticed that free oxygen present with the steam will combine with Fe_3O_4

produced to form the red oxide Fe_2O_3.

There are some metals which, though susceptible to attack by oxygen or air, would hardly be attacked by pure water vapour, simply for reasons of chemical equilibrium. In these instances, the dissociation pressures of the oxide are higher than the partial pressure of oxygen in water vapour[91], for instance, Mo at 1000°C, Co, Ni, Cu at 500 and 1000°C. Standard free energies have been used [92] to compile the information contained in Appendix 1 for 525°C.

Copper would hardly be expected to be attacked appreciably by water vapour at temperatures approaching the melting point[93]. The oxidation rate of copper in oxygen at 800°C is independent of water vapour content up to 3.9%[94], although a slightly reduced oxidation rate has been reported [95] for moist compared with dry air.

2.8.2. Steam treatment of sintered parts.

Porosity[96] is a characteristic feature of articles made from metal powders and although they may appear dense to the naked eye, they are in reality full of pores. Most of the pores are interconnected so that liquids or gases may pass through the sintered articles.

When porous iron articles are treated in steam this reaction takes place

$$3Fe + 4H_2O \longrightarrow Fe_3O_4 + 4H_2$$

Magnetite Fe_3O_4 is formed wherever the steam is in contact with the surface. In the sintered case the steam reacts not only with the outer surface but with all surfaces which are exposed within the porous passages. When solid

steel is treated only a very thin skin, (0.0025 mm), of oxide forms on the exterior, but in the porous case the oxide is found throughout the mass of the porous article with a thickness of 0.005 mm. Greater layer thicknesses are not possible, because the iron oxide then no longer allows any further water vapour to pass through it.

Generally components are steam treated at temperatures ranging between 450°C and 570°C. The Fe_3O_4 which deposits on the iron parts during the process is very dense and hard and has good corrosion resistance properties.

At the reaction temperatures used, the steam in the furnace is supersaturated and, therefore, behaves as a diatomic gas which causes a deposition of Fe_3O_4 on all the internal surfaces. However, with sintered iron articles a considerably longer treatment is required, because of the time required for diffusion of the superheated steam into the network of pores, and the diffusion in the opposite direction of the hydrogen produced by the reaction inside the sintered body.

During investigations at 570°C Lenel[96] found weight gain increases of 3.9% after 10 minutes, 6.7% after 30 minutes and 7.8% after 60 minutes, the latter being a maximum value, when the reaction extended to the deepest layers of the body. Theoretically, if the entire mass of sintered iron were converted to Fe_3O_4, the calculated increase in weight would be about 38.2%. Since only 7.8% weight gain was actually measured, this indicates that only 20% of the original sintered iron structure is converted to iron oxide.

Kanapicky[97] has investigated the influence of porosity on per cent gain in weight during steam treatment at 600°C for 1 hour.

In the same investigation into the properties of sintered iron bodies with and without steam treatment, tests have been done[97] on flat sintered test pieces, compacted at various pressures to obtain densities of between 6.3 and 7.6 $^{g}/cc$. The parts were steam treated at 570^{o}C. The results show that at a density of 6.7 $^{g}/cc$ the hardness value is roughly doubled by steam treatment. It was found that the increase in hardness depended solely on the amount of iron oxide in the iron body, and that the method of manufacture of iron powder used for sintering was unimportant.

Franklin and Davies[98] have investigated low-density sintered iron specimens when steam oxidised at two temperatures, 520^{o}C and 650^{o}C. It was demonstrated that reduction in interconnected porosity was due to complete sealing of all surfaces passages into the interconnected pore network, and that a substantial interconnected pore network existed beneath the specimen surface.

It was shown that treatment at 650^{o}C produces very rapid oxidation but, due to surface sealing, a lower oxide content was achieved after long treatment times than would be achieved at normal treatment temperatures.

Razavizadeh and Davies[99] have investigated the effect of density, (6.0, 6.4, and 6.8 $^{g}/cc$), and powder type, (A.S.C. and sponge), on steam treatment at 450^{o}C, 525^{o}C and 600^{o}C.

It was shown that:

(i) The type of iron powder used has an important influence on the rate of pore closure during steam treatment at low temperature.

(ii) In order to obtain the maximum increment of hardness, steam treatment should be practised at 450^{o}C or 525^{o}C.

(iii) After steam treatment under comparable conditions the hardness of sponge iron powder specimens is always greater than that in those produced from A.S.C. powder.

(iv) At steam treatment temperatures of 450°C the oxide formed is Fe_3O_4 but at higher temperatures a mixed structure of Fe_3O_4 and Fe_2O_3 is produced.

During the steam treatment of iron-copper alloys, (as discussed in section 1.8.1), copper does not oxidise in steam and only iron oxides are formed.

Addition of copper slightly improves the oxidation resistance of iron.

Phadke and Davies[17] investigated the steam treatment of sintered Fe-2% Cu alloy at 500°C and the possibility of combining this treatment with precipitation hardening.

The results showed that:

(i) Significant improvement in hardness can be achieved during simultaneous steam oxidation and ageing heat-treatment.

(ii) The degree of hardness increase due to steam oxidation was found to be nearly the same in pure iron and in the Fe - 2% Cu alloy.

Sunter and Cosh[100] have investigated the effect of steam streatment on 97.9% Fe, 1.1% Cu., 1.0C% alloy at 510°C for 55 minutes.

The results indicate that both steam treatment and oil impregnation are effective methods of reducing corrosion, though steam

treatment would be undesirable if the part were to be exposed to a weak acid electrolyte.

2.9. Operating Precautions.

Steam treatment is a rather inexpensive, safe treatment which has gained considerable acceptance in powder metallurgy[16] since it satisfies the requirements of many applications. The process involves the exposure of powdered iron parts to a steam atmosphere in a furnace with internal pressure, equal to $1000\,N/m^2$, (4 in:H_2O). This usually prevents significant amounts of air being pulled into the furnace. When properly operated, the treatment forms a controlled oxide primarily of Fe_3O_4 with a small amount of FeO.

Three general precautions must be observed to obtain satisfactory results.

(i) Parts must be clean. Where parts are machined, sized or coined subsequent to sintering, it is necessary to remove the lubricants picked up in these operations prior to steam treatment.

(ii) Steam must not be introduced into the chamber until the coldest part of the load is at a temperature greater than $100^{o}C$. Otherwise, a hydroxide of iron is formed on those parts whose temperature is less than $100^{o}C$, and this decomposes to typical red rust according to equation

$$2Fe(OH)_3 \longrightarrow Fe_2O_3 + 3H_2O$$

(iii) All air must be absent from the furnace chamber at temperatures

greater than 425°C. If air is present the oxide formed will have variations of a dull, non-uniform colour and the part frequently will be covered with a brown velvety fuzz which is a form of Fe_2O_3 mentioned above.

The formation of the controlled oxide coatings results from the reactions between superheated steam and iron

$$Fe + H_2O \longrightarrow FeO + H_2$$

$$3FeO + H_2O \longrightarrow Fe_3O_4 + H_2$$

These equations do not complete the story in that the oxygen source must result from a fractional decomposition of the steam at the temperatures used for the process. In this decomposition there are two reversible reactions which can compete against each other depending on conditions in the chamber,

$$H_2O \rightleftarrows H_2 + \tfrac{1}{2}O_2 \qquad \text{and}$$

$$H_2O \rightleftarrows OH + \tfrac{1}{2}H_2$$

The first is the normal reaction which occurs at temperatures greater than 425°C when no air is present to provide additional oxygen. It is much faster than the second reaction and the Fe_3O_4 is formed readily. If air is present the second reaction will have sufficient energy to be predominant and the hydroxide of iron, $Fe(OH)_3$, is formed which is unstable and breaks down to a form of Fe_2O_3 as previously indicated. It is important to note that the amount of oxygen and hydrogen in the chamber resulting from the fractional decomposition of steam is extremely small.

2.10. Applications of steam treatment.

The majority of steam atmosphere furnaces have been supplied for treatment, after final grinding, of high-speed tools such as drills, reamers, hobs, milling cutters and saws. The blue-black oxide film of Fe_3O_4 is tough, hard and tightly adherent with a high degree of corrosion resistance. Extensive laboratory and production tests by drill manufacturers show that steam treatment improves useful product life by 50% or more.

The effects of steam treatment in prolonging tool life in this application are threefold.[88]

(i) The film of Fe_3O_4 is sufficiently porous to retain cutting oil so that lubrication at the point of contact during machining is improved, thereby reducing frictional heat.

(ii) The iron oxide coating prevents machining chips from welding to the lip of the cutting edge.

(iii) Steam treatment relieves stresses in the tool conferred by grinding.

In the fabrication of non-ferrous materials such as brass, bronze, beryllium, copper and aluminium, chemical and mechanical cleaning operations must be employed to remove surface oxide formed during annealing, stress relieving and other heat treatments carried out in air. Heat treatment in steam substantially reduces, and in some cases eliminates, such cleaning operations.

2.11. Applications to sintered iron parts.

Typical items commonly treated include gears, cams, shock absorbers, pistons, seals and compressor parts.

Formation of a Fe_3O_4 layer of up to 0.005 mm thick results in increased hardness, compressive strength and wear resistance.

After steam treatment, iron powder parts can be oil-dipped[101] to increase resistance to corrosion. On bearing surfaces, for instance, where alternating heating and cooling results in condensation of moisture, the oxide-impregnated part retains oil sufficiently to resist the effect of moisture.

The hard oxide also provides a better breaking-in condition when starting up or wearing-in the part. When the oxide on the external surface particles wears away, the oxide in the pores continues to offer a network of hard wear-resistant material.

CHAPTER 3

3. PRECIPITATION HARDENING.

3.1. History.

The major commercial interest in the precipitation reaction stems from its usefulness as a strengthening mechanism. It is this mechanism which has made possible the use of lightweight aluminium alloys in industry.

It was discovered by accident in 1906 by Wilm[102]. During the course of experiments to investigate the solid solution strengthening effects of magnesium additions to an Al-Cu-Mn alloy he found by accident that ageing a quenched alloy produced a considerable increase in hardness. Wilm could observe no microstructural changes during the strengthening period, and the source of the increased strength remained a mystery. In 1920[103] Merica et al correctly deduced that the strengthening resulted from formation of submicroscopic precipitates produced at temperatures below the solvus line. However, it was not until the development of the electron microscope in 1950 that the nature of precipitate formation became physically clear.

3.2. Driving Energy for Precipitation.

A necessary condition for precipitation is that a phase becomes thermodynamically unstable and tends to decompose into two phases of differing compositions. This requirement is usually accomplished by cooling at a rate rapid enough to avoid diffusion of the solute which is necessary for formation of the precipitate phase. The new phase forms because by so doing it lowers the free energy of the system. The alloy becomes either unstable or metastable depending upon whether the composition

lies within the spinodal or outside it and decomposes in two distinct modes by spinodal decomposition or by nucleation and growth.

3.2.1. Spinodal points.

Fig. 8a shows a simple solid solution phase diagram which contains a miscibility gap at low temperature. At any temperature below $T_{max.}$ the free energy curve of the solid solution will be shown in Fig. 8b. The equilibrium phase mixture at the temperature to which this free energy curve refers is obtained by drawing a common tangent between the two minima in the free energy curve, the points of tangency determining the compositions of the two phases. This part of the curve is hypothetical in that it gives the free energy of the super-saturated solid solution within the miscibility gap. The magnitude of the difference between the hypothetical free energy curve and the line of common tangency gives a measure of the thermodynamic driving force causing decomposition.

There are two points of inflexion, S_1 and S_2 on the free energy curve at positions between the two minima, and the locus of the point of inflexion on the free energy curve at all temperatures below $T_{max.}$ defines the so-called spinodal line, the dashed line in Fig. 8a. Both the mechanism of formation and the resultant morphology of the decomposition products of the super-saturated alloy depend upon whether the alloy is inside or outside the spinodal region. If the temperature and composition are such that the alloy is transformed in the region between the phase boundary and the spinodal line there is a nucleation barrier to decomposition.

3.2.2. Barrier to nucleation.

In Fig. 9a if alloy C_N suffers a composition[104] fluctuation which results in some parts of the alloy having a composition C_N^+ the matrix phase must then have a composition C_N^-. The total free energy of the alloy is given by the weighted average of the free energy of the two compositions, i.e. point N in the figure. To accomplish such a composition fluctuation the free energy of the alloy must increase by an amount ΔG_N. If the composition fluctuation is to increase to the extent of forming a stable two phase mixture of the equilibrium phases α_1 and α_2, the free energy of the alloy must continue to increase until the composition fluctuation goes beyond the composition $C_N^{'+}$ corresponding to the position b' on the free energy curve, at which point the free energy of the alloy begins to decrease. The increase of free energy that is needed to obtain a two phase structure from the supersaturated alloy represents the barrier to nucleation which must be overcome if stable nuclei are to form. Thus, alloys between the equilibrium and spinodal lines undergo a nucleation and growth transformation.

For alloys lying within the spinodal region there is no thermodynamic barrier to nucleation. Considering the alloy of compo siton C_S in Fig. 9b, composition fluctuations yielding regions of composition C_S^+ leave the matrix of composition C_S^-. The free energy of the alloy now lies on the line joining the free energies of the two different compositions (i.e. point S in the diagram). This means that the free energy of the alloy has decreased by an amount ΔG_S due to the composition fluctuations, and increasing changes in composition lead to progressive decreases in free energy. That is the alloy C_S is unstable to small fluctuations in composition, and therefore decomposition of all supersaturated solid solutions within the spinodal region takes place

spontaneously.

3.2.3. Free energy change and formation of precipitates.

Free energy is the most important factor in the sense that if it is positive there is no driving force for nucleation and, hence, no nucleation. Consider a single α-phase alloy of composition X_o that has been quenched below a solvus line to some temperature. Fig. 10 presents[105] the free energy composition diagram for this α-phase alloy and locates its free energy per mole at G_o. If a small amount of precipitate forms with composition X_2 this in turn requires the remaining α phase to lower its composition to X_1. Consider that the precipitate is a G.P. zone having the same crystal structure as the matrix and assume that its free energy G_2 is given at point A. Thus the free energy change associated with the formation of the precipitate is,

$$\Delta G' = G(\text{Final}) - G(\text{initial})$$

$$= (n_1G_1 + n_2G_2) - (n_1 + n_2)G_o \qquad (1)$$

where, $\Delta G'$ is the total free energy change upon formation of the precipitate.

n_2 is the number of moles per precipitate.

n_1 is the number of moles in the α matrix after precipitation.

From the lever law

$$\frac{n_1}{n_2} = \frac{X_2 - X_o}{X_o - X_1} \qquad (2)$$

Combining Equations 1 and 2 gives

$$\Delta G' = n_2[G_2 - G_o - (X_2 - X_o)\frac{G_o - G_1}{X_o - X_1}] \qquad (3)$$

At the instant of nucleation the amount of precipitate that has formed will be very small so that it may be assumed that $X_1 \simeq X_o$. Under this condition equation 3 becomes

$$\Delta G_B = \frac{\Delta G'}{n_2} \text{ [initial precipitate]} = [G_2 - G_o - (X_2 - X_o)(\frac{dG}{dX})_{X_o}]$$

This equation gives the desired expression for the free energy per atom in the nucleus and it may be interpreted quite easily by graphical means.

The term $G_2 - G_o$ is seen directly on the ordinate. The term $(X_2 - X_o)(\frac{dG}{dX})_{X_o}$ can be determined from the following calculations.

$$\text{Slope at composition } X_o = \tan\alpha = [\frac{dG}{dX}]_{X_o}$$

and $\tan\alpha$ in triangle BMF is $\tan\alpha = \frac{BM}{X_2 - X_o}$

Combining these two equations gives $BM = (X_2 - X_o)[\frac{dG}{dX}]_{X_o}$

Hence, it is seen that formation of the precipitate of composition X_2 leads to a free energy change, ΔG_B, which is represented by (A - B) on the plot.

(A - B) is positive so this precipitate cannot form because

$$G_2 - G_o - (G_B - G_o) \Longrightarrow G_2 - G_B = A - B > o$$

But β precipitate of composition X_3 has negative free energy. From the above calculation

$$CM' = (X_3 - X_o)[\frac{dG}{dX}]_{X_o} \Longrightarrow G_3 - G_o - (G_C - G_o) \Longrightarrow G_3 - G_C = D - C < o$$

Thus from the above discussion it may be concluded that any precipitate having free energy per mole below the line tangent at X_o will have a

negative value of ΔG_B and its formation is thermodynamically favoured. This is a very useful guide because it allows the determination of ΔG_B for any potential precipitate by a simple graphical construction.

As an example consider an alloy of composition X_o in Fig. 11. The alloy is first homogenized above the solvus temperature and then quenched to either the high temperature, T_h or the low temperature T_L. Prior to any precipitation at the quenched temperature the α phase of composition X_o is a metastable phase with free energy of $G_{(\alpha)}$ at temperature T_h and T_L. From the above discussion there are three types of precipitate which may form and these are GP zones, an intermediate phase or the equilibrium phase.

The $G_{(\beta)}$ curve refers to the equilibrium precipitate and $G_{(int)}$ for the intermediate precipitate. The G_s curve for GP zones will be assumed to be the same as $G_{(\alpha)}$ because these zones have the same crystal structure as the parent α phase. From Fig. 11 it can be seen that at T_h quenching temperature only equilibrium precipitate can form because free energy is below the tangency line. At T_L all three precipitates can form and it shows more negative free energy for equilibrium precipitate. Consequently GP zones and intermediate phase may only form at lower temperature.

Referring to Table 2[105] it is seen that at temperature T_L all three precipitates have a negative free energy of formation and any of them could, in principle, form. One might expect the equilibrium precipitate always to form in preference because it has the largest driving force, for formation. However, it will be seen in the next sections that surface energy and strain energy will inhibit formation of any precipitate, and it is precisely because these factors are lower for the

intermediate precipitate and GP zones that they do form before the equilibrium.

Q Temperature	ΔG_β(GP)	ΔG_β(int)	ΔG_β(equil.)
T_h	Positive ⟶	Positive ⟶	Negative
T int	Positive ⟶	Negative ⟶	More negative
T_L	Negative ⟶	More negative ⟶	Most negative

Table 2[105] Variation of free energy of formation of three precipitates at three different temperatures.

3.3. Nucleation.

Nucleation that occurs completely at random throughout a system is said to be homogeneous. Usually there are regions where nucleation is observed to take place more rapidly. These are regions where there is disarray, such as grain boundaries, dislocations and vacancy clusters, since these regions will have high free energy per atom and so will be the first to become unstable during the transformation. Nucleation occurs preferentially at these places during heterogeneous nucleation.

3.3.1. Nucleation from pure liquid metal.

During solidification of a pure metal, no composition change is involved and the strain energy associated with a nucleus of solid growing in a liquid is negligible.

The only factors involved in the system are the difference in volume free energy and surface energy. Let the latter be ΔF_s. The

difference in volume energy of the two phases A and B (ΔF_V) will be, by definition zero at T_L, the melting point of the metal, but will increase as the temperature decreases.

For a given degree of supercooling, the release of volume free energy on forming a nucleus of the solid phase, must be offset by the absorption of energy involved in creating the interface. If the particle of A is large the interfacial free energy can be ignored in comparison with the volume free energy, but this will not be justified if the nucleus is very small.

If the nucleus is considered to be a sphere with radius r, then the change of the volume free energy for this sphere will be $-\frac{4}{3}\pi r^3 \Delta F_V$. The energy required to create the interface will be $4\pi r^2 F_s$.

$$\text{Thus,} \qquad \Delta F = (-\tfrac{4}{3}\pi r^3 \Delta F_V + 4\pi r^2 \Delta F_s) \qquad (4)$$

The surface energy term is initially larger than the volume energy term, but increases less steeply with change in r, so that the value of free energy passes through a maximum value at r_o, the critical size for nucleation. Equation 4 is represented in Fig. 12.

Homogeneous nucleation requires that thermal fluctuations produce nuclei large enough to exceed r_o, otherwise the second phase cannot nucleate. If nucleus radius is smaller than r_o it can lower the total free energy by re-dissolution.

The value of r_o will be given by differentiation of equation 4 with respect to r and equating to zero.

$$\frac{dF}{dr} = -4\pi r_o^2 \Delta F_V + 8\pi r_o \Delta F_s \Longrightarrow$$

$$r_o = \frac{2\Delta F_s}{\Delta F_V}$$

3.3.2. Nucleation in the solid state.

In solid-solid transformations the difference in specific volumes of the matrix and precipitate phases introduces an extra energy term, the strain energy ΔF_E, because in this case the volume change of the transformation cannot easily be accommodated by the matrix material due to its rigidity, so,

$$\Delta F = -{}^{4}/_{3}\,\Pi r^3 \Delta F_V + 4\Pi r^2 \Delta F_S + \Delta F_E$$

Before considering the effect of precipitate on interfaces the way in which the size of a stable nucleus varies with temperature needs to be considered.

It was assumed that ΔF_S is independent of temperature. On the other hand, the volume free energy varies with temperature, becoming larger at low temperatures because the degree of super-saturation increases, (solubility decreases), as the temperature decreases. This effect is shown qualitatively in Fig. 13, where it can be seen that the critical radius decreases with decrease of temperature. At a temperature just less than the solvus line, r_o is very large. The rate of homogeneous nucleation is, therefore, very small at this temperature. As the temperature is decreased, the critical radius rapidly decreases in size and so does the energy necessary to form a critical embryo.

3.3.3. Incoherent nucleation.

An incoherent nucleus has no lattice continuity with the matrix, and the strain associated with the formation of an embryo in a crystal is that associated with the hydrostatic strain produced by placing an inclusion into a hole which is either slightly too large or too small for it.

This dilation, (uniform expansion or contraction) can be accommodated by plastic flow if the two phases are sufficiently soft, or by elastic strain if they are rigid. The resultant strain energy will be negligible in the first case but in the second case it is dependent upon the values of the elastic moduli and upon the particle shape of the second phase. Russell[106] has shown that if a precipitate forms with an incoherent interface it will almost always be strain free.

On the assumption that the strain is accommodated predominantly in the matrix, Nabarro[107] has calculated the strain energy of an incoherent spherical nucleus as a function of its shape. He has shown that maximum strain energy is present when the precipitate is spherical.

3.3.4. Coherent nucleation.

The energy of coherent or quasi-coherent interfaces is less than that of the incoherent type and a considerable reduction in the free energy of formation of a nucleus results if the embryos are bounded by coherent interfaces. Phases joined by coherent interfaces are crystallographically related so that specific crystallographic planes in the two crystals are parallel and certain directions in these planes coincide. Consequently, coherent precipitates having large associated strain energy fields tend to form as plate-shaped particles on {100} matrix planes in F.C.C. and B.C.C. lattices because the modulus of elasticity is a minimum along <100> direction.

Nicholson et al[108] have shown that in Al - 4% Cu alloy in which plate shaped precipitates of θ'' have a coherent interface with the

matrix the orientation relationship is $\{100\}_{\theta''} \parallel \{100\}_{matrix}$.

3.3.5. Heterogeneous Nucleation.

As mentioned before defects such as vacancies, dislocations, grain boundaries act as nucleation centres for heterogeneous nucleation. These defects have high free energy per atom and so will be the first to become unstable during the transformation. A review of the subject has been given by Nicholson[109].

3.3.5.1. Vacancy clusters. This type of heterogeneous nucleation occurs in age-hardening alloys that are quenched from high temperature and aged at low temperature. The rapid quench retains an excess of vacancies in the lattice at lower ageing temperature, which assists both in the diffusion of the solute to a precipitate nucleus and also in the nucleation event itself. Most of the evidence for vacancy assisted heterogeneous nucleation comes indirectly from studies of the rate of nucleus formation. For instance, some of the excess vacancies that are retained in the lattice during quenching are annihilated at grain boundaries which are preferred sites for nucleation.

Seitz[110] suggested that the very high diffusion rates observed during GP zone formation are due to a concentration of vacancies in excess of the equilibrium concentration. Various investigations[111, 112] of the rate of GP zone formation in a number of systems are in accord with the excess vacancy explanation. Diffusion in substitutional alloys occurs by a vacancy mechanism so that an n-fold increase in the number of vacancies gives an n-fold increase in diffusion rate.

3.3.5.2. Dislocation lines. Nucleation is strongly dependent upon the state of strain of the nucleus structure. The growth of a cluster will be promoted by either a compressive or a tensile strain. Since dislocations are closely associated with regions of both, they should assist the formation of a cluster whichever the cluster requires. In such cases the compressed and stretched regions above and below edge dislocations will materially reduce the elastic energy required to form a nucleus.

Transition phases usually nucleate at or on dislocations. Several factors contribute to this:-

(i) The concentration of solute will probably be higher around a dislocation due to segregation at dislocations[113].

(ii) The atom positions at the core of the dislocations can be distorted until the crystal structure is similar to that of the precipitate, e.g. nucleation of a hexagonal precipitate along helical dislocations in a F.C.C. matrix as in Al - 16% Ag[114] alloys.

The attraction between silver atoms and dislocations may not be simply due to relief of strain, because atoms of aluminium and silver have very similar atomic sizes. Thus it is probable that there is chemical or electrical attraction between silver atoms and dislocations.

(iii) A pure screw dislocation is not such a favourable site for solute segregation as an edge dislocation. However, screw dislocations can climb into helices by absorbing vacancies, so that they become mainly of edge character and are then favourable places for segregation of solute atoms (e.g. θ' precipitate in Al - 4% Cu[115] alloys aged at 160°C).

3.3.5.3. Grain boundaries. The large energy of high-angle grain boundaries is removed when precipitation occurs there because a non coherent high-angle boundary is similar to a non-coherent interface between precipitate and matrix. Such a boundary is able to reduce the surface energy necessary for nucleation. Other reasons why grain boundaries are preferred nucleation sites include:-

(i) diffusion along boundaries is rapid at temperatures below about 0.6 T_m[116].

(ii) Grain boundaries act as a sink for vacancies, and consequently nucleation of precipitates on them.

3.3.5.4. Precipitate Free Zones (P.F.Z.) When grain boundaries act as sinks for vacancies[117] and when the precipitate requires vacancies for its formation and growth, a precipitate free zone forms near a grain boundary, (for example in Al - Zn - Mg and Al - Mg alloys)[118]. In these systems the precipitates are less dense than the matrix and, therefore, localized compressive stresses are created in the matrix near these precipitates. The stresses are greatly reduced by precipitation of vacancies within this region with the result that such precipitates act as vacancy sinks. The nucleation and growth of these precipitates being vacancy sensitive is greatly hindered in the absence of vacancies and P.F.Z. results.

3.4. Precipitate Sequences.

The precipitation sequence is summarized in general terms in Table 3.[119] The term ΔG_B is the driving force for the precipitation

reaction and it must be negative in order to cause precipitation. This free energy is a function of the extent to which the alloy is quenched below the solvus temperature. At high temperature only the equilibrium precipitate forms, because it is the only precipitate having a negative ΔG_B. At low temperature the driving force ΔG_B is largest for the equilibrium precipitate. However, the two factors of strain energy E and surface energy tend to inhibit nucleation of the equilibrium precipitate because the rate of nucleation of solid precipitate from a solid solution is a function of both ΔG^*, the free energy of formation of a critical sized nucleus, and of D, the diffusion coefficient of the solute in the matrix phase. Both the thermodynamic and kinetic factors are a function of temperature: ΔG^* depends upon the degree of supersaturation, which is directly related to temperature, (Fig. 12) and diffusion is a thermally activated process.

The rate of nucleation at any temperature is given by the product of the thermodynamic term and the kinetic term, so that

$$I = K \exp[-(\Delta G^* + Q)/KT]$$

where I is the rate of nucleation, and the remaining factors have been defined previously.

In Fig. 14a. is shown the value of I as a function of temperature where T_o is a temperature on the solvus line.

At very low temperatures the rate of nucleation is low because the diffusion rate is low. At the higher temperature the rate of nucleation is low because of the high value of ΔG^*. At intermediate temperatures the rate of nucleation increases to a maximum.

From Fig. 14b. it is apparent that the time required to reach a given stage of precipitation, (i.e. to precipitate N nuclei), is proportional to $\exp(\Delta G^*/KT)$. On the other hand zones and sometimes intermediate precipitates give higher nucleation rates due to their lower surface energy. The activation energy for nucleation of the intermediate precipitate may be decreased by reducing the strain or surface energy by heterogeneous nucleation. An example of this reference occurs in Al - Cu[120] alloys and is shown schematically in Fig. 15.

	Driving Force, ΔG_B		Factors Inhibiting Nucleation		Mode of Formation
Precipitate	Low Temp. Inside Spinodals	High Temp. Just Below Solvus	Strain Energy, E_s	Surface Energy γ	
GP zone	Small negative	Positive	Low (Frequently along certain <hkl> dir.)	Low	Spinod. decomp. or homog. nucl. and growth
Intermed-iate	Intermed-iate neg-ative	Positive	Med-high (can be lowered by precipitation on dislocations)	Low-medium	Hetero-geneous nucl. and growth
Equilib-rium	Large negative	Negative	Low	High (can be lowered by precipitat-ion on sur-faces [grain boundaries]	Hetero-geneous nucl. and growth

Table 3[119] Summary of the major factors involved in the Precipitation Sequence.

3.5. Reversion

It was pointed out in the section on nucleation that clusters which are just large enough to be stable nuclei at low temperatures are

of sub-critical size at a higher temperature and, therefore, will dissolve. This resolution called retrogression or reversion is accompanied by loss of properties previously acquired by virtue of the GP zones or nuclei of the transition or equilibrium lattice. Correlated hardness and X-ray effects have been reported which clearly show retrogression in cold-hardened Al - Cu alloys[121]. Alloys aged at high temperature can also experience retrogression when they are reheated to a still higher temperature[122]. A surprising example was found by Gruhl et al[123] who reported that reversion occurred in Cu - Be alloys during cold working. They ascribed this resolution to the heat generated during the plastic deformation.

3.6. Precipitation coarsening.

Overaging is softening resulting from prolonged ageing. It may be stated that it is connected with the continued growth of precipitate particles. Growth will continue as long as the metal is maintained at a fixed temperature. This does not mean that all particles continue to grow, because this is an impossibility once the solute has attained an equilibrium concentration.

It merely means that certain particles, (the larger ones), continue to grow, while the smaller ones disappear.

The growth of precipitate is directly related to the surface tension at the interface between the matrix and the particles. Because of the boundary surface energy, the free energy per atom in a large particle is lower than in a small particle. This free-energy difference is the driving force that causes the dissolution of small particles and growth

of large ones.

According to equation 4 $$\Delta F = -4/3 \Pi r^3 \Delta F_V + 4\Pi r^2 \Delta F_S$$

This is the total free energy of a given amount of precipitate. The free energy per unit volume would be

$$\Delta F' = \frac{\Delta F}{4/3 \Pi r^3} = -\Delta F_V + \frac{3\Delta F_S}{r}$$

or $$\Delta F' = -A_1 + \frac{A_2}{r}$$

The free energy per atom of the precipitate is proportional to the free energy per unit volume, so that

$$F_a \approx -A_1 + \frac{A_2}{r}$$

where F_a is the free energy per atom. This quantity varies inversely as the radius of the particle. The larger the radius, the more negative the free energy of the second phase and, therefore, the more stable it is in the precipitate. Conversely, the smaller, the less stable it is. Under conditions such as these, solute atoms tend to leave smaller particles and enter the matrix, while at the same time they leave the matrix to enter the larger particles. Diffusion of solute through the matrix makes it possible for this process to continue.

3.7. Theories of hardening.

In general, the increase in hardness is synonymous with an increased difficulty of moving dislocations. Either a dislocation must cut through the precipitate particles in its path, or it must move between them. In either case, it can be shown that a stress increase is needed to move the dislocation through a lattice containing precipitates. The

mechanism of Fig. 16 has been proposed by Orowan[124] and in this case the particle spacing is large enough and the particles so hard that the dislocation cannot pass through them.

As the applied shear stress is increased the dislocation bows out sufficiently so that it begins to meet at points such as A and B at time t_2. Notice that the sense of the dislocation at A will be opposite to that at B. Consequently when these dislocation segments meet they will annihilate, causing the main dislocation to separate from the looped regions as shown at t_3. Every time a dislocation passes the particles by this looping mechanism it leaves one loop around each particle as shown at t_4. The stress T_o[113] to expand a dislocation loop out to a radius of curvature $d/2$ is

$$T_o = \frac{Gb}{d}$$

where G is the shear modulus, b is the Burger's vector and d is the spacing between precipitates.

If the precipitate spacing and strength are such that the dislocation can pass through them, the stress at which the particles deform would be as follows. Consider the balance of forces existing in the model Fig. 17. The force per unit length on the dislocation is the applied stress T times the Burger's vector b. Thus the force resisted by each particle is Tb times the length of dislocation per particle or roughly Tbd. Thus the work done in moving the dislocation through a particle of diameter 2r is Tbd(2r).

The crystal structure of the precipitate may be ordered, in which case if the Burger's vector of the moving dislocation is not equal to the repeat distance of the ordered structure, work must be done to create the disordered interface across the slip plane. The passage of the dislocation through the precipitate alters the numbers of atom at the surface of the precipitate and hence alters the number of nearest neighbours of a particular type, which again requires work.

Kelly et al[125] have shown that the applied stress required to move a dislocation through a coherent spherical particle can be expressed as

$$T = \frac{f\gamma_p}{b} + \frac{Cf\gamma_s}{r}$$

where T = applied shear stress

b = Burgers vector

f = volume fraction of precipitate

γ_p = energy of the new interface within the particle

γ_s = precipitate-matrix interfacial energy

C = a numerical constant = $\frac{\sqrt{6}}{\pi}$

r = mean radius of the spherical particle

The first term on the right represents the stress required to disorder the precipitate and as particles thicken it will dominate. The second term represents the stress needed to produce the additional particle-matrix interface by slip.

If the particles are not ordered internally then γ_p equals zero

$$T \geqslant \frac{\sqrt{6}}{\pi} \frac{f\gamma_s}{r}$$

3.8. Precipitation in iron - copper alloys.

Copper precipitates from α or γ iron as a F.C.C. phase without formation of intermediate compounds. In the first stage of the precipitation, spherical particles with diameter < 100Å are formed at a high rate. During the second stage, the particles grow at a rate given by Zener's equation for growth of a spherical precipitate. In the third stage, growth is slower. Rod shaped particles form after long ageing times at 700°C[126]. Maximum strengthening has been observed at the beginning of the second stage of precipitation.

There have been several investigations dealing with the precipitation of copper from iron. Hardness has been found to pass through a maximum during ageing at temperatures between 400 and 700°C [127, 128]. Hardness begins to increase as soon as ageing starts and without an incubation period.

3.8.1. Solid solution.

A solubility that decreases with decreasing temperature makes it possible to obtain supersaturated solid solutions with concentrations up to the maximum solubilities. Then the alloy has to be heated above the α or γ solubility line, Fig. 18. The homogeneous solid solution can be quenched from the homogeneous α or γ field. Alloys with a concentration close to that of maximum solubility have to be quenched from the temperature of maximum solubility, (e.g. 8% cu from 1050°C in γ field or 1.5% Cu from 850°C in α field).

In systems with an extended γ-field, (Fe - Cu), relatively imperfection-free supersaturated solid solution can be obtained only by quenching from the α-field. Then the temperature of maximum solubility

is less than 900°C and the rate of quenching is, therefore, not very critical. Much higher supersaturations can be obtained by quenching from the γ-field. The transformation that takes place during quenching is martensitic at high solute concentration but massive at low solute concentration[129]. Both transformation mechanisms lead to homogeneous solid solutions which differ only in the density and distribution of lattice imperfections.

Hornbogen et al[126] have shown that there is no great difference in the hardness curves after quenching from the γ or the α field. The initial hardness of a sample quenched from the γ field is higher but both reach about the same maximum hardness and the reaction is only slightly accelerated by quenching from the higher temperature. Metallographic examination showed the same shape and size of the ε particles but some copper precipitated as films along sub-boundaries in those samples which were quenched from the γ-field.

3.8.2. Nucleation and growth.

The supersaturated solid solution is thought to decompose first into spherical GP zones of copper which have the matrix b.c.c. crystal structure. The GP zones have never been observed directly but the very rapid onset of precipitate growth is usually taken as strong circumstantial evidence for GP zone formation.

Hornbogen[130] showed the small particles which are present in large numbers after 25 hours ageing at 500°C in Fe - 1.2% Cu alloy. The appearance of these fine dispersed particles of high copper content[126] is an indirect proof of the state of clustering that is believed to have existed in this alloy before nucleation occurred.

Nucleation of copper-rich particles requires little strain energy, because the atomic volumes of matrix and of precipitate are about equal. Therefore, the nucleation barrier is determined only by the surface energy between the F.C.C. particle and the B.C.C. matrix.

Nucleation must originate from copper-rich clusters that have formed in the B.C.C. matrix. Nucleation occurs at high angle boundaries, at low angle boundaries, or at single dislocations and all take place with about the same time dependence.

Clusters of copper, (B.C.C. zones), of an average diameter of 90Å grow at a rate that can be explained by the concentration of excess vacancies in the material. Presence of excess vacancies due to the quenched-in vacancies leads to rapid diffusion during clustering of copper[131], because the excess of quenched-in vacancies is not annealed immediately (or is eventually permanently trapped), so that the speed of diffusion can be kept high for a long time.

The enhancement of diffusion can be estimated by multiplying the normal diffusion coefficient by the relative concentration of excess vacancies[131].

$$D_C = D\frac{CT_2}{CT_1} \quad , C_T = e^{U_f/RT}$$

where U_f is the energy of formation of a vacancy.

When all the vacancies are still present the enhancement will decrease as the vacancies decay but it explains the time dependence of formation of the first particles, which are almost pure copper. When these zones reach a critical size, they transform into the F.C.C. lattice.[132]

Spherical clusters can be expected due to the similarity in size of the iron and the copper atoms[133].

After vacancy decay, the epsilon particles grow slowly by normal volume diffusion. The rate of growth can be described by Zener's equation[134] which states that the second stage of precipitation is proportional to the square root of time.

$$S = \alpha(Dt)^{\frac{1}{2}}$$

where S is the particle diameter, D the volume diffusion coefficient and α a constant that depends upon the concentration distribution inside and outside the growing particle. This equation can be applied because the particles are almost spherical.

The deviation from Zener's parabolic growth law after long ageing times has been explained by Ilschner[135]. He assumes that the reaction slows down after the diffusion zones of the particles begin to overlap.

3.8.3. Transition of particles.

After long times of ageing some percentage of the particles, (depending on temperature) change from spherical to rod shape.

This phenomenon may be explained by the fact that in particles of a size 50 to 300Å, surface energy is the factor that determines the spherical shape. When particles grow larger this factor becomes less important. Nabarro[107] showed that the strain energy of a noncoherent ellipsoidal particle will decrease in the following sequence

sphere ⟶ needle ⟶ disc. This could explain why particles

more than 300Å in diameter tend to take the shape of rods because above this size the surface energy which led to the spherical shape is overcome by the strain energy of noncoherent particles in spite of the small difference in atomic volume of copper and iron. Disc-shaped copper particles might be observed after very long periods of ageing at high ageing temperatures.

After 24 hours ageing at 700°C[126] the F.C.C. spheres of ε-phase coarsen into rod like precipitates which have a definite orientation relationship with the matrix α-iron, $[110]_\varepsilon || [110]_\alpha$. The closest packed directions of the two phases are parallel along the axis of the rod-shaped precipitate.

3.8.4. Hardening mechanisms.

The mechanism of hardening of iron by a softer phase like copper can be explained as follows:

(i) In the early stage of precipitation, when the particles are coherent or semicoherent with respect to the matrix, the strengthening effect is generally associated with the stress required to shear the particles.

(ii) As particles grow and become noncoherent, shearing of these particles becomes more difficult. The material softens as the interparticle spacing increases. In this overageing stage, softening cannot be related to change of volume fraction of particles, and the initial flow stress associated with the stress to bow out dislocations between the particles[124].

(iii) In the later stage of overageing, dislocations can be generated at particle-matrix interfaces.

3.9. Precipitation-hardening in sintered iron-copper alloys.

Precipitation-hardening phenomenon may be utilized to enhance the properties of alloy steels made from metal powders.

The precipitation of the ε-phase has been shown significantly to improve the properties of copper-bearing steels. A further advantage of this type of steel is that after the sintering treatments the compact may be re-pressed or coined while it is in the soft condition, and it can then be resintered, solution-treated, and precipitation hardened to develop maximum properties.

Harrison et al[14] have shown the effect of precipitation-hardening on the tensile strength of alloys with copper contents varying from 1 to 10%, on densities from 6.5 $^{g}/_{cc}$ to beyond 7.00 $^{g}/_{cc}$ at different ageing temperatures between 200°C and 550°C for 1 hour.

The results show that those samples with 5% Cu and a density of 6.5 $^{g}/_{cc}$ which were quenched in oil and precipitated hardened at 500°C have the highest tensile strength. Comparison between oil-quenched and furnace-cooled samples showed that the optimum composition range lies between 2 and 3% copper under the above condition.

Stern et al[136] demonstrated the effect of precipitation hardening on hardness of alloys with 2% Cu, 0.03 % C after various times at temperatures of 400, 500, 600, 700°C. The samples were quenched from a temperature of 1150°C in brine. The results show that decrease in

ageing temperature causes an increase in the time required for the appearance of maximum hardness, and that the value of maximum hardness increases with decreasing temperature. However, at an ageing temperature of 400°C, the value of maximum hardness is less than at 500°C. A similar phenomenon was observed by Krishnadev et al[137] who investigated the ageing process in cast materials. The principal factor responsible for an increase in hardness during the initial stage of the ageing process is the clustering of the copper atoms. At a more advanced stage ε-phase precipitates. The number, size, and distance between these precipitates also influence the hardness. At 400°C, maximum hardness was observed after 100 hours. The effect of the clusters during this prolonged treatment, (most of which have probably dissolved), is not great, while ε-phase are sufficiently large, but the number of ε-phase precipitates after 2 hours treatment at 500°C is at a minimum. The factor which determines maximum hardness is the clustering process.

There has been a limited amount of research into the precipitation hardening of sintered materials.

It was observed by Watanabe et al[138] that the effect of precipitation hardening on the strength is greater for high density compacts which explains the effect of pores on precipitation.

Phadke and Davies[139] showed the effect of different copper content, (2% to 8% Cu), on precipitation hardening of iron-copper alloys at density 6.8 $^{g}/_{cc}$ during ageing at 500°C. They demonstrated that:

(i) Supersaturation, grain, subgrain and plate boundaries, defect structure of massive martensite regions and possibly free void surfaces may account for the increase in the rate of precipitation reaction with increasing copper content.

(ii) Massive martensite was found in 4% and 6% copper alloys after water quenching.

(iii) The magnitude of hardness increases over the solution treated value was nearly the same in the three alloys but the percentage increase in hardness was highest in 2% cu alloy.

(iv) Peak hardness was attained at times similar to wrought alloys[140].

CHAPTER 4

4. WEAR

4.1. Friction.

It is now generally agreed that when two surfaces are pressed together, either statically or in sliding contact, real contact occurs only at the tips of the surface irregularities, where plastic deformation takes place under intense local stresses. The work of deforming or shearing these irregularities during sliding gives rise to the frictional force and the deformation leads to wear and to metal transfer between the surfaces. These ideas have been developed mainly by Bowden and Tabor[141]. In reaching their conclusions they pursued three general lines of investigation. Firstly they examined the nature of surface contact between solids at rest, secondly the phenomena associated with sliding and thirdly the nature of the surface damage.

4.1.1. Contact between static metal surfaces.

When the finished flat surface of a metal is examined under high magnification it will show a series of irregular hills and valleys of random heights and depths. These irregularities will be present even with the best possible workshop finishes, (for instance between 5 - 100, 10 - 50, and 1 - 5 micro inches[142] after machining, grinding and diamond dust polishing respectively).

When two flat solid surfaces are placed in contact, the real area of contact is only a limited number of the highest asperities in intimate contact.

For example, when two unloaded flat steel surfaces are placed in contact, the real contact area is not more than about $^{1}/_{1000}$ of the surface area. Since the real area of contact is so minute, an applied load of only a few pounds is sufficient to cause very high pressures.

As soon as the yield stress of the contacting solid is reached, the loaded asperities will yield plastically, partly collapsing until the load is distributed over a greater area. Further loading will cause further yielding and collapsing of asperities until equilibrium is established when the supporting area of intimate contact is just sufficient to prevent further plastic deformation. Such high pressures are reached locally during loading that asperities in contact tend to form junctions by a process of cold welding. The total area of cold welded junctions increases with increase of pressure.

4.1.2. Sliding metal surfaces in contact.

When an attempt is made to slide one of the contact metals over the other, resistance to motion is encountered which is termed frictional resistance. This resistance is equivalent to the sum of the shearing forces required to break the metal-to-metal junctions. It follows then that the basic mechanism of sliding friction is that the normal load W is supported by minute junctions, which are continually being formed and broken, between the surfaces as they slide over each other. Since the surfaces are in plastic equilibrium the mean pressure Pm over the real area of contact A, is constant, and the value of the mean shear stress Sm needed to shear the junctions depends on the strength of adhesion at the interface. Hence the total frictional force is $F = ASm$, and $A = \frac{W}{Pm}$

$$\text{Thus,} \qquad F = \left(\frac{Sm}{Pm}\right) W \qquad (1)$$

Since the first Law of Friction states that $F = \mu W$, (μ is Coefficient of Friction), it is apparent that (Sm/Pm) must be in some way identified with μ.

It can be seen that Sm and Pm are two constants referring to the bulk mechanical properties of the metal surface. Pm can be identified with the yield stress P of the softer metal, since shearing usually occurs within the bulk of the softer metal and Sm is approximately equal to the shear strength S of the softer metal.

$$\text{Thus,} \qquad \mu = \frac{\text{Shear strength of softer metal}}{\text{Yield stress of softer metal}} = \frac{S}{P}$$

From this, two conclusions follow. The first is that S and P being strength properties of the same metal, vary together and their ratio is roughly the same for all metals. This explains why the coefficients of friction of a very wide range of metals do not vary by a large factor; generally they lie between 0.5 to 1.5. The second conclusion is that, since shear strength and yield stress vary together as the temperature is varied, temperature changes over a limited range should not have a significant effect on the coefficient of friction of dry metals. This is also found to be generally true so long as heating does not affect the nature of any surface films which may be present on the metals.

4.1.3. Mechanism of metallic friction.

In addition to friction which is a surface phenomenon, deformation and distortion are other effects which can be observed at

relatively great depths below the interface of the sliding solids. Observations show that two distinct types of interaction, shearing and ploughing, may take place. Ploughing defines the action whereby hard surface asperities plough out grooves in a softer metal. Frictional resistance F may be approximately expressed

$$F = S + P$$

Where S is the shearing force and P the ploughing force. For a hard metal sliding on a soft metal the ploughing term may be appreciable and the simple expression given by equation (1) would have to be modified, since in the foregoing analysis ploughing interaction is neglected. However, in the majority of sliding processes the ploughing force appears to play only a relatively minor role in the total frictional force and as a first approximation, may be neglected.

4.1.4. Surface damage.

Most engineering mechanisms in which sliding of metals takes place can be roughly classified as follows.

(i) A hard metal sliding on a soft metal e.g., steel on copper.

(ii) A soft metal sliding on a hard metal e.g., copper on steel.

(iii) Similar metals sliding on each other e.g., nickel on nickel.

In general, each of the above classes of sliding is characterized by a typical kind of surface damage, the nature and degree of which is to some extent modified by the relative proportions and geometrical relationships of the surfaces. The typical damage for each of the classes would be as follows:-

(i) A hard slider ploughs out a groove in the soft metal.

(ii) A soft slider continually tends to weld to the hard surface and fragments remain adhering to it. Little or no damage is experienced by the hard metal.

(iii) Similar metals sliding on each other give rise to the most severe surface damage due to the work hardening of the contacting asperities on both surfaces.

4.2. Wear characteristics.

Friction and wear are not intrinsic material properties but are characteristics of the engineering system. Any change in load, speed, or environmental conditions may cause catastrophic changes in the wear rate of one or both of the surfaces in contact[143].

Wear is one of the three most commonly encountered industrial problems leading to the replacement of components and assemblies in engineering, the others being fatigue and corrosion.

Wear is rarely catastrophic but it reduces operating efficiency by increasing the power losses, oil consumption, and the rate of component replacement. Sufficient is known about wear mechanisms and their solution to encourage greater application of this knowledge. There are, however, a number of problems which cause considerable difficulty in translating the results of research into industrial practice.

However, the formulation of a precise and all embracing definition of wear is difficult. A Committee of the Institution of Mechanical Engineers decided on the following definition.

"The progressive loss of substance from the surface of a body brought about by mechanical action".

Krogelskii[4] defines wear as "the destruction of material produced as a result of repeated disturbances of the frictional bonds". Neither definition is perfect. For instance, the first appears to eliminate spark erosion as a form of wear, and the second perhaps places too much emphasis on fatigue effects in wear.

4.3. Wear in industry.

Wear encountered in industrial situations can be broken down into the following categories.[144] Abrasive, adhesive, corrosive, surface fatigue, and there are two other minor types of erosion and fretting. However, there are situations where one type changes to another, or where two or more mechanisms operate together.

4.4. Adhesive wear.

Adhesive wear occurs when surfaces slide against each other, and the pressure between the contacting asperities is high enough to cause local plastic deformation and adhesion. Adhesion is favoured by clean surfaces, non-oxidising conditions, and by chemical and structural similarities between the sliding couple. Adhesion occurs between a few asperities which increase in size as motion continues. Eventually the junctions rupture at their weakest point due to shearing of these junctions, usually resulting in metal transfer from one surface to the other. This type of wear occurs primarily in highly stressed machine elements such as bearings. Wear decreases if the asperity is harder because the contact

area is lower, (area of contact is inversely proportional to HV), and increases if asperity is chemically clean because bonding and welding is more likely. Archard[145] has produced a formula which shows the dependence of wear rate on a number of important factors. The wear constant K represents the properties of the friction couple and only has any real meaning provided that the wear mechanism does not change, i.e. there is no change from mild to severe wear.

$$\text{Wear volume} = \frac{K \cdot S \cdot P}{Pm}$$

Where K = wear constant,

S = sliding distance,

P = applied load,

Pm = flow stress of wearing surface.

There are, however, some ways to reduce wear loss in metals under metal-to-metal contact such as alloy addition.

The surface texture of the wear track is greatly influenced by the microstructure of the material.[146] A discontinuous structure is an advantage in order to inhibit severe growth[147]. Thus carbon steels are less prone to adhesive wear than is homogeneous austenitic stainless steel or pure iron. It has been suggested that with ferrite-pearlite structures in steels, wear is limited to adhesion and fracture within the ferrite constituent only[148]. A grain boundary network of ferrite, (e.g., as found in cast steel), is thus undesirable. A general increase in carbon content which has the effect of reducing free ferrite and increasing hardness is thus beneficial in increasing wear resistance.

Eyre and Wilson[5] evaluated the effect of microstructure of grey cast iron on wear.

(i) The principal effect of ferrite is to increase running-in wear and to markedly decrease the mild/severe transition load.

(ii) The effect of phosphorus is to reduce running-in wear and to increase the mild/severe transition.

(iii) Nodular iron is inferior in most respects to flake iron, because equilibrium mild/wear rate decreased as the graphite interparticle distance decreased and would, therefore, appear to be related to availability of graphite as lubricant between the sliding surfaces. Graphite has good thermal stability and does not begin to oxidize until a temperature of about 400°C is reached when it is converted into carbon dioxide. In inert atmospheres it is stable up to temperatures above 1400°C.

The other way to reduce wear rate is to use a polymeric or ceramic material to slide against metals.

Many surface diffusion treatments, such as Tufftriding or Carburizing, depend upon their ability to enhance wear properties by chemical contamination to produce non-adhesive or anti-welding characteristics.

Wear under adhesive conditions is subject to sharp transitions in behaviour. Variations in load and speed may bring about marked thermal changes which precede, and cause, wear change. Welsh[149] was one of the first to examine systematically the concept of mild wear, (oxidation),

and severe wear, (metallic), and the sharp transition between these which he refers to as T_1 and T_2 transitions, (Fig. 19). Below T_1, wear occurs by the removal of oxide debris from an oxidised surface supported on a work hardened substrate. T_1 marks the transition to severe wear initiated by the breakdown of the protective surface oxide produced at lower loads. Plastic deformation of the substrate occurs, caused by a higher bulk temperature, and the wear rate increases considerably with the production of metallic debris. Between T_1 and T_2 severe wear occurs. At the T_2 transition the surface temperature is high enough for phase hardening to produce a hard structure (white layer) which prevents deformation and helps to establish an oxidised surface once more. The wear rate is reduced considerably but is not as low as the wear rate below the T_1 transition.

4.5. Abrasive wear.

The term abrasive wear covers two types of situation. In both cases wear is occasioned by the ploughing-out of softer material by a harder surface. In the first instance a rough hard surface slides against a softer surface. In the second case abrasion is caused by loose hard particles sliding between rubbing surfaces.

However, the second mechanism is still of great importance. Not only do most mechanisms work in an environment containing much airborne dust and dirt, but also the products of corrosive wear are more often than not abrasive in character. Particles of hard metal produced by the abrasive wear mechanism can also cause abrasion. Generally abrasive wear arises from the penetration and micro-cutting of one material by another.

Rabinawicz et al[150] constructed a simple model of a conical abrasive grain penetrating and abrading a plain surface and showed that

$$V = \frac{AWL}{H}$$

where V = volume of material removed,

W = load normal to the abrading surface,

L = sliding distance,

H = Hardness of softer material,

A = area of cross section of groove.

This equation predicts that total volume wear is directly proportional to load, sliding distance and area of cross section.

4.6. Fatigue wear.

Adhesive and abrasive wear mechanisms depend on direct contact between solids and they produce a wear pattern that is progressive from the start of rubbing. If the surfaces can be separated by a lubricating film, (and abrasive particles excluded), then these wear mechanisms cannot operate. This is the situation in well-designed rolling element bearings, where it is found that a fatigue mechanism of failure takes place. For this case, although direct contact does not occur, the opposing surfaces experience large stresses, transmitted through the lubricating film during the rolling motion. These show that the maximum shear stresses occur some distance below the surface as illustrated in Fig. 20. As rolling proceeds, the directions of the shear stresses for any element change sign. Fatigue failure is dependent on the amplitude of the reversed shear stresses and if in rolling contact these are above the endurance limit, failure will eventually occur.

However, materials are rarely perfect and the exact position of ultimate failure will be influenced by inclusions, porosity, micro-cracks and other factors.

Suh[151] in his delamination theory explains the effect of factors such as inclusions, porosity, dislocations and hard particles on crack and sheet formation at low sliding speeds.

As the dislocation density builds up at the sub-surface layer, cracks and voids can form. The rate of void formation may be increased when there are hard particles present in the metal, since the motion of the mobile dislocations generated by the applied load may be blocked by the particles. When these hard particles are stronger than the cohesive strength of the matrix, cracks and voids can be nucleated under the stress of dislocation pile-ups.[152] Small cracks can also form when these hard particles break up under the dislocation pile-up stress. Voids can also be created during plastic deformation by the decohesion of the matrix-particle interface and by the plastic flow of the matrix around a hard particle[153]. Crack formation around hard particles is likely to be one of the most important mechanisms of void formation, since in most commercial grade metals there are many hard particles such as, oxides, borides, carbides and nitrides.

In single phase metals voids may nucleate through the coalesence of microvoids and vacancies during plastic deformation of the sub-surface layer.

The formation of cracks and voids at the sub-surface does not guarantee the formation of wear particles. Loose particles can form only

when these cracks and voids join together so that the strength of the sub-surface layer is less than the shear stress applied at the interface between the slider and surface. Thus, the result should be a separated thin sheet. These cracks and voids may link together by three different mechanisms, growth of voids, crack propagation, and the plastic deformation of the metal. After these wear sheets are created, some of them may be entrapped between the two sliding surfaces. These trapped particles may either be rolled into a spherical shape, broken into small pieces or remain the same, depending on the material properties of the loose particles and the sliding condition. When the metal is relatively brittle, the delaminated sheets may break into pieces and form many small wear particles. On the other hand the sheet of ductile metal may remain intact or simply roll into a large particle.

4.7. Effects of various factors on adhesion wear under unlubricated sliding conditions.

4.7.1. Effects of oxide film.

Most metals are covered by an oxide film and even after cleaning by machining or grinding acquire a film of oxide of between 5 and 50 molecular layers in five minutes or less.[144]

Unless the load is very small, the oxide film does not prevent intermetallic contact, so, as mentioned in the earlier discussion, the adhesive wear mechanism of metals can be divided into two regions, mild wear and severe wear. In the mild wear region, which occurs at lower load, the contact resistance is high, the wear debris is fine and consists mainly of metal oxide, and the rubbed surfaces become polished. In the severe wear region, at higher loads, the contact resistance is low, wear debris includes coarse metallic particles and the rubbed surfaces are rough.

Eyre et al[154] examined the effects of load and sliding distance on adhesive wear of 1% and 3% Cr steel.

At low loads and sliding speeds during equilibrium mild wear, ferric oxide (Fe_2O_3) forms. As the speed and load were increased, Fe_3O_4 became the predominant oxide in the debris, and it is believed that this oxide which is of higher iron content than Fe_2O_3 may account for the slightly higher wear rate indicated by a slight change in slope of the mild wear curve coincident with the oxide change. If this wear rate change was due to load or sliding speed only, it would be unlikely that a change in slope would occur.

Quinn[155] has shown a similar change in mild wear rate for steel but does not offer an explanation for this change. Thus, mild and severe wear may be related to both oxidation and the metallurgical changes taking place in the surface layer.

In this section the effect of oxide films on adhesive wear has been considered, but oxide films will also have a large influence on abrasive wear, since many metal oxides are hard and when present in the form of wear debris act as abrasive particles.

The wear between metals may be reduced by coating the surfaces with a thin layer of metal which has higher wear resistance than the substrate metal.

Rhodium and chromium are both hard, and electroplated coatings of these metals have been used successfully for the protection of cylinder liners, crankshafts and similar applications. The wear resistance

properties of these films have been demonstrated by Moor et al[156].

Films of soft metals such as indium and lead have been used on harder metal substrates. An example of their effective use has been in lubricating the dies used in deep drawing operations.

Besides these methods there are a number of chemical techniques which increase the wear resistance of the surface. Examples are the phosphating, sulphinising, boronising, and steam treatment of steels. Ferrous surfaces can be hardened by nitriding and carburising. Also hard surface layers can be produced by heat treatment. For instance, large cast iron rolls for rolling mills are chill cast so that the higher rate of cooling at the surface produces a hard surface whereas the centre is composed of a less brittle structure.

4.7.2. Effects of temperature.

In general the hardness of a metal is temperature dependent, the higher the temperature, the lower the hardness. Thus the tendency for asperities to adhere and the wear rate to increase with decreasing hardness. This effect has been demonstrated by Hordon[157]. In order to counteract this effect it is necessary to use metals with high hot-hardness for bearing materials operating at high temperature, such as tool steel, and alloys with base composition of cobalt, chromium and molybdenum, and above 850°C it is necessary to use cermets or ceramics.

The second effect of temperature is phase changes caused by increase of temperature as a result of frictional heating, because the mutual solubility of metal pairs is a function of temperature. It is therefore quite possible that increases in solubility with increasing

temperature could adversely effect tribological properties.

Changes of temperature have a marked effect both on rate of oxidation and on types of oxide formed as discussed in chapter 2.

This effect of temperature has been demonstrated by Kragelskii[158] by rubbing pure Armco iron against itself at different speeds, (and hence different interface temperatures). At low speeds the wear rate was high, with evidence of much adhesion, but at higher speeds the wear rate fell by almost three orders of magnitude and the surface became smooth and polished. The temperature of the interface at the transition speed was calculated to be about 1000°C. To prove that this was a temperature rather than a speed effect the experiment was repeated at very low speed while high current pulses were passed through the contacts to raise them to the same temperature. The wear rate was again very low and the surfaces were polished.

4.7.3. Effects of speed.

If the temperature of the sliding elements is a controlling factor in the mild/severe wear transition, it would be expected that the sliding speed would also be an important variable.

Eyre et al[5] indicated the variation in the mild/severe transition load with increase in sliding speed for nodular cast iron. They showed that the load at which a mild form of wear changes to a severe form decreases to a minimum value before again increasing. Severe wear takes place within the concave curve. Below a critical load mild wear predominated at all speeds.

Examination of the debris from these regions showed that in the low speed mild wear region Fe_2O_3 and Fe_3O_4 were the predominant oxides, while in the high speed mild wear region FeO was obtained.

4.7.4. Effects of load.

An increase in load causes an increase in the frictional force, and hence a temperature rise produces the effects discussed earlier. Also an increase of load can cause a transition from mild wear to severe wear to occur.

The transition from mild to severe wear is attributed to the interaction of the plastic zones beneath the contacting asperities[159]. During mild wear the situation is as shown in Fig. 21a where there is no interaction between the plastic zones. As the load is increased, the plastic zones interact as in Fig. 21b and the subsurface regions become entirely plastic and severe wear occurs.

4.8. Effect of factors on abrasive wear under unlubricated conditions.

4.8.1. Load and sliding distance.

Volume wear usually increases linearly with load and sliding distance[160]. If deviations occur they are usually due to a reduction in particle size of the abrasive or clogging of the surface.

4.8.2. Hardness.

There are three principal ways of strengthening the structure of steels by a) alloying b) heat treating and c) work hardening.

Khrushchov[161] et al and Larsen-Badse[162] have shown that a linear relationship exists between the relative wear resistance,

($E = \frac{\text{Linear wear of standard}}{\text{Linear wear of material}}$), and Vickers hardness. Pure metals and annealed steels show direct proportionality between E and hardness.

For heat treated steels, Khrushchov found different results. The samples he tested were quenched in oil and tempered at different temperatures to give different hardness values. Heat treated carbon steels showed improved abrasion resistance over the annealed state.

The behaviour of heat treated carbon steels is thought to be a function of carbon content.

When metals undergo abrasion, it is found that their surfaces work harden to very high levels, the degree varying between classes of material and depending on the severity of the abrasion process[163].

Larsen-Badse[162] examined the wear resistance of heat treated steels as a function of tempering temperature. The results indicated that wear resistance was proportional to the volume fraction of cementite in each sample. High carbon steels have higher wear resistance for the same tempering temperature. Wear resistance declines with increasing tempering temperature.

He showed conclusively that wear resistance is not a direct function of carbon content, i.e. steels of different carbon content but with the same surface hardness will have the same wear resistance.

It is also necessary to take into account the hardness of the abrasive particles. Richardson[164] showed, in his work at the Agricultural Research Institute, that the hardness of the surface resisting wear must be greater than half the hardness of the abrasive if any real improvement

in wear resistance is to be achieved. He showed a relationship between hardness and wear resistance and that the hardness of the material must exceed some critical value K_T to bring about any marked improvement,

$$\text{where} \qquad K_T = \frac{H_v \text{ surface}}{H_v \text{ of abrasive}}$$

K_T must be greater than 0.5. However, it is unnecessary to increase the hardness of the material beyond 1.3 times that of the abrasive because no further significant improvement is obtained.

In any recommendation about hardness care is required in applying this knowledge, particularly if surface rather than bulk hardening is used. There is some evidence to suggest a relationship between the hardness of the surface layer, its thickness and the hardness of the substrate material. These effects are shown by Eyre[165] on a boronised coating of approximately 0.1 mm on steel. He showed that under abrasive conditions low wear is obtained at loads of 150 gm: on 0.15% C steel. The same coating thickness will produce a low wear rate at 150 gm and lower wear rate at 300 gm on a higher carbon steel (0.4 % C).

4.9. Anti-friction materials.

Anti-friction materials are widely used for rubbing components, and in particular for bearings. Bearing materials operate in the presence of a liquid lubricant which must be effective in preventing the formation of intermetallic junctions between the sliding surfaces. The most difficult conditions exist during starting up, when no oil wedge has yet been formed and the surfaces are only separated by a very thin film of lubricant. In very severe operating conditions where overloading may occur, the thickness of the lubricant film is greatly reduced so that

surface damage and scoring are encountered which may ultimately lead to catastrophic damage.

For many years, the principal bearing materials used have been white metals, i.e. tin and lead-base alloys, cadmium alloys, soft aluminium alloys and lead bronzes.

Khrushchov[166] has listed the following factors on which anti-friction behaviour depends.

(i) During sliding under conditions of boundary lubrication, anti-friction behaviour is governed by those properties of the bearing materials which ensure the lowest surface temperature and hence protect the boundary lubricant film from destruction. These properties include,

(a) high thermal conductivity,

(b) high thermal capacity,

(c) a special design of the surface to improve the supply of lubricant to the contact regions or to increase the rate of heat removal from these regions,

(d) the ease with which the bearing material can be plastically deformed or will wear during sliding in order to redistribute the load and the local specific pressures and temperatures, (the so-called running-in ability),

(e) the ease with which the bearing material can deform elastically under load because of its low elastic modulus, so as to attain a more uniform distribution of the load over the surface.

(ii) Anti-friction behaviour is also dependent on the ability of the

bearing material to form a strong boundary lubricant film, i.e. one which will be destroyed only at high temperatures and pressures. Different pure metals interact with lubricants in different ways because of their different thermal properties.

(iii) Anti-friction behaviour depends on those properties of the bearing material which facilitate the rapid reformation of a boundary lubricant film over the regions where it has been destroyed, e.g., as a result of overheating, failure of the lubricant supply, etc. One of these properties, for example, may be related to the production of lubricant from within the pores of the bearing metal itself during localized heating. This is important during the operation of porous anti-friction bearings and porous surface coatings.

In the development of anti-friction materials, extensive use has been made of Charpy's rule[4] which may be stated in the following form: All alloys used as anti-friction materials have one common characteristic: they consist of hard grains dispersed in a ductile matrix. This type of structure common to almost all alloys, is generally accepted as the most effective and satisfies most of the requirements for bearing materials. The pressure can be transferred to the hard grains, giving a low coefficient of friction and preventing scoring of the journal, whilst the ductility of the alloy matrix enables the bearing to conform to the journal and hence removes the possibility of producing localized high pressures which are the main cause of bearing damage.

A complete theory of anti-friction materials must include a combination of the fundamental physical and mechanical properties of materials. According to Jaeger's[4] formula the temperature rise produced by frictional heating depends on the following factors.

(i) The sliding speed

(ii) The pressure at the contact spot which, in conditions of plastic deformation, equals the hardness of the material.

(iii) Thermal conductivity and diffusivity.

Hence, an anti-friction material should have low hardness, high thermal conductivity and high thermal diffusivity.

In the majority of engines produced today the top compression ring material is an alloy cast iron.

Physical properties and descriptions of these alloys are shown in Tables 4a, 4b[2] respectively.

Factors which must be considered for replacement of these alloys with other materials are, wear resistance, thermal conductivity, and coefficient of friction, at least comparable with data established for current centrifugally-cast piston ring material. It must also be compatible with materials used for cylinder bores.

Fig. 22[2] summarizes some previous work on alloy cast iron as standard cylinder-liner and piston ring materials.

4.10. Wear of sintered iron-base products.

It is well known that anti-friction alloys are characterized by the presence of hard and soft structure components. In porous products the pores are the softer "structural element" and the basic metal the

harder.

Sintered iron parts are becoming more widely used particularly for components requiring low friction and high wear resistance, (sintered plain bearings), and sintered piston rings for internal combustion engines are now generally accepted, particularly for diesel engines, where they compete with cast iron.[167]

Iron-graphite with a porosity of 20 - 30%, iron-copper and iron-copper-graphite are some of the materials used. In recent years porous tin bronze has been ousted by porous iron and iron-graphite material, as being in less short supply and having better anti-friction properties.

Porous bearings have a number of advantages compared to other bearings. Porous bearings "run-in" excellently and are simple in use, the presence of lubricant in the voids and the simplification of its feed, the wear of the bearings and the shaft is reduced and the design of the sub-assemblies can be simplified. In addition finished articles have a form that requires no further machining.

Porous bearings can be impregnated with oil and, therefore, possess the property known as "self-lubrication". The self-lubrication of a porous bearing is based on the fact that during operation as the bearing heats up, the oil held in the voids and very small channels of the material by capillary forces, is gradually forced out, and forms a lubricating film on the working surface. When it is stopped and allowed to cool down this oil is partially sucked back into the voids. At low loads the lubricant contained in the voids of the bearing itself is sufficient for several months' operation, so lubricant consumption as

compared with an ordinary bearing is extremely low.

Porous bearings made of iron powder frequently break down due to seizing of the working surfaces and it is not recommended that they should be used at high loads.

The addition of graphite to iron or brass powder considerably improves the resistance to wear. The coefficients of friction of iron and iron-graphite bearings are about 2 - 3 times lower than those of some Babbitt metals and the wear is 10 times less[168].

Porous bearings are suitable for use in cases where regular lubrication is difficult, where the lubricant must not get into the products, (e.g. in the food and textile industries), where there is dust in the surrounding atmosphere, and where there are frequent stops and starts. The use of porous bearings is particularly economic where the mass production of bearings of a definite size is required. Porous bearings are being successfully used in the automobile, tractor, aviation and textile industries, in machine tool construction, electrical industry, and in other branches of the national economy.

Shahparast and Davies[169] examined the wear characteristics of sintered iron-lead and iron-lead-tin alloys as bearing materials. They showed coefficient of friction decreased with increasing lead up to 5% and wear decreased continuously with increasing lead content up to 12%. The wear track formed by iron - 10% lead exhibits a very smooth surface, whereas the track formed by a pure sintered iron pin displays considerable surface damage.

Addition of tin to the iron - 10% lead alloy improves the wear resistance of the alloys particularly at higher loads, while the

coefficient of friction remains almost unchanged.

Odenhausen[170] reported that addition of 5 - 10% lead to pure sintered iron produces an improvement in the coefficient of friction, wear resistance and thermal conductivity.

Porous iron treated with steam atmosphere at a temperature of 450 - 600°C[171] improves the adhesion wear resistance considerably.

Porous bearings impregnated with plastics which has been suggested by Bal'shin[172] are just as suitable for working in heavy conditions.

Amsallem[173] et al reported on the friction and wear behaviour of sintered iron, (D = 7. $^{g}/_{cc}$, AHC powder), against XC38 steel with 0.5 $^{m}/s$ sliding speed and loads of 40 N to 360 N.

Test showed that:

(i) Maximum wear rate occurred at a load of about 80 N,

(ii) Wear in nitrogen increases linearly with load.

(iii) In air, there is a specific load interval, (about 40 - 160 N), within which the sintered part is submitted to localized oxidation, frictional contact is partly on Fe_2O_3 and partly on iron and there is high abrasive type wear. Above this load the oxide coating: Fe_3O_4 becomes more uniform with increase of load and below 40 N load the wear of the sintered part is low and not greatly affected by the environment.

In air or nitrogen, sintered iron work hardens by frictional contact: hardness increases with increasing load, and sintered iron work

hardens to a depth of 5 - 10 times that of solid iron.

Sintered and solid iron have similar wear and friction characteristics in an air environment.

Eyre[174] et al demonstrated the effects of density, sintering conditions and addition of P on adhesion wear of sintered iron at a constant speed of 300 cm/s.

They concluded that:

(i) Sintered iron exhibits running-in wear and a mild severe transition.

(ii) Wrought and sintered pure iron have almost identical wear properties.

(iii) Large variations in the pressing and sintering conditions do not significantly alter the friction and wear behaviour under dry sliding conditions.

(iv) Impregnation of the inherent porosity of sintered metals reduces wear considerably and increases their load-bearing capacity. These improved properties are maintained until all available lubricant has been used.

(v) The addition of phosphorus causes a large improvement in wear resistance.

(vi) For sintered iron excellent results have been obtained sliding against grey cast iron. Under these conditions no adhesive wear occurs because of the presence of graphite which acts as a solid lubricant.

Sintered iron and iron plus 2% copper[175] are very similar but the mild/severe transition load of the latter is slightly higher.

Hewitt[2] et al compared the wear properties of Fe - base sintered alloys over a large range of compositions of Cu, Sn, C under different treatments (Tufftriding, steam treatment) and different impregnants with cast iron.

Oil impregnated specimens of SP 20, (A work-hardening nickel containing alloy with 0.8% C), showed the least wear and Tufftrided oil-impregnated has the least wear rate in comparison with other treatments.

Generally they concluded that sintered rings have significant advantages over conventional rings, particularly in engines which are prone to give scuffing problems. The lubricant can be readily impregnated into the body of the ring and is thereby immediately effective.

The results of their wear tests are shown as histograms in Fig. 23. This figure is a useful basis for comparison of sintered variations (Table 4b) and one or two less common materials with traditional materials in Fig. 22.

CHAPTER 5

5. PRACTICAL WORK

5.1. Aim of experimental work.

Iron articles produced by powder-metallurgy techniques can never reach the strength values of iron produced by normal methods, even when a resintering process is used. In order to increase their strength and particularly their hardness, (reducing the amount of porosity and increasing the bulk strength), it is therefore necessary to subject them to special treatments and special alloy additions.

Copper additions to iron powder are used in industry to produce high strength sintered parts. It is estimated that over 90% of the sintered ferrous parts produced currently contain copper. In the furnace cooled condition the increase in strength is due to precipitation of copper from the solid solution produced during sintering and also due to some solid solution hardening. As with wrought metals, the methods of increasing the strength of sintered parts form an important research area. In the case of Fe - Cu alloys higher strengths may be obtained by employing separate solution and ageing or steam treatments.

Steam treatment is remarkable because it affects both the surface and the internal structure of the sintered parts and results in products having increased hardness, greater abrasion resistance and improved corrosion resistance in comparison with untreated products.[176]

Therefore the subject of simultaneous precipitation hardening and steam oxidation in sintered iron-copper alloys was chosen for this research project.

This work forms a continuation of previous studies by Phadke - Davies[17] and Razavizadeh - Davies[99] at this University, during which the progress of oxidation of sintered Fe and Fe - 2% Cu alloy was followed by determination of weight changes, hardness, and the % open porosity.

In these investigations the following variables were studied:

(a)[17] -100 mesh Sponge iron and - 200 mesh electrolytic copper, pressed to a density of 6.8 $^{g}/_{cc}$ and sintered at 1150^{o}C for 1 hour were treated in steam and inert gas at 500^{o}C for periods from 10 to 100 minutes.

(b)[99] - 200 mesh and - 300 mesh A.S.C. and Sponge iron, pressed todensities of 6.0, 6.4, 6.8 $^{g}/_{cc}$ and sintered at 1120^{o}C for 1 hour were treated in steam at 450^{o}C, 525^{o}C, and 600^{o}C for periods from 5 to 250 minutes.

In the present project specimens prepared from - 100$^{\#}$ A.S.C. iron and - 100$^{\#}$ pre-alloyed powders containing 2, 4, 6 and 8% Cu, pressed to densities 6.0, 6.4, 6.8 $^{g}/_{cc}$ and sintered for 1 hour at 1120^{o}C were treated in superheated steam and inert gas at 525^{o}C for periods ranging from 5 to 100 minutes and under vacuum for 500 hours.

The study was preceded by examination of the effects of copper on steam oxidation and on dimensional change in these alloys after sintering. Alloys were solution treated by water quenching and also by rapid cooling at an average rate of 80^{o}/min in the sintering furnace. Subsequent ageing was done in either inert gas or in steam. The progress of oxidation was followed by determination of % weight gain, hardness, % of open porosity, radial-crushing-stress, and wear resistance (abrasive).

Both types of powder used are representative of the powders used in industrial practice. - 100 mesh powder was used to compare the influence of particle, size, distribution on the rate of pore closure with results obtained on - 200 mesh and - 300 mesh iron in previous work[99], and also to have a range of coarse and fine powder for closest packing, (minimum amount of porosity). Different percentages of copper in each powder type were used in the belief that this might prove to be an important variable on oxidation and precipitation hardening. The three densities were chosen to be representative of low, medium and high densities and the sintering conditions were selected to be representative of those employed in industrial practice. The duration of steam treatment was chosen from the previous results[99] in which it was found that after 100 minutes of treatment most of the open pores were filled by oxide and percentage of weight gain was almost constant. The temperature which was used for steam treatment is a normal temperature for ageing[17] and a controlled temperature[99] for oxide formation.

5.2. Raw materials

(a) - $100^{\#}$ pure iron sieved from 100 mesh A.S.C. grade, supplied by Hoganas (G.B.) Ltd.

(b) - 100 mesh pre-alloyed powder of nominal composition 2%, 4%, 6% and 8% Cu sieved from 100 mesh pre-alloyed powder supplied by Davy Loewe Ltd., Bedford.

A screen analysis was determined on all powders according to the Metal Powder Industries Federation (M.P.I.F.) standard No. 5 - 21 and the results are quoted in Table 5. The pre-alloyed powders were annealed by passing through the furnace under cracked ammonia at 760°C, and then

ball-milled for 30 minutes. Screen analysis was determined after annealing and the results are quoted in Table 7.

5.3. Physical properties.

The apparent densities and flow rates of all powders were determined according to the M.P.I.F. standard 3 - 45 before and after annealing. The results are quoted in Tables 6 and 8 respectively.

5.4. Pressing and density.

Two floating die sets were used which produced cylindrical and rectangular specimens of 1.6 cm diameter and 4 cm^2 area respectively.

The density for all the samples was measured by using the relationship: $D = {}^{weight}/_{volume}$.

5.5. Sintering.

A 6" belt furnace with cracked ammonia atmosphere was used. The samples were sintered in trays on the belt for 1 hour at the maximum temperature of $1120^{o}C$ and then cooled at the fastest cooling rate of average 80^{o}/mins. This furnace was water cooled at both ends.

5.6. Solution treatment.

Half of the furnace cooled samples of Fe - 2% Cu, Fe - 4% Cu, Fe - 6% Cu and Fe - 8% Cu were solution treated in a small tube furnace of 3 cm diameter and 10 cm hot zone under nitrogen at $950^{o}C$, $1000^{o}C$, $1050^{o}C$ and $1100^{o}C$ respectively for 1 hour and then water quenched.

NOTE: In future sections wherever there is reference to water quenched samples, it means sintered samples which have been subsequently solution treated and water quenched. Furnace cooled samples are those which have been sintered only.

5.7. Ageing treatment.

The water quenched samples of all compositions were aged in a small tube furnace of 4 cm diameter and 10 cm hot zone under nitrogen for times ranging from 5 minutes to 100 minutes and in evacuated capsules for 500 hours.

5.8. Steam treatment.

A schematic diagram of the steam treatment furnace is shown in Fig. 24. It consists of a single silica tube furnace of 7 cm inner diameter and 10 cm hot zone length. Temperature was controlled to an accuracy of $\pm$ 5^{o}C by placing a Chromel/Alumel thermocouple in the middle of the hot zone and a copper boiler with a capacity of 1500 cc water was used. The boiler consisted of three tubes, one large (2.5 cm diameter) for confidence of water level, and two narrow (1 cm diameter). One of the latter connects to the tap of the boiler for a constant head of water and the other to the tube of the furnace.

At the point of entry of steam to the furnace there is a round copper diaphragm of 6 cm diameter. This slowed down the rate of flow of steam and the steam became superheated during passage through the furnace. The rate of steam production in the boiler was 14 cc per minute. Fig. 25 shows the steam rate per minute.

The pressure of the gas (H_2O) in the furnace is at least equal to atmospheric pressure (approximately 10^5 N/m^2). Because the furnace was connected to the open air the pressure in the furnace could not be less than atmospheric pressure. At the same time steam was being generated in the boiler and a continuous flow of steam was passing through the furnace and was released to the air. Thus it could be assumed that the pressure of the gas in the furnace was greater than atmospheric pressure and

there was no flow of air through the furnace.

Three sets of results were obtained, for treatments carried out with densities of 6.0, 6.4 and 6.8 $^{g}/_{cc}$ at 525^{o}C. In each case, specimens were treated for periods of time from 10 to 100 minutes. These specimens were weighed to an accuracy of 0.001 gr and were introduced into the furnace tube with steam already flowing and with the furnace at operating temperature. It was estimated, by placing a thermocouple inside a hole which was made by drilling in the middle of a cylindrical specimen, that the specimens attained the furnace temperature after approximately 3 minutes. The specimens after each particular treatment of time and temperature were removed, cooled and re-weighed. These specimens were assessed by determining the % weight gain and hardness.

5.9. Open, total porosity and hardness.

The percentages of total and open porosity were determined according to the M.P.I.F. standards No. 35.

Vickers hardness values were measured on cylindrical specimens and 4 impressions were made on each side of the sample, then the average of these readings is the value of hardness. A 20 kg. load was used in all tests.

5.10. Crushing test.

Radial crushing stress was determined on sintered and steam treated, (50 minutes at 525^{o}C), ring shaped samples of 0.8 cm wall thickness and constant length of density 6.4 $^{g}/_{cc}$, using the relationship:

$$P = \frac{KLT^2}{D - T} \quad \text{(according to the M.P.I. standard No. 16-55T).}$$

where, P = crushing strength

K = radial crushing stress

L = bearing length

T = wall thickness of bearing

D = outside diameter of bearing.

5.11. Resistivity test.

To show the effect of water quenching on trapping of vacancies the compacted samples of Fe - 2% Cu alloy at density 6.0 $^{g}/_{cc}$ with rectangular shape were sintered for 1 hour at 1120^{o}C and then furnace cooled. Half of these samples were solution treated for 1 hour at 1000^{o}C and then water quenched. Measurements of resistivity were done by Kelvin Bridge using a special adaptor which was able to measure the resistivity over a constant length of 3 cm.

5.12. Open porosity network.

To show the open porosity network in sintered products, cylindrical specimens of density 6.0 $g/_{cc}$ with composition of Fe - 2% Cu alloy were impregnated under vacuum with ERL.4206 (vinyl , cyclohexane , dioxide) which has the lowest viscosity of all the plastics[177]. They were then left in an oven at 60^{o}C for approximately 50 hours, until the resin had polymerised. Samples were then treated in dilute hydrochloric acid at room temperature for 48 hours to dissolve the surface metal of samples.

Samples were removed from acid and were photographed by S.E.M.

5.13. Type of oxide.

For finding the type of oxide, pure iron, pure copper and alloys of Fe - 2% Cu to Fe - 8% Cu, (W. quenched and F. cooled), which had been steam treated for 100 minutes at 525^{o}C were exposed to X-ray with radiation of cobalt by Fe filter for 8 hours.

5.14. Wear test.

Fig. 26 shows the different parts of the reciprocating wear test machine used. The sample (A) was held by a rectangular block clamp which in turn was fixed on a screw clamp on the table of the machine (B). The table was moved along the square bed by arm (C). An electric motor (D) provided a cyclic motion of the table by an eccentric screw junction which works as a cam system and could be adjusted for producing 5 different of stroke. The speed of the motor was adjustable by a control knob (E) with numbers 0 to 200, to produce speed from 10 to 91.5 r.p.m.

A right circular cone of diamond with a circular tip of 0.2 mm ± 0.01 mm radius and included angle of cone 120^{o} ± 20' was the abrasive element at the end of the shaft (G). The shaft was passed through a circular hole into the gate (F), and the cone was placed on the specimen (A). The load (L) was applied on the top of the shaft (G). The number of passes was checked by an ordinary watch (N).

5.15. Preparation of samples for metallography.

In studies of microstructure of sintered powder samples using optical microscopy the preparation of specimens with a special technique

is very important. Generally, conventional polishing and etching techniques are applicable to the powder metallurgy product during sintering and further treatment. However extreme caution is necessary.

According to Tomkins' recommendation[178] care is required:

(a) In polishing, to avoid deformation (tearing or dislocation) of particles, which would give a distorted picture of the structure such as shape, size and distribution of pores and even diminish the pores.

(b) In etching, because of the ready absorption of the etchant by the capillary action of the pores, which would result in internal corrosion.

In steam treated samples some open porosity becomes closed by formation of oxide within the channels, so for showing these oxides and remaining pores the procedures are more difficult. An attempt was made to produce samples free from scratches and the following procedure was adopted.

(i) For pre-grinding 180, 320, 400 and 600 grit silicon-carbide papers were used successively. Grinding was continued for 10 - 15 minutes at each stage and between stages the samples were cleaned ultrasonically for 3 minutes in distilled water.

(ii) Specimens were initially polished for 20 minutes using a cloth impregnated with 6 μm diamond for 20 minutes.

(iii) White spirit was used as lubricant on the diamond cloth.

(iv) Samples were etched for 15 to 20 seconds using Nital 1 in order

to show the difference between pores and oxides under optical microscope.

In water quenched and aged samples the same procedure for grinding and polishing was used.

Due to the different phases in water quenched samples, after polishing samples firstly were etched in Nital for 15 seconds to show the ferrite and martensite phases and secondly in alcoholic ferric chloride for 10 seconds to reveal the copper under optical microscope.

In aged samples the etchant was alcoholic ferric chloride for more than 1 minute to become overetched for using under S.E.M.

CHAPTER 6

6. RESULTS AND DISCUSSION.

6.1. NOTE.

Due to the large number of variables examined and the large number of tests carried out it was decided to show the results in tabular form. The various columns in the forthcoming tables will be discussed here separately where necessary.

For convenience of reference to samples the codes in Table 9 were used.

6.2. Powder preparation.

Pre-alloyed powder is usually produced by an atomisation process. This consists of the melting of iron and copper, stirring the liquid and atomising with water. During the melting iron and copper are liquid, (single phase) and atomisation by water should not provide opportunity for any diffusion of copper. Thus this process should result in the production of a powder in which each particle is homogeneous. Usually particles will be covered by a layer of oxide. The powder agglomerates are ground to powder and then annealed in cracked ammonia.

6.2.1. Results and discussion.

As received powders for this project were very hard, which meant that it was not possible using laboratory equipment, to compact it to high densities. This observation possibly shows that the powders were not

annealed after ball-milling. To remove the effects of cold work and the oxide layer on the surface of particles, powders were annealed at 760^{o}C for 20 minutes under cracked ammonia. This process made the powder softer, due to relief of cold work and also the precipitation of copper.

The physical properties of powders should not change during annealing but because of ball-milling after annealing, the fraction of finer particles increased, and the apparent density and flow rate changed, as shown in Tables 5 to 8.

Observation of powders using a Stereoscan microscope showed some copper rich phase in Fe - 8% Cu. The only explanation for this is that there has not been enough time for diffusion of copper and iron in the liquid phase before passing through the orifice for atomisation. This copper rich phase solidified during atomisation, and remained as such in the powder particles.

Tables 7 and 8 show the Particle Size Distribution (P.S.D.), Apparent Density (A.D.) and flow rate for four alloy powders after annealing. As quoted, by increasing the copper content A.D. increases because copper has slightly higher density than iron. Flow rate of all alloys was not measurable because by comparison of P.S.D. before and after annealing the fraction of finer powders after annealing is greater and the friction between particles is higher.

6.3. Green density.

6.3.1. Results and discussion.

The results in Table 10a show that similar pressures were applied to obtain constant densities in alloys 2 to 6% Cu. These results agree

with A.D. results which are almost the same for alloys of 2 to 6% Cu, because as mentioned in Chapter 1, the higher the apparent density the lower the pressure required to attain a constant density.

The pressures required to attain constant density in Fe - 8% Cu are less than those needed for lower copper contents. It has been stated previously that some copper rich phase was present in this alloy. This is softer than the iron rich phase, so lower pressure will be required for constant densities.

Figs. 27 and 28 show the pure iron (- 100# A.S.C.) and pre-alloyed (- 100# Fe - 4% Cu) particles respectively. The particles of pure iron are irregular in shape and the surfaces are rough. Pre-alloyed particles are smooth and more regular in outline, approximate more closely to spherical in shape, are smaller in size and appear to be more dense. The other compositions of iron - copper alloys have similar appearance to Fe - 4% Cu.

In Figs. 29 and 30 the top surfaces of samples pressed to a green density of 6.4 $^{g}/_{cc}$ from pure iron and Fe - 4% Cu respectively are shown. Less deformation is evident in Fig. 30 and furthermore total porosity appears to be less in the former and individual pores tend to be smaller. Because iron particles are more irregular, (less spherical), and coarser than Fe - 4% Cu, their ability to respond to compaction is higher than Fe - 4% Cu pre-alloyed.

6.3.1.1. Comparison of compressibility of pre-mixed and pre-alloyed powders. Because of the high ductility of copper which is present as free copper in pre-mixed alloys compressibility is good and compacts of high green strength

can be produced.

During the production of pre-alloyed powder and subsequent to atomisation the powder agglomerate is ground to powder by ball-milling and then annealed. At the end of this process powders are soft and have good compressibility due to removal of cold working stresses and the presence of precipitated copper.

Holcomb[15] has reported that pre-alloyed powder supplied by DOMTAR[179] has good compressibility. Also he mentioned that DOMTAR process includes ball-milling of sinter-cake and annealing of powders. The as-received powders which were used in this project were hard and before annealing they had very poor compressibility.

6.4. Sintering.

During sintering the particles "weld" together and the point contacts formed during compaction become areas of contact or necks. When this process has advanced to a certain degree the cavities between particles gradually close and tend to become spherical.

The mechanism of sintering for Fe - Cu alloys in this project starts from compacted iron with precipitated copper. Thus the difference between sintered properties of pre-alloyed and pre-mixed powders arises from the location of copper within the iron lattice rather than as discrete copper particles. Pre-alloyed powders are a more intimate mixture of base metal and alloying elements, the diffusion paths required for saturation are shorter and the saturated condition is more closely approached during a conventional sinter.

Unlike compacts prepared from pre-mixed powders, pre-alloyed compacts do not grow during sintering, because no liquid phase is formed. Acceleration of the stages of sintering may result from re-solution of copper precipitates within the pre-alloyed grains.

Pre-alloyed powders (maximum 8.4% Cu) sinter by a solid state process[42] in the same way as pure iron but at copper contents greater than 8.4% some liquid phase sintering will occur.

6.4.1. Results and discussion.

6.4.1.1. Dimensional changes. The dimensional change during sintering of pre-alloyed powder differs from that during sintering of pre-mixed powders, because there is no free copper in compacted samples. Thus diffusion of precipitated copper does not cause expansion in grains like diffusion of free-copper and pre-alloyed powders shrink on sintering.

As shown in Table 11 the shrinkage is almost the same in iron - copper alloys up to 8% Cu. Decreased shrinkage at 8% Cu results from the phenomenon responsible for expansion in alloys prepared from pre-mixed powders. The copper from copper-rich phase in this powder has melted, penetrated the particle grain boundaries, causing expansion which partially counteracts the shrinkage.

6.4.1.2. Comparison with other investigations. Comparison of dimensional changes in this work at a sintered density of 6.9 $^{g}/_{cc}$ (Table 11) with Trudel[42]'s results in Fig. 31 for pre-alloyed powders shows about 0.6% more shrinkage in the former case, and also in the 8% Cu alloy shrinkage is less than in lower copper content alloys. In the present work

sintering time was 1 hour whereas Trudel used a sintering time of 30 minutes and it can be argued that increase of time is accompanied by increased elimination of pores which is reflected in increased shrinkage.

Holcomb[15]'s results are shown in Fig. 32. Decreased shrinkage at 8% Cu and 0.09 % C, relative to 2% and 5% Cu at the same carbon level, results from the phenomenon responsible for copper growth in premixes. The copper-rich phase in this alloy has melted[15] and penetrated the particle grain boundaries, expanding the compact and counteracting the shrinkage to some extent.

The addition of graphite reduces shrinkage at low copper content, due to expansion of the alloy lattice on solution of carbon. Coincidence of results for both carbon levels at 8% Cu is fortuitous. The expansion due to carbon is equivalent to that due to the copper-rich phase in the absence of carbon. The effects are not additive because prior solution of carbon diminishes grain boundary penetration by the liquid copper and subsequent saturation of the lattice.

Comparison of the above results with this work at a sintered density of 6.5 $^{g}/_{cc}$ (Table 11) shows much less shrinkage in the former. The reason for this is the absence of carbon in the specimens used in the present investigation.

6.4.1.3. Effect of density on dimensional change. As shown in Table 11 the percentage of shrinkage decreases as density increases. This can be explained because of the greater driving force for shrinkage arising from greater surface area to volume ratio of low density compacts.

6.5. Solution treatment.

Water quenching from the austenite region using a belt sintering furnace is not possible. Thus to prevent the separation of copper from iron it was decided to solution treat the furnace cooled samples for 1 hour at a temperature appropriate for each alloy using a small furnace.

Comparison of hardness values in Table 13 shows that solution treated hardness increases with increasing copper content.

Solution treated hardness is dependent upon the amount of copper in solution, grain size, structure of massive phase, degree of sintering and porosity.

1. Amount of copper in solution.

When a foreign atom dissolves in a solid metal it may act as an atomic sized obstacle to the motion of dislocations. Suppose that each foreign atom produces a restraining force F upon the dislocation line. According to Kelly[180] the increment in applied stress necessary to overcome this restraining force per length of this would be:

$$\Delta T = \frac{F}{db}$$

where d is spacing of foreign atoms along the line, which is a function of the atom size, their distribution within the structure and the fractional concentration of these foreign atoms, and b is the burgers vector.

2. Grain size.

The flow stress of a metal is almost universally[181] observed to increase as the grain size decreases. According to Petch

et al's[182] equation.

$$\sigma = \sigma_o + K/\sqrt{d}$$

where σ_o and K are constant, and d is the grain diameter.

The strengthening produced by the microstructure, results from the blockage of dislocation motion by the interfaces of the microstructure. If a source within a given grain is feeding dislocations into a grain boundary, the dislocation motion will eventually become blocked at that boundary. Thus a smaller grain size causes more blockage of dislocations and the flow stress of the material increases.

3. Effect of second phase on grain size.

Since grain boundaries are regions of lattice misfit, the strain energy of the boundary, as well as that of the lattice surrounding a foreign atom, can be reduced by the migration of the foreign atom to the neighbourhood of the grain boundary. In this manner it is possible to imagine grain boundary atmospheres similar to dislocation atmospheres and that these atmospheres can effectively hinder the motion of a grain boundary. Weining et al[183] have shown experimentally that the grain growth expansion of copper is decreased by increasing the aluminium in solid solution.

4. Structure of phases.

Structure of a water-quenched sample depends on the cooling rate from the single phase, (solid solution). At constant cooling rate solute content determines whether the product of transformation is massive ferrite or massive martensite.

5. Degree of sintering and porosity.

These two factors will be discussed during the explanation

of microstructure of solution-treated alloys.

6.5.1. Results and discussion.

Microstructures of solution treated samples in Figs 33 (2% Cu) and 34 (4% Cu) show a uniform single phase of massive ferrite. There is no evidence of a copper-rich phase at grain boundaries. Scattered small amounts of copper-rich phase can be seen in Fig. 37 in the 8% Cu alloy. No massive martensite regions were found in 2% or 4% Cu alloys but some areas were found in 6% Cu (Fig. 35) and 8% Cu alloys. A greater amount of massive martensite could be observed in the 8% Cu alloy, (Fig. 36). Overall grain size is almost the same in all four alloys.

These observations and hardness results suggest that the degree of supersaturation was higher in higher copper content alloys and also that in lower solute content alloys massive transformation occurs at higher cooling rate or alternatively lower solute content reduces the effect of quenching on transformation. For these reasons in 2% and 4% Cu alloys the product of transformation is massive ferrite, whereas in alloys of increased solute content some transformation to massive martensite occurs.

In sintered products the porosity will have a direct effect on hardness and an indirect effect on grain size, (same effect as second phase particles). A quantitative explanation of hardness is impossible but a qualitative comparison is given below.

Tables 12 and 13 show that the % of total porosity and % open porosity in 4% Cu and 6% Cu alloys are almost the same but by increasing the copper content from 4% to 6% the increment in hardness is about 20% at a density of 6.0 $^{g}/_{cc}$. This shows the effect of copper content in

solution. The decrement in hardness of Fe - 8% Cu alloy is due to the greater amount of porosity. The increased porosity could be attributed to the reduced shrinkage which occurred during sintering.

Comparison of 2% Cu and 8% Cu alloys at a density of 6.0 $^{g}/_{cc}$ shows that the amount of porosity is almost the same but the hardness of 8% Cu alloy is 100% increased which shows the effect of copper in solution.

The other factor which accounts for decrement of hardness in Fe - 8% Cu alloy is the presence of some copper-rich phase.

6.6. Steam treatment.

6.6.1. Results.

Tables 14, 15, 16 and 17 compare % weight gain obtained during steam treatment for various constant times for each alloy in the water-quenched and furnace-cooled conditions, and for each density.

Reference to these tables and Fig. 38 shows that for pure iron maximum % weight gain decreased as compaction pressure increased.

Figs. 38 and 39 also show that the same trend is apparent for alloys of constant copper content both in the furnace cooled and water quenched conditions.

These Figures also reveal that:

(i) at constant density for alloys of comparable composition the maximum % weight gain was always greater for samples which had been furnace cooled.

(ii) at constant density the maximum % weight gain decreased as copper content increased from 2% to 6%.

(iii) irrespective of density or alloy composition the maximum % weight gain (saturation) was reached more rapidly in furnace cooled samples.

(iv) except in furnace cooled samples compacted to a density of 6.0 $^{g}/_{cc}$, alloys containing 8% Cu were subject to greater weight gain than 6% Cu alloys.

The results from the above experiments are dependent upon open porosity and open porosity will have a major influence on sintered materials during oxidation. In order to show the effect of copper on steam oxidation of iron the results need to be shown independently of porosity.

Fig. 4o and Table 13 show the variations of open porosity in furnace cooled and water quenched samples in all three densities for pure iron and each iron-copper alloy. The results shown in Tables 18, 19 and Fig. 41 are the variations of % weight gain/% open porosity after 100 minutes of steam treatment. It can be seen that this ratio decreases as copper content increases and is independent of open porosity. However, pure iron was subject to slightly less oxidation than the alloy containing 2% Cu.

6.6.2. Discussion.

During the steam oxidation process the sintered iron base parts were subjected to action of superheated steam at a temperature of 525^{o}C. The iron oxidized to magnetite Fe_3O_4 by this reaction, (Appendix 1)

$$3Fe + 4H_2O \longrightarrow Fe_3O_4 + 4H_2$$

The oxide forms a passive layer on the external surface of the product and also on the pore surfaces.

Figs. 42 and 43 show - 100 mesh Fe - 8% Cu, D = 6.4 $^{g}/_{cc}$ as sintered and after 100 minutes steam treatment at 525^{o}C respectively.

Fig. 43 shows that oxide covered the particles and there is clear evidence of oxide formation on surfaces in comparison with Fig. 42.

This film prevents contact between the pure iron and the surrounding atmosphere. Because the volume of the oxide is greater than that of the pure iron from which it forms, the pores are filled by oxide and the open porosity is decreased.

In iron-copper alloys according to Wagner's theory[72], oxidized layers of iron consist of metal deficit semiconductor. Thus by adding copper with lower valency oxidation rate can be decreased.

Considering the equilibrium:

$$(O_2) = 2\square Fe^{++} + 2\oplus\bar{e} + 2FeO$$

Small additions of copper with lower valency (1) than the iron (2, 3) should fill the cation vacancies and electron defects respectively. Thus the concentration of $\square Fe^{++}$ cation deficits, is reduced by the copper ions which have only one charge in place of two (Cu^{+}), and the number of $\square\ Fe^{++}$ vacancies is smaller than that of the electron defects represented by Fe^{3+} as illustrated by Fig. 44.

Fig. 41 shows the effect of Cu addition on oxidation of iron in furnace cooled and water quenched samples. Independent of open

porosity, it can be seen that by increasing the copper content resistance to oxidation is increased, because higher copper content causes fewer $\square Fe^{++}$ vacancies than electron defects.

In Fig. 41 oxidation of pure iron in the same condition is less than that of Fe - 2% Cu, because by comparison of Figs 27 and 28 it can be seen that the particle size of iron is coarser than that of pre-alloyed powder. Thus greater surface area is exposed to steam for oxidation in the latter. It can be seen in Fig. 41 that furnace cooled samples show more response to oxidation than water quenched samples. It is possible that during cooling some of the copper precipitated from solution so that the number of iron vacancies is more in comparison to water quenched samples. Thus resistance to oxidation decreases in furnace cooled samples at the beginning of the steam treatment.

As shown by theory, (Appendix 1) and experiment, copper does not oxidise at $525^{o}C$ in steam. Thus particles precipitated during steam treatment which are almost pure copper do not oxidise in steam. In water quenched samples all of the copper is present in solid solution at the start of steam treatment and, therefore, the initial rate of oxidation is reduced. In contrast, in furnace cooled samples some copper will not provide oxidation resistance to the sample. Thus, the initial rate of oxidation for furnace cooled samples will be accelerated.

By increasing the pressure the amount of open porosity is materially reduced so that the amount of open porosity at the end of steam treatment decreases correspondingly. In addition it is reasonable to argue that in specimens prepared at higher pressure the channels

connecting individual pores will be narrower and become blocked with oxide more rapidly during steam treatment.

Figs 45, 46 and 47 show the formation of oxide on the particles of specimens treated under the same conditions with different amounts of copper. Comparatively the porosity in 6% Cu alloy is coarser and more interconnected than in 4% Cu alloy. In 8% Cu alloy the percentage of porosity is greater but individual pores are smaller than in lower copper content alloys. Fig. 48 shows the same condition as Fig. 47 but at a density of 6.8 $^{g}/_{cc}$. It appears that the percentage of porosity is significantly less than in the lower density alloy.

6.6.2.1. Comparison with previous works. Table 20 shows a comparison of previous results obtained by Lenel[96] at 575°C, Razavizadeh-Davies[99] at 525°C and 600°C using - 300# A.S.C. powder, Franklin-Davies[98] at 520°C and 650°C using ROSPL MP32, and the present work at 525°C using - 100# A.S.C. at D = 6.0 $^{g}/_{cc}$. Generally it can be concluded that:

(i) By increasing the temperature to 575°C % weight gain will increase, because increasing the temperature increases the coefficient of diffusion of atoms. Thus filling of pores by oxide at lower temperature will occur at a slower rate than at high temperature. Thus after steam treatment at 525°C the % weight gain will be smaller than it is after treatment at 600°C.

(ii) At temperatures of 600°C or higher, increasing the time to more than 30 minutes causes a decrease in total weight increment. This is due to the fact that at sufficiently high temperature the capillary inlets eventually become blocked by oxidation

products and since the access of oxidising reagent to the interior of the test piece is inhibited, a part of the internal surface ceases to take part in the oxidation process. As a result, the oxidation rate cannot be described by a quadratic equation.[184]

Comparison of Franklin's[98] results and Razavizadeh's[99] results at 520°C and 525°C respectively shows that the % weight gain in the former is mostly smaller than in the latter. Also results at 650°C and 600°C from these two studies show an apparent inconsistency.

During the latter investigations all specimens were prepared by compaction in a die whereas those used by Franklin were isostatically pressed. As a result there will be a more uniform distribution of porosity in these specimens and it is probable that the shape of the channels connecting the pores to each other will be different. It is also important to note that in Franklin's work a different type of powder was used.

Razavizadeh[99] reported that change of particle size distribution from - 200# to - 300# has a minor influence on the rate of oxidation. Results from the present investigation using - 100# are in close agreement with those obtained in the earlier investigation using - 300# powder, (Table 20).

Table 21 shows a comparison of previous and present results at different density. It can be seen that at each density level the % weight gain is appreciably greater than that reported by Kanopicky[97]. Again it can be argued that a change in the form and distribution of porosity and powder type is responsible for this inconsistency.

Phadke-Davies[17] reported the effect of 2% Cu on steam oxidation of sintered iron at 500°C in pre-mixed (- 100# Sponge iron and - 200# electrolytic copper) alloy in D = 6.8 $^{g}/_{cc}$.

Comparison of these results with the present investigation in - 100# atomised Fe - 2% Cu (pre-alloyed) after 100 minutes steam treatment at 525°C of furnace cooled sample in D = 6.8 $^{g}/_{cc}$ confirms their finding about the effect of copper on steam oxidation.

Phadke's results[17] show 1.8% weight gain in a sample of 10.5% open porosity ($^{1.8}/_{10.5}$ = 0.17%). The present work shows 2.3% weight gain in a sample of 12% open porosity ($^{2.3}/_{12}$ = 0.19%). Thus the results in this range of temperature and density reveal that:

(i) Resistance to steam oxidation is not obvious by addition of 2% Cu to iron alloy, which confirms present results.

(ii) Higher amount of weight gain in the present investigation depends upon higher amount of open porosity (which has direct relation to alloy preparation) and higher temperature of steam treatment.

6.7. Type of oxide.

6.7.1. Results.

Referring to calculations in Tables 22 and 23 for all compositions of iron - copper alloys in water quenched and furnace cooled conditions there was no evidence of copper oxides. Most of the iron-oxides are Fe_3O_4 and αFe_2O_3, with free copper in Fe - 6% Cu and Fe - 8% Cu alloys.

Table 24 and X-ray film show steam oxidation of pure copper and again there is not any evidence of copper oxide.

Tables 25, 26 and X-ray film are the results of steam treatment on pure iron, which show, formation of Fe_3O_4 and αFe_2O_3.

Calculations for the above results were determined, using Bragg law relationship

$$n\lambda = 2d \sin \theta$$

where λ is wave length, λ for cobalt radiation (λ_1 = 1.7903 single Peak, λ_2 = 1.7890 double Peak)

θ is impinging angle,

d is distance between crystal planes (Å)

n is number of wave length (1)

$D = R_2 - R_1$ is diameter (mm).

6.8. Effect of variables on hardness.

6.8.1. Pressure.

Generally hardness is proportional to compaction pressure. Table 13 shows the variation of hardness after sintering and solution-treatment in four alloys. It is apparent that at the higher pressure the rate of increase in hardness was less than the rate at lower pressure.

6.8.2. Precipitation hardening in W.Q. samples by inert gas.

6.8.2.1. Results. Table 27 and Figs 49 and 50 show the kinetics of ageing in inert gas for 2, 4, 6 and 8% Cu alloys. The ageing curves reveal the following characteristics:

(i) There is no incubation period before precipitation starts in any

of the alloys.

(ii) As the amount of copper increases, the time required to attain peak hardness decreases.

(iii) The peak hardness increases with copper percentage up to 6% Cu but there is a slight decrease in the 8% Cu alloy. However, when the % increase in hardness after ageing in D = 6.8 $^{g}/_{cc}$ is compared with the water quenched, it is seen that the percentage increase in alloys is nearly identical at about 40%.

(iv) Increase in hardness after ageing over the solution treated value is greater at higher density for all of the alloys.

6.8.2.2. Discussion.

6.8.2.2.1. Rate of precipitation. The absence of an incubation period indicates a rapid rate of precipitation. To explain the high rate of precipitation, it can be assumed that, in common with wrought alloys, zones form first and the presence of excess quenched in vacancies leads to rapid diffusion during clustering[126]. The enhancement of diffusion in wrought material can be estimated by multiplying the normal diffusion (D) coefficient by the relative concentration of excess vacancies[131], using the relationship

$$D_C = D^{\frac{CT_2}{CT_1}}, \quad CT = e^{-U_F/RT}$$

where CT is the vacancy concentration at absolute temperature T.
U_F is the energy of vacancy formation.

R is the gas constant.

D_C is the increased value of the diffusion coefficient due to excess vacancies.
T_2 is quenching temperature.

T_1 is ageing temperature.

In sintered product it needs to be shown that even due to the presence of porosity which acts asafree surface for removing the vacancies, quenching from solution-treatment temperature could trap excess vacancies.

Quantum theory[185] says that in a perfect crystal, (all atoms stationary in their regular positions), an electron moves through the crystal quite easily. The motion can be described by a kind of wave that glides through the regular array of atoms without meeting any resistance. Any departure from perfect periodicity, however, disturbs this wave motion of the electron and scatters it from its intended path. The thermal vibrations represent such a departure so that the resistivity of metals increases with increasing temperature. A vacancy is an even more radical disturbance of the periodicity and therefore appears as a serious obstacle to the electron motion. These facts form the basis for resistivity test.

The results of this experiment were quoted in Table 28 which shows that the average resistivity in a water quenched sample is about 6 micro-ohm greater than in furnace cooled samples. Thus excess concentration of vacancies could be trapped by quenching in sintered products.

The results of Norton[127] on wrought alloy and Phadke-Davies[139] in sintered alloy do not show any incubation period during ageing at temperatures between 400°C and 700°C.

6.8.2.2.2. Peak hardness and time relationship. Explanation of the second feature is that super saturation increased with the copper content of the mixture and the time required to attain peak hardness decreases as the super saturation increases. This happens due to the fact that, as

the number of solute atoms in the matrix increases the chance of assembling sufficient atoms to form a nucleus increases.

Similar results for alloys of 2 to 8% Cu at 500°C ageing temperature were found by Phadke-Davies[139].

6.8.2.3. The magnitude of solution treated and peak hardness.

The solution treated hardness and its relationship to the amount of copper in solution, grain size, structure of phases, sintering, and porosity were discussed in section 6.5.

6.8.2.3.1. The magnitude of peak hardness.

The peak hardness condition is influenced by the number, size and distribution of precipitates.

The number of precipitates can be expected to increase and their size to decrease with increasing supersaturation[186]. However, it was not possible to observe the microstructures of alloys at peak hardness by electron microscopy. Therefore, in order to observe the precipitates the alloys were aged for 500 hours at 525°C. After this treatment, the precipitates were visible in the electron microscope. The microstructures of aged alloys (Figs. 51 to 53), provided a valuable support for the results obtained from the kinetics of ageing as followed by hardness measurement. It can be seen that the number of precipitates and their uniformity increased with copper content of the alloy.

From Figs. 49 and 50 it is seen that the difference in hardness between the aged and solution treated values increases by increasing the copper content up to 6% Cu and decreases at 8% Cu alloy.

As mentioned before by increasing the copper content, the magnitude of hardness in solution-treated and aged alloys is increased. By referring to Table 12 and the discussion in section 6.5.1. the amount of porosity in 2, 4, 6% Cu alloys is almost the same. Thus the probability of heterogeneous nucleation in these alloys should be the same, but in 8% Cu alloy the amount of porosity is greater and also the presence of massive martensite, (high dislocation density) will provide more sites for heterogeneous nucleation. The difference between solution-treated and aged alloy is decreased in comparison with lower copper content alloys. This explanation is supported by the results obtained by Hornbogen[126] on cast material which showed the effects of plate boundaries of the massive phase on precipitation. The fact that he obtained the same peak hardness in alloys quenched from the α or γ regions, means that the magnitude of hardness increase was actually lower on quenching from the γ regions, when it is recalled that the as quenched hardness of samples quenched from the γ region is higher. This can be understood in terms of more rapid and preferential growth of precipitates situated on grain boundaries, which would decrease the number of homogeneous precipitates and increase the spacing between the particles.

There are several areas in the microstructures of aged alloys showing preferential precipitation on grain boundaries. Fig. 53 shows this effect very clearly. It is seen that the size of precipitates on grain boundaries and martensite plate boundaries is larger and in the immediate neighbourhood of boundaries precipitation is almost absent.

Fig. 54 was especially taken from the same sample before ageing, to show the different phases of ferrite and martensite.

6.8.2.4. Peak hardness and density relationship.

Examination of Table 27 and Figs. 49 and 50 reveals that in any composition from 2 to 8% Cu the increment in hardness during ageing is dependent on density. Increase in hardness at peak is greater in higher density samples. As mentioned before at higher density the % of porosity is less. However, since a pore surface is similar to a grain boundary, it may be inferred that like precipitation on grain boundary, copper precipitates on pore surfaces. In addition to minimizing interfacial energy and enhancing diffusion, a free surface also helps precipitation by accommodating strains associated with the formation of a precipitate with a crystal structure different from that of the matrix[117]. It may be assumed that zones located near pore surfaces transform earlier to ε particles and grow larger similar to grain boundary precipitation.

The other explanation for precipitation on pore surfaces, could be due to a high concentration of vacancies around the pores, because pore surfaces act in the same way as free surfaces in the crystal lattice.

From the above discussion, it could be concluded that increase of porosity causes more heterogeneous precipitation, and that the percentage of increment in hardness will be greater in higher density specimens.

Figs. 55, 56 and Table 29 show the microhardness in different areas of Fe - 4% Cu in D = 6.0 $^{g}/_{cc}$ and D = 6.8 $^{g}/_{cc}$. Minimum hardness is around the pores, and maximum is in the middle of grains.

Comparison of these two Figures reveals lower hardness in D = 6.0 $^{g}/_{cc}$ in different area. Hardness in the grains is less, because the percentage of homogeneous nucleation is less in lower density (more pore surface).

6.8.3. Steam treatment as ageing in (W.Q.) samples.

6.8.3.1. Results.

In data recorded in Tables 14, 15, 16 and 17 for water quenched samples, (density 6.8 $^{g}/_{cc}$), steam treatment was used as an ageing treatment and Table 27 shows the results of ageing in inert gas. These results are plotted in Figs. 57a, 57b, 58a and 58b to show the comparison between steam treatment and ordinary ageing in iron-copper alloys.

In Fig. 57a it can be seen that for Fe - 2% Cu steam treatment can improve the hardness as a simultaneous ageing and oxidation treatment. There is about a 10% increase in hardness in comparison with ageing in inert gas.

Fig. 57b shows the same procedure for Fe-4% Cu but in this alloy the situation is reversed and there is about an 8% decrease in hardness if steam treatment is used as ageing treatment. This decrement in hardness for Fe - 6% Cu is about 7.5% and for Fe - 8% Cu is about 8.5% (Appendix 2).

Fig. 59 shows the variation in peak hardness of samples in solution treated, aged, and steam treated conditions for four alloys.

Comparison of the curves for solution treated and inert gas aged specimens shows that, at constant copper content, the increment of hardness is comparable.

In steam treated specimens a different pattern from 2 to 8% Cu was shown.

Fig. 60 shows the straight relation between hardness and % weight gain in pure iron.

6.8.3.2. Discussion.

According to Wagner's theory[72] if a metal (Fe) is exposed to gas (H_2O) at a proper temperature, gas and metal decompose to ions and electrons (equation A).

$$\left.\begin{array}{l} Fe \longrightarrow Fe^{++} + 2\bar{e} \\ H_2O \rightleftharpoons H_2 + \tfrac{1}{2}O_2 \\ O_2 + 4\bar{e} \longrightarrow 2\bar{O} \end{array}\right\} \quad (A)$$

One molecule of oxygen which chemisorbed on the surface of the metal would effect the migration of two Fe^{++} ions and two electrons with formation of two vacant Fe^{++} ($\square Fe^{++}$) and two vacant electron sites ($\oplus$) (equation B).

$$O_2 = 2\square Fe^{++} + 2\oplus\bar{e} + 2FeO \quad (B)$$

Iron ions are cations and oxygen ions are anions so they migrate to each other and oxide forms. Thus when iron ions diffuse towards the metal/oxide interface vacancies diffuse in the opposite direction and they possibly condense at the grain boundaries or vanish in the grain boundaries and pore surfaces. Thus the vacancy concentration of the matrix decreases.

The mobility or diffusion coefficients for cations, anions and electrons are not equal and because of this difference a separation of charges takes place in a growing oxide scale. The resulting space charge also creates an electric field which opposes a further separation of charges and a stationary state is reached for which no net current flows through the scale.

According to Shewmon[187] when cast alloys are quenched from the solution treatment temperature, most of the copper stays in solution, and the high concentration of vacancies remains. This gives rise to two effects which are important in the early stage of ageing.

(i) These excess vacancies slowly precipitate or "condense out" many clusters and form dislocation loops.

(ii) Others are annihilated on existing dislocations thus modifying the shape of the dislocation.

These new and modified dislocations thus increase by an order of magnitude the number of dislocation sites at which precipitate particles can nucleate.

Hornbogen et al[126] suggested that in Fe - 1.2% Cu alloy clusters of copper grow at a rate which can be explained by the concentration of excess vacancies in the material, which are preferred sites for nucleation of copper particles within the lattice.

It was shown, (Section 6.8.2.), by resistivity test that in sintered products excess vacancies can be trapped by quenching as in cast materials.

Thus if steam treatment is used as an ageing treatment, due to oxidation theory, most of the preferred sites, (vacancies), for nucleation of ε copper are annihilated or have probably condensed at the grain boundaries and pore surfaces. Thus most of the particles nucleate in these regions which are heterogeneous sites for nucleation and hardness

value is less than the hardness obtained by ageing in inert gas, because during ordinary ageing nucleation is more homogeneous.

Calculations in Appendix 2 show that by increasing the copper to iron ratio this situation is worse, because by increasing the copper resistance to oxidation increases, due to the smaller number of vacancies for diffusion, and as a result fewer nucleation sites for homogeneous nucleation of copper particles exist.

It should be noticed that the worse effect in higher copper content alloys has nothing to do with the amount of porosity which are heterogeneous sites for nucleation, because, as shown in Table 12, the amount of porosity in 2, 4 and 6% Cu is almost the same.

Improvement of hardness by steam treatment of Fe - 2% Cu alloy is due to formation of oxide and precipitation hardening during steam treatment. Also heterogeneous nucleation in this alloy is less than in higher copper content alloys. Despite these considerations, as shown in Appendix 2, there is 90% of age hardening by steam treatment in comparison with ageing in inert gas.

Figs 61a and 62a show the difference between the location of precipitated particles during ageing in inert gas and ageing in steam for Fe - 2% Cu alloy. It can be seen that the amount of precipitated particles along grain boundaries and pore surfaces as a result of steam ageing is more than ageing in inert gas.

Figs 63a and 64a were taken of Fe - 8% Cu alloy to show the effect of steam treatment as an ageing process. Figs. 61b, 62b, 63b, and 64b show the copper line and copper image probe and provide evidence that

the distribution of copper in ordinary aged samples is more homogeneous than in steam treated samples.

To provide further support for this conclusion alloys were steam treated for 75 minutes at 525°C for nucleation of copper during steam treatment and then they were kept in vacuum capsules for 498.75 hours at 525°C. Comparison of Figs 65 and 66 with Figs. 51 and 52, for samples which were kept in vacuum capsules for 500 hours at 525°C without any steam treatment, reveals that during 75 minutes steam treatment most of the particles nucleated and grew at grain boundaries and pore surfaces, and during the rest of the time up to 500 hours they became coarser and connected to each other, so that they look almost as a line on grain boundaries. This situation is less obvious in samples aged in inert gas for 500 hours, because the distribution of copper is more homogeneous at the beginning of precipitation.

Figs. 67 and 68 were especially taken to show the concentration of precipitated particles on pore surfaces and grain boundaries in comparison to the grains.

6.8.4. Influence of density on response to steam treatment.

6.8.4.1. Results of water quenched samples.

Reference to Fig. 69b for water quenched samples of Fe - 2% Cu alloy reveals that:

(i) For all three densities maximum hardness is reached after 25 minutes. Increasing the period of steam treatment to more than 25 minutes causes reduction of hardness in D = 6.8 $^{g}/_{cc}$ while in densities of 6.0 and 6.4 $^{g}/_{cc}$ hardness remains constant.

(ii) Maximum hardness at peak and after 100 minutes steam treatment belongs to density 6.8 and 6.4 $^{g}/_{cc}$ respectively.

Fig. 70b for water quenched samples of Fe - 4% Cu alloy shows:

(i) In densities of 6.4 and 6.8 $^{g}/_{cc}$ maximum hardness is reached after 10 minutes but in density 6.0 $^{g}/_{cc}$ maximum hardness is attained after 25 minutes and after these two periods of treatment hardness starts to decrease.

(ii) Maximum hardness at peak and after 100 minutes steam treatment belongs to density 6.8 and 6.0 $g/_{cc}$ respectively.

Fig. 71b shows data for water quenched samples of Fe - 6% Cu alloy and it can be seen that:

(i) Maximum hardness in D = 6.8 and D = 6.4 $^{g}/_{cc}$ is reached after 10 minutes but in D = 6.0 $^{g}/_{cc}$ maximum hardness occurs after 50 minutes. Reduction in hardness for D = 6.8 $^{g}/_{cc}$ starts after 10 minutes but in D = 6.4 and D = 6.0 $^{g}/_{cc}$ no reduction was observed up to 100 minutes.

(ii) Maximum hardness at peak and after 100 minutes of steam treatment belongs to D = 6.8 and D = 6.0 $^{g}/_{cc}$ respectively.

Data recorded in Fig. 72b for Fe - 8% Cu alloy shows that:

(i) Maximum hardness in D = 6.8, 6.4 and 6.0 $^{g}/_{cc}$ is reached after 10, 25 and 50 minutes respectively, and after these periods of treatment reduction in hardness starts.

(ii) The value of hardness at the end of treatment is almost the same for all three densities, and maximum hardness at peak

belongs to D = 6.4 $^{g}/_{cc}$.

6.8.4.2. Results of furnace-cooled samples.

In furnace cooled samples the variation of hardness with density is less than in water quenched samples.

From Fig. 69a it can be seen that:

(i) Maximum hardness for all three densities is reached after 50 minutes of steam treatment and from this time up to 100 minutes hardness remains constant.

(ii) Maximum hardness at peak and after 100 minutes steam treatment belongs to density 6.0 $^{g}/_{cc}$.

Fig. 70a for Fe - 4% Cu alloy shows that:

(i) Maximum hardness is again after 50 minutes in all three densities and by increasing the period of treatment, the value of hardness in density 6.8 $^{g}/_{cc}$ starts to decrease.

(ii) Maximum hardness at peak and after 100 minutes steam treatment belongs to D = 6.4 $^{g}/_{cc}$.

For Fe - 6% Cu alloy which was shown by Fig. 71a:

(i) In density 6.4 and 6.8 $^{g}/_{cc}$ maximum hardness is attained after 25 minutes treatment and in D = 6.0 $^{g}/_{cc}$ even after 100 minutes hardness still increases.

(ii) Maximum hardness at peak and after 100 minutes steam treatment belongs to D = 6.0 $^{g}/_{cc}$.

Alloy of Fe - 8% Cu in Fig. 72a show the same situation as Fe - 2% Cu alloy in Fig. 69a.

6.8.4.3. Discussion.

The effect of steam treatment on hardness depends on the three factors of, density, precipitation hardening and formation of oxide.

6.8.4.3.1. In water quenched samples.

The effect of pressure on density, (porosity), was mentioned in section 6.8.1. Increasing the pressure reduces the amount of porosity, thus increasing the density, and as a result increases the hardness.

An explanation of the effect of amount of copper in solution, ageing by steam treatment and effect of density on precipitation was given in sections 6.5, 6.8.3. and 6.8.2.4 respectively.

The third factor has a general effect on hardness. The hardness of oxide coating is high in comparison with that of normal metal. During steam treatment the voids are filled up by the oxide and thus the resistance to deformation under load is increased.

The effect of steam treatment on hardness is more evident in lower density, due to the fact that % open porosity is greater than in specimens prepared at higher density. In specimens produced at lower density most of the voids are interconnected and controlled oxide coating is developed on the walls of the voids throughout the section as well as on the external surfaces. Thus, there is a larger increment of hardness on specimens produced at lower density than on those produced at higher density.

6.8.4.3.2. In furnace-cooled samples.

In furnace cooled samples apart from the first factor which has a general effect on hardness, the effect of both other factors on hardness in furnace cooled samples is different.

Compared with the kinetics of ageing by steam treatment in severely quenched alloys in Figs. 69b to 72b, the ageing process in the furnace cooled alloy was retarded and the peak hardness reached was almost the same (Figs. 69a to 72a). This can be attributed to a decreased vacancy and solute concentration due to precipitation during cooling from the sintering temperature. Stosuy[188] has previously noted that copper dissolved during sintering precipitates during furnace cooling and the fineness of precipitation depends upon the cooling rate. The precipitates formed in wrought Fe - Cu alloy during air cooling were identified as particles of equilibrium ε by Pickering[189].

In this project the belt speed during cooling was adjusted to 10 ^{minute}/meter, and cooling rates in the temperature ranges 1100 to 850^{o}C, 850 to 500^{o}C, 500 to 350^{o}C, and 350 to 200^{o}C were 100^{o}C/minute, 130^{o}C/minute, 60^{o}C/minute, and 50^{o}C/minute respectively. Therefore, it appears that some precipitates of ε phase can form during cooling through the high temperature range from 850^{o}C. (The temperature 850^{o}C corresponds to the temperature at which separation of ε phase takes place according to the Fe - Cu phase diagram). The effect of precipitation during cooling is not confined to a decrease in the solute concentration. In Fe - Cu alloys coherent copper rich zones form first and later they transform in situ to

equilibrium ε phase[126]. Therefore, in the presence of equilibrium ε phase formed during cooling, metastable zones which may form during subsequent ageing probably dissolve without growing and the resulting coarse precipitation decreases the peak hardness.

As was shown in Fig. 39, formation of oxide in furnace cooled samples is greater than in water quenched samples due to the increase of open porosity, and also from Fig. 40 and discussion in section 6.6.2., resistance to oxidation in furnace cooled samples is less than in water quenched samples. Thus a larger amount of oxide forms and this partly compensates for the reduction of hardness attributable to precipitation of copper from Furnace Cooled specimens. However, longer times are required for the attainment of peak hardness.

It was shown in Figs 57 and 59 that during the ageing of water quenched samples in inert gas as the amount of copper increases, the time required to attain peak hardness decreases. In furnace cooled samples the amount of solute available for precipitate formation is less than in water quenched samples of equivalent composition. Thus it needs a longer time to assemble sufficient atoms to form a nucleus.

For example, calculation of the hardness of a sample of Fe - 2% Cu alloy of D = 6.8 $^{g}/_{cc}$ which had been furnace cooled and subsequently aged for 25 minutes in steam and of a sample which was water quenched shows that:

After 25 minutes of ageing the weight gain is 1.8% and the hardness values for pure iron due to a weight gain of 0% and 1.8% are 49 and 98 H.V., (Fig. 60), respectively. The hardness increase due to steam oxidation alone is then 49 H.V. units. The hardness value of Fe - 2% Cu alloy after 25 minutes in steam is (170 - 49) or 121 H.V. Similar

calculation for a water quenched sample gives, 1.5% Weight gain which corresponds to 41 H.V. units, and observed hardness after 25 minutes, is (Fig. 69b), 180 H.V. Thus the hardness value on ageing for 25 minutes in steam is (180 - 41) or 139 H.V.

Comparison of these two calculations reveals that after 25 minutes ageing in the same composition of alloy, furnace cooled samples have 13% reduction in hardness during ageing. Thus these calculations confirmed the above discussion for retardation of peak hardness.

The results of the present work after 100 minutes steam treatment of furnace cooled sample in D = 6.8 $^{g}/_{cc}$ of Fe - 2% Cu alloy at 525^{o}C, basically confirm Phadke's result,[17] but higher hardness value in the former case is due to the greater amount of oxide, (more porosity), and higher temperature of treatment which has a direct effect on oxidation and precipitation rate.

6.8.4.4. Conclusion.

The effect of mentioned factors together on hardness suggest that:

(i) Higher pressure during compaction increases the hardness.

(ii) Effect of steam treatment and inert gas treatment as ageing treatment is more pronounced at higher density.

(iii) Effect of steam treatment as oxidation treatment is more pronounced at lower density.

(iv) The time required to peak hardness decreases as the amount of copper increases.

(v) In the peak hardness condition the maximum hardness belongs to D = 6.0 $^{g}/_{cc}$ but in the initial stages lower density samples have less hardness. The maximum hardness increment occurs in Fe - 2% Cu alloy at D = 6.0 $^{g}/_{cc}$, which has almost 260% increase in furnace cooled and 240% increase in water quenched conditions.

(vi) Water quenched samples of 4, 6, 8% Cu after 100 minutes of steam treatment have lower hardness in comparison with furnace cooled samples, but in 2% Cu alloy hardness values are almost the same.

(vii) There is a possibility of increasing the hardness of furnace cooled samples in low and medium densities by increasing the period of steam treatment to more than 100 minutes.

(viii) The results indicate that in order to improve response to subsequent ageing of Fe - Cu alloy of any given composition by steam treatment, it is necessary to reduce high concentration regions, grain boundary area, and void surfaces.

Furnace cooled samples of Fe - 2% Cu alloy in medium density which have been steam treated for 50 minutes at 525^{o}C have the optimum strength of the four alloys.

6.9. Radial crushing strength (R.C.S.)

6.9.1. Results.

Tables 30, 31 and Fig. 73 show the radial crushing strength of ring shape samples in the sintered and steam treated conditions (50 minutes at 525^{o}C), with the same dimensions and at a density of 6.4 $^{g}/_{cc}$.

This information reveals that steam treatment improves the radial crushing strength of sintered pure iron by up to 32% but this treatment decreased resistance to crushing in 2, 4, 6% Cu alloys and in 8% Cu is not harmful.

Radial crushing strength in furnace cooled samples increases as the amount of copper increases, up to 6% Cu, but in 8% Cu R.C.S. decreases.

6.9.2. Discussion.

As mentioned in section 4.10 one of the applications of sintered iron and sintered iron-copper alloys is in the field of bearing products, and radial crushing strength is a standard test to assess the strength of these materials under load.

Since steam treatment gives an oxide layer not just to the surface, (to improve surface properties like wear) but also to the interior of the pores, (to improve bulk properties like hardness and compressive strength)[190], it was decided to assess the effect of this treatment on R.C.S. of bearing shape samples.

Fig. 73 shows R.C.S. of sintered iron is improved by steam oxidation. It can be argued that oxide has filled the voids. Thus density and hardness of article are increased, and as a result resistance to crushing increases.

During steam treatment of iron-copper alloys in addition to formation of oxide in the porosity and on the surface of articles, there is precipitation hardening by copper. The presence of precipitated

particles will increase the strength with the change in ductility. Variation of ductility depends on the ageing temperature[191]. The loss of ductility of an alloy aged at low temperature is generally less than that in the same alloys aged at high temperatures. The reduced ductility is intimately associated with the presence of localized precipitation at grain boundaries. In Al-Mg-Si[192] alloys the increase in brittleness has been related to increased continuity of the grain boundary network by precipitated particles.

At low temperature where nucleation is greater, hardening by general precipitation can proceed at a rate which is relatively faster with respect to localized precipitation. At high temperature most of the precipitate forms by growth of a few heterogeneously nucleated particles.

In sintered products the presence of porosity helps to increase the amount of heterogeneous precipitation.

Fig. 73 for iron-copper alloys shows steam treatment has no beneficial effect on R.C.S. of sintered alloys.

Consideration of factors such as density, porosity, temperature, and ageing treatment by steam explains this phenomenon.

Density of 6.4 $^{g}/_{cc}$ has about 18% porosity which means that the possibility of heterogeneous nucleation is high. Temperature of 525^{o}C is a relatively high temperature for ageing and the possibility of grain boundary's nucleation is high (below 0.6 Tm)[193], and thirdly ageing in steam helps to promote heterogeneous nucleation in comparison with ageing in inert gas.

Thus from the above discussion it can be concluded that steam treatment of iron-copper alloys increases the strength of sintered products by formation of oxide and precipitated particles but presence of these particles reduces the ductility which as a result reduces the R.C.S.

Increase of copper content up to 6% increases the R.C.S. as a result of solid solution strengthening effects but further increase to 8% causes a decrease because of the increased porosity and because some copper rich phase exists in this alloy which has an effect on R.C.S. similar to that on hardness.

Steam treatment of Fe - 8% Cu alloy has no effects on R.C.S. This is possibly due to the presence of some copper rich phase in this alloy which partly compensates for the brittleness produced by localized precipitated particles on grain boundaries and pores surfaces.

6.10. Wear properties.

For this experiment abrasive wear by a reciprocating machine was studied, and results were obtained from sliding distance (number of passes), scar width, and volume wear with different loads in the same condition of preparation (D = 6.8 $^{g}/_{cc}$, furnace cooled, 100 minutes steam treatment) and test (room temperature, atmospheric pressure, and 0.5 cm/sec speed).

6.10.1. Results for sintered and steam treated iron.

Tables 32 to 43 and Figs. 74a, 74b show the effect of load and sliding distance on sintered and steam treated pure iron.

Increasing the load increases the scar width almost in a regular manner but increasing the sliding distance up to 180 passes

increases the scar width. Increasing the number of passes to more than 180 has no effect on the width of scar and this phenomenon is more evident in tests under lower load.

Steam treated samples have more resistance to abrasive wear especially at lower load and shorter sliding distance. This advantage was continued even at 1000 cm sliding distance under loads up to 5 kgs but at higher load the scar widths of sintered and steam treated specimens are almost the same.

6.10.2. Results for sintered and steam treated Fe - 2% Cu alloys.

Reference to Tables 32 to 43 and Figs. 75a and 75b shows that the same results were obtained by increasing the load and sliding distance. Comparison of results from sintered and steam treated samples shows that the advantage of steam treatment is obvious up to 1000 cm but at greater distances sintered and steam treated samples even under lowest load behave similarly and at higher load sintered samples had better resistance to abrasive wear.

6.10.3. Results for sintered and steam treated Fe - 4% Cu alloys.

These results are shown in Tables 32 to 43 and Figs. 76a and 76b. The results followed the same pattern as previously. The advantage of steam treatment continues up to 180 cm over the whole range of loads but at longer distances even under lower load sintered samples had smaller scar width, (lower wear rate).

6.10.4. Results for sintered and steam treated Fe - 6% Cu alloys.

By examination of Tables 32 to 43 and Figs. 77a and 77b, it can be concluded that the advantage of steam treatment in this alloy for

abrasive wear was continued up to 100 passes but at longer distances the resistance to wear is lower in steam treated samples. The order of scar width by increasing the load and number of passes is the same as for previous alloys.

6.10.5. Results for sintered and steam treated Fe - 8% Cu alloys.

The results presented in Tables 32 to 43 and Figs. 78a and 78b, for Fe - 8% Cu show that steam treatment can improve the resistance to abrasive wear up to 1000 passes in all ranges of tested load, (1 to 5 Kgs.), and it neither shows any advantage nor disadvantage in longer distance up to 5 Kgs. At higher loads the difference in scar width is not significant.

Relationship between load and scar width is a parabolic relation, and scar width after 200 passes under any load is constant, almost the same as previous results.

6.10.6. Variation of scar width with load in different alloys.

According to Tables 42, 43 and Figs. 79aand 79b the different copper content alloys were examined in the same condition of density, sliding distance and speed with variation of load in sintered and steam treated condition. Fig. 79a shows that by increasing the copper content the scar width decreases, but in steam treated condition, (Fig. 79b), the resistance to wear is not in order of increasing copper content.

By comparison of Fig. 80a, 80b it can be concluded that the resistance to abrasive wear in sintered and steam treated conditions is related to their hardness in sintered and steam treated conditions.

6.10.7. Volume wear as a function of load.

Calculations for volume wear and information about abrasive indentor, shape of scar are quoted in Appendix 3.

6.10.7.1. Volume wear in sintered and steam treated pure iron.

Volume wear was measured after 1000 cm sliding distance and data are shown in Tables 44, 45 and Fig. 81. The volume wear of sintered samples is greater than that of steam treated samples at loads up to 7 Kgs. Under higher loads the situation is reversed. This advantage exists at longer sliding distance because it was shown in Fig. 74 that after 200 passes the scar width is almost constant.

6.10.7.2. Volume wear in sintered and steam treated iron-copper alloys.

Tables 44, 45 and Fig. 82a do not show any advantage or significant disadvantage for Fe - 2% Cu steam treated samples at 1000 cm sliding distance.

In the case of Fe - 4% Cu steam treated samples exhibit higher volume wear as shown in Fig. 82b and this situation is worsened by increasing the load.

Volume loss of Fe - 6% Cu is almost the same as Fe - 4% Cu because disadvantage of steam treatment is quite obvious from 100 cm in lowest load (1 Kg.). The results of this alloy are shown in Figs. 77 and 83a.

Fig. 83b shows the effect of steam treatment on Fe - 8% Cu. In this alloy the situation is not so bad as Fe - 4% Cu and Fe - 6% Cu and it is almost the same as Fe - 2% Cu and probably up to 5 Kgs steam

treatment does not have harmful effects on abrasive wear.

6.10.8. The relation of wear and hardness.

Reference to Fig. 80a and Table 13 shows that by increasing the Cu content the hardness of sintered samples increases up to 6% and decreases at 8% Cu.

In abrasive wear one of the most important factors is hardness and wear is inversely proportional to hardness. Fig. 84 confirms this relationship and shows that the minimum volume loss is in Fe - 6% Cu which has maximum hardness. In the case of steam treated samples Fig. 85 shows the relationship between hardness and volume wear which is confirmed by Fig. 80b. Minimum wear rate is in 6% and 8% Cu and wear rate in 4% Cu is more than 2% Cu. This shows that increase in hardness during steam treatment has a relation to precipitation and oxidation.

The result in Fig. 86 shows the volume wear of two alloys with the same hardness and it can be seen that wear rate (volume wear) in steam treated samples of Fe - 4% Cu under any load is more than sintered samples of Fe - 6% Cu, and it is more obvious at higher loads.

6.10.9. Discussion.

Abrasive wear with reciprocating machine was used in this project due to four reasons.

(i) Surface finishes should be considered at the design stage of any metal component when decisions can be made as to the most suitable methods of introducing special engineering properties. Having designed a component to be manufactured from a selected material by a special process and then imposed surface condition

in relation to wear, corrosion or heat resistance, bearing properties or even appearance it will be necessary to finally reappraise the original component design and consider in what way it may be affected by finishing. This is particularly so with components produced by powder metallurgy as the vast majority are porous in their final form, having densities of from 70 to 80% of solid metals.

Among the many ancillary finishing processes carried out on powder metal components is steam treatment.

In this process iron oxide coating forms on the outer surface of the part and the steam diffusing through the pores effects an internal oxide coating.

For investigation of wear property there are two methods in this department.

1. Adhesive wear test, in which standard test pieces should be machined from rectangular powder samples.

2. Abrasive wear test, in which samples can be used without any machining after sintering and steam treatment.

Figs. 87 and 88 show a comparison of machined surfaces after sintering and then steam treated, and a surface just after steam treatment respectively.

It can be seen that machining after sintering removes the surface porosity and damages the porosity network by closing the channels

which are passages for diffusion of steam, and generally can reduce the effect of steam treatment by at least 50%.

Because of the above problems it was decided to use an abrasive wear test for wear properties of sintered and steam treated speciments.

(ii) During the "running-in" in actual case of piston ring high spots will be removed by adhesive wear and plastic deformation. After the "running-in" period the removed particles act as abrasion particles between the rubbing surfaces. Besides these particles, corrosion is thought to be a major mechanism of wear of piston rings and cylinders in car engines. The presence of sulphur and additive in the petrol may be one cause of corrosion, but the major cause is carbonic acid formed from the combustion products, CO_2 and water. Burwell[194] describes the situation as follows:

A car is started from cold in the morning and driven to work, where it is parked and cools down, possibly to sub-zero temperatures. In the evening the process is repeated. Thus two cycles from cold to hot to cold are repeated daily even though the total distance driven might be small. Each time the engine is cooled the carbonic acid condenses on the cylinder walls, producing abrasive corrosion products (e.g. Fe_2O_3). The next start-up wears away these corrosion products producing additionally some abrasion.

Thus the loose particles which are detached from the steam treated samples during test are a mixture of iron and iron

oxide (Fe_2O_3, Fe_3O_4) and have the same effect as removed spots (during "running-in") and corrosion product respectively. Thus an abrasive wear test covers these effects as in a real case.

(iii) Reciprocating abrasive wear test was used, because in actual case a piston ring passes a constant length of cylinder from top to bottom to top, which in a reciprocating machine abrasive element passes a constant length on the specimen from right to left to right.

(iv) The most important factor in abrasive wear is hardness, which is an especially very important factor in the present project due to alloy addition, ageing and steam treatment.

6.10.9.1. Abrasive wear.

The hard asperities of the slider will plough into the soft surface layer of the specimen during sliding. This should result in a smooth surface appearance with parallel ridges due to the ploughing action, where no abrasive wear particles have been separated. By increasing the load this smooth surface converts to rough with formation of cracks and wear sheets.

According to delamination[151] theory voids in single phase metals deform in the deformed layer beneath the wear track by coalescence of micro-voids and vacancies during plastic deformation of the sub-surface layer. Figs. 89 and 90 show the general views of plastic deformation produced by 1 Kg load on pure Fe and Fe - 8% Cu alloy after 1000 cm sliding distance.

Voids and cracks can link by shearing and growing of voids or by propagation of cracks between these voids. Thus the strength of the sub-surface layer is less than the shear stress applied at the interface between the slider and the surface, so the result should be a separated thin sheet. After these wear sheets are created, some of them may be entrapped between the two sliding surfaces. These trapped particles may either be rolled into a spherical shape or broken into small pieces or remain the same, depending on the material properties of the loose particles and the sliding conditions. When the metal is relatively brittle, the delaminated sheets may break into pieces and form many small particles.

Figs. 91 and 92 show debris from a steam treated sample of Fe - 8% Cu alloy and a sample of sintered Fe - 8% Cu alloy after 1000 passes at 9 Kgs load respectively.

In Fig. 91, Fe_3O_4 was produced as a plate-like debris with one smooth surface, (the face in sliding contact), and one rough surface, (the underlying oxide/metal interface). Fe_2O_3 shows granular shape. Fig. 92 shows all debris has the same sheet shape with rough surfaces, and in comparison with Fig. 91 this sheet shape debris is much bigger, because the sheets were produced from a sintered specimen which is almost pure Fe*. Because Fe is more ductile than iron oxide, they did not break under load during sliding and they look thinner.

Fig. 93 shows formation of wear sheet in the wall of the track of sintered Fe - 2% Cu alloy under 7 Kgs load.

* Probe analysis for iron in Fig. 92 showed average reading of 18900 and for Fig. 91 showed average of 21000 which is relatively higher amount of iron in iron-oxide particles (Fe_3O_4, Fe_2O_3).

Powder product materials are porous and these pores act as cracks especially open pores which are connected to a free surface.

Figs. 94 and 95 show the porosity network of surface and wall of specimen respectively. These figures reveal distribution of pores and bonds between the particles, (neck surfaces).

The easiest location for crack formation is the bond between the particles[195] and dislocation area (grain boundaries). Formation of a crack in a steam treated specimen will occur more readily, owing to the presence of many hard particles such as oxide and precipitated particles in the component, since the motion of mobile dislocations generated by the applied load may be locked by the particles or can be created during plastic deformation by the decohesion of the matrix/particle interface and by plastic flow of the matrix around a hard particle.

The tracks show, (Figs. 96a and 96b), transverse cracks on the wall and bottom of the scar with formation of detached wear sheets. These cracks are, remained pores, which were not removed completely by ploughing and those cracks that formed from neck surface by plastic deformation of the sub surface layers.

From the appearance of the crack it can be concluded that when the angle between neck and sliding direction is zero the possibility of crack formation is minimum, at 90^{o} the possibility is maximum and when $0<\alpha<90$ the possibility is moderate, due to opening up of particles in direction of slider.

6.10.9.2. Effect of variables on volume wear.

(i) Load and sliding distance.

It was shown in results that after 200 cm under any load, scar

width is mostly constant.

Figs. 97a and 97b are taper sections of Fe - 8% Cu after 1000 passes (cm) sliding distance in sintered and steam treated samples under a load of 5 Kgs.

It can be seen that material has deformed by the sliding of a loaded abrasive element on it. This deformation after 200 passes makes material work-hardened to a constant extent and there is no further wear loss at longer distance, provided that the material can withstand the load. Alternatively it could be possible that with a constant wear track, material collapsed as a result of complete propagation of cracks to the surface. These figures also show more deformation in sintered Fe - 8% Cu alloy.

Table 46 shows variation of sub-surface hardness with sliding distance. According to James et al[196] increase in hardness as a result of deformation may be due singly or in combination to:

(a) The development of a 'work hardening' dislocation network,

(b) strain-induced phase changes,

(c) strain-induced precipitation.

In the sintered steels examined[196], the formation of martensite within metastable austenite was found to be the principal mechanism giving rise to hardening during working.

(ii) Sintered and steam treated pure iron.

Percentage of open porosity in the sintered samples is greater than in steam treated samples. Thus the possibility of formation of a crack by plastic deformation in sintered specimens is higher. This causes more wear sheets formation and an increase in the wear rate in the sintered case.

Formation of oxide has straight relation to density (porosity) and density of tested samples is relatively high (D = 6.8 $^{g}/_{cc}$), so there is not enough passage for steam to the deeper parts of specimens. Also it was said[99 - 184] that at high oxidation temperature and high density the capillary inlets eventually become blocked by oxidation products and, since the access of oxidising reagent to the interior of the test piece is inhibited, a part of the internal surface ceases to take part in the oxidation process.

Fig. 98b (steam treated) shows less wear rate in comparison with Fig. 98a (sintered) under 3 Kgs load. By increasing the load to more than 6 Kgs, (Fig. 81), the situation is reversed. Because penetration depth of the abrasive element is greater than the maximum depth of oxide layer, abrasive element and abrasive particles run on sintered metal and the broken oxide between the sample and abrasive element acts as another abrasive on the metal. Thus as long as the indentor and abraded particles are running on oxide layer, (maximum 6 Kgs), wear rate in steam treated samples is less than that in sintered samples.

Figs. 99a and 99b show more wear damage in sintered and steam treated pure iron under 9 Kgs load in comparison with Figs. 98a

and 98b respectively.

(iii) Sintered and steam treated iron-copper alloys.

Presence of precipitated particles in steam treated alloys are the centres for nucleation of voids and cracks.

During steam treatment the concentration of precipitated particles around the pores which are filled by oxide is higher. Thus voids which formed by these particles grow and elongate through the oxide layer and through the neck surfaces to the free surface.

For this reason delamination is more in steam treated alloys than sintered (solid-solution) and iron steam treated.

Figs. 96a and 96b show increased wear damage in steam treated Fe - 4% Cu alloy under 5 Kgs load.

Figs. 100 and 101 show the formation of crack in walls and delaminated wear sheets in bottom of track in Fe - 6% Cu alloy under 5 Kgs load respectively. It is clear that percentage of damage in steam treated samples is more than in sintered samples.

(iv) Hardness - Wear relationship.

Presentation of Fig. 86 reveals that two alloys with the same hardness have different wear rates, and steam treated Fe - 4% Cu alloy is less resistant to abrasive wear than sintered Fe - 6% Cu alloy in the tested loads.

Thus it can be concluded that the hardness-wear relationship should be compared with the materials in identical conditions.

Figs. 84 and 85 present data using this basis of comparison. In steam treated iron-copper alloys, (three phases), or sintered alloys (single phases), higher hardness alloys have lower volume-wear. It is also apparent that sintered alloys with lower hardness have lower volume-wear than steam oxidised alloys with higher hardness.

6.10.9.3. Comparison with previous investigations.

From the results of Hewitt et al[2] in Fig. 22 it can be seen that MK 9 and MK 11 Tufftrided cast iron with 0.01 gr. and 0.055 gr weight loss, are the best combination for ring piston and liner material respectively. Replacement of cast iron for piston ring material with sintered Fe base material, (Fig. 23), gives the least weight loss in SP 20 with MK 24 (liner material) with 0.02 gr and 0.04 gr wear rate respectively.

By reference to Fig. 23 (part variation) it can be seen that steam treatment or oil impregnated SP 20 with MK 24 has lower weight loss, (almost 0.02 and 0.05 gr respectively) than just sintered SP 20.

Data recorded in Fig. 23, (part treatment), reveals that addition of 1% C to SP 20 followed by Tufftriding and oil impregnation provides a piston ring material which when used with MK 2 as liner material has the least or almost the same weight loss in comparison with cast iron as ring piston and liner material.

Because of different sintered materials and conditions of test there is no possible quantitative comparison between the results of Hewitt

et al[2] and the present work, but a general qualitative comparison confirms that steam treatment can improve wear resistance of sintered iron base alloys which have no copper content.

Comparison of abrasive and adhesive wear is not possible due to different mechanisms. In the former case the mechanism depends mostly on the hardness, abrasion of loose particles, fracture and in the latter case it depends mostly on welding of loose particles and oxidation. The most important difference, is that in the former case relation between wear rate and load is linear but in the latter case there is transition between wear rate and loads.

Thus a quantitative comparison between previous work on sintered material during adhesive wear with the present investigation is not possible. However, the general conclusion from other investigations[174] is that wrought and sintered pure iron have almost identical wear properties and excellent results have been obtained during sliding against grey cast iron.

Addition of 2% Cu alloy[175] to sintered pure iron has not much effect on adhesive wear properties, but addition of 2% Cu improves abrasive wear resistance of sintered pure iron, (present investigation).

Amsallem[173] et al reported that friction and wear behaviour of sintered iron ($D = 7\ ^{g}/_{cc}$, A.H.C. Powder) are similar during adhesive wear.

Comparison of previous results[2, 173, 174, 175] confirms that wear properties of sintered iron base materials have mostly the same wear properties as wrought Fe base alloys.

7. General Conclusions.

1. Pre-alloyed iron/copper powders, up to 8% Cu, shrink during sintering.

2. Addition of copper up to 8% Cu increases the resistance to oxidation of iron.

3. Resistance to oxidation in furnace cooled samples is less than in water quenched samples.

4. After a certain time, dependent on initial porosity, (density), surface pores become sealed and open porosity decreases to a very low level. Further oxidation occurs only at the surface because steam can no longer permeate through the interconnected pore network to the interior of the specimen.

5. Effect of steam treatment is more pronounced in lower densities.

6. The oxidation induced increase in weight of porous iron specimens cannot be described by a quadratic equation. This confirms the findings of Fedorchenko et al[184].

7. Oxidation of iron and iron-copper alloys is accompanied by a marked increase in hardness and considerable changes in internal structure.

8. At a steam treatment temperature of 525^{o}C for iron and iron-copper alloys the oxide formed is mostly Fe_3O_4 and Fe_2O_3 but copper is not oxidised by steam at 525^{o}C.

9. Precipitation hardening response of iron-copper alloys up to 8% Cu is higher in higher density.

10. There is no incubation period before precipitation starts in any alloy.

11. As the amount of copper increases, the time required to attain peak hardness decreases.

12. The peak hardness increases with copper percentage up to 6% Cu but there is a slight decrease in the 8% Cu alloy.

13. Steam treatment as an ageing treatment improves the hardness of Fe - 2% Cu, but by increasing the copper up to 8% hardness decreases in comparison with ageing of these alloys in inert gas.

14. The increment of hardness during steam treatment is slightly more pronounced in furnace cooled samples than water quenched samples.

15. Steam treatment improves the radial crushing strength of sintered iron but this treatment decreases the R.C.S. of sintered iron-copper alloys up to 6% Cu and in 8% Cu has no advantage or disadvantage.

16. R.C.S. in sintered samples increases as the amount of copper increases, (maximum up to 6% Cu).

17. Resistance to abrasive wear in sintered and steam treated samples increases as the amount of copper increases.

18. Steam treatment improves the resistance to abrasive wear of iron under lower loads (maximum 6 Kgs) but under higher loads has a disadvantageous effect.

19. Steam treatment decreases the resistance to abrasive wear of sintered iron-copper alloys.

20. Increasing the hardness increases the resistance to abrasive wear, but it should be noticed that improving of hardness must be in the same condition.

21. From the point of physical properties such as dimensional change, oxidation resistance and mechanical properties such as hardness, radial crushing strength, wear properties, and consideration of economic points such as price of copper and equipment for separate treatment, steam treatment of furnace cooled samples of Fe - 2% Cu alloy have the optimum properties.

8. Suggestions for Further Work.

1. Influence of copper addition on steam oxidation of cast iron/copper alloys.

2. Effect of carbon (up to 0.8%) on dimensional changes of samples during sintering.

3. Effect of changes in speed on abrasive wear of samples.

4. Examination of resistance of samples to corrosion and fatigue.

5. Investigation of precipitation and steam oxidation of Distalloy (Fe - 1.5% Cu - 1.7% Ni - 0.5% Mo).

6. Influence of alloy additions on kinetics of steam oxidation.
   In this connection it would be of considerable interest to compare the effects of alloy elements which stabilize Ferrite (e.g. Mo,P, Si, Sn) with those which stabilise austenite (e.g. C, Mn, Cu, Ni).

9. REFERENCES

1. The metals society symposium on the corrosion and protection of porous metal compacts., 19 April, 1977, Loughborough University.

2. J.C. Hewitt, A. Clayton and G.J. Cox, Powder Metallurgy, 18 (1975) 168.

3. Jaeger from I.V. Kragelskii (1965)325 "Friction and Wear" Butterworths, London.

4. I.V. Kragelskii (1965) 328 "Friction and Wear" "London Butterworths".

5. T.S. Eyre and F. Wilson J.A.S. of Lubrication Engineers 29 (1973) 65.

6. R.L. Sands and C.R. Shakespeare (1966) Powder Metallurgy, "London George Newnes Limited".

7. A. Blainey, Symposium on Powder Metallurgy 1954 (Special Report No. 58) 223, 1956 London (Iron and Steel Institute.

8. N. Collasi and N. Fongi, Metallurgy I'tal 46 (1954) 111.

9. C.S. Smith and E.W. Palmer, Trans. A.I.M.E. 105 (1933) 133.

10. C.S. Smith and E.W. Palmer, Trans. A.I.M.E. 105 (1933) 165.

11. P.W. Taubenblat, Intern. Journal Powder Metallurgy 10(1974) 169.

12. R.E. Smallman (1970) 514 Modern Physical Metallurgy, London 3rd edition, "Butterworths".

13. W.J.M. Salter, J.I.S.I., 204 (1966) 478.

14. L. Harrison and R.H.T. Dixon, Powder Metallurgy, No. 9 (1962) 247.

15. R.T. Holcomb, Intern. Journal Powder Metallurgy 2 (1972) 69.

16. J.H. Eggeston and F.H. Spangler (1972) CM72 - 812 "Heat treatment of powder iron products"

17. V.B. Phadke and B.L. Davies, Powder Metallurgy International 9 (1977) 168.

18. K. Razavizadeh (1977), M. Phil. Thesis, Brunel University, Metallurgy Dept., Uxbridge, Middx.

19. J.F. Watkinson, Powder Metallurgy, No. 1, 2 (1958) 13.

20. P. Ulfgummeson, Powder Metallurgy 15 (1972) 67.

21. Davy-Loewe Ltd., Bedford, England.

22. U.S. Patent 1,986,197.

23. U.S. Patent 2,027,532.

24. C. Goetzel, 1 (1949) 218 "Treatise on Powder Metallurgy" Interscience Publishers Ltd., London.

25. U.S. Patent 2,754,193.

26. B. Meddings, H.R. Huffman, and V.N. Mackiw 23 (1963) 28, "New types of metal powder", Metallurgical Society Conferences ed. H.H. Hausner, Gordon and Breach Science Publisher, New York, London.

27. J.A. Lund, W.R. Irvine and Y.N. Mackiw, Powder Metallurgy, No. 10 (1962) 218.

28. U.S. Patent 2,754,194.

29. A.F. Krovic, Progress in Powder Metallurgy 28 (1972) 53.

30. L.F. Narris and G. Passavano, J. Amer. Ceram. Soc., 46 (1963), 449.

31. W.D. Kingery and M. Berg, J. Appl. Physics 26 (1955) 1205.

32. R.L. Coble, J. Amer. Ceram. Soc., 41 (1958) 55.

33. G.C. Kuczynski, Acta. Met., 4 (1956) 58.

34. G. Passavano, A.S.T.I.A. Rep. (AD - 207974) (1957 - 58).

35. H.J. McQueen and G.C. Kuczynski, J. Amer. Ceram. Soc., 45 (1962), 343.

36. A.L. Pramatis and L. Seigle (1960) 71, Powder Metallurgy ed. W. Leszynski Interscience Publishers New York, London

37. W.W. Mullins, Journal Appl. Physics, 28 (1957) 333.

38. L. Seigle, A.L. Pranatis, and L.S. Castlemon (1958), "Fundamentals of Sintering III" Report No. Sep.250 Sylvania Research Labs.

39. J. Wulf, R. Volterra and J. Libsch (1942) 379, Powder Metallurgy, ed. J. Wulf., Amer. Soc. for Metals, Cleveland.

40. M. Cohen, D. Bakalar, and F.S. Buffington, Aug. (1949), "Self diffusion in iron", Symposium on the Physics of Powder Metallurgy, Sylvania Electric Product Inc., Bayside, Long Island, New York.

41. I. Jenkins, Powder Metallurgy 7 (1964) 68.

42. Y. Trudel and R. Angers, The Intern. . . Journal Powder Metallurgy 11 (1975) 5.

43. J.E. Elliot, Metallurgia, 59 (1959) 17.

44. D. Berner, H.E. Exner, and G. Petzow, Modern development in Powder Metallurgy 6 (1973) 237.

45. Y. Trudel and R. Angers, Modern development in Powder Metallurgy 6 (1973) 305.

46. T. Krantz, International Journal Powder Metallurgy 5 (1969), 35.

47. G.S. Smith, Trans. A.I.M.E. 175 (1948) 15.

48. L.H. Vanvlack, J. Metals 3 (1951) 251.

49. V.B. Phadke and B.L. Davies, Intern. Journal Powder Metallurgy 13 (1977) 253.

50. P.F. Pulvernet, 11th Annual Meeting Met. Powder. Assoc., 1 (1955), 94.

51. Bockstiegel, Stahl und Elsen 79 (1959) 1187.

52. J.E. Elliot, Metallurgia, 52 (1955) 226.

53. D. Yarnton and M. Argyle, "A Practical Course in Powder Metallurgy" published by Cassell Ltd.

54. A.L. Ruoff (1973) 237, "Materials Science" Prentice-Hall Inc., Englewood Cliffs, New Jersey.

55. C.J. Leadberter, L. Northcott, and Hargreaves, Symposium on Powder Metallurgy, (1947) 15, (Special Report No. 38), London (Iron Steel Inst.).

56. G. Zoff, Powder Metallurgy No. 7 (1961) 218.

57. G. Arthur, J. Inst. Metals 83 (1954 - 55) 329.

58. A.S.T.M. Standard on metal powders and metal powder products (1961) 2nd edn. Cleveland, Ohio. (Amer. Soc. Test. Mat.)

59. W.C. Winegard and C. Cand. Journal of Physics 30 (1952) 422.

60. T.S. Hutchinson and D.C. Baird (1963) 70 "The Physics of engineering solids" J. Wiley & Sons Inc.

61. K. Hauffe, Wiss Z. Univ. Greifswald 1(1951-52)1

62. E. Brauns and A. Rahmel, Werkst. U. Korrosion Mannkeim 7 (1956) 448.

63. H. Pefiffer and K. Hauff Z. Metallk 43(1952) 364.

64. G. Sainfort, Mem. Sci. Rev. Metall. 56(1959) 704.

65. O. Kubaschewski and B.F. Hopkins (1962) 22 "Oxidation of Metals and Alloys" "Butterworths, London.

66. L.S. Darken and R.W. Gurry. J. Amer. Chem. Soc. 67 (1945) 1398.

67. Perkofstad (1966) 21 "High temperature oxidation of metals" John Wiley & Sons, Inc., New York.

68. D.M. Young and B.M.W. Trapnell (1964) chemisorption "Butterworths".

69. D.O. Hayward and B.M.W. Trapnell (1964) "chemisorption" "Butterworths".

70. P.G. Shewmon (1969) 372 "Transformation in metals" "McGraw Hill".

71. J. Benard, F. Gronlund, and M. Duret. Z. Elektrochem 63(1956) 799.

72. O. Kubaschewski and B.F. Hopkins (1962) 82 "Oxidation of metals and alloys". "Butterworths London".

73. C. Wagner (1951) 153 "Atom movements" Amer. Soc. Metals, Cleveland.

74. M.H. Davies, M.T. Simnad and C.F. Birchenal, J. of Metals. Trans. A.I.M.E. 3 (1951) 889.

75. J. Paidassi, Acta. Metallurgica 6 (1958) 184.

76. O. Kubaschewski and B.F. Hopkins (1962) 110 "Oxidation of Metals and Alloys" "Butterworths London".

77. L.B. Pfeil, J. Iron and Steel Inst. 123 (1931) 123.

78. B.M. Larson and K. Heindlhofer, Trans. Amer. Soc. Steel. Treat. 21 (1933) 865.

79. J.E. Stead, J. Iron Steel Inst. 94 (1916) 243.

80. L.B. Pfeil. J. Iron and Steel Inst. 119 (1929) 501.

81. E. Scheil and K. Kiwit, Archiv. Eisenhuttenwesen 9 (1936) 405.

82. W. Hatfield, J. Iron Steel Inst. 115 (1927) 483.

83. R. Hales and A.C. Hill, Corrosion science 12 (1972) 843.

84. D. Caplan and M. Cohen, Corrosion science 6 (1966) 321.

85. I. Svedung, B. Hammar, and N.G. Vannerberg, Oxid. Metals 6 (1973) 1.

86. Z. Bret, Werkstaffe U. Korr 22 (1971) 386.

87. B. Hammar and N.G. Vannerberg, Scandinavian J. Metallurgy 3 (1974) 123.

88. T.H. Sanderson (1974.5) 109 Heat treatment of metals, "Steam atmosphere heat treatment" Leeds and Northrup Ltd.

89. O. Kubaschewski and B.E. Hopkins (1962) 270 "Oxidation of Metals and alloys". "Butterworths London".

90. C. Upthegrave and D.W. Murphy, Trans. Amer. Soc. Steel. Treat. 21 (1933) 73.

91. O. Kubaschewski and E.L. Evans (1958) "Metallurgical thermo-chemistry" "Pergamon, London".

92. J.D. Fast 1 (1965) 32, "Intraction of metals and gases" Macmillan & Co. Ltd.

93. M. Farber, J. Electro Chem. Soc. 106 (1959) 751.

94. N.B. Pilling and R.E. Bedworth, J. Inst. Met. 29 (1923) 529.

95. W.E. Campbell and U.B. Thomas, Trans. Electro Chem. Soc. 91 (1947) 623.

96. F.V. Lenel (1942) 518 Powder Metallurgy ed. J. Wulf (The Amer. Soc. for Metals) Cleveland, Ohio.

97. Kanopicky, from F.W. Regel 24 (1963) 91 "Engineer Digest".

98. P. Franklin and B.L. Davies, Powder Metallurgy 20 (1977) 11.

99. K. Razavizadeh and B.L. Davies, Powder Metallurgy 22 (1979) 187 - 192.

100. B.J. Sunter and B.D. Cosh, Powder Metallurgy 17(1974) 319.

101. F.L. Spangler (1955) 103 Iron Powder Parts improved by heat treatment, Leeds and Northrup Ltd.

102. H.Y. Hansker and H.C. Stumpf 27 (1965) 271 - 330, The Sorby Centennial Symposium on the history of Metallurgy., Metallurgical Society Conference, Gordon and Breach, New York.

103. P.D. Merica, R.G. Waltenberg and H. Scott, Trans. Met. Soc. A.I.M.E. 64 (1920) 41.

104. R. B. Nicholson, J. Sheffield Univ. Met. Soc. 5 (1966) 19.

105. J.D. Verhoeven (1975) 384, Fundamentals of Physical Metallurgy, John Wiley & Sons, New York, London, Sydney, Toronto.

106. K.C. Russell (1970) 219 - 268. Phase-transformation. American Society of Metals, Park, Ohio.

107. R.N. Nabarro, Proc. Roy. Soc. A 175 (1940) 519.

108. R.B. Nicholson and J. Nutting, Pil. Mag. 3 (1958) 531.

109. R. B. Nicholson (1968) 269, Phase transformation A.S.M., Ohio.

110. F. Seitz, L'Etat Solide, Institute Solvay (1952) 401.

111. D. Turnball and H.N. Treafties, Acta. Met. 5 (1957) 534.

112. H. Herman, J.B. Cohen and M.E. Fine, Acta. Met. 11(1963) 43.

113. P.G. Shewmon (1969) 308, Transformation in Metals, McGraw Hill, 1st edition.

114. R.B. Nicholson and J. Nutting, Acta. Met. 9 (1961) 332.

115. G. Thomas and J. Nutting (1956) 57., "The mechanism of phase transformation in metals", London.

116. C.E. Birchenall (1950) "Atom movement" A.S.M. Seminar.

117. J.B. Clark, Acta. Met. 12(1964) 117.

118. R.B. Nicholson (1963) 861, "Electron microscopy and strength of crystal", Interscience, New York.

119. J.D. Verhaeven (1975) 398, Fundamental of Physical Metallurgy, John Wiley & Sons, New York, London, Sydney, Toronto.

120. E.C. Rollason, J. Inst. Metals, 86 (1957 - 58) 77.

121. V. Gerold, Zeischrift Fur Metallkunde, 45 (1954) 593 - 599.

122. W. Koster, L'Etate Solide "9th Solvay Conference Brussels" (1952) 235 - 271.

123. W. Gruhl and O. Gruhl, Metall. 8 (1954) 20 - 23.

124. E. Orawon, A.I.M.E. (1956) 69.

125. A. Kelly and R.B. Nicholson, Prog. Mat. Sci., 10 (1961) 151.

126. E. Hornbogen and R.C. Glenn, Trans. Amer. Inst. Min (Metall) 218 (1960) 1064.

127. H. Buchholz and W. Koster., Stahl U. Eisen, 50 (1930) 687.

128. T. Norton, A.I.M.E. Trans. 116 (1935) 386.

129. W.D. Swanson and J. Gordon, J. of the Iron and Steel Inst., Feb. (1964) 104.

130. E. Hornbogen, Acta. Met. 10 (1962) 525.

131. T. Federighi, Acta. Met. 6 (1958) 379.

132. E. Hornbogen, Z. Metallk 50 (1959) 70.

133. A. Guinier, Z. Metallk 43 (1952) 217.

134. C. Zener, J. Appl. Physics 20 (1949) 950.

135. B. Ilschner, Arch. Eise huttenu, 26 (1955) 59.

136. A. Stern, L. Levin, and S.F. Dirnfeld, Internal. Journal of Powder Metallurgy 8 (1972) 20.

137. M. R. Krishnadev and I. Lenay, J.I.S.I. 62 (1970) 458.

138. T. Watanabe, Rep. Govt. Industries Research 7 (1958) 105, Inst. Nagoya, Japan.

139. V.B. Phadke and B.L. Davies, Powder Metallurgy International 9 (1977) 64.

140. E.A. Wilson, J.I.S.I., 206 (1968) 164.

141. F.P. Bowden and D. Tabor (1950), The friction and lubrication of solid. London, Oxford University Press.

142. P. Freeman (1962) 121, Lubrication and Friction, London, Sir Isaas Pitman and Sons Ltd.

143. H. Czichos, Tribology (1974) 14 - 20.

144. J. Halling (1975) 95 and 114 Principles of Tribology, "Macmillan Press Ltd."

145. J. Archard, Wear 2.6 (1959) 438 - 455.

146. Z. Kolazsvary and E. Filep, Wear 13 (1969) 54.

147. W. Hirst, Engineering, 209 (5427)(1970) 477.

148. T.S. Eyre, M.Sc. Thesis (1967) University of London

149. N.C. Welsh, Phil. Trans. Roy. Soc. 257 (1965) 31 - 70.

150. E. Rabinawicz, L.A. Dunn and P.G. Russell, Wear 4 (1961) 345 - 355.

151. N.P. Suh, Wear 25 (1973) 111.

152. E. Rabinawicz, (1966), Friction and Wear of Material, Wiley, London.

153. F.A. McClintoch, S.M. Kaplan, and C.A. Berg, Inter. J. Fract. Mech. 2 (1966) 614.

154. T.S. Eyre and D. Maynard, Wear 18 (1971) 301 - 310.

155. T.F.J. Quinn, Proc. Inst. Mech. Engrs. 182(N)(1967 - 681) 201.

156. A.J.W. Moore and D. Tabor, C.S.I.R. (Australia) Tribophysics, Report A 46 (1942).

157. M.J. Hordon, A.S.T.M., STP 431 (1967) 109 - 127.

158. I.V. Kragelskii (1965) 91, "Friction and Wear" "Butterworths London"

159. M.C. Shaw, NASA Lewis Research Center, Cleveland, Ohio, TM-X-52748, (Nov. 1968).

160. T.S. Eyre, Tribology Intern. Oct. (1976) 203.

161. M.M. Khrushchov (1957) 655 - 659, Proc. Conf. Lub. and Wear, London I.M.E.

162. J. Larson- Badse, Trans. Metallurgical Soc. Am. Inst. Min., Met. Pet. Eng. 236 (1966) 1461 - 1466.

163. K.H.R. Wright, Tribology 2 (3) (1969) 152.

164. R.C. Richardson, Wear 11 (1968) 245.

165. T.S. Eyre, Wear 34 (1975) 383 - 397.

166. M.M.Khrushchov (1950) 52, Friction and Wear in Machines, b, Izd. Akad. Nauk, USSR.

167. M.J. Neale, I. Mech. E. (1970-71) 21-32.

168. S.A. Tsukerman (1965) 112 Powder Metallurgy "Pergamon Press Ltd".

169. F. Shahparast and B.L. Davies, Wear 50(1978) 145 - 153.

170. H. Odenhausen, Chem. Zentralbl, 11 (1944) 154.

171. A. Lazos, Private Communication.

172. M. Yu. Balshin (1948), Powder Metallurgy "Mashgiz".

173. C. Amsallem, A. Gaucher, and G. Guilhot, Wear 23 (1973) 97 - 112.

174. T.S. Eyre and R.K. Walker, Powder Metallurgy, No. 1 (1976) 22 - 30.

175. T.S. Eyre, Private communication.

176. F.W. Regel, Engineers Digest 24 (1963) 91.

177. A.M. Glauert, (1975) 137, Practical methods in electron microscopy "North Holland Publishing Company".

178. D.W. Tomkins and D.S. Coleman, Powder Metallurgy 19 (1976) 53.

179. Domtar Process. DOMTAR Chemicals Ltd., Metal powders Division, Montreal, Canada.

180. P.M. Kelly, J. Aust. Inst. Metals 16 (1971) 104.

181. J.D. Verhoeven (1975) 516, Fundamentals of Physical Metallurgy "John Wiley & Sons, New York, London, Sydney, Toronto.

182. R. Armstrong, I. Codd, R.M. Douthwaite and N.J. Petch. Phil. Mag. 7 (1962) 45.

183. S. Weining and E.S. Machlin Trans. A.I.M.E. 209 (1957) 843.

184. I.M. Fedorchenko, A.P. Lyapunav and V.V.Skorokhad, Powder Metallurgy No. 12 (1963) 27.

185. L.A. Girifalco, (1964) 36 Atomic migration in crystals "Bloisdell Publishing Company".

186. J.W. Martin, (1968) 19, Precipitation hardening "Pergamon Press".

187. P.G. Schewmon (1969) 303, Transformation in metals "McGraw Hill Book Company".

188. A. Stosuy, 7 (1972) 203, "Atlas of microstructures of industrial alloy". 8th ed. Ed. Taylor Lyman, A.S.M., Ohio.

189. F.B. Pickering, "Low alloy steels" I.S.I. No. 114 (1968) 131.

190. Technical Report No. 1031, A.D. Smith - Inland Inc. Powder. Met. Division, Box 1634, Milwaukee, WI 53201.

191. J.B. Newkirk (1959) 100, "Precipitation from solid solution", American Society for Metals, Cleveland, Ohio.

192. I.R. Harris and P.C. Varley, J. Institute of Metals, 82 (1954) 379 - 393.

193. J.D. Embury and R.B. Nicholson, Acta. Met. 13 (1965) 403.

194. J.T. Burwell, Wear, 1 (1957) 119 - 141.

195. P. Franklin and B.L. Davies, Powder Metallurgy No. 1 (1978) 7.

196. B.A. James, J.E. Garner and G.T. Brown, Powder Metallurgy 20 (1977) 221 - 226.

APPENDIX 1

$$H_2O \rightleftharpoons H_2 + \tfrac{1}{2}O_2$$

$$Kp = \frac{PH_2O}{PH_2 \cdot PO_2^{\frac{1}{2}}}$$

$$PO_2 = \left(\frac{PH_2O}{PH_2}\right)^2 \cdot \frac{1}{Kp^2} \qquad (a)$$

Approximate values of Kp can be found with the help of standard Tables[92] which give the value at 25°C and by using the equation:

$$\text{Log } Kp = -\frac{\Delta H^o_{298}}{4.575T} + \frac{\Delta S^o_{298}}{4.575} \qquad (b)$$

where ΔH^o is enthalpy of formation in K $^{cal}/_{mole}$

ΔG^o is Free enthalpy in K $^{cal}/_{mole}$

ΔS^o is entropy in $^{cal}/_{deg\ mole}$

ΔS^o can be calculated using the formula:

$$\Delta S^o = \frac{\Delta H^o - \Delta G^o}{T}$$

For example, at 1000°K, by using the value at 25°C and equation (b) $Kp \approx 10^{10}$. Substituting in (a) gives:

$$PO_2\,(1000^oK) \approx 10^{-20}\left(\frac{PH_2O}{PH_2}\right)^2$$

With equal partial pressures of hydrogen and water vapour we have

$$PO_2\,(1000^oK) = 10^{-2}\ \text{atm.}$$

The use of gas mixture, $(H_2 + H_2O)$, presents a fine method of adjusting very low but accurately known oxygen pressure.

By using this formula it is possible to find the value of $\frac{PH_2O}{PH_2}$ for a metal that reacts with water vapour at any temperature.

For example $3Fe + 4H_2O \rightleftharpoons Fe_3O_4 + 4H_2$

	ΔH^o_{298}	ΔG^o_{298}
Fe_3O_4	- 267	- 242
H_2O	- 57.8	- 54.63

$\Delta H^o_{298} = - 267 + 4 \times 57.8 = - 35800$ cal.

$\Delta G^o_{298} = - 242 + 4 \times 54.63 = - 23500$ cal.

$\Delta S^o = \frac{- 35800 + 23500}{298} = - 41.2$ cal/deg mole

By putting these values in equation (b) we obtain

$$\text{Log}\left(\frac{PH_2}{PH_2O}\right)^4 \simeq \frac{35800}{4.575T} - \frac{41.2}{4.575}$$

$$\text{Log}\left(\frac{PH_2O}{PH_2}\right)^4 \simeq - \frac{7825}{T} + 9.05$$

Where T is the Absolute Temperature in the experiment.

When T = 798K, $\text{Log}\left(\frac{PH_2O}{PH_2}\right)^4 = 0.75$ and $\text{Log}\left(\frac{PH_2O}{PH_2}\right) = - 0.18$

Thus, $\text{Log}\left(\frac{H_2O}{H_2}\right) = \text{Log Kp} = - 0.18.$

For the reaction of $2Cu + H_2O \rightleftharpoons Cu_2O + H_2$

the following values are valid, according to standard table at 25^oC.

$\Delta H^o = - 40 + 57.8 = 17800$ cal

$\Delta G^o = - 35.0 + 54.6 = 19600$ cal

$\Delta S^o = \frac{- 1800}{298} = - 6.04$ cal/deg mole

Substitution in equation (b) gives

$$\text{Log}\left(\frac{PH_2O}{PH_2}\right) = \text{Log Kp} = \frac{3890}{T} + 1.32 \Longrightarrow \frac{3890}{798} + 1.32 \Longrightarrow 6.14$$

NOTE:

If the standard free energy, $\Delta G^o_T = - RT \log Kp$ in a reaction between a metal and water vapour at a special temperature is negative (Copper at

$525^{o}C \Longrightarrow \Delta G^{o}_{798} = - R \times 798 \times 6.14 = - 4899.7R$) it means that reaction proceeds to reduction of oxide and if it is positive (Iron at $525^{o}C \Longrightarrow \Delta G^{o}_{798} = - R \times 798 \times - 0.18 = + 143.6R$) it means it will oxidise the metal. When Kp, $(\frac{PH_2O}{PH_2})$, is unity the standard free energy is zero.

APPENDIX 2

Fig. 60 shows Vickers hardness as a function of weight gain for pure iron of D = 6.8 $^{g}/_{cc}$ at different times of steam treatment.

Fig. 59 shows the peak hardness of four alloys by ageing in inert gas and steam. Time to peak hardness in inert gas and steam can be found from Figs. 57 and 58.

In Fe - 2% Cu after 25 minutes of ageing in steam the weight gain is 1.5% and the hardness during ageing in inert gas is 160 H.V. (Fig. 57a). From Fig. 60 the hardness value for pure iron due to weight gains of 0% and 1.5% are 48 and 90 H.V. respectively. The hardness increase due to steam oxidation alone is 42 H.V. units. Therefore the hardness of Fe - 2% Cu alloy on ageing for 25 minutes in steam is expected to be (160 + 42 = 202), but hardness by steam treatment at peak (25 minutes) is 182. Thus about 90% of precipitation hardening can be achieved by steam treatment.

In Fe - 4% Cu

Steam treatment hardness at peak (15 minutes) = 160 H.V.

Aged hardness at peak (15 minutes) = 180 H.V.

Weight gain after 15 minutes = 0.9%.

Hardness of pure iron with 0.9% weight gain = 73 H.V.

Thus 73 - 48 = 25 H.V. is due to formation of oxide

180 + 25 = 205 H.V. is maximum hardness by precipitation and oxidation

$\frac{160}{205}$ x 100 = 78% of precipitation hardening can be achieved.

In Fe - 6% Cu

Steam treatment hardness at peak (10 minutes) = 180 H.V.

Aged hardness at peak (10 minutes) = 240 H.V.

Weight gain after 10 minutes = 0.84%

Hardness of pure iron with 0.84% weight gain is 72 H.V.

Thus 72 - 48 = 24 H.V. is due to formation of oxide

240 + 24 = 264 H.V. is maximum hardness by precipitation hardening and oxidation.

$\frac{180}{264}$ x 100 = 68% of precipitation hardening can be achieved.

In Fe - 8% Cu.

Steam treatment hardness at peak (5 minutes) = 170 H.V.

Aged hardness at peak (5 minutes) = 224 H.V.

Weight gain after 5 minutes = 1.2%

Hardness of pure iron with 1.2% weight gain = 84 H.V.

Thus 84 - 48 = 36 H.V. is due to formation of oxide.

224 + 36 = 260 H.V. is maximum hardness by precipitation hardening and oxidation.

$\frac{170}{260}$ x 100 = 65% of precipitation hardening can be achieved.

APPENDIX 3

Rockwell indentor specification:

A right circular cone with a circular tip of 0.2 mm ± 0.01 mm radius, and included angle of cone = 120^{o} ± 20' was used as abrasive.

Volume wear:

The actual shape of track must be the same as indentor shape (ABC) but owing to repeating the indentor on a constant length, the horizontal facing of wear track would be AXYC (solid line).

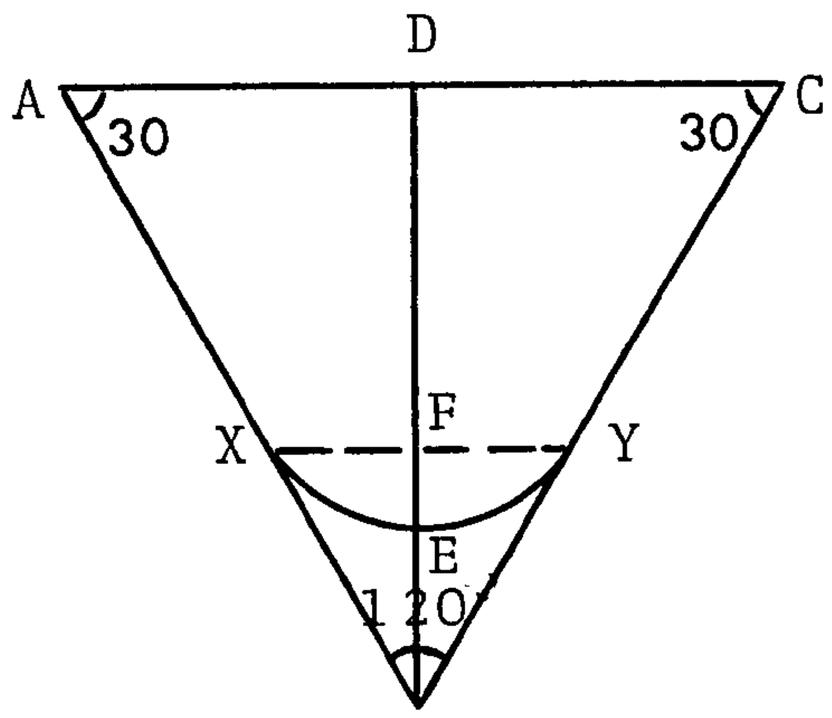

B

When the track width exceeds 0.138 mm (XY = 0.138 by measurement from Fig. 89) and if AC is the track width then the area of the track is

Area of ΔABC - area of ΔXBY + area of XFYE.

(i) Area of ΔABC = area of ΔABD + area of CBD

$$= 2 \times \tfrac{1}{2}BD \times AD = BD \cdot \left(\frac{\text{track width}}{2}\right)$$

$$= 2 \times \tfrac{1}{2} \tan 30 \times AD \times AD$$

$$\text{Area of } \Delta ABC = \tan 30 \times (AD)^2$$

(ii) Area of $\Delta XBY = 2 \times \frac{1}{2}(BF) \times \frac{XY}{2}$ but $\frac{XY}{2} = 0.069$ mm

$= 2 \times \frac{1}{2} \times \tan 30 \times 0.069 \times 0.069.$

$= 2 \times \frac{1}{2} \times \tan 30 \times (0.069)^2 = 275 \times 10^{-7} cm^2$

(iii) Area of XFYE = Area of segment - Area of ΔXYZ

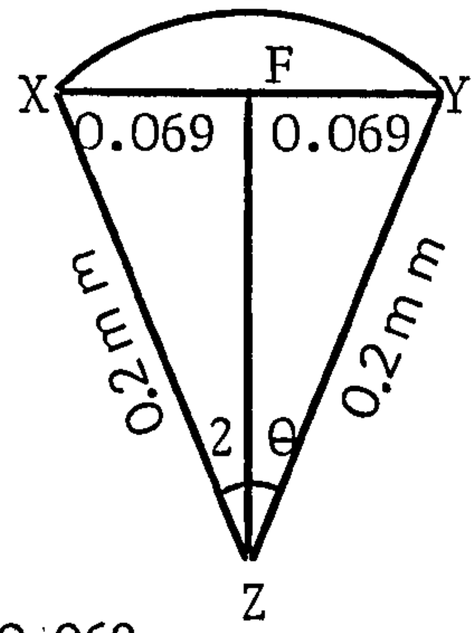

$\text{Sin } \theta = \frac{0.069}{0.2} = 0.345 = 20^o, 18' \Longrightarrow 2\theta = 40^o, 36'$

1. Area of segment $= \frac{\Pi r^2 \times 40^o, 36'}{360^o} = 0.014 \text{ mm}^2$

2. Area of ΔXYZ = 2 x area of ΔXFZ

$= 2 \times \frac{1}{2} \times ZF \times 0.069$

$ZF = \sqrt{(0.2)^2 - (0.069)^2} = 0.188$ mm

$\therefore$ Area of DXYZ $= 2 \times \frac{1}{2} \times 0.188 \times 0.069 = 0.01297 \text{ mm}^2$

Area of track $= 0.57 \times (AD)^2 - (275 \times 10^{-7} - 103 \times 10^{-7})$

Thus area of track $= 0.57 \times (AD)^2 - 172 \times 10^{-7} \text{ cm}^2 = S$

Volume wear = Area of Track x Length of Track (1 cm)

$= S \times 1 \Longrightarrow V$

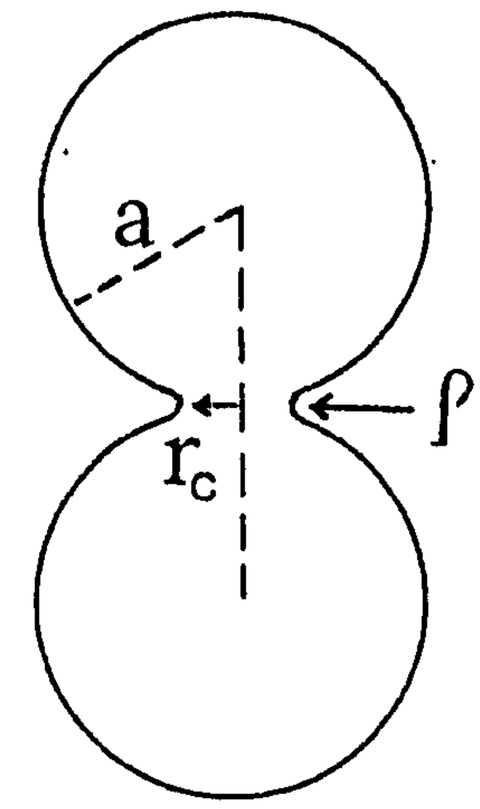

Fig. 1. Neck Formation

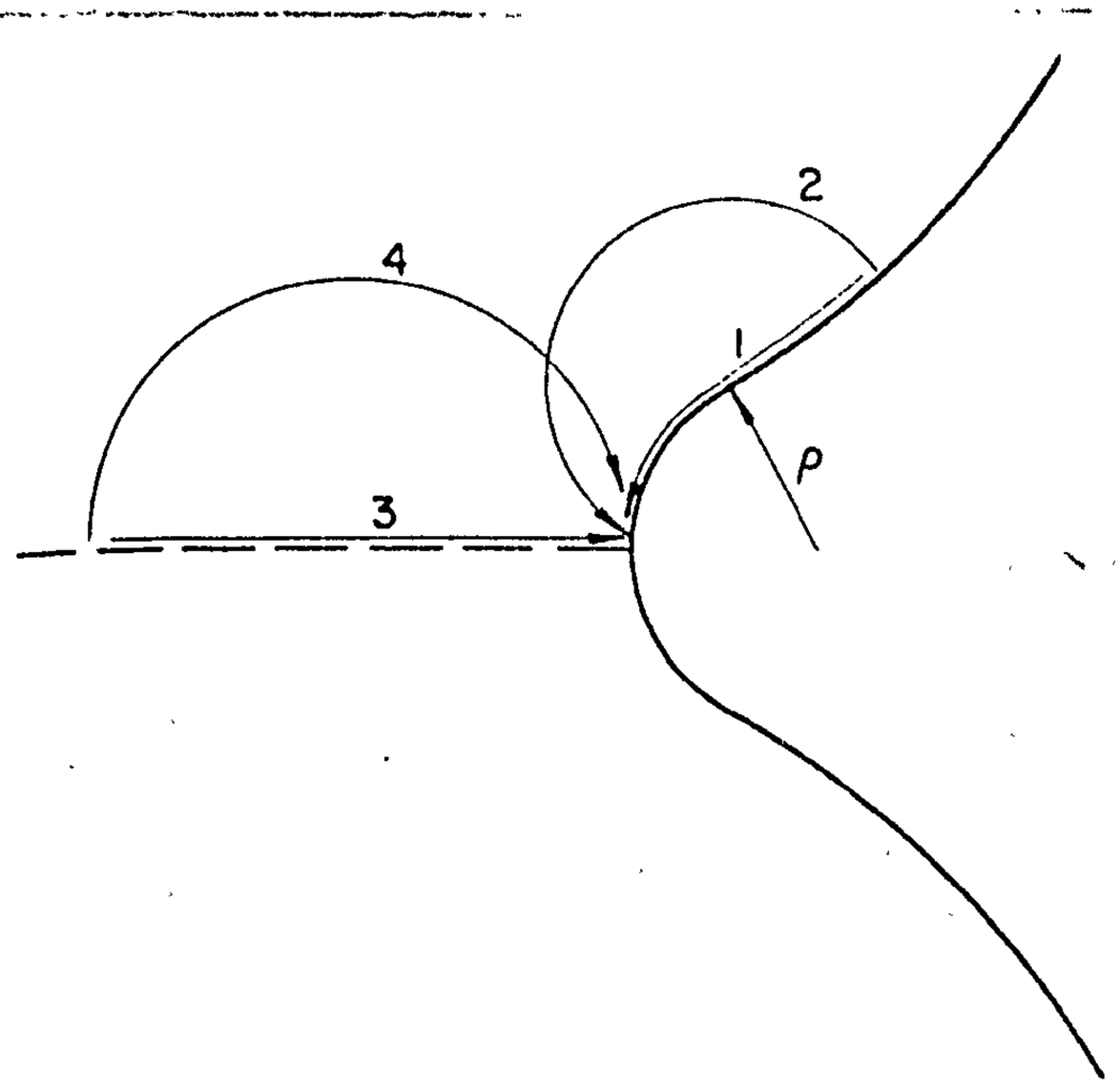

Fig. 2. Flux paths in sintering process

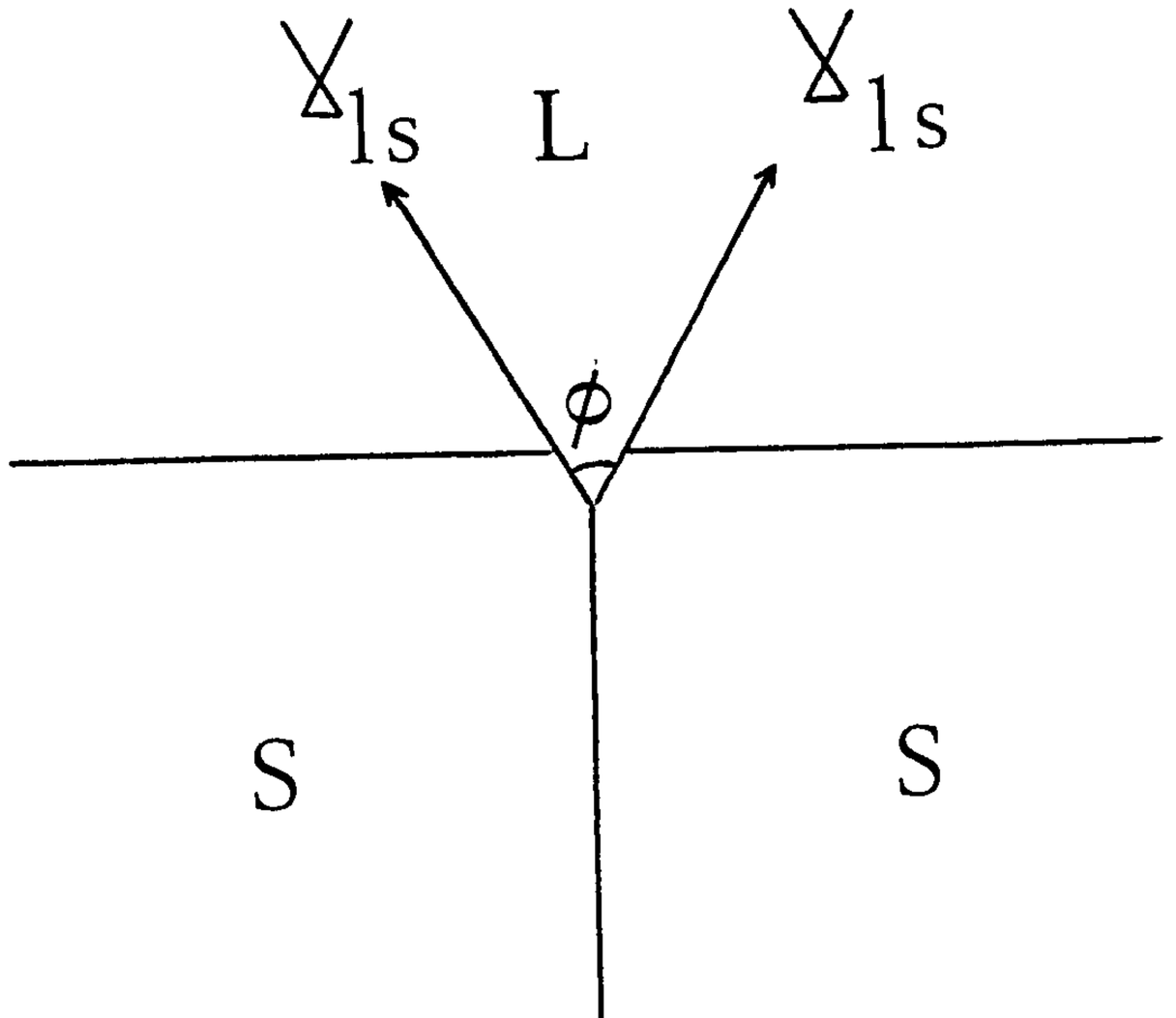

Fig. 3. Dihedral angle formed at junction of grain boundary and liquid.

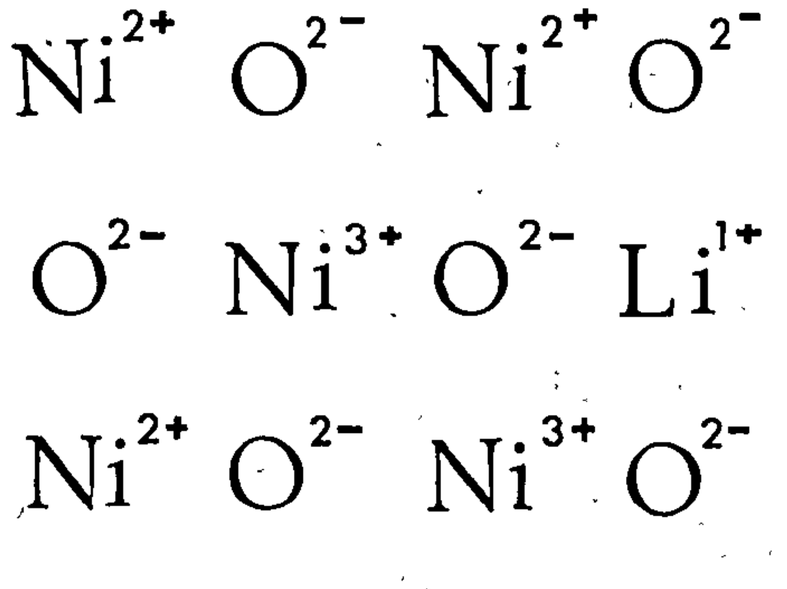

Fig. 4a. Defect structure of an NiO-LiO_2 oxide.

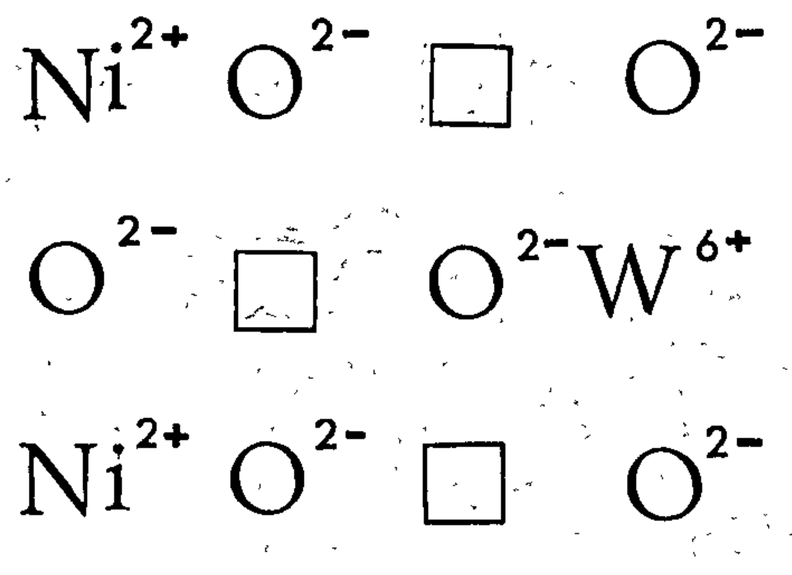

Fig. 4b. Defect structure of an NiO-WO_3 oxide

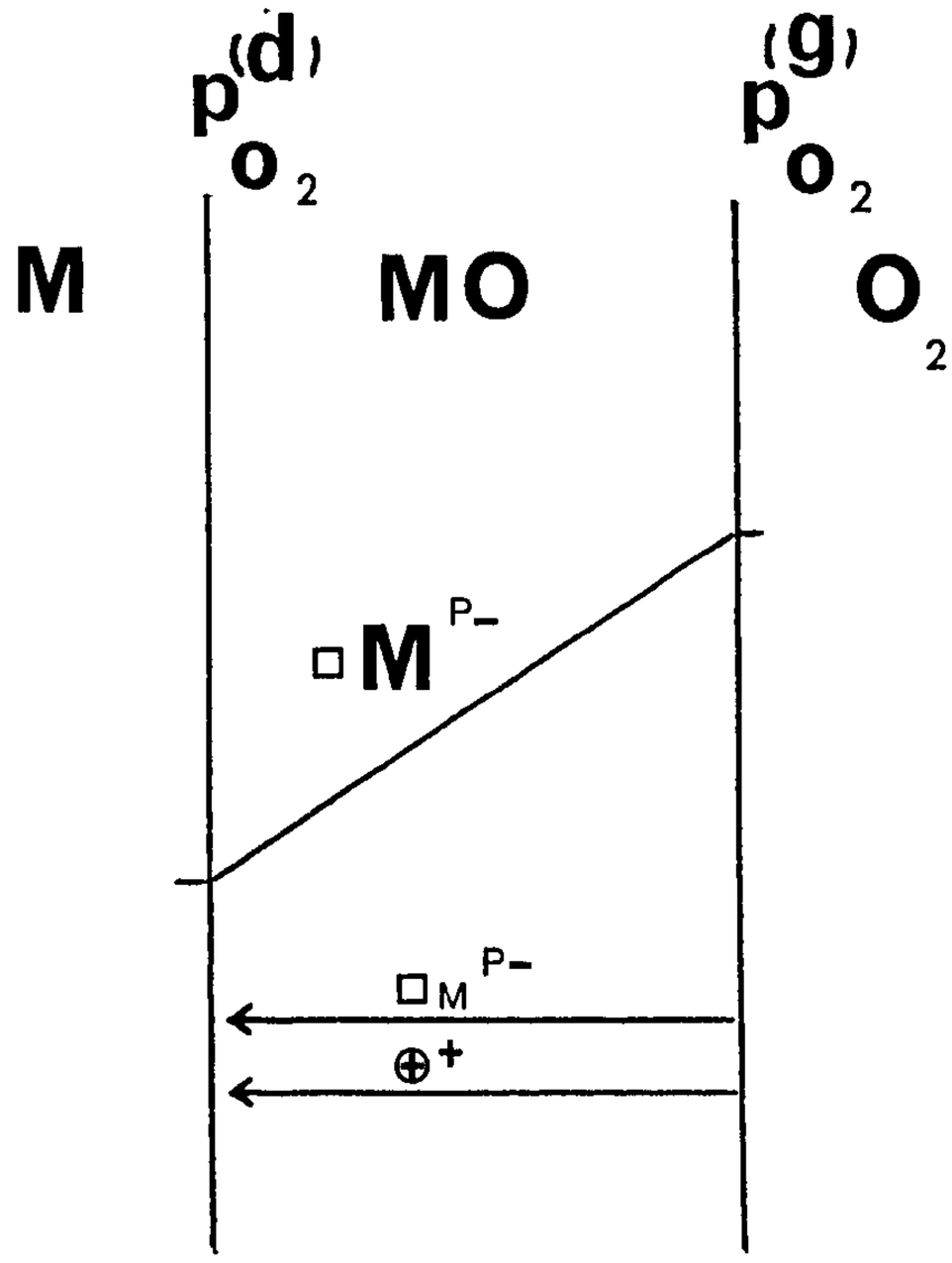

Fig. 5a. Concentration gradient in an oxide scale containing metal ion vacancies.

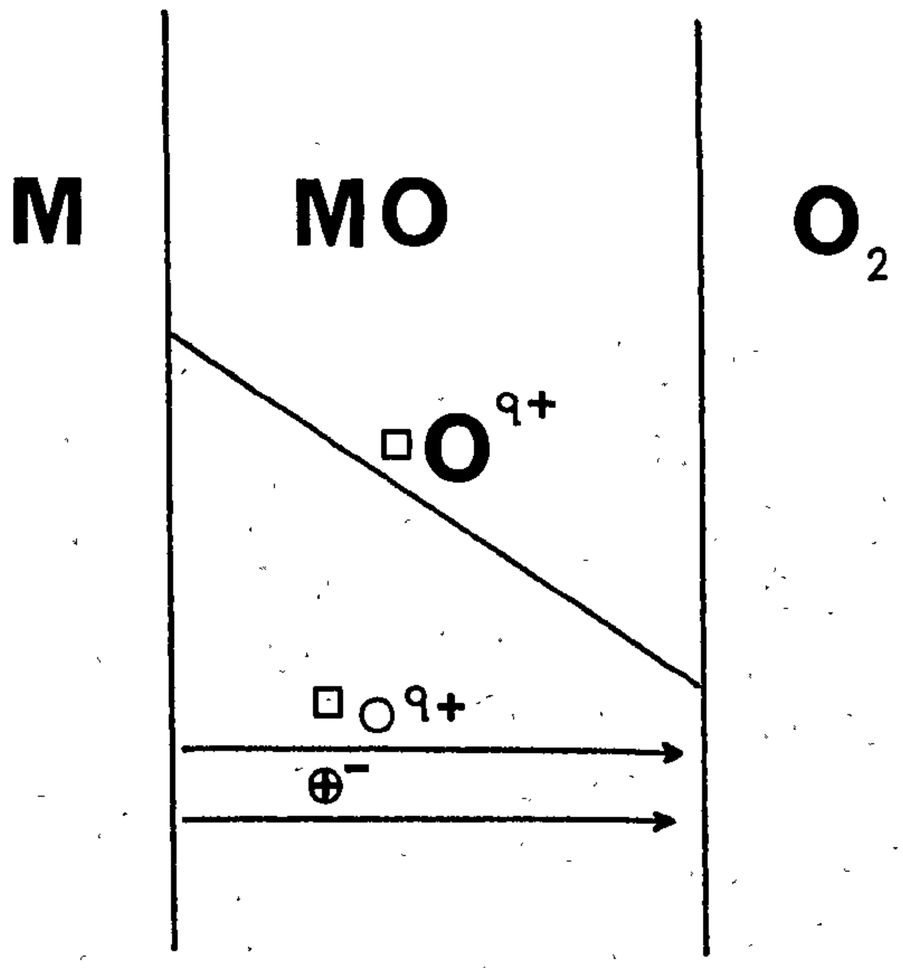

Fig. 5b. Concentration gradient in an oxide scale containing oxygen ion vacancies.

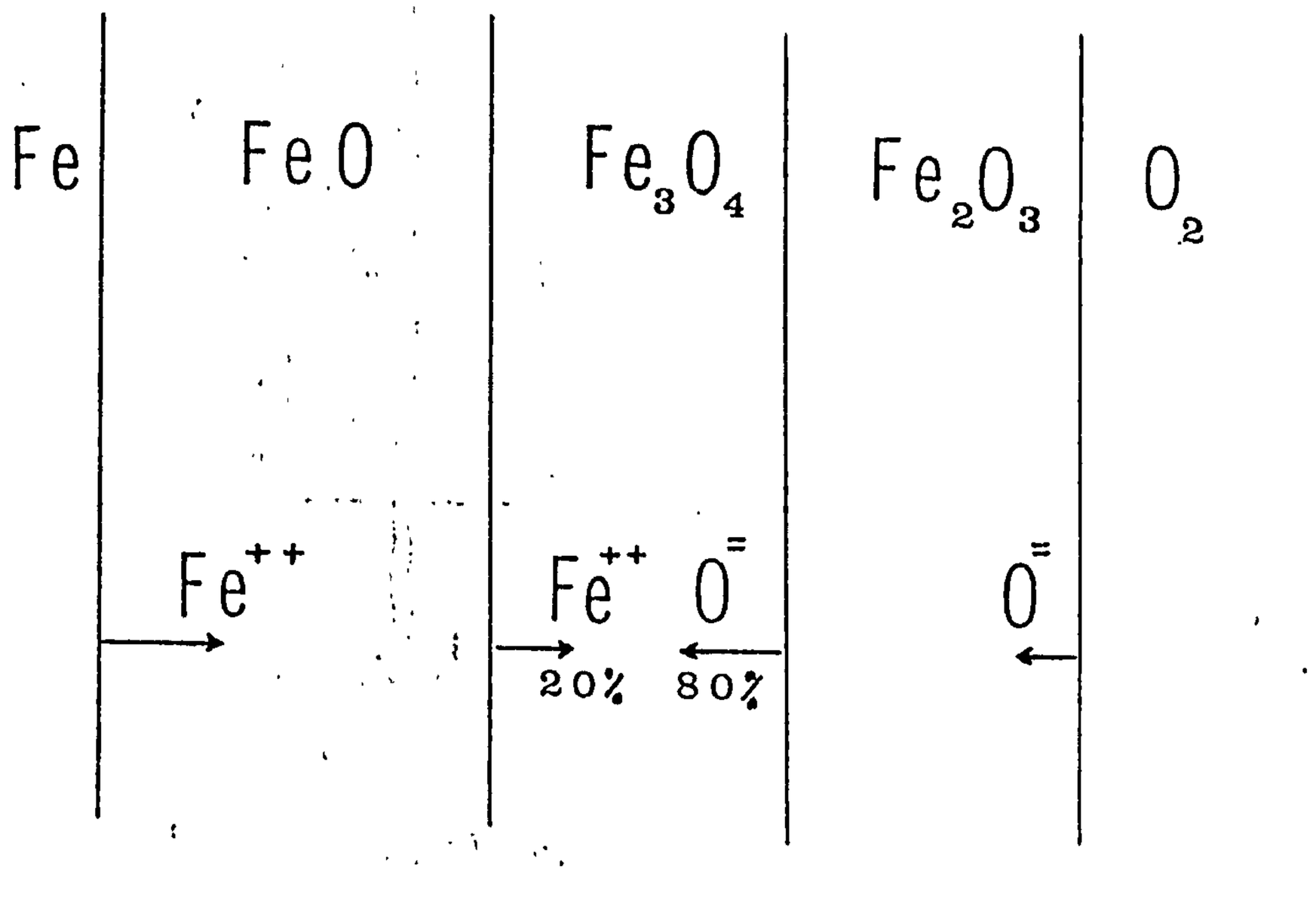

Fig. 6 . Oxidation process in iron

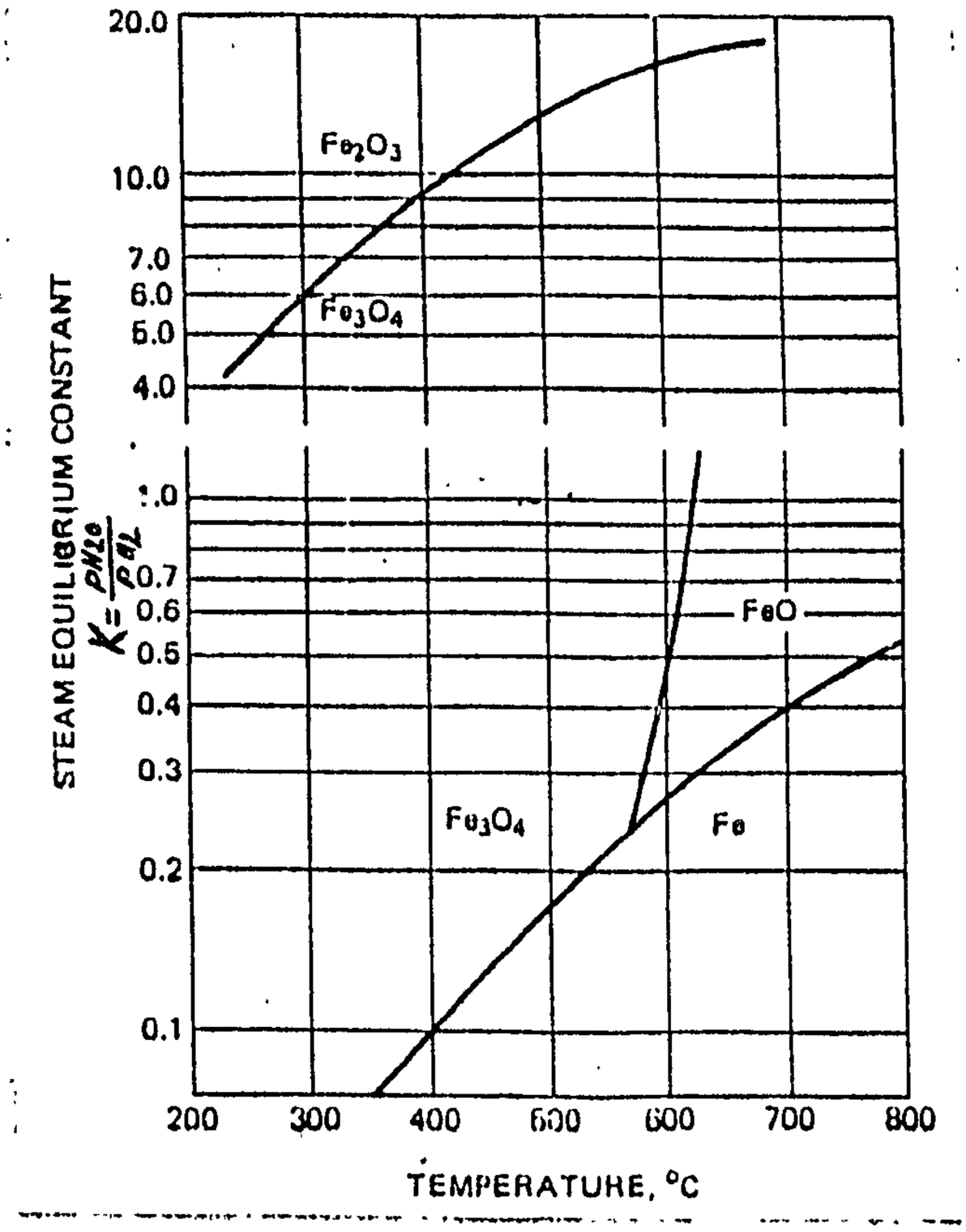

Fig. 7. Regions of the formation of FeO, Fe_2O_3, and Fe_3O_4.

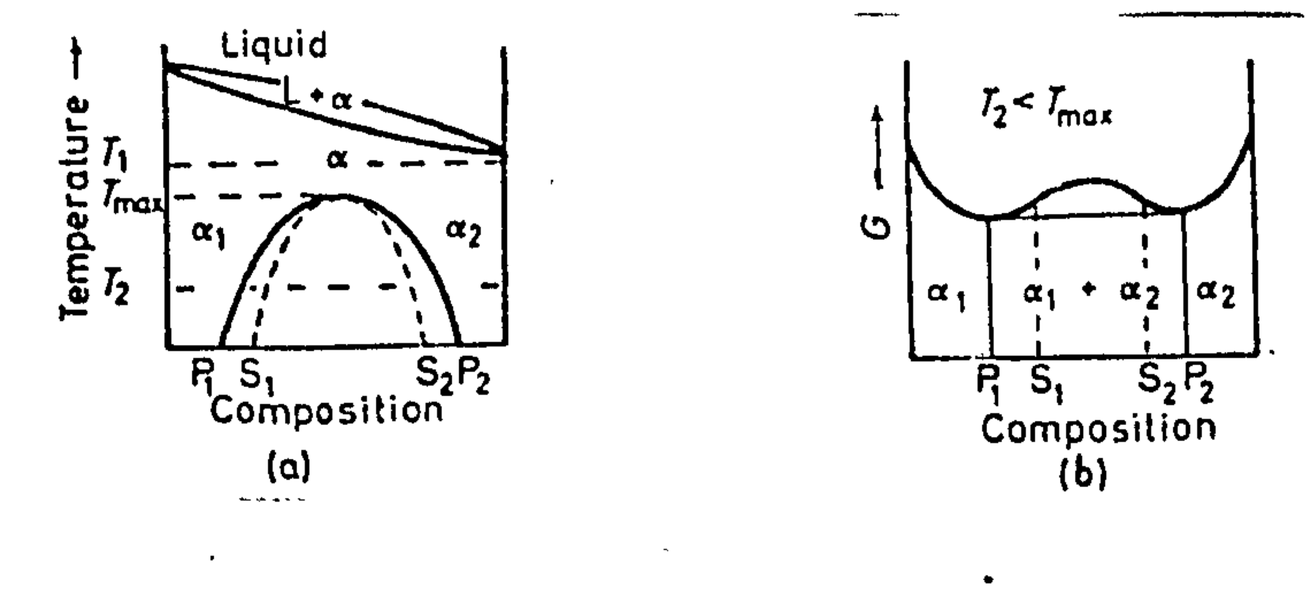

Fig. 8. a): Equilibrium diagram containing miscibility gap in the solid state.

b): At T_2, the free energy curve possesses a central maximum and this gives rise to two inflexion points, S_1 and S_2. The common tangent between the minimum points defines the composition of the equilibrium phases, P_1 and P_2.

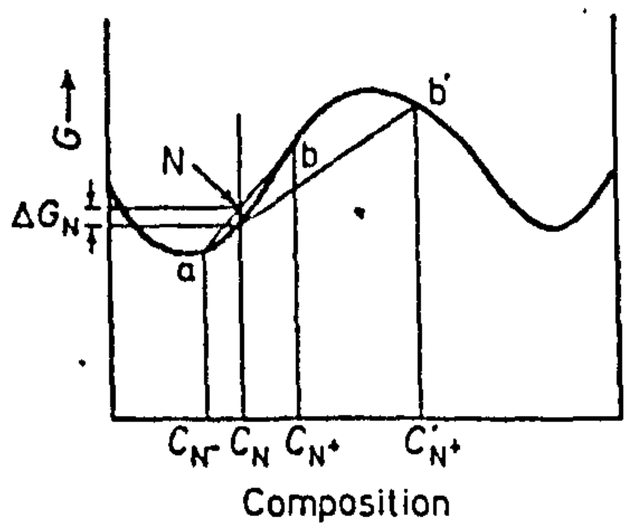

Fig. 9a. Schematic drawing showing the positive activation energy required for a composition fluctuation in alloys located outside the spinodal region.

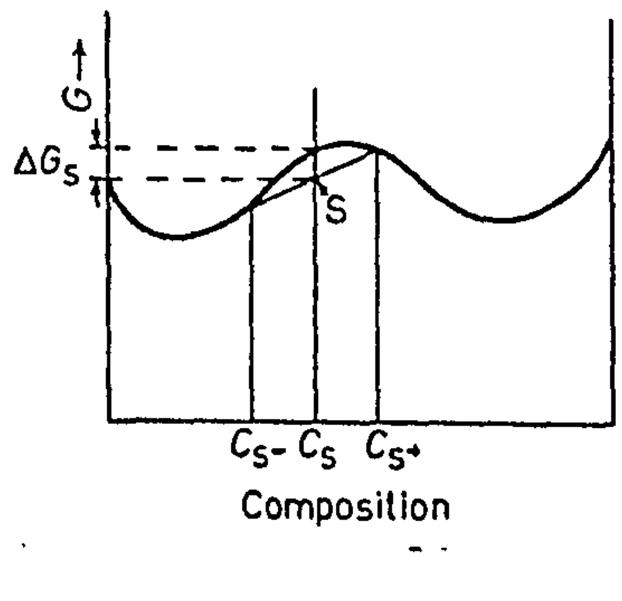

Fig. 9b. Schematic drawing showing the decrease in free energy of an alloy undergoing spinodal decomposition.

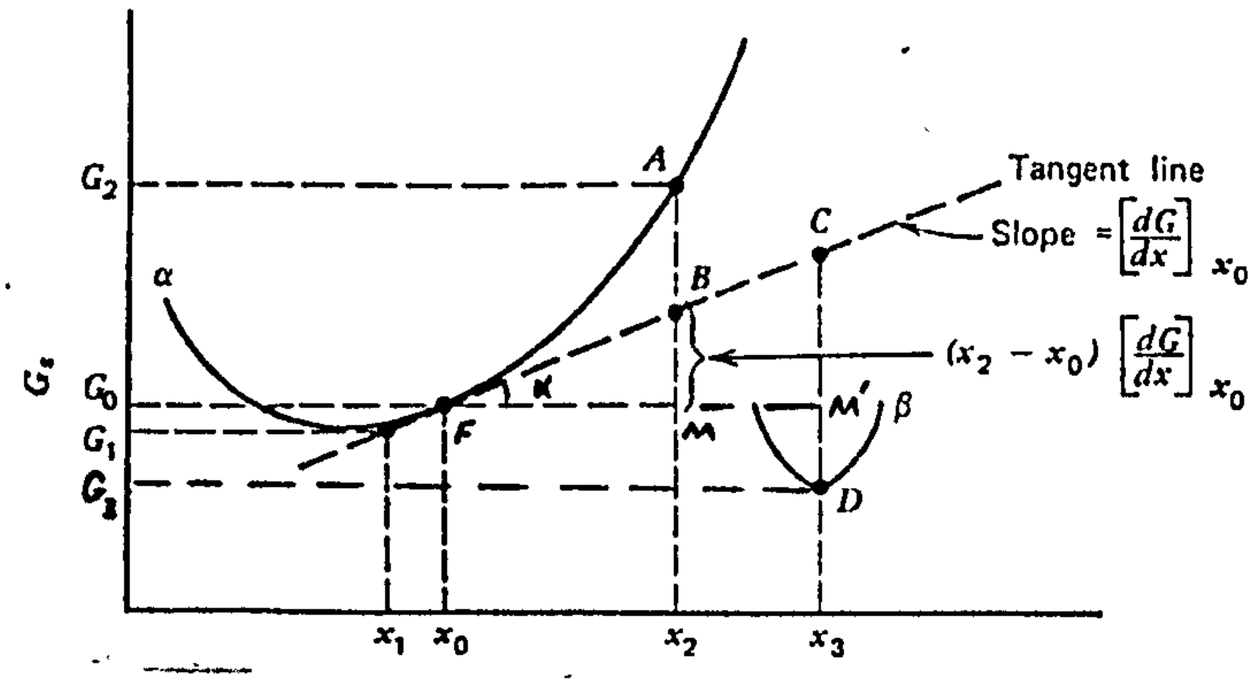

Fig. 10. Construction for graphical determination of the free energy of the initial precipitate.

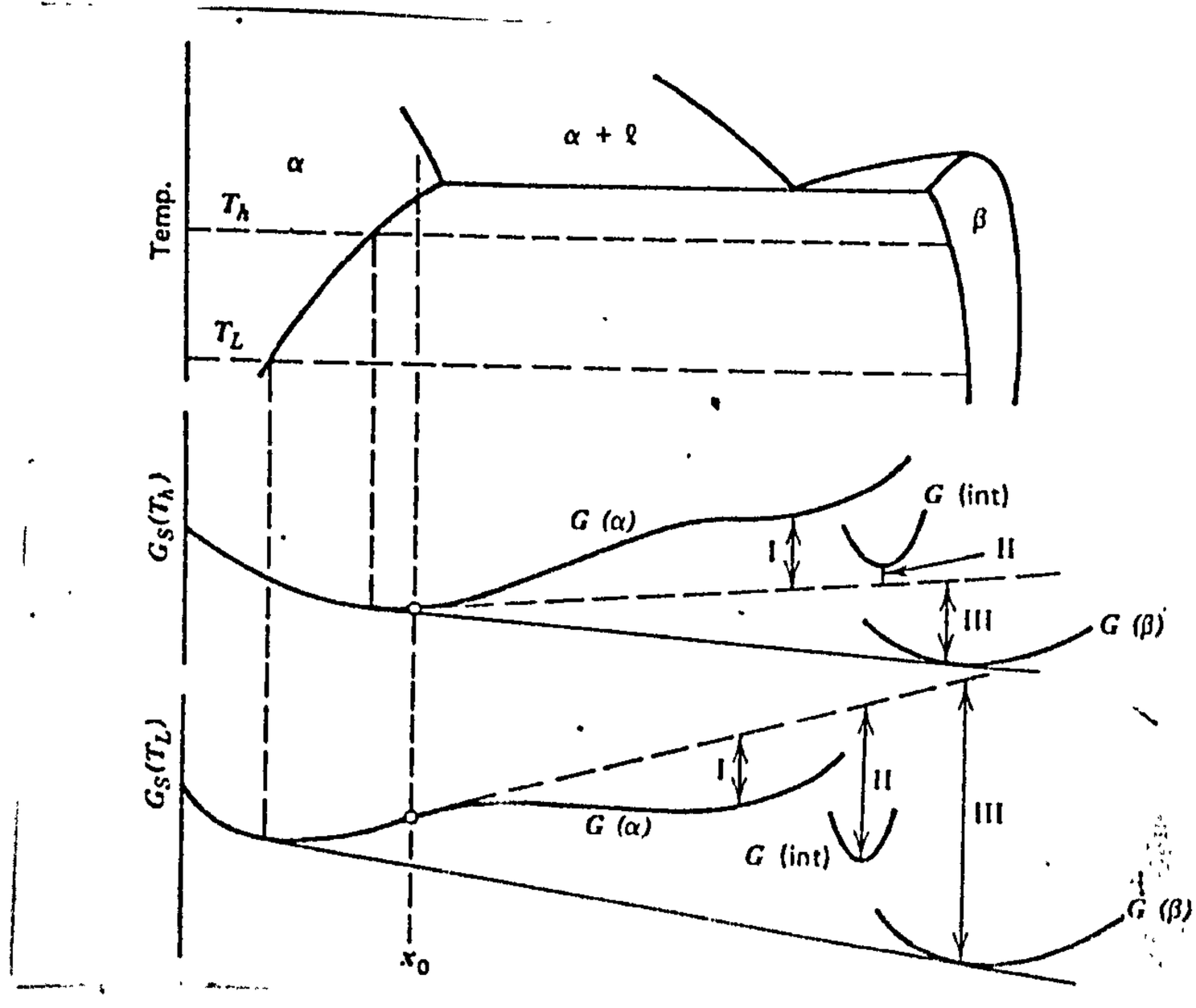

Fig. 11. Construction illustrating the free energy of initial precipitates of (I) GP zone, (II) intermediate precipitate, and (III) the equilibrium precipitate at two different temperatures, T_h and T_L.

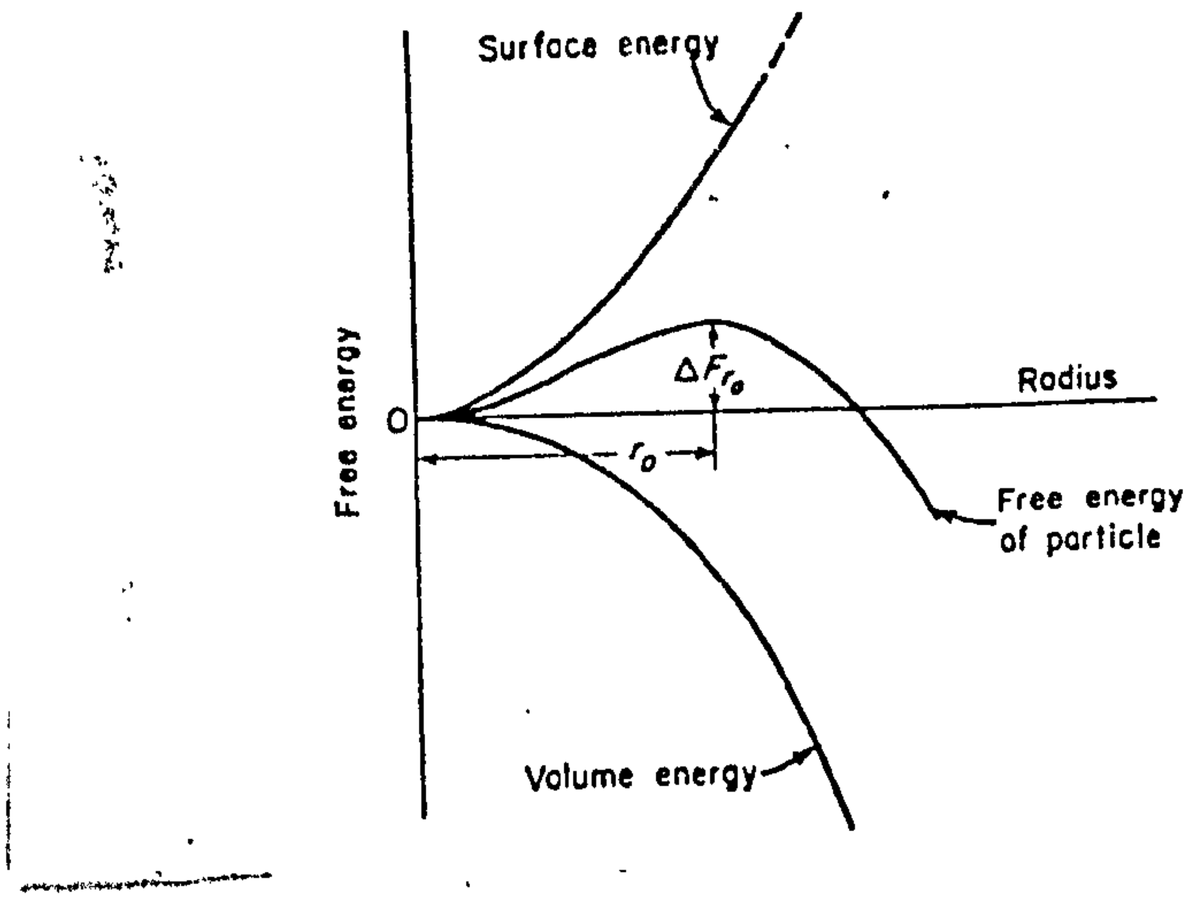

Fig. 12. Free energy of a precipitate particle as a function of its radius.

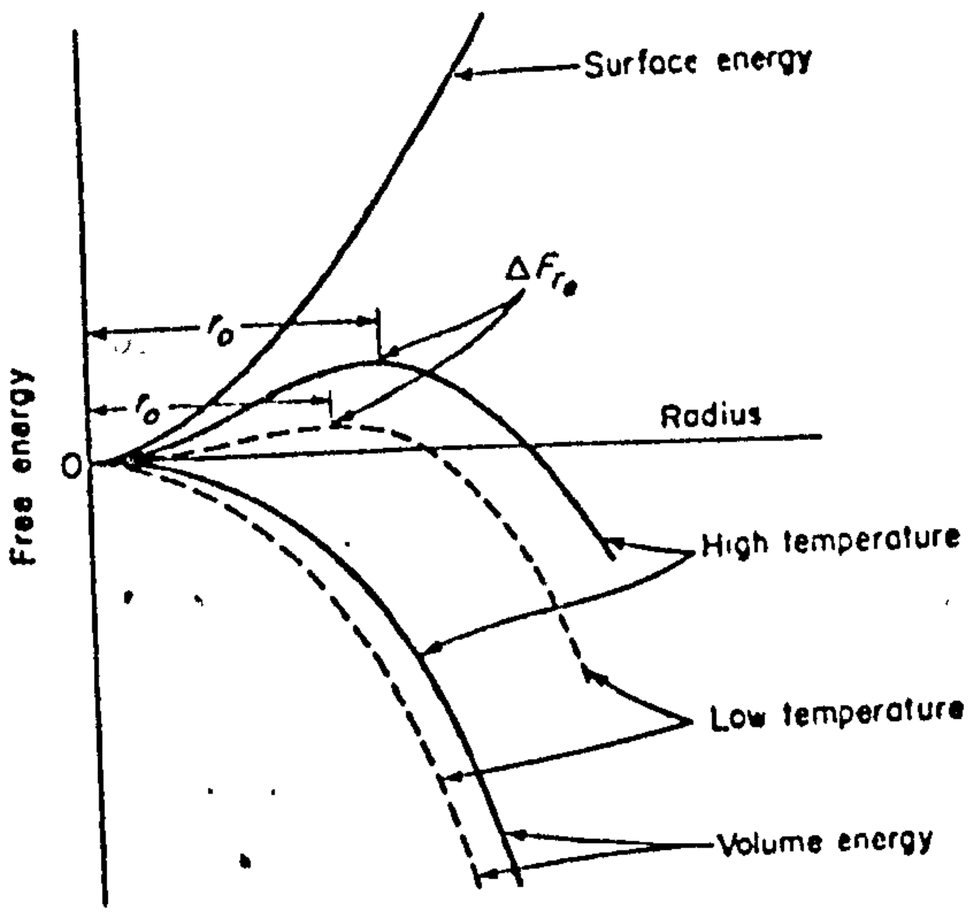

Fig. 13. Effect of temperature of precipitation on the free energy of a precipitate particle as a function of its radius.

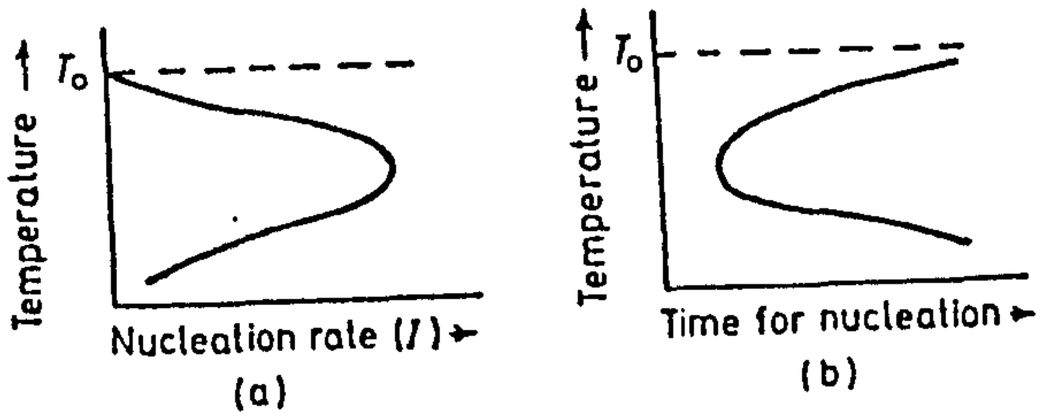

Fig. 14. a. Rate of nucleation, I, as a function of temperature.
b. Time required for initiation of nucleation as a function of temperature.

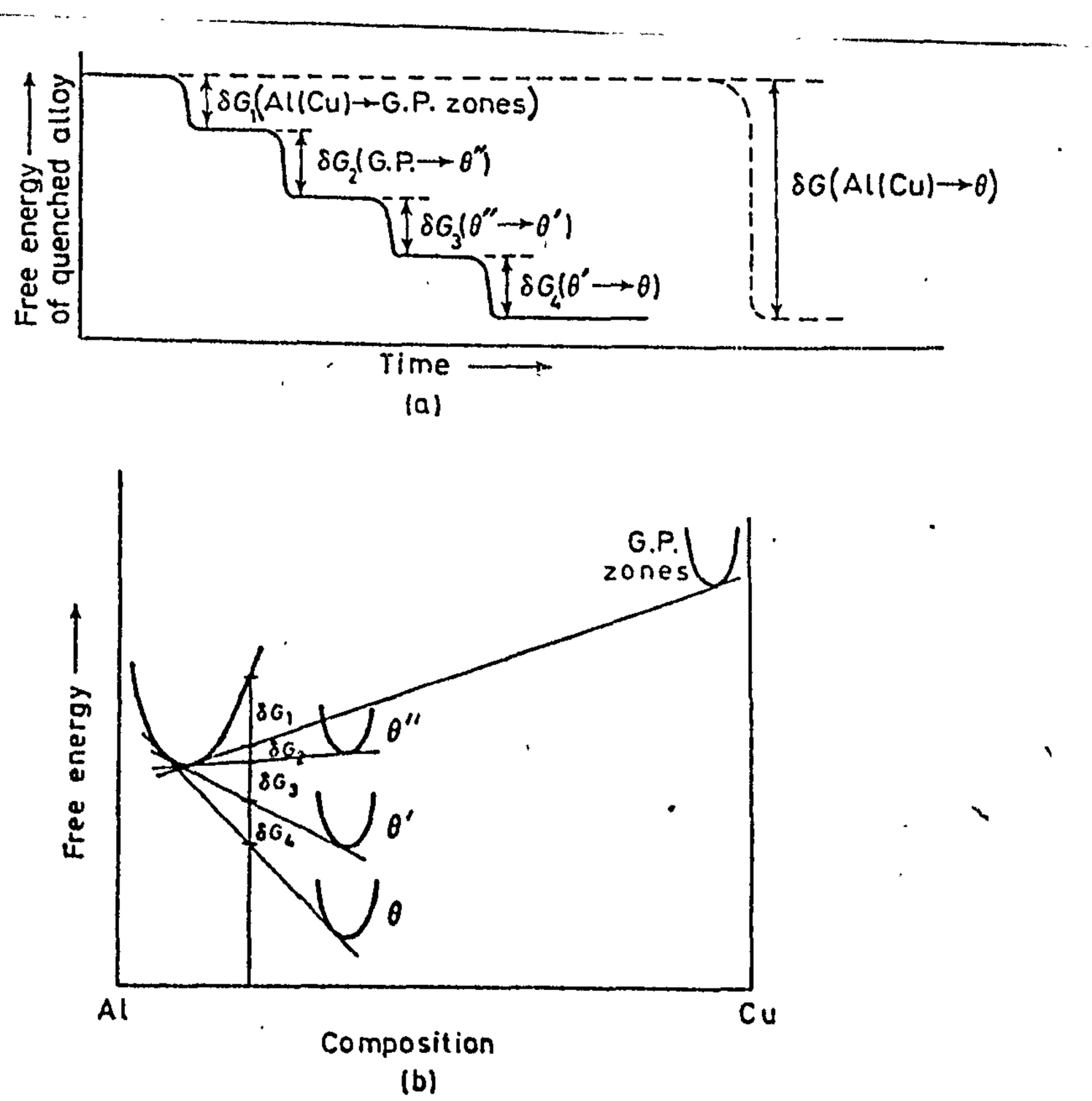

Fig. 15. Free energy changes of an alloy during precipitation for the cases of a) sequential nucleation of metastable precipitates, and b) direct nucleation of the stable θ precipitates.

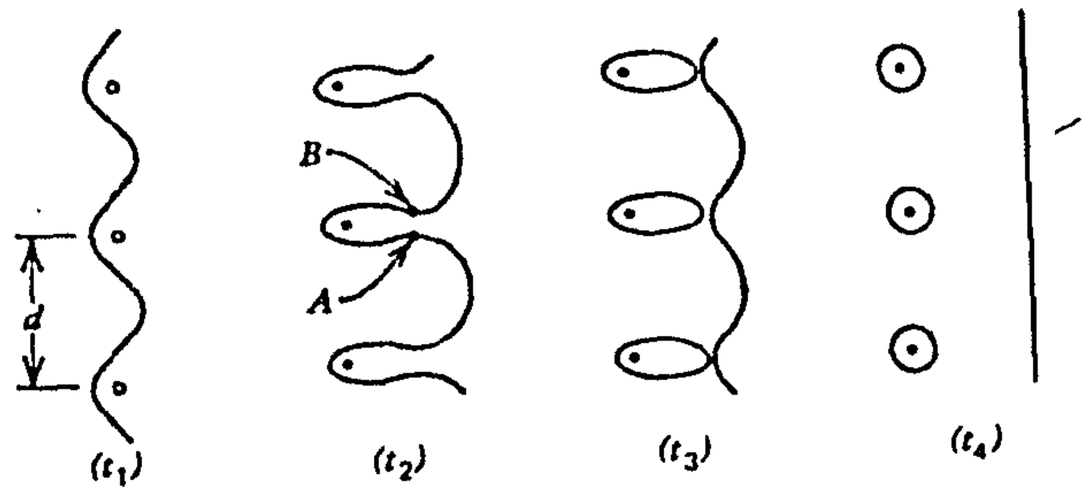

Fig. 16. Interaction of a dislocation line with a row of precipitate particles.

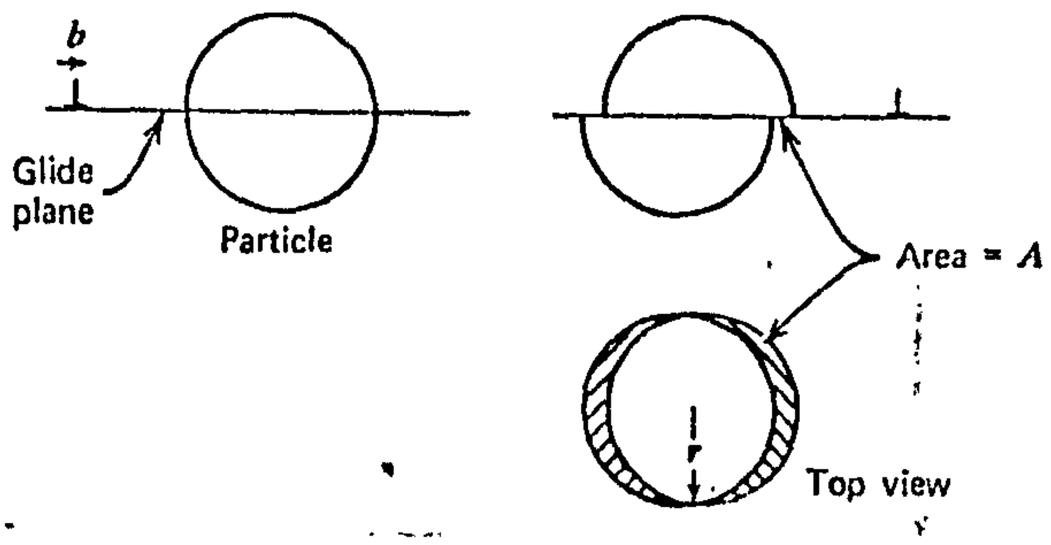

Fig. 17. The "cutting" of a particle by glide motion of a dislocation.

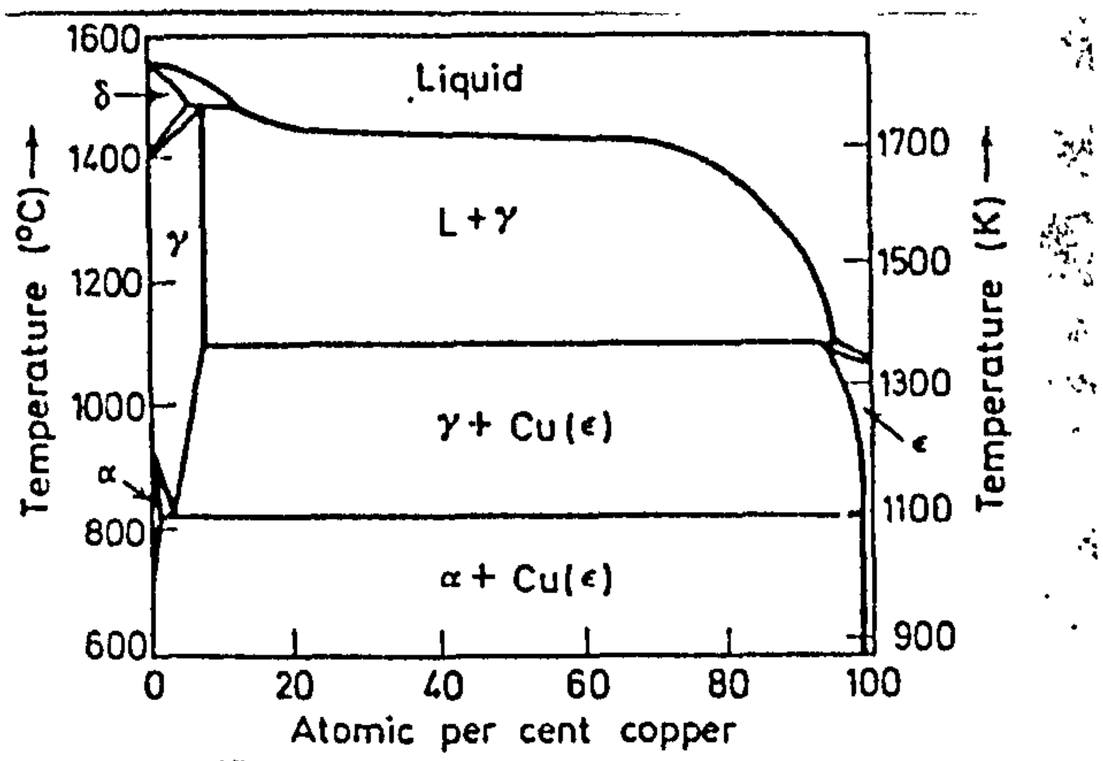

Fig. 18. The iron-copper equilibrium diagram

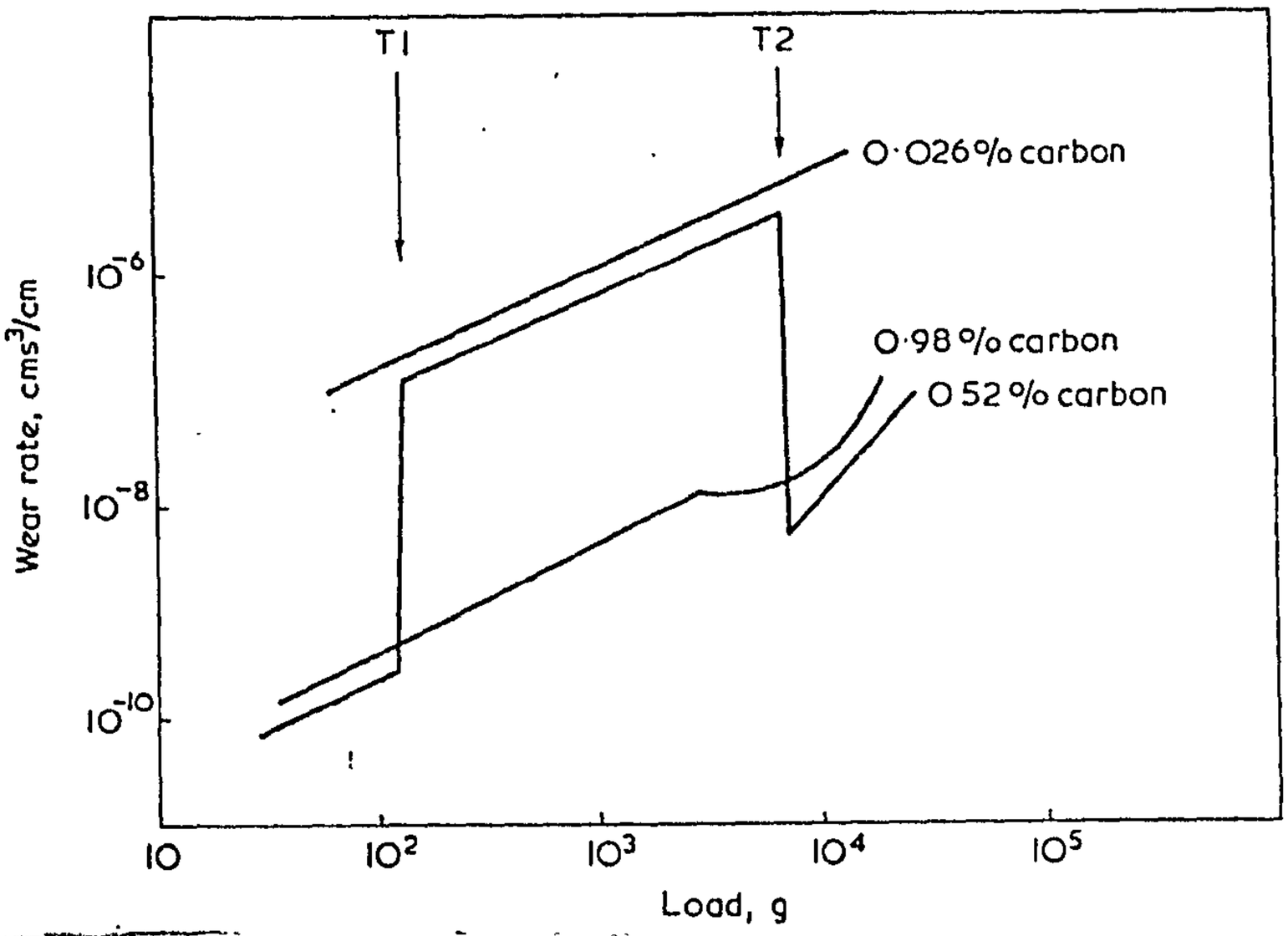

Fig. 19. Wear of different steels under adhesive conditions.

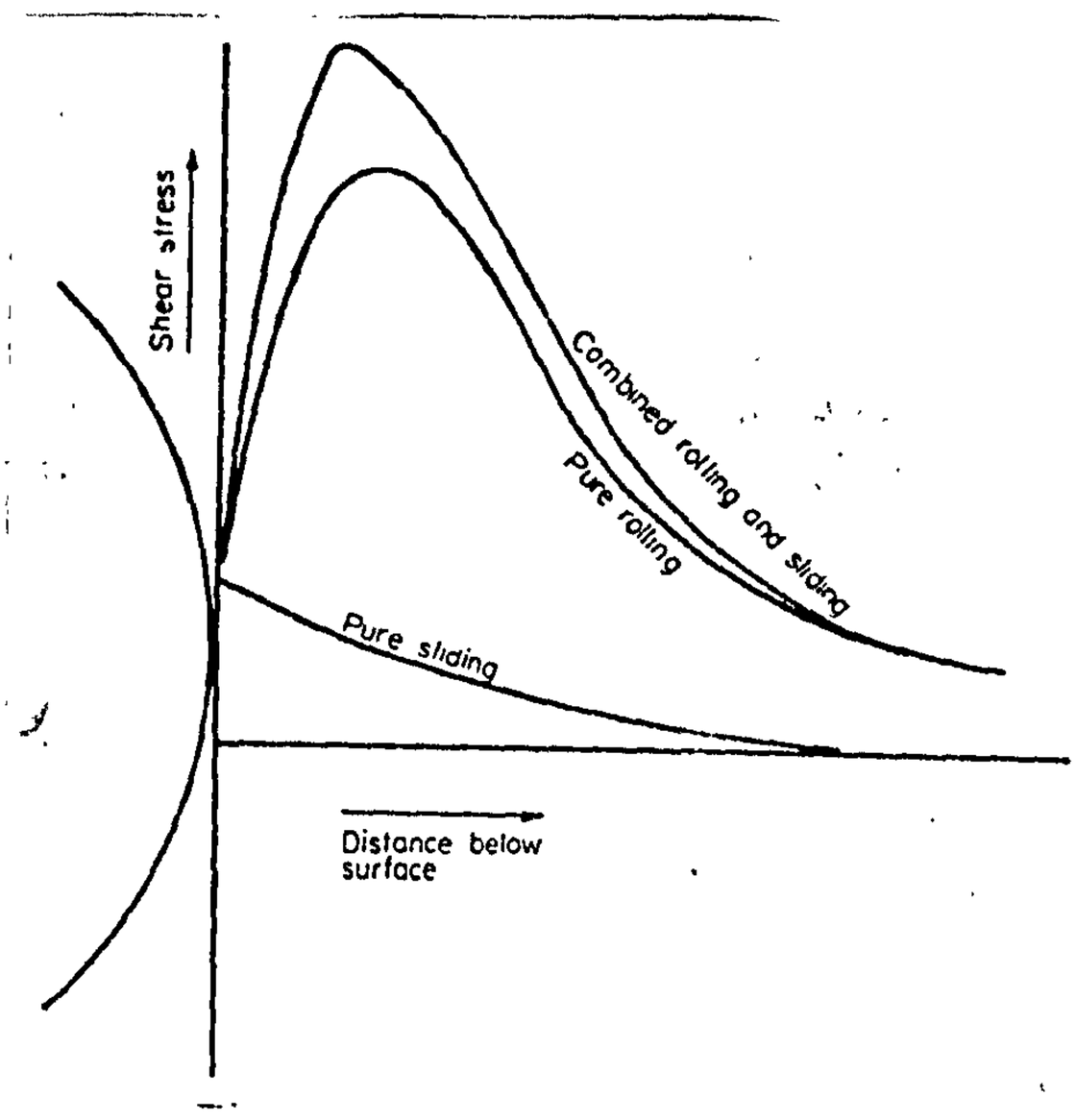

Fig. 20. The variation of shear stress with distance below the surface.

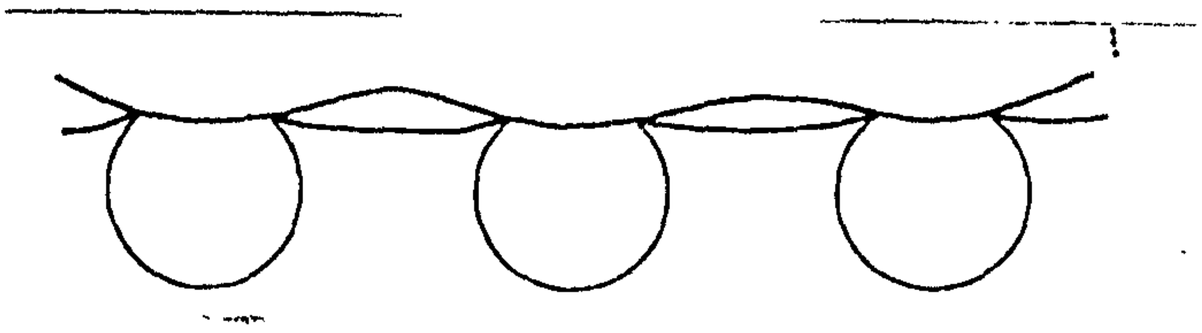

Fig. 21a. The independent plastic zones under the contacting asperities of a plane slider under relatively low loads.

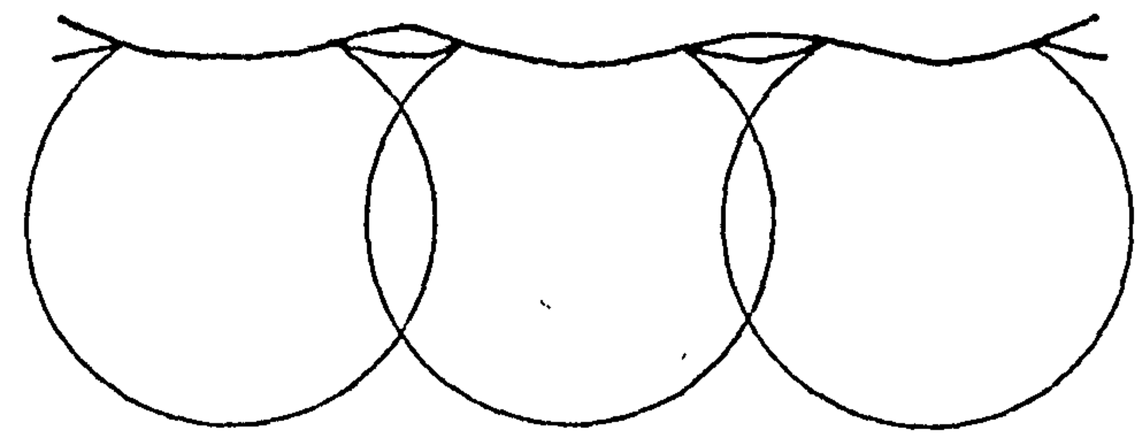

Fig. 21b. The interation of the plastic zones of a plane slider under high loads.

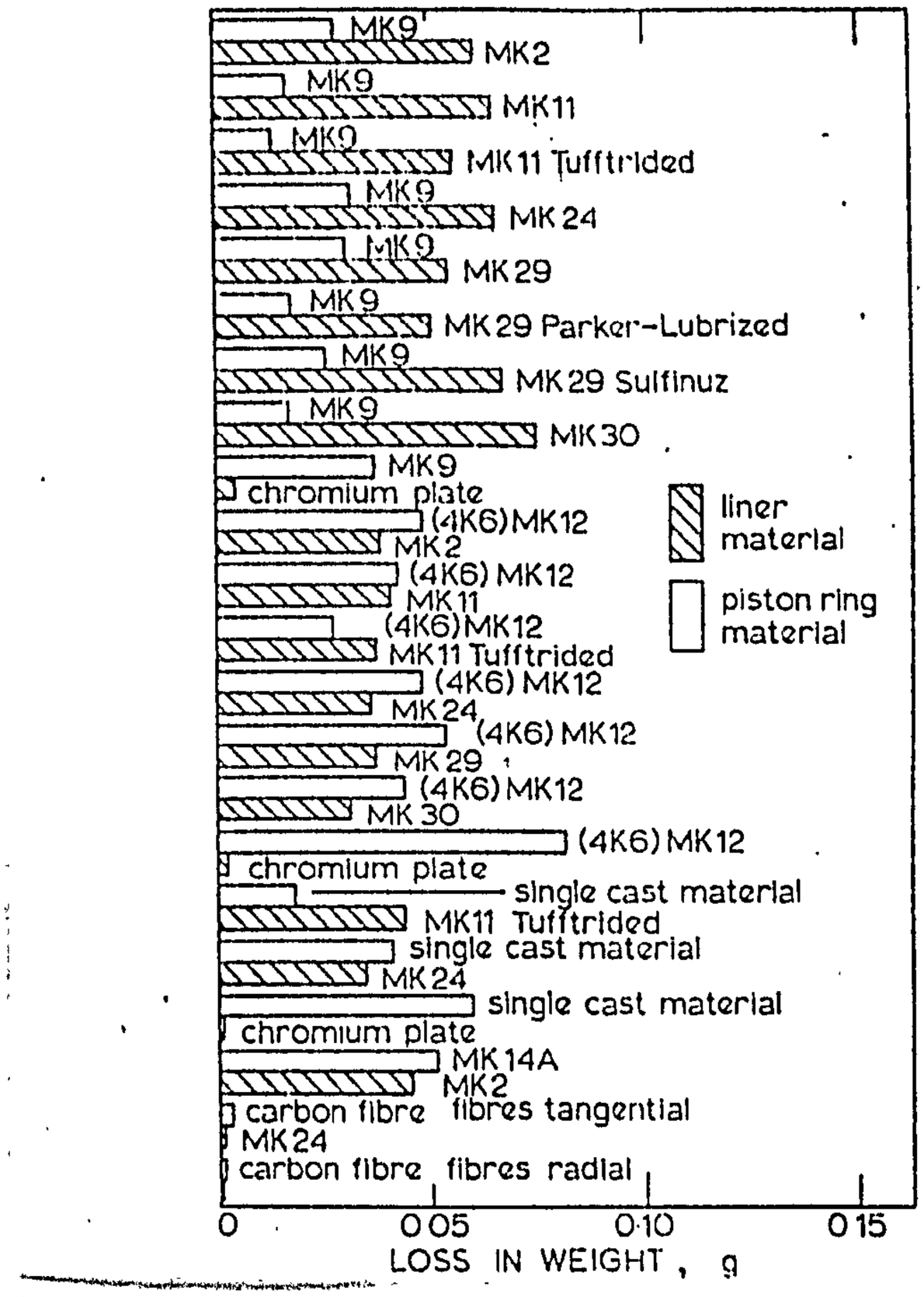

Fig. 22[2]. Comparative wear tests of standard cylinder-liner and piston-ring materials.

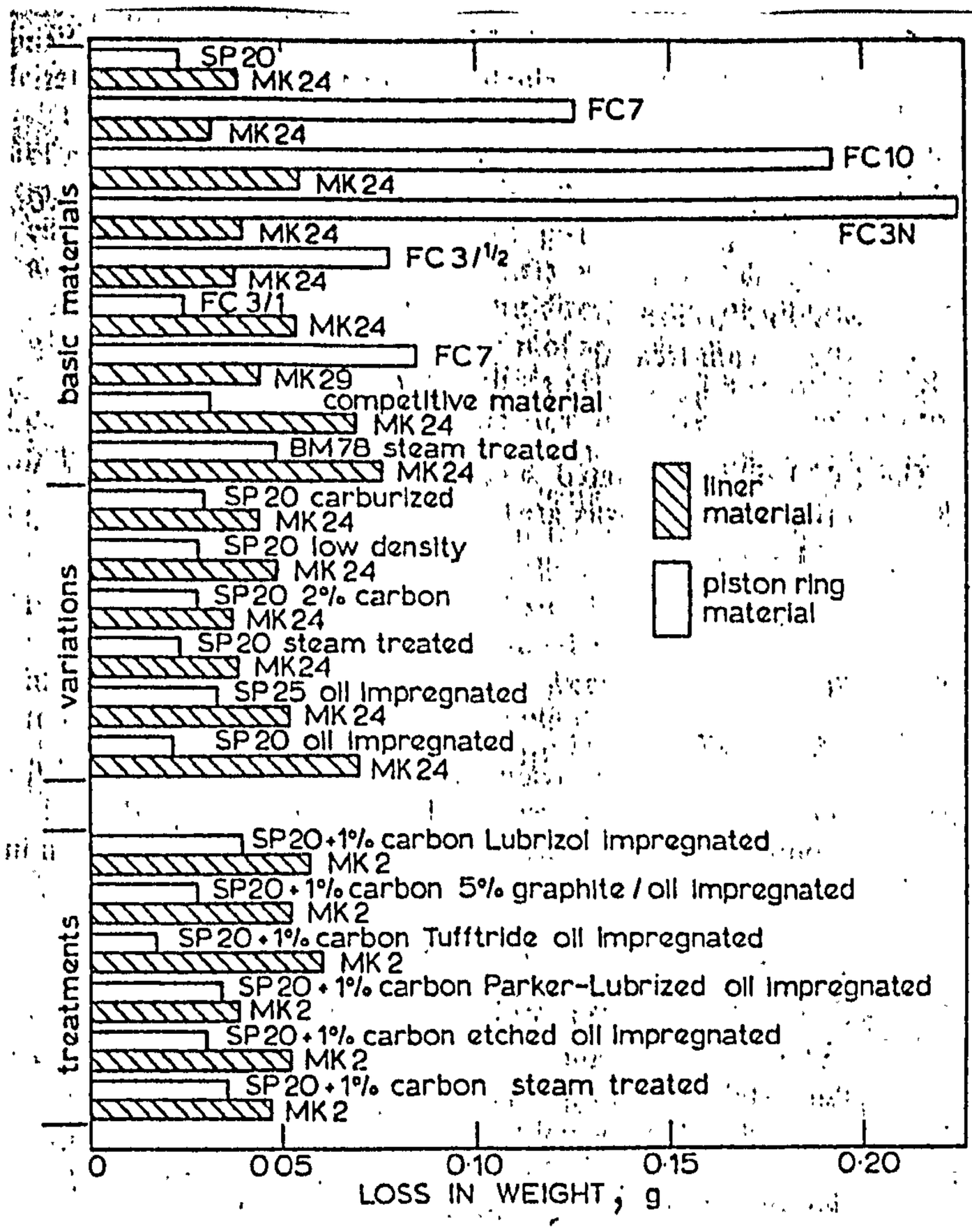

Fig. 23[2]. Comparative wear tests of centrifugally cast liner and sintered ring materials.

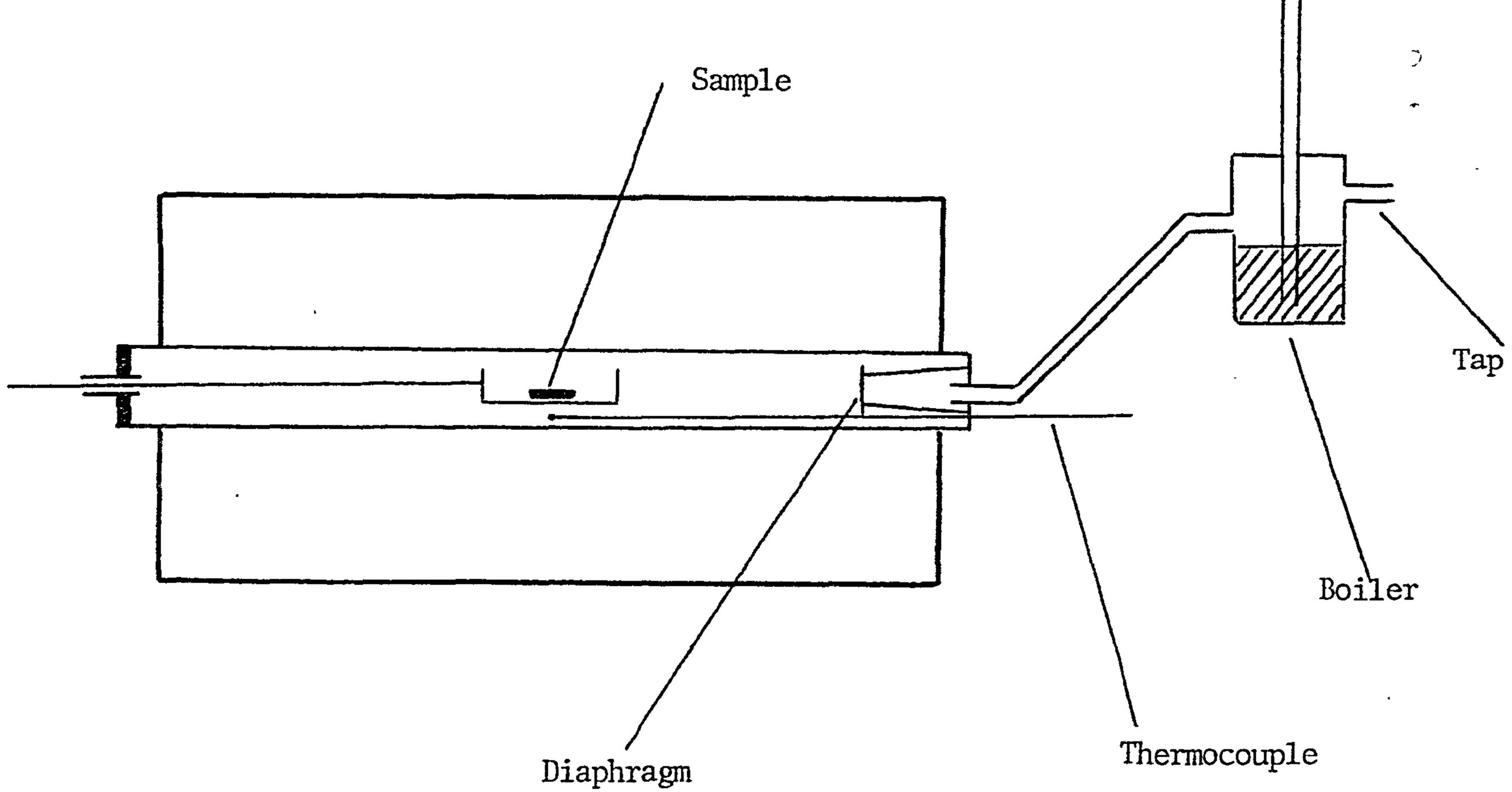

Fig. 24. Schematic diagram of steam treatment equipment.

Steam Rate Per Minute

Approx. 14 cc

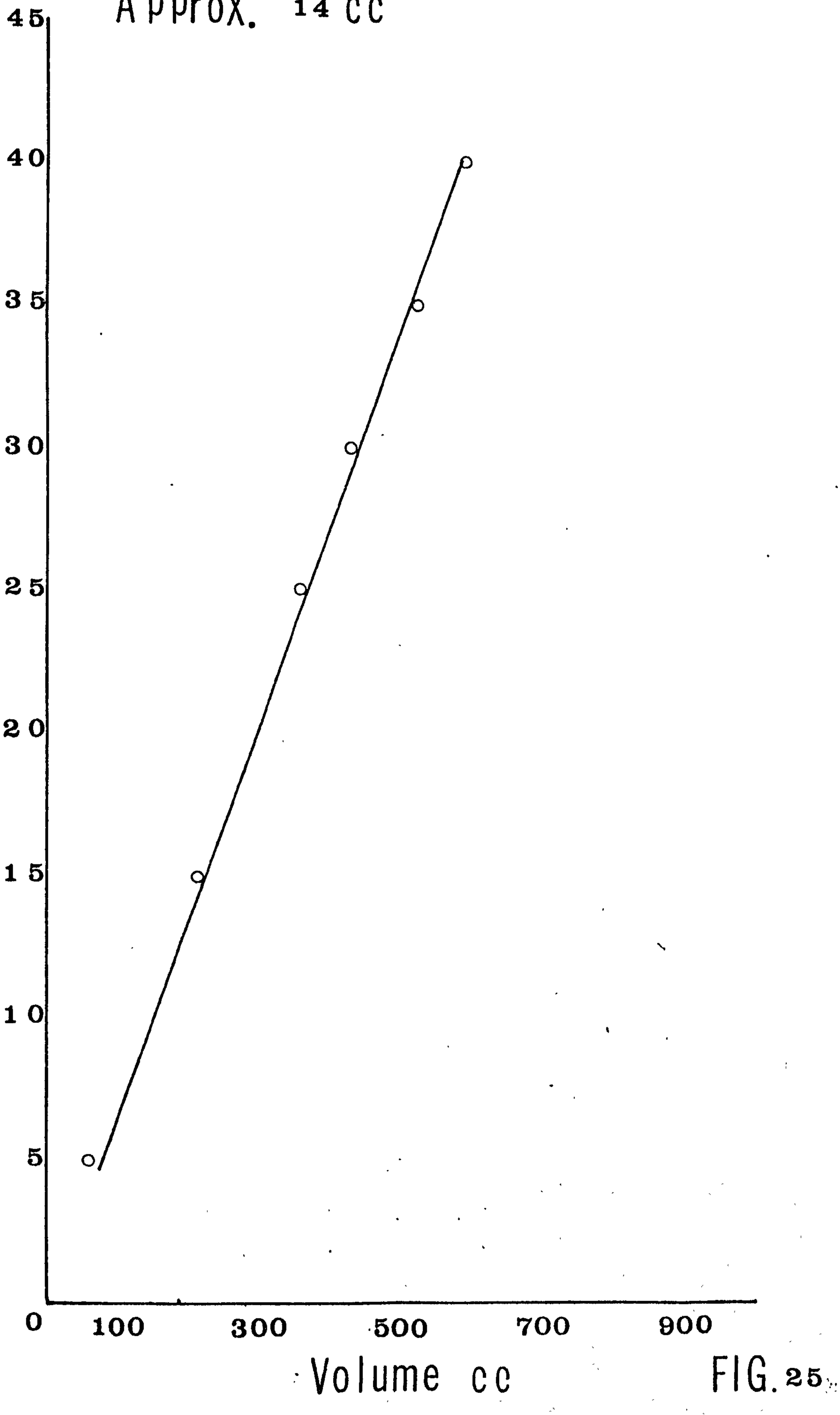

FIG. 25

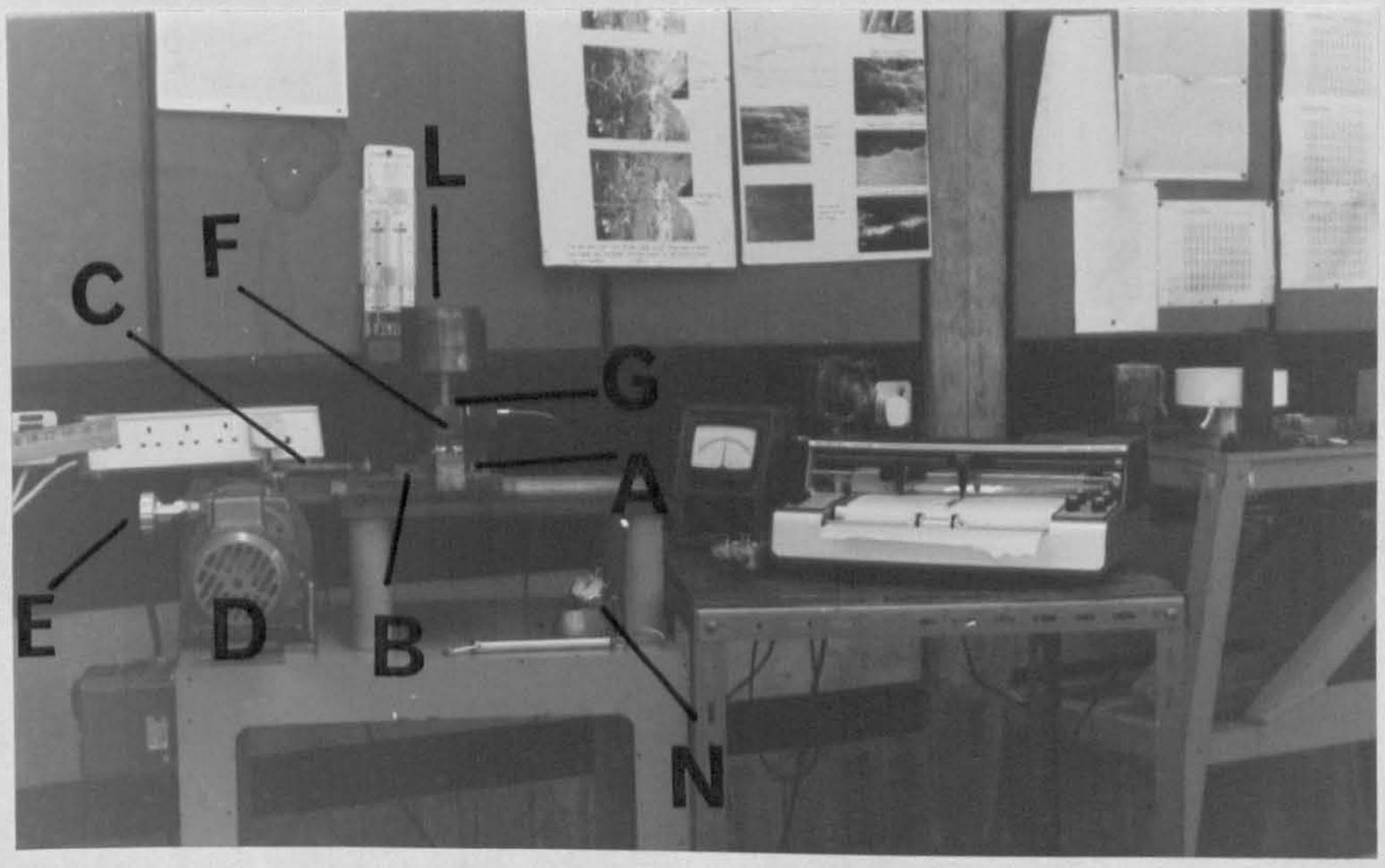

Fig. 26. Wear equipment.

A: Sample

B: Wear Machine

C = Arm of square bed.

D = Electric motor.

E = Control knob for speed.

F = Gate.

G = Shaft.

L = Load

N = Stop Watch.

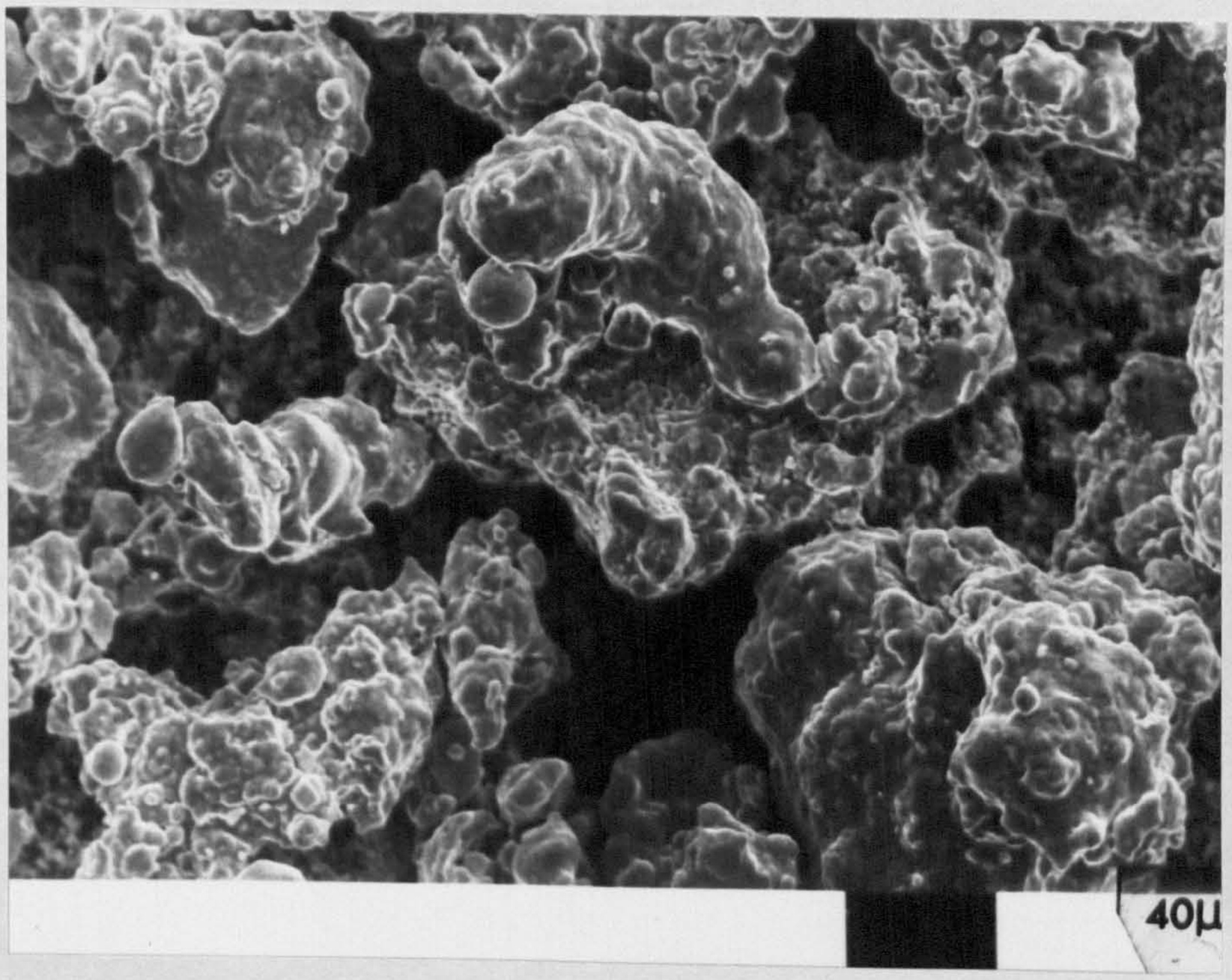

Fig. 27. - 100# A.S.C. powder (pure iron)
As received x 500

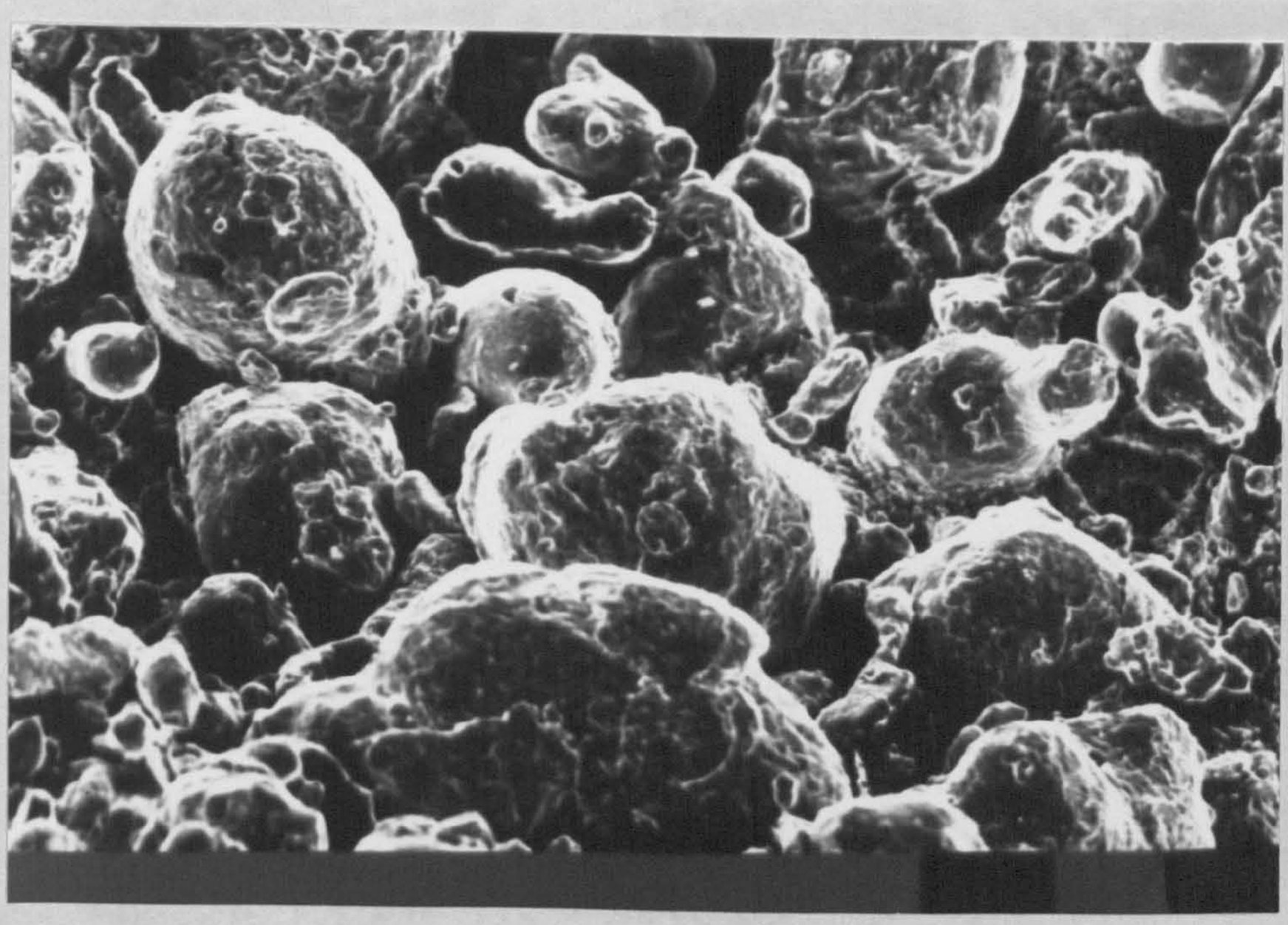

Fig. 28. - 100# Pre-alloyed powder (Fe + 4% Cu)
after annealing. x 500

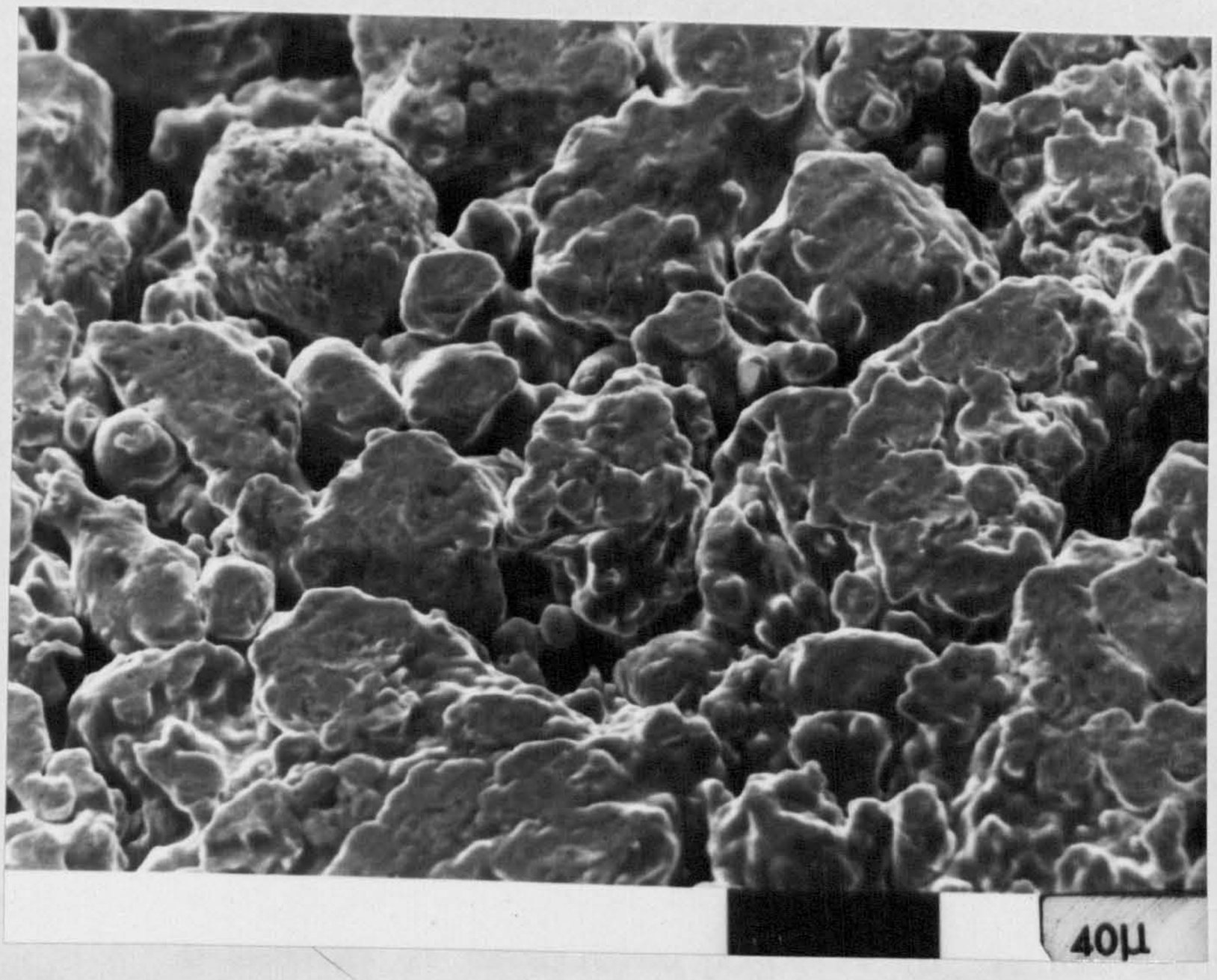

Fig. 29. - 100# A.S.C. (Fe) D = 6.4 g/cc
(compacted) x 500

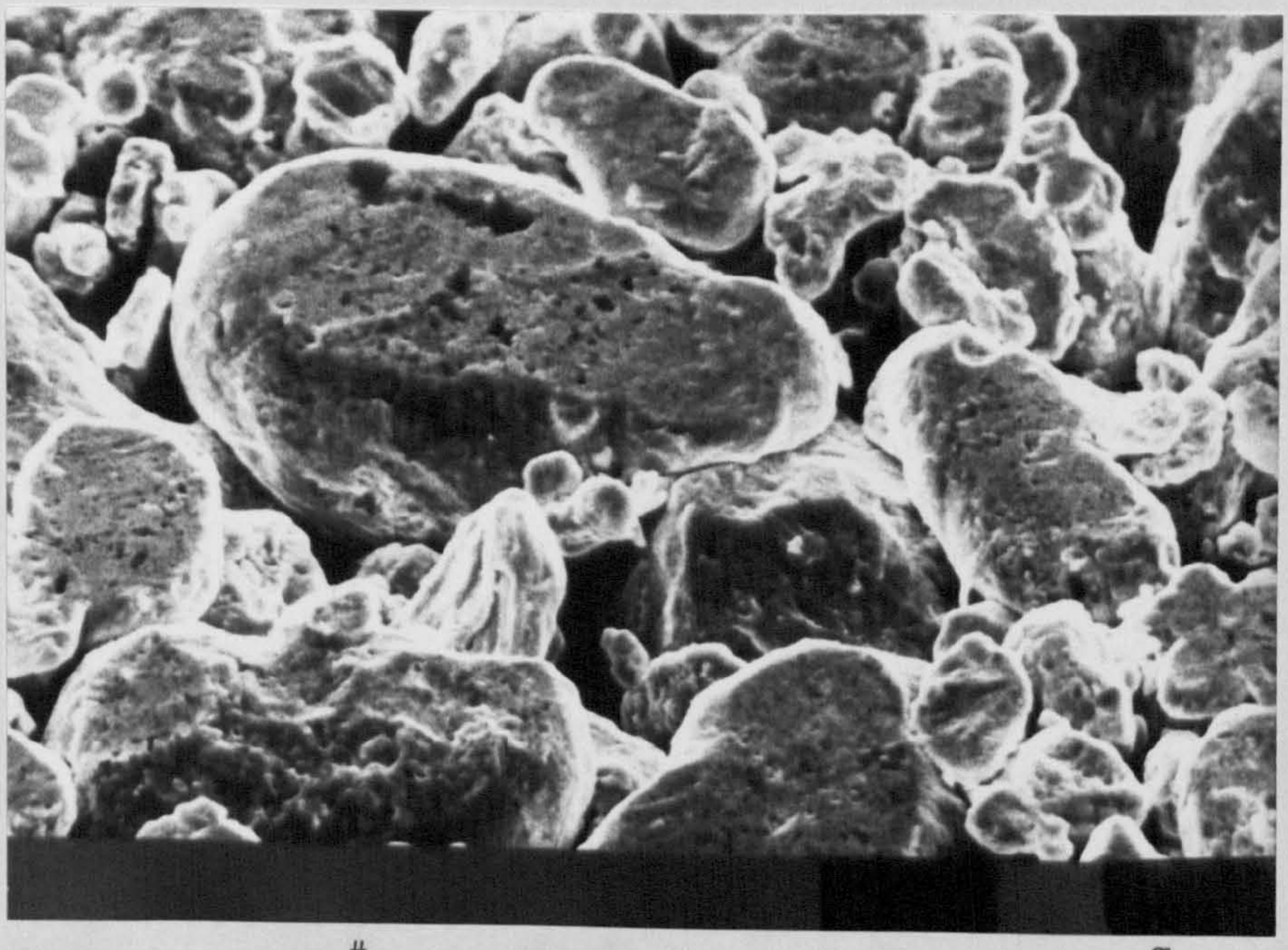

Fig. 30. - 100# Pre-alloyed (Fe + 4% Cu) D = 6.4 g/cc
(compacted) x 500

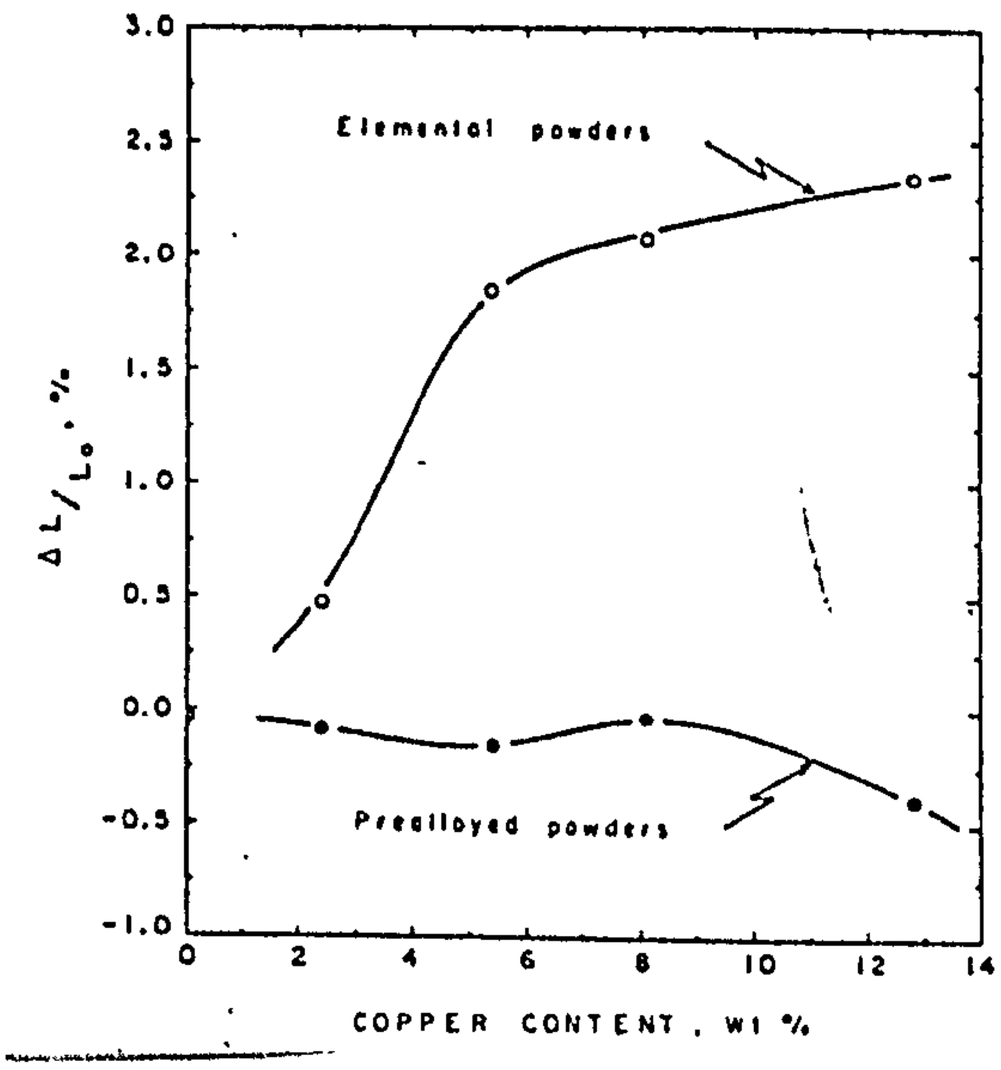

Fig. 31[42] Dimensional changes of Fe - Cu alloys made from elemental or prealloyed powders. (L_o is die length)

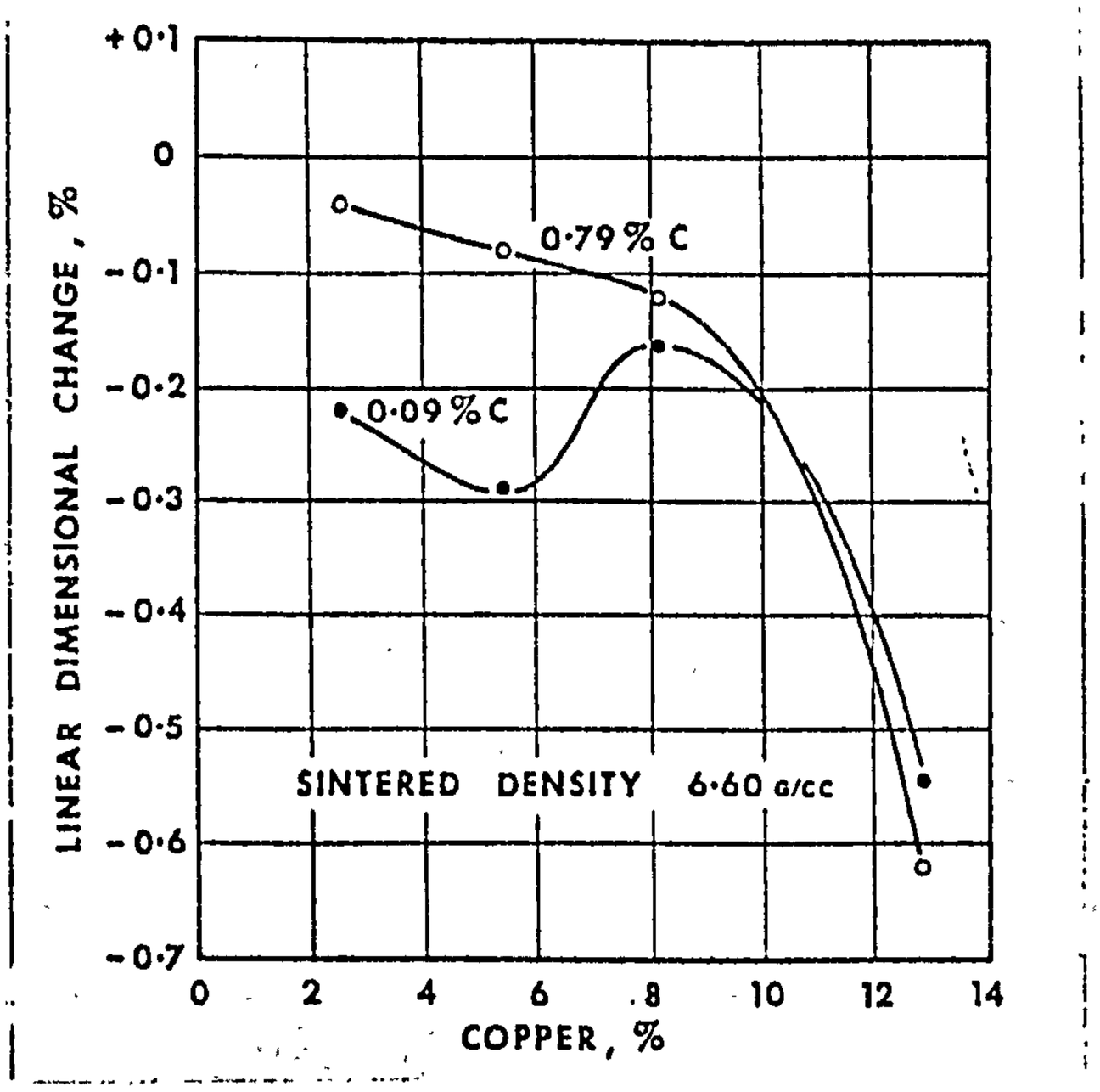

Fig. 32[15]. Dimensional change vs Copper content. Fe - Cu Prealloys.

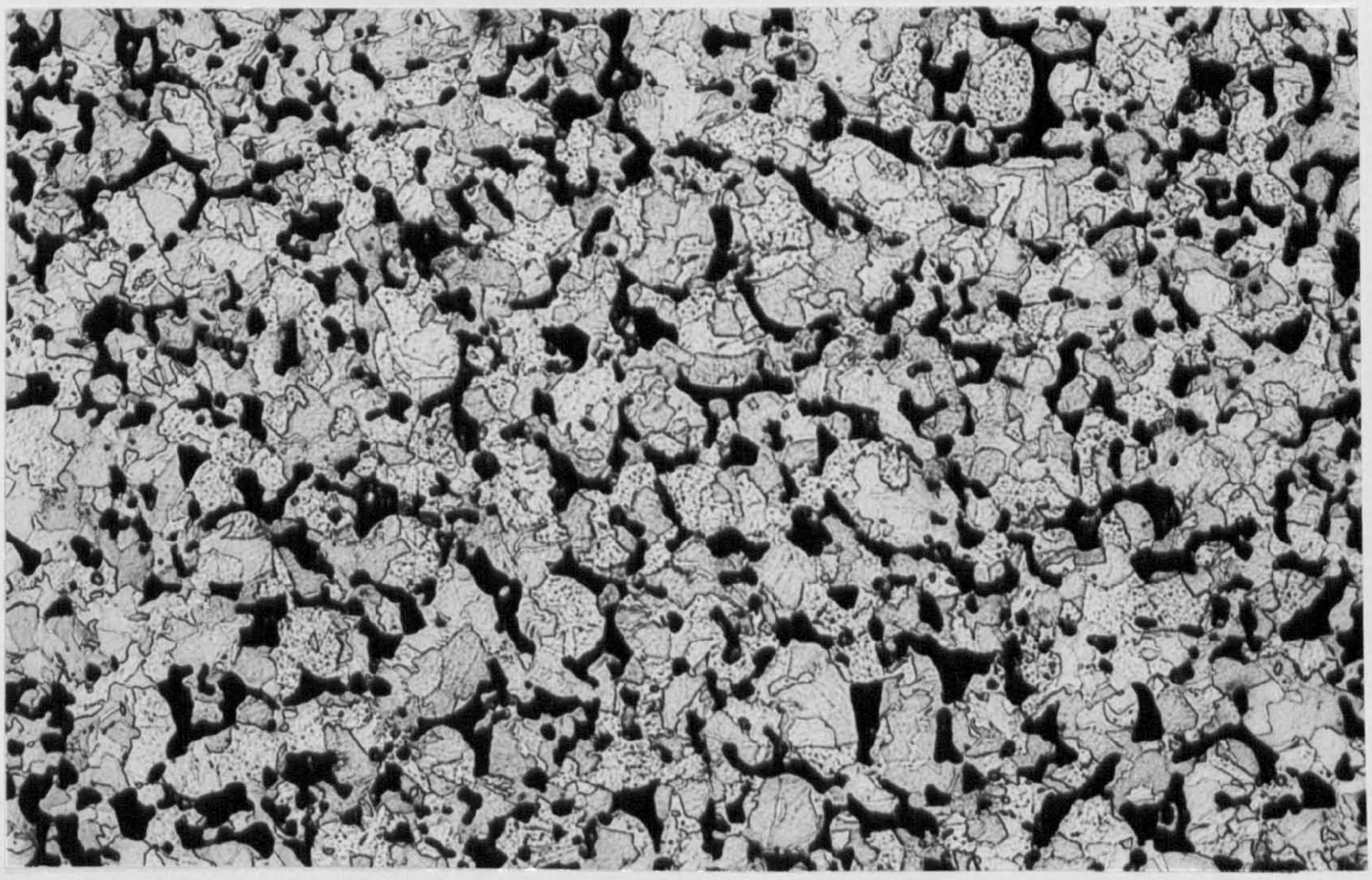

Fig. 33. - 100# Pre-alloyed (Fe + 2% Cu)

D = 6.8 g/cc (W.Q.) x 200

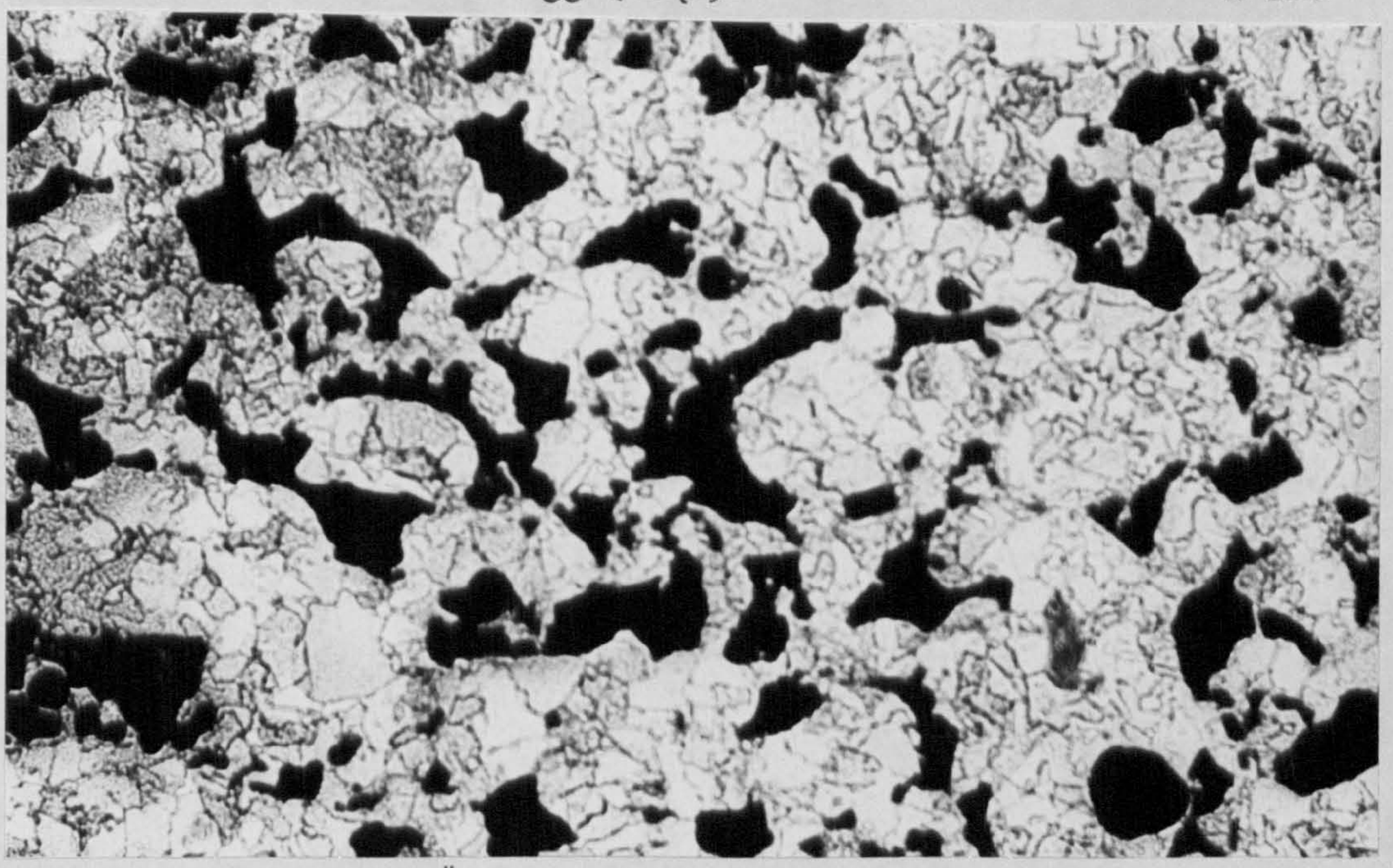

Fig. 34. - 100# Pre-alloyed (Fe + 4% Cu)

D = 6.8 g/cc (W.Q.) x 200

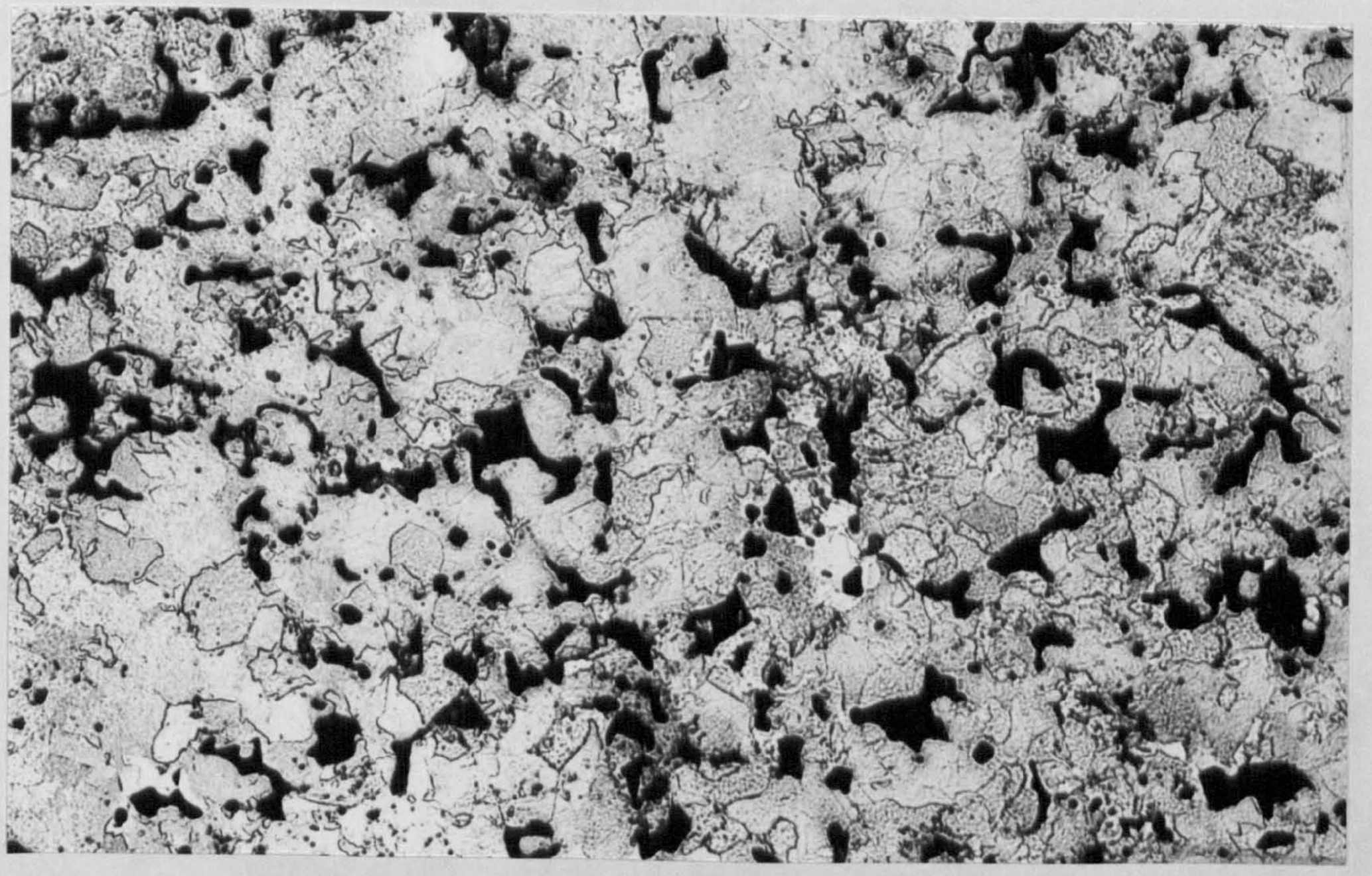

Fig. 35. - 100# Pre-alloyed (Fe + 6% Cu)

D = 6.8 $^{g}/_{cc}$ (W.Q.) x 200

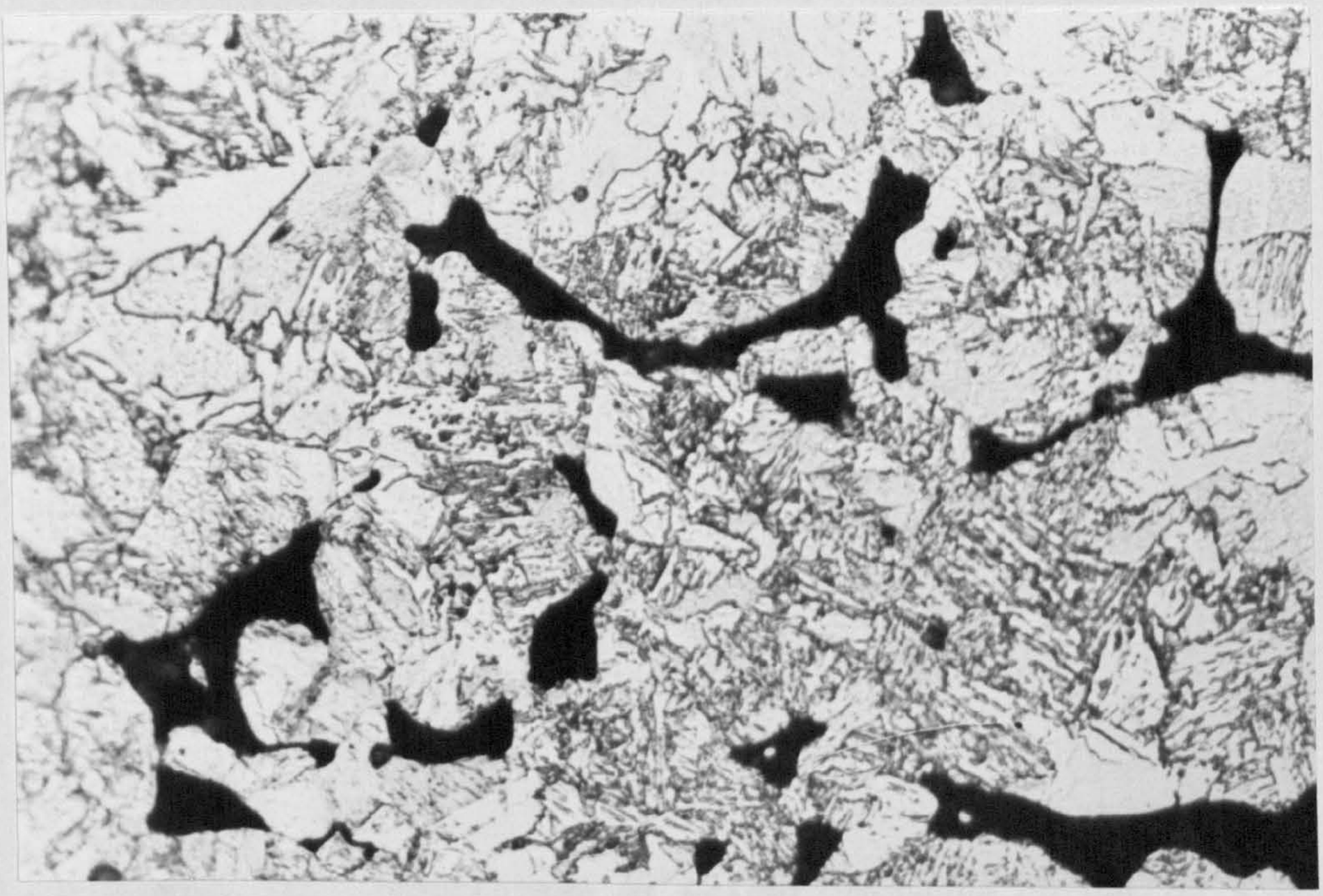

Fig. 36. - 100# Pre-alloyed (Fe + 8% Cu)

D = 6.8 g/cc (W.Q.) x 200

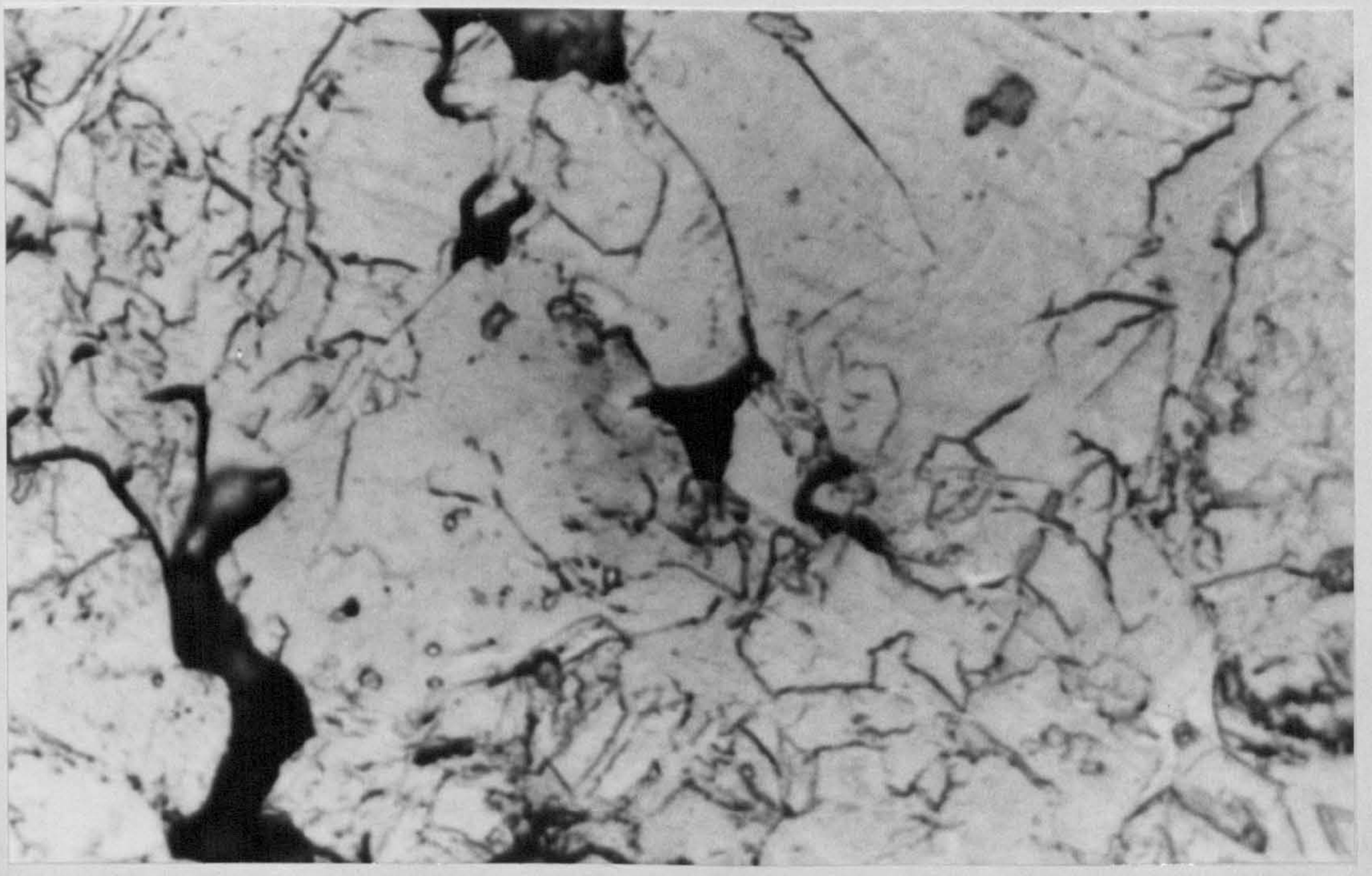

Fig. 37. - 100# Pre-alloyed (Fe + 8% Cu)

D = 6.8 g/cc (W.Q.) x 1000

Key for Figs. 38 and 39

● ●	Fe
△ △	Fe + 2% Cu
▲ ▲	Fe + 4% Cu
□ □	Fe + 6% Cu
■ ■	Fe + 8% Cu

Fig. 38. Percentage of weight increase curves as a function of steam treatment time for iron and iron/copper alloys in water quenched samples.

Fig. 39. Percentage of weight increase curves as a function of steam treatment time for iron and iron/copper alloys in furnace cooled samples.

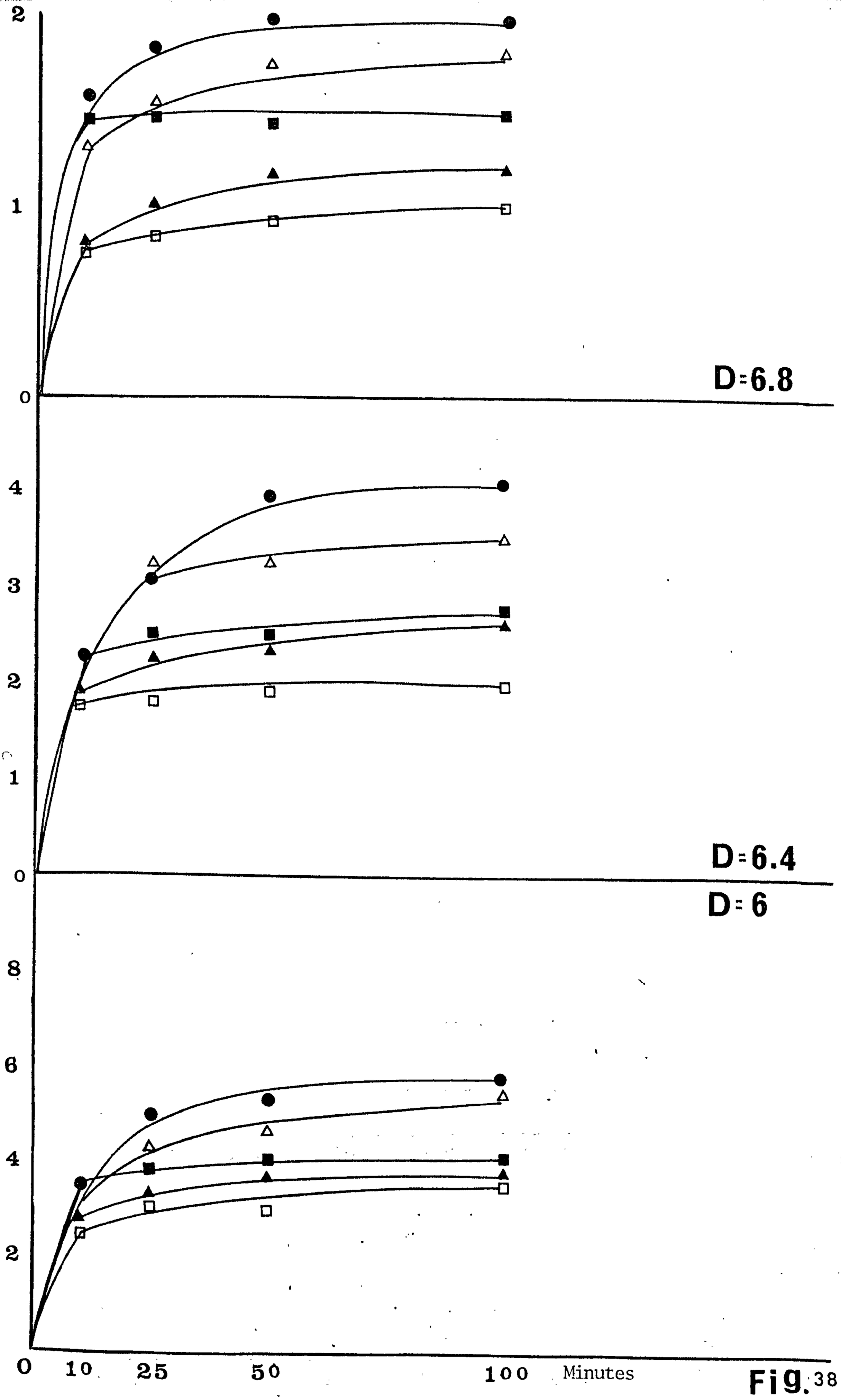

Fig. 38

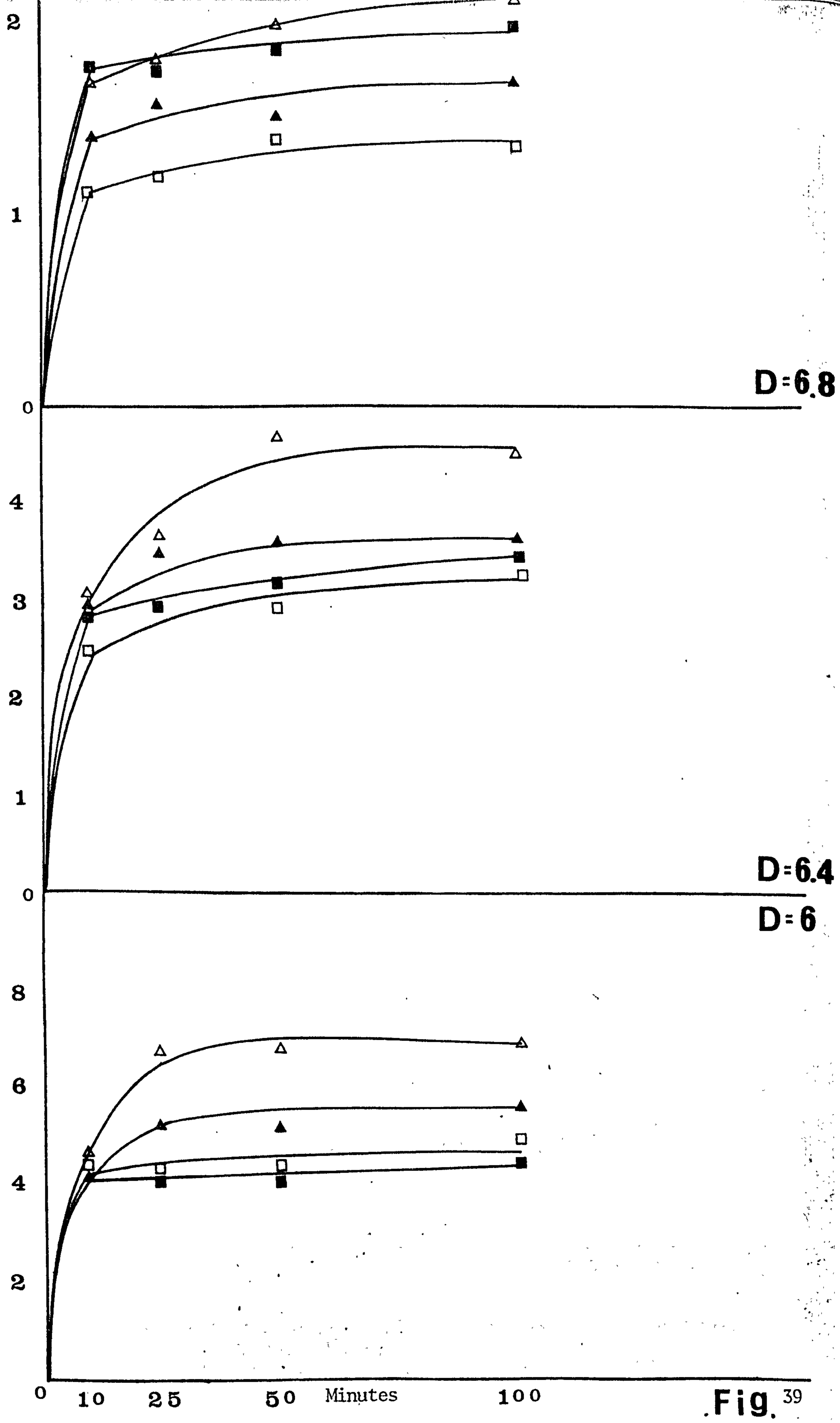

Fig. 39

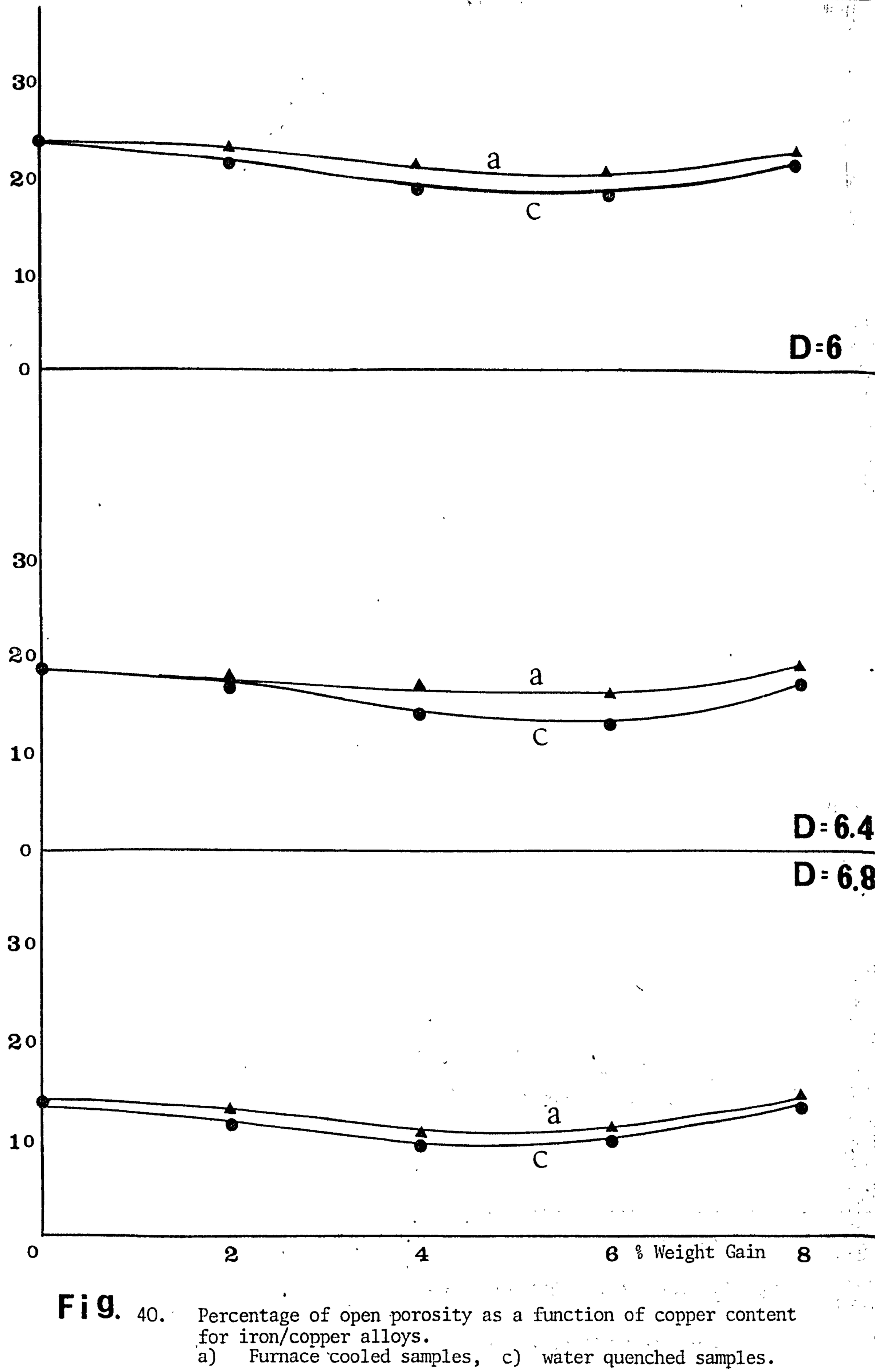

Fig. 40. Percentage of open porosity as a function of copper content for iron/copper alloys.
a) Furnace cooled samples, c) water quenched samples.

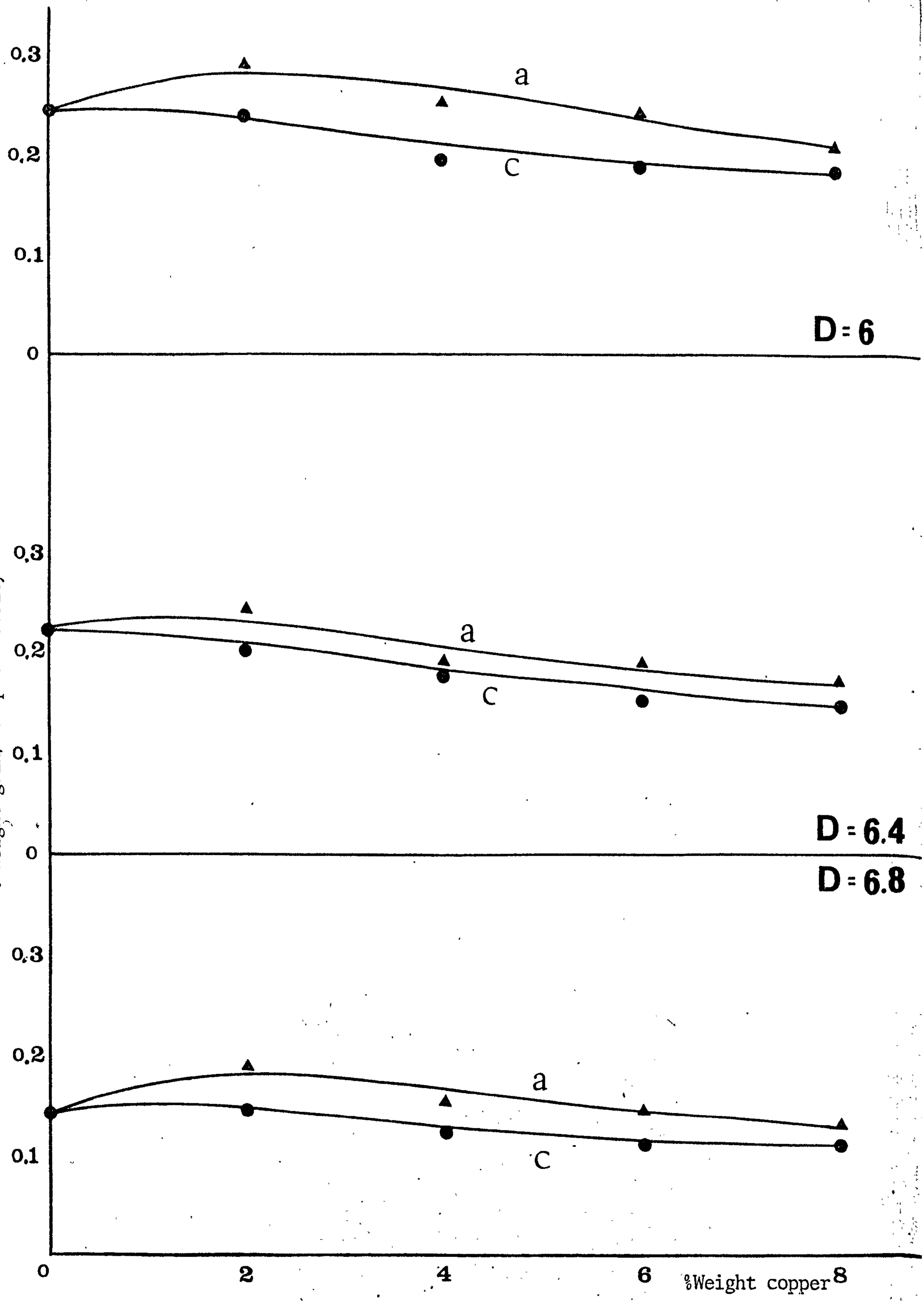

Fig. 41. Percentage of weight gain/open porosity as a function of copper content for iron/copper alloys.

a) Furnace cooled samples, c) Water quenched samples.

Fig. 42. - 100# Pre-alloyed (Fe + 8% Cu)
D = 6.4 $^{g}/_{cc}$ (sintered) x 2K

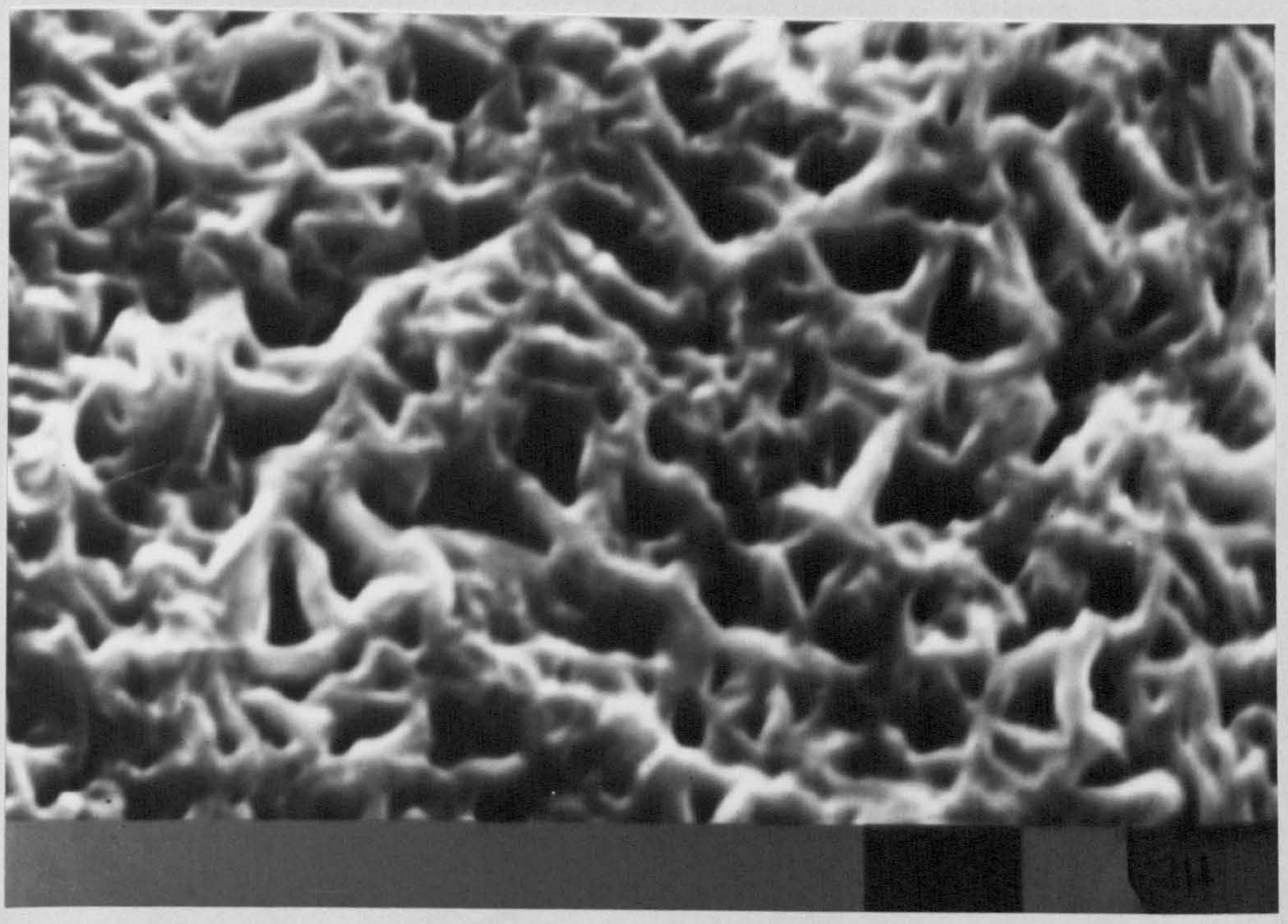

Fig. 43. - 100# Pre-alloyed (Fe + 8% Cu) D = 6.4 $^{g}/_{cc}$
steam treated (100 minutes
(525° C x 10K

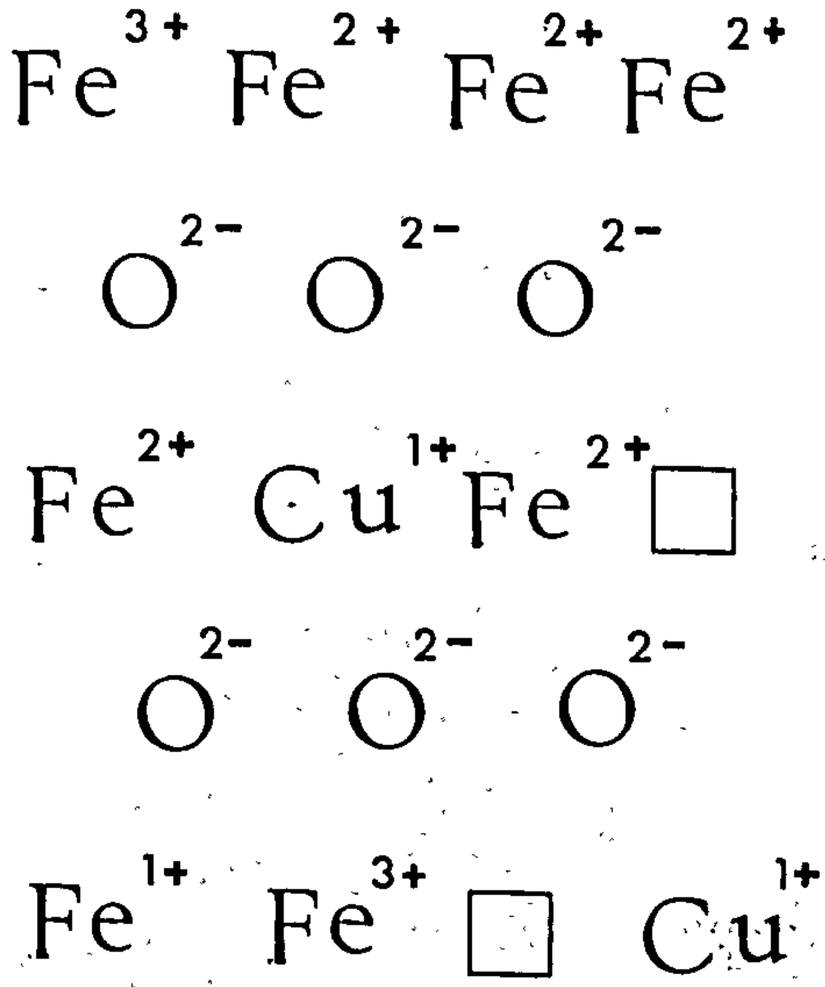

Fig. 44. Defect structure of an FeO - CuO oxide

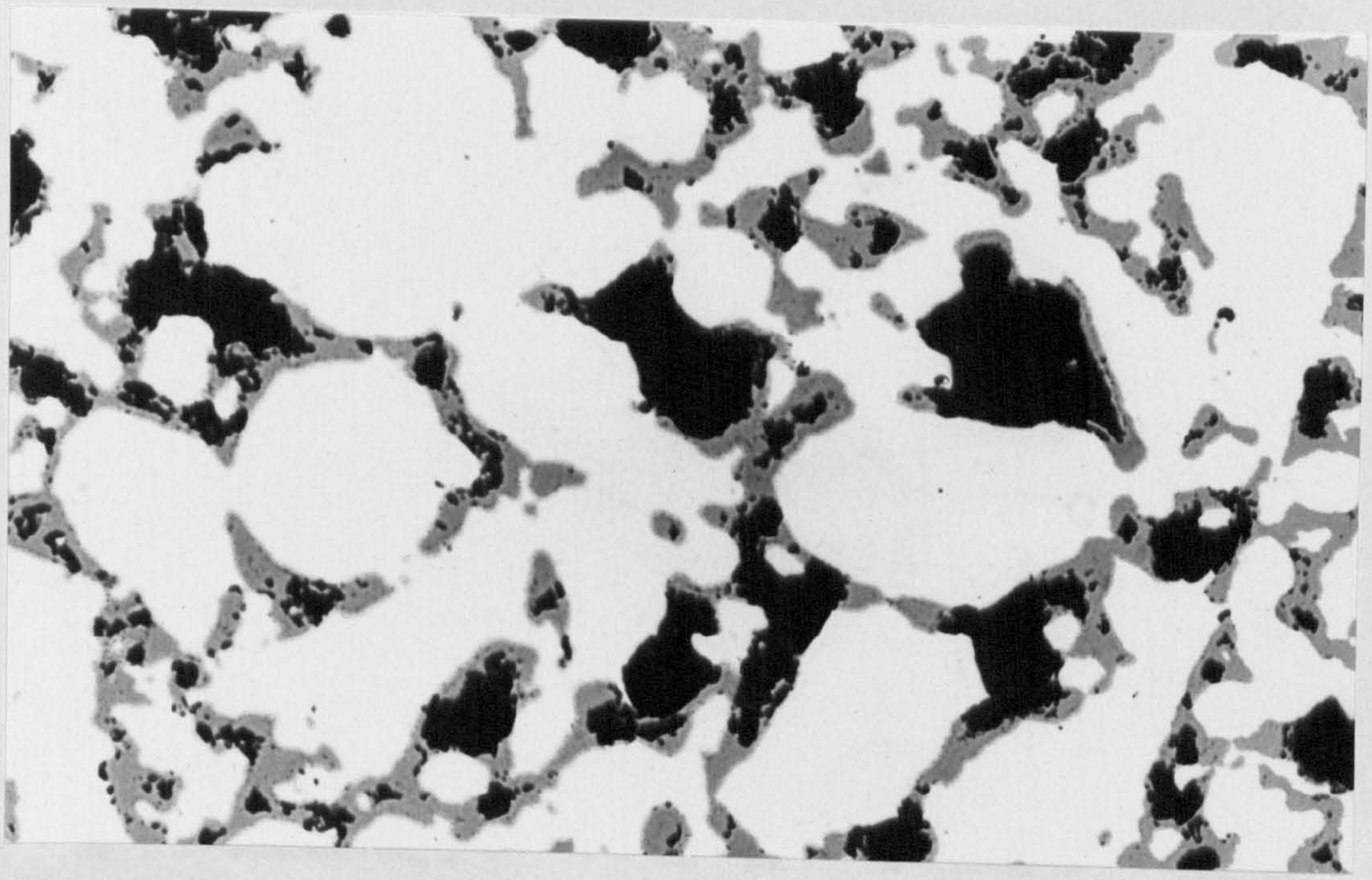

Fig. 45. - 100# Pre-alloyed (Fe + 4% Cu) D = 6.0 g/cc
steam treated (100 minutes
(525°C
x 200

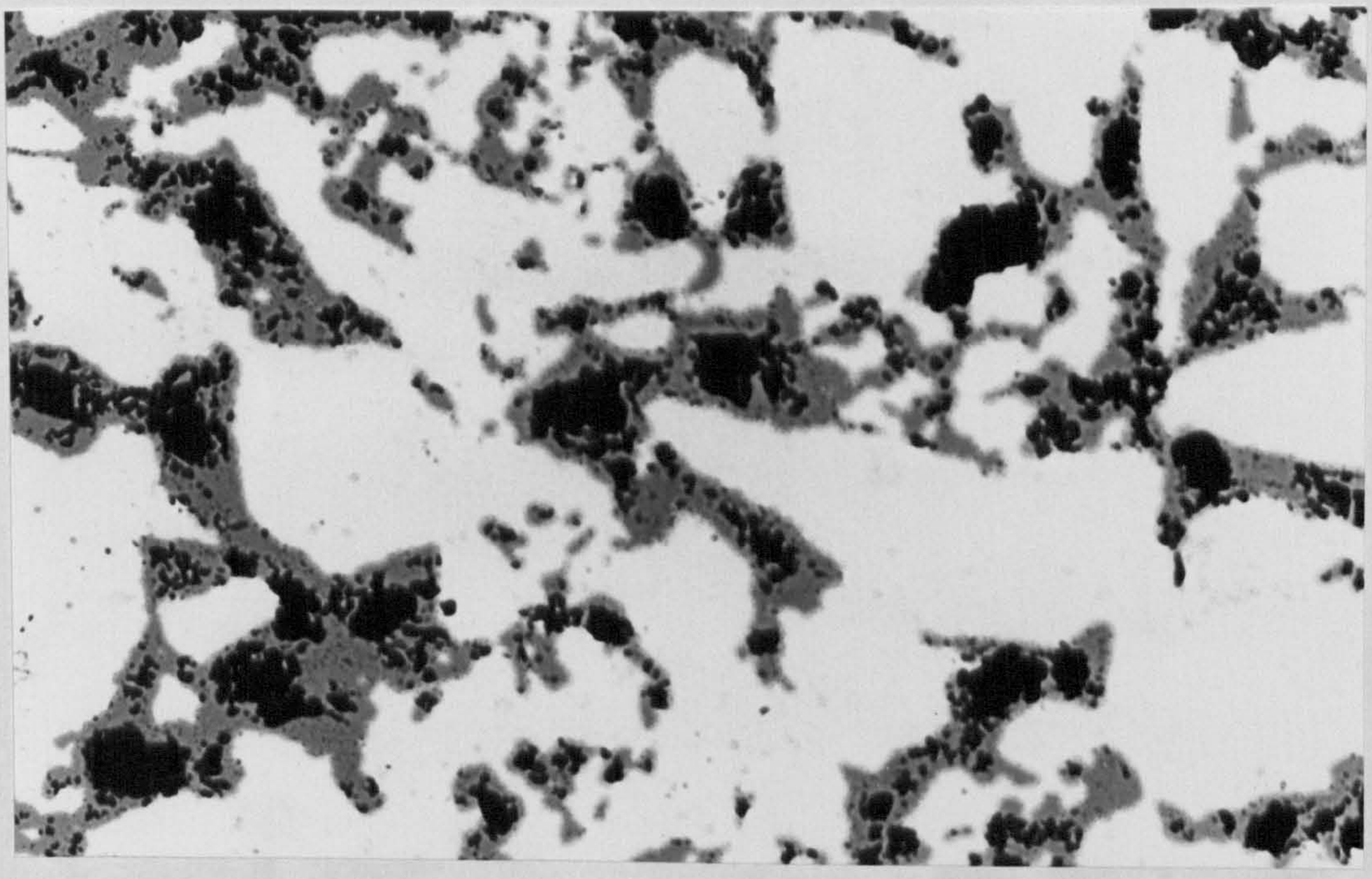

Fig. 46. - 100# Pre-alloyed (Fe + 6% Cu) D = 6.0 g/cc
steam treated (100 minutes
(525°C
x 200

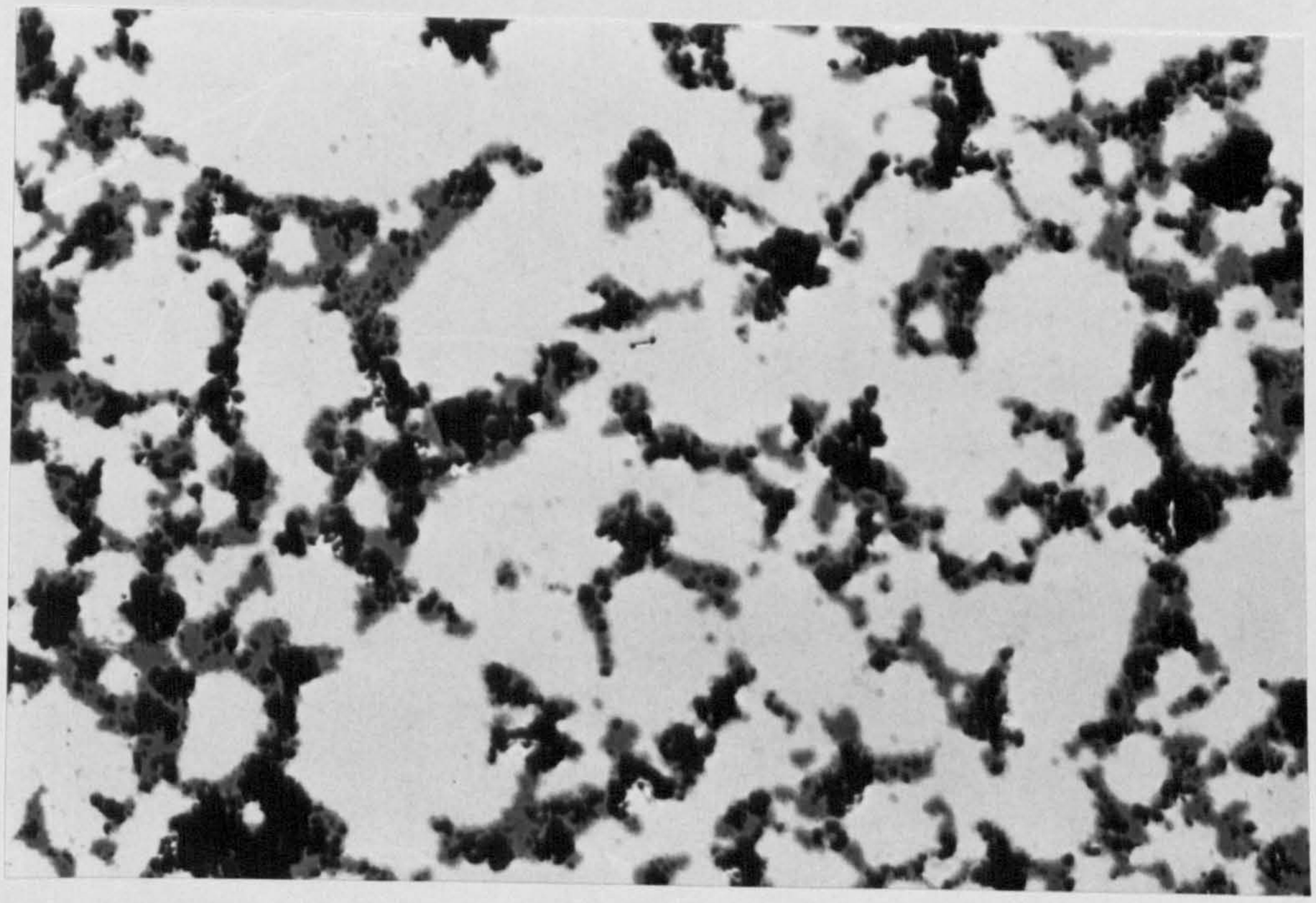

Fig. 47. - 100# Pre-alloyed (Fe + 8% Cu) D = 6.0 $^{g}/_{cc}$

steam treated (100 minutes, (525° C x 200

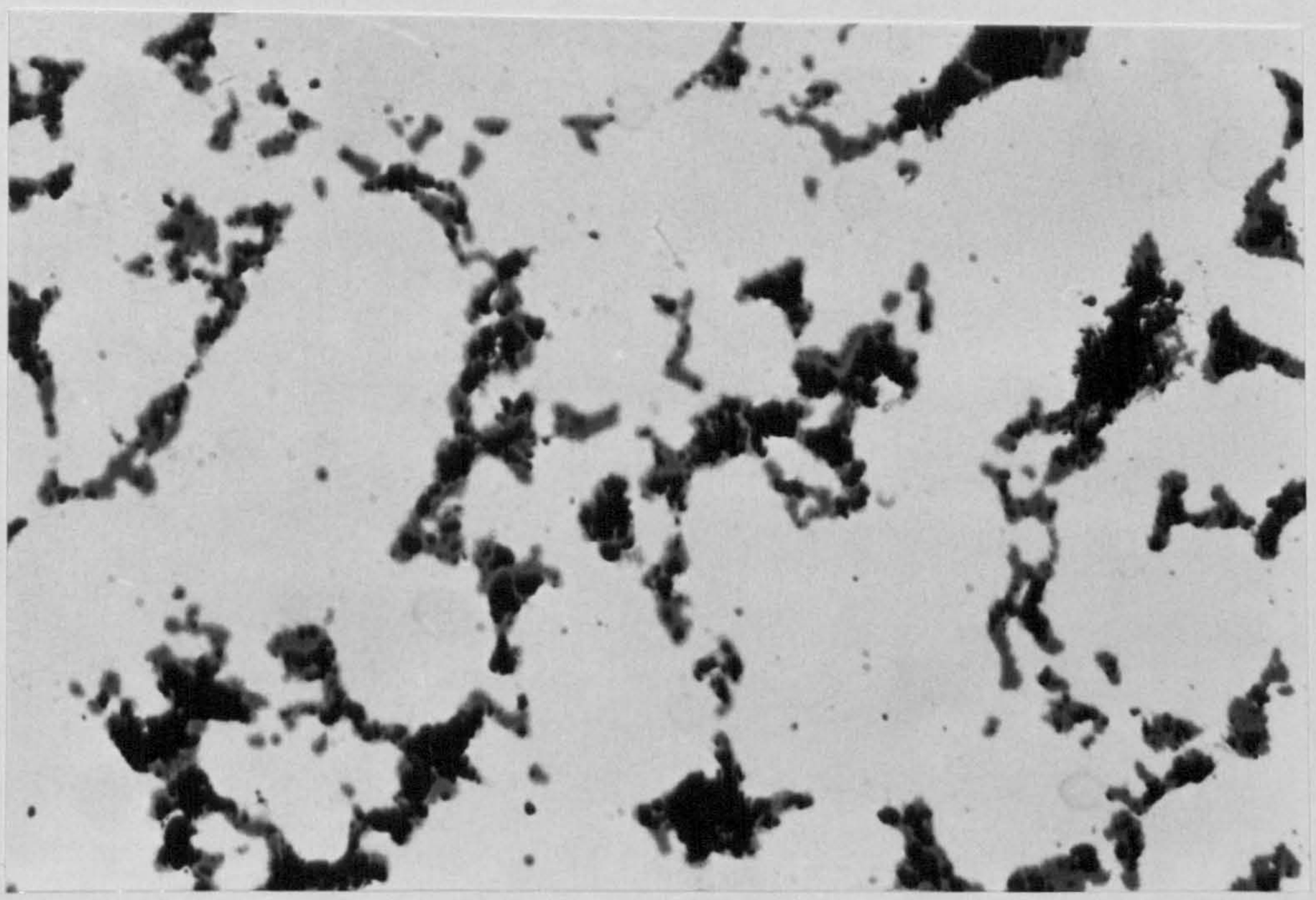

Fig. 48. - 100# Pre-alloyed (Fe + 8% Cu) D = 6.8 $^{g}/_{cc}$

steam treated (100 minutes, (525° C x 200

Key for Figs. 49 and 50

● ● Density 6.8 $^{g}/_{cc}$

○ ○ Density 6.4 $^{g}/_{cc}$

△ △ Density 6.0 $^{g}/_{cc}$

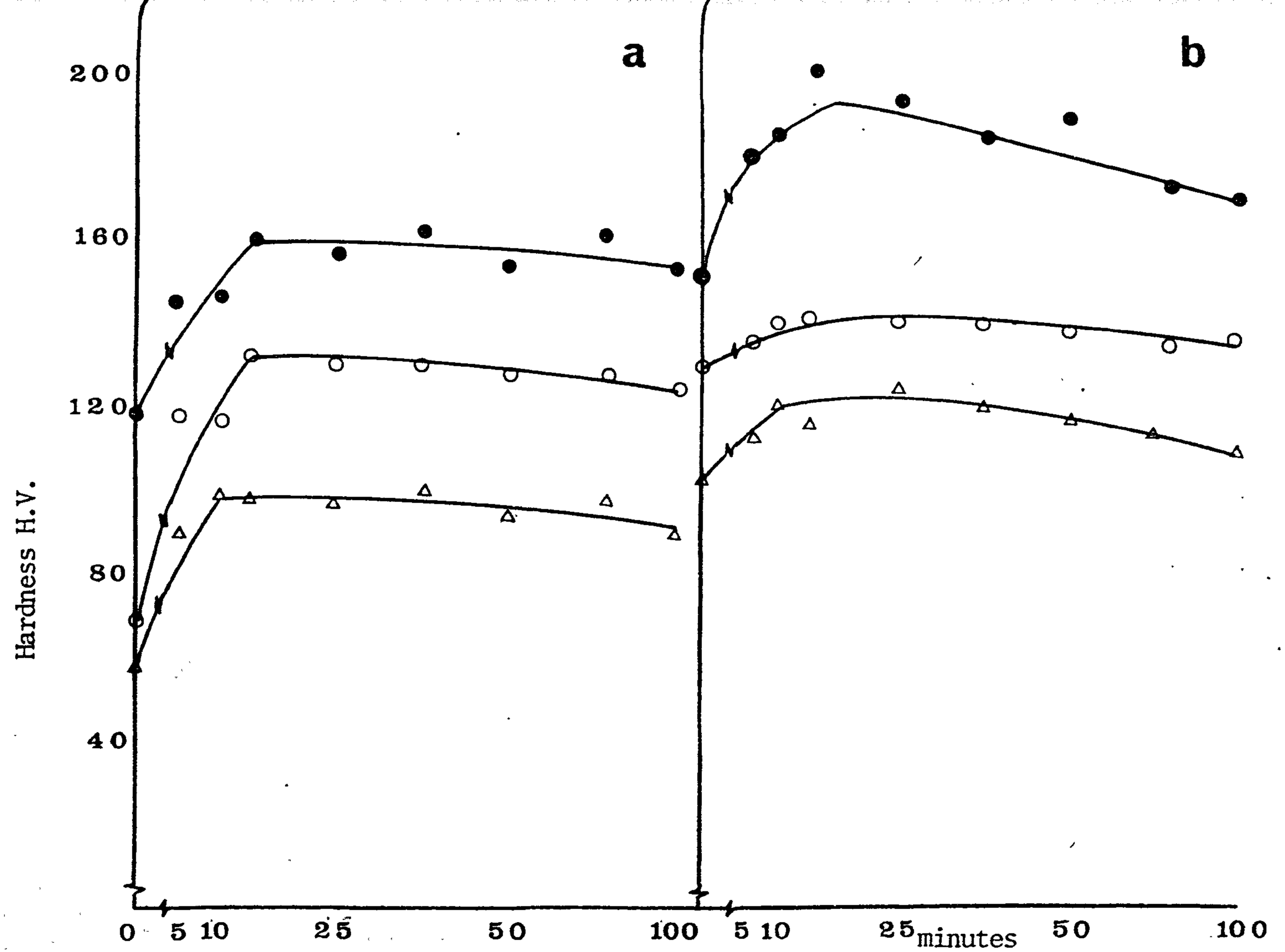

Fig. 49. Vickers hardness as a function of treatment time by inert gas in water quenched samples.
a) Fe + 2% Cu alloy b) Fe + 4% Cu alloy

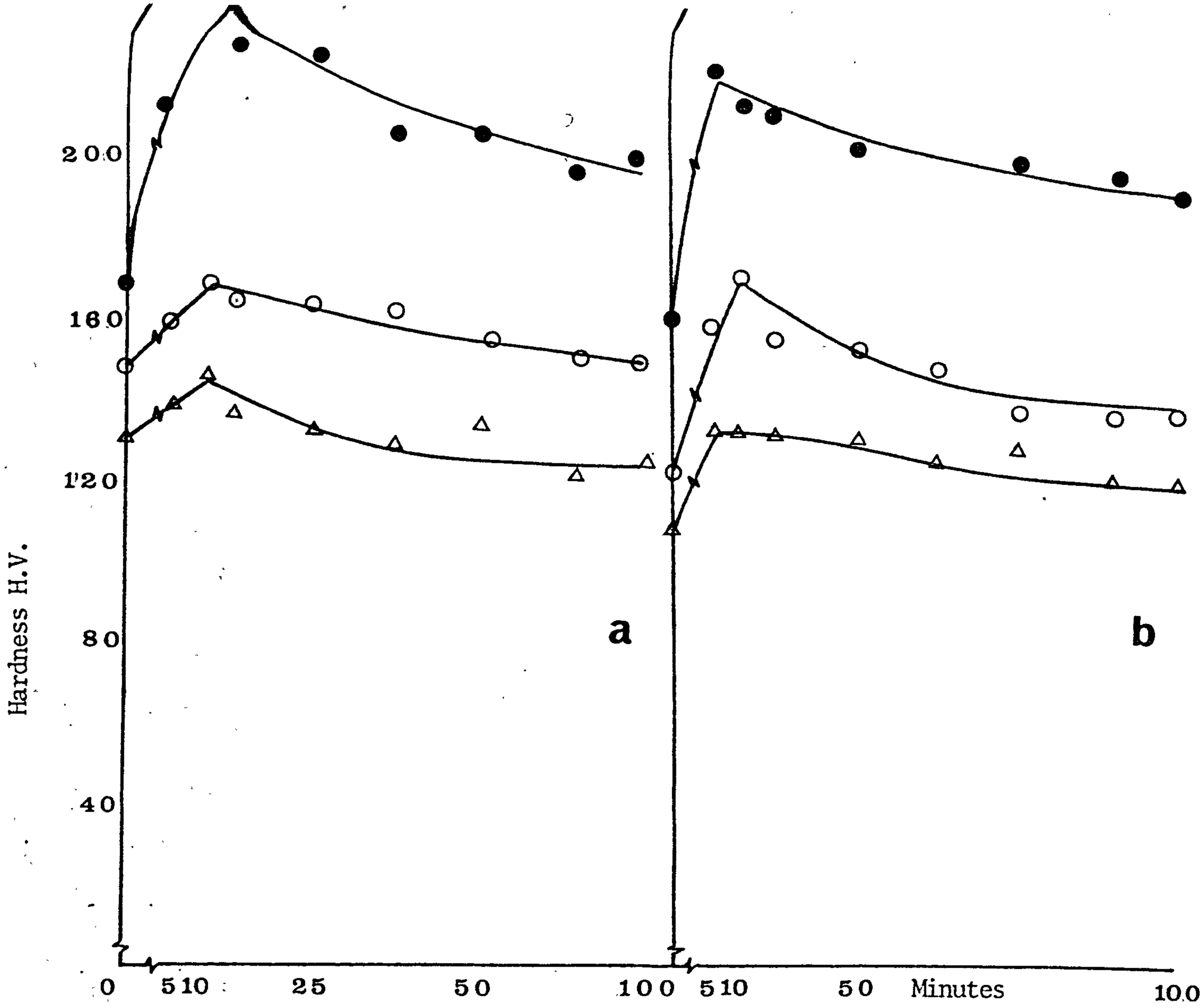

Fig. 50. Vickers hardness as a function of treatment time by inert gas in water quenched samples

a) Fe + 6% Cu b) Fe + 8% Cu

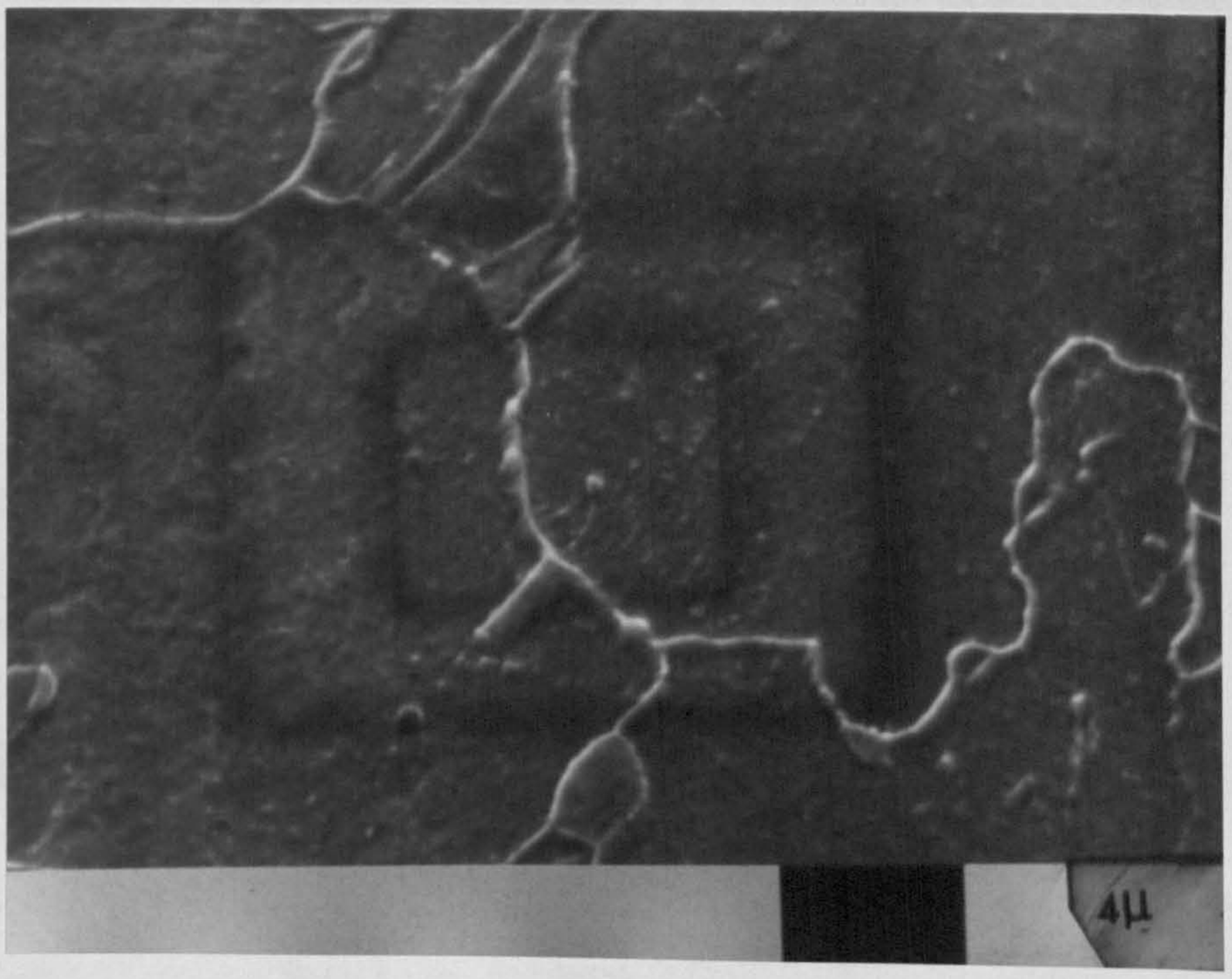

Fig. 51. - 100# Pre-alloyed (Fe + 2% Cu) D = 6.8 g/cc

(W.Q.) Aged (500 hours (525° C x 5K

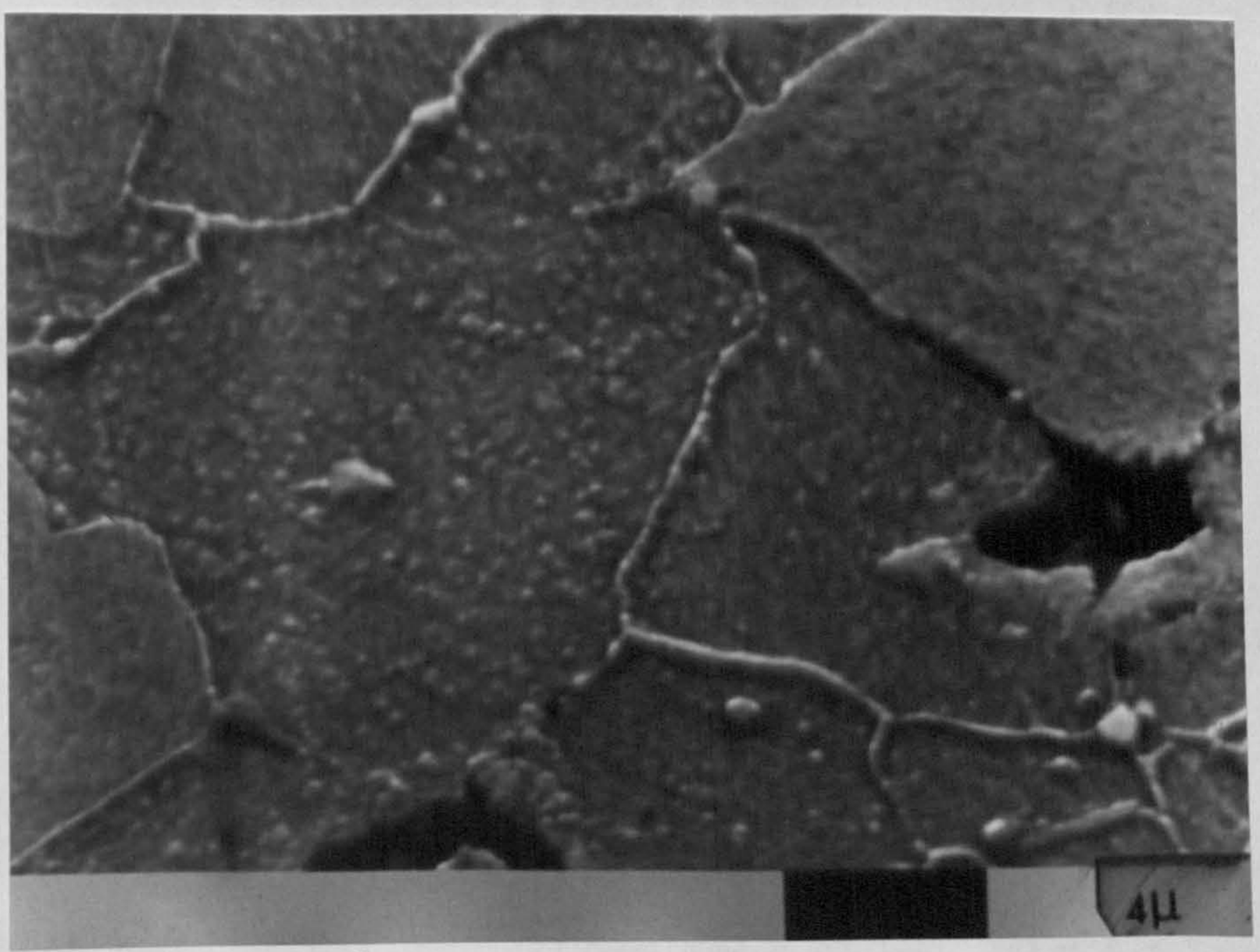

Fig. 52. - 100# Pre-alloyed (Fe + 6% Cu) D = 6.8 g/cc

Aged (500 hours (525° C x 5K

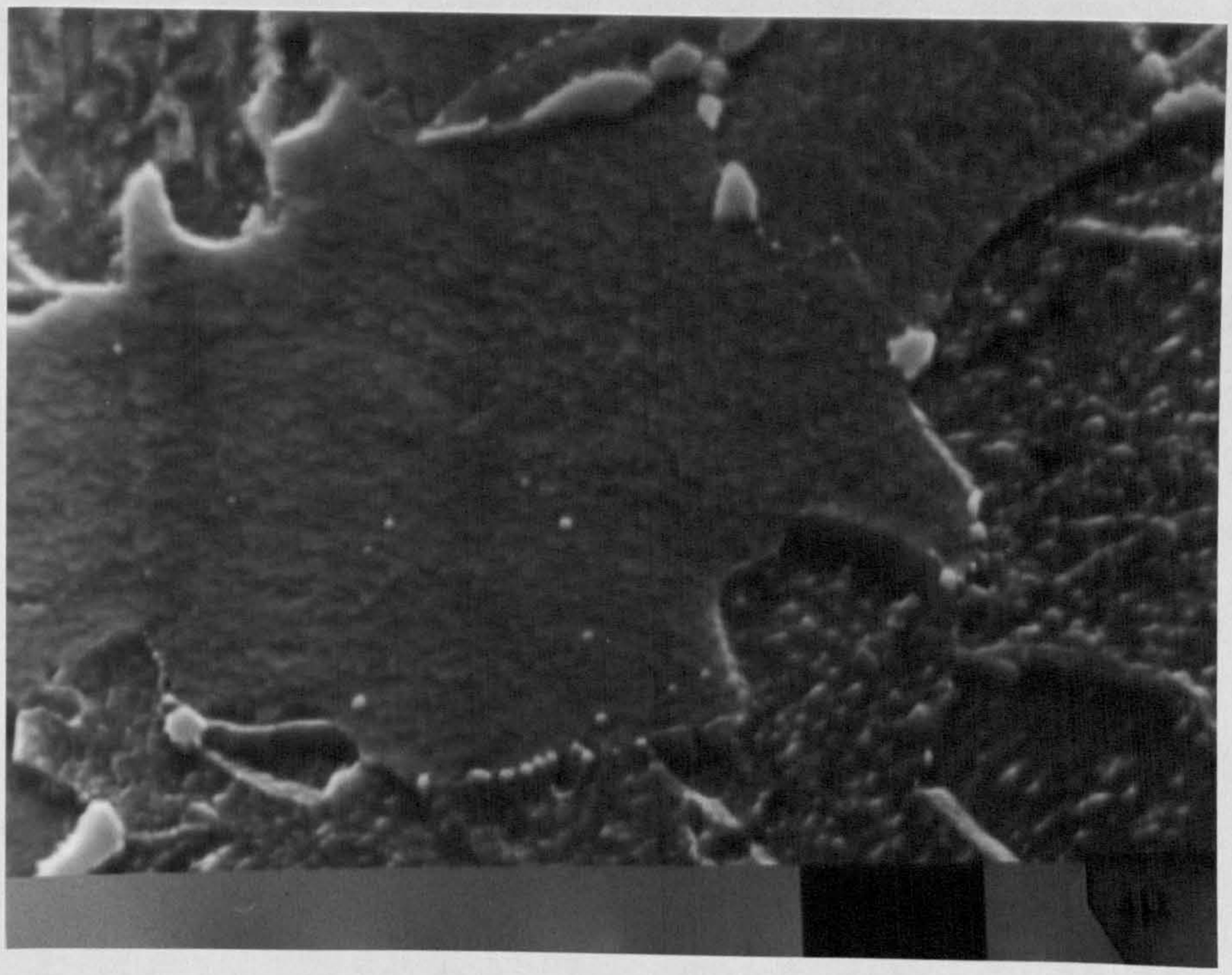

Fig. 53. - 100# Pre-alloyed (Fe + 8% Cu) D = 6.8 $^{g}/_{cc}$

(W.Q.) Aged (500 hours
(525° C

x 5K

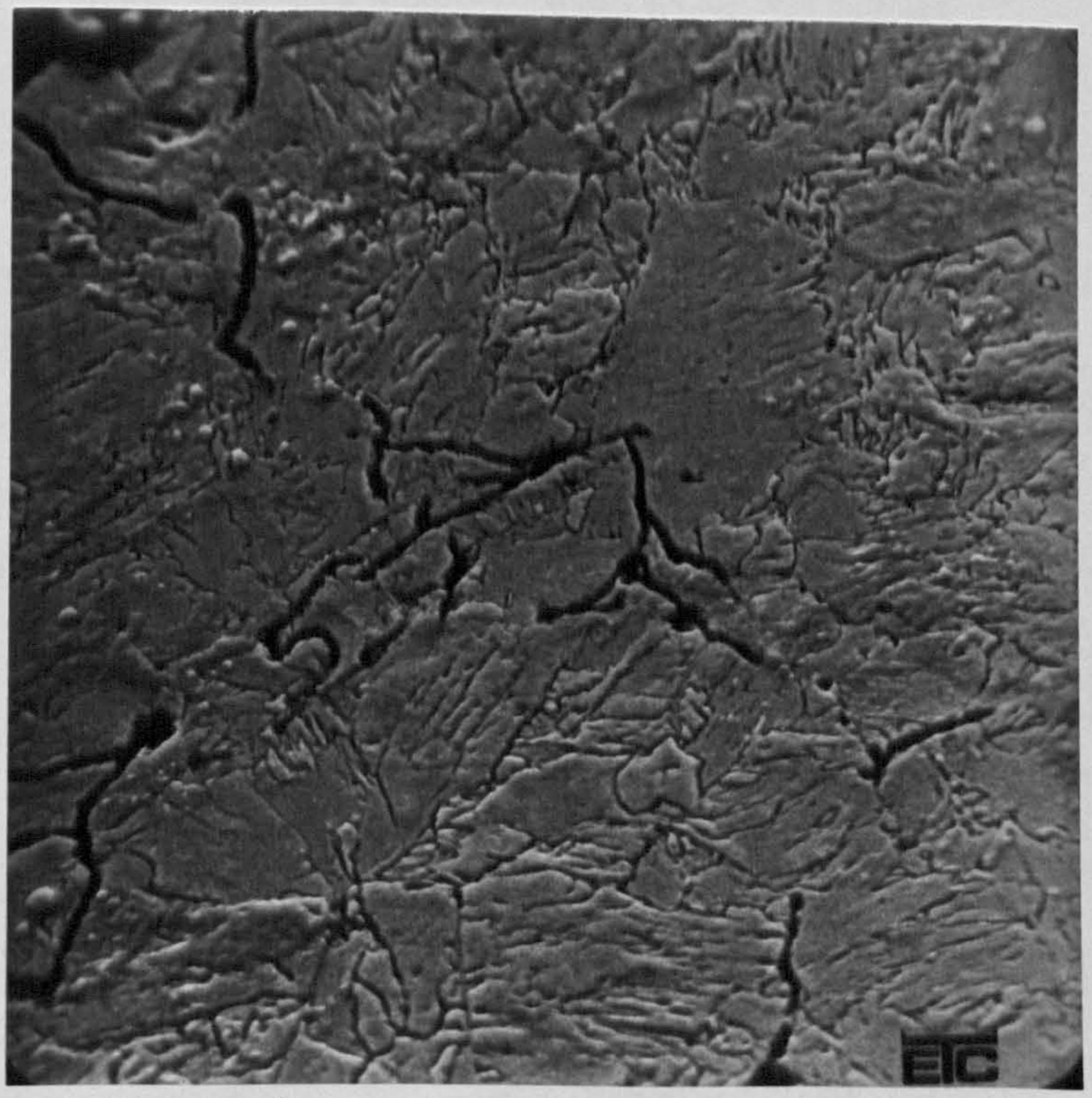

Fig. 54. - 100# Pre-alloyed (Fe + 8% Cu) D = 6.8 $^{g}/_{cc}$

(W.Q.)

x 1.2K

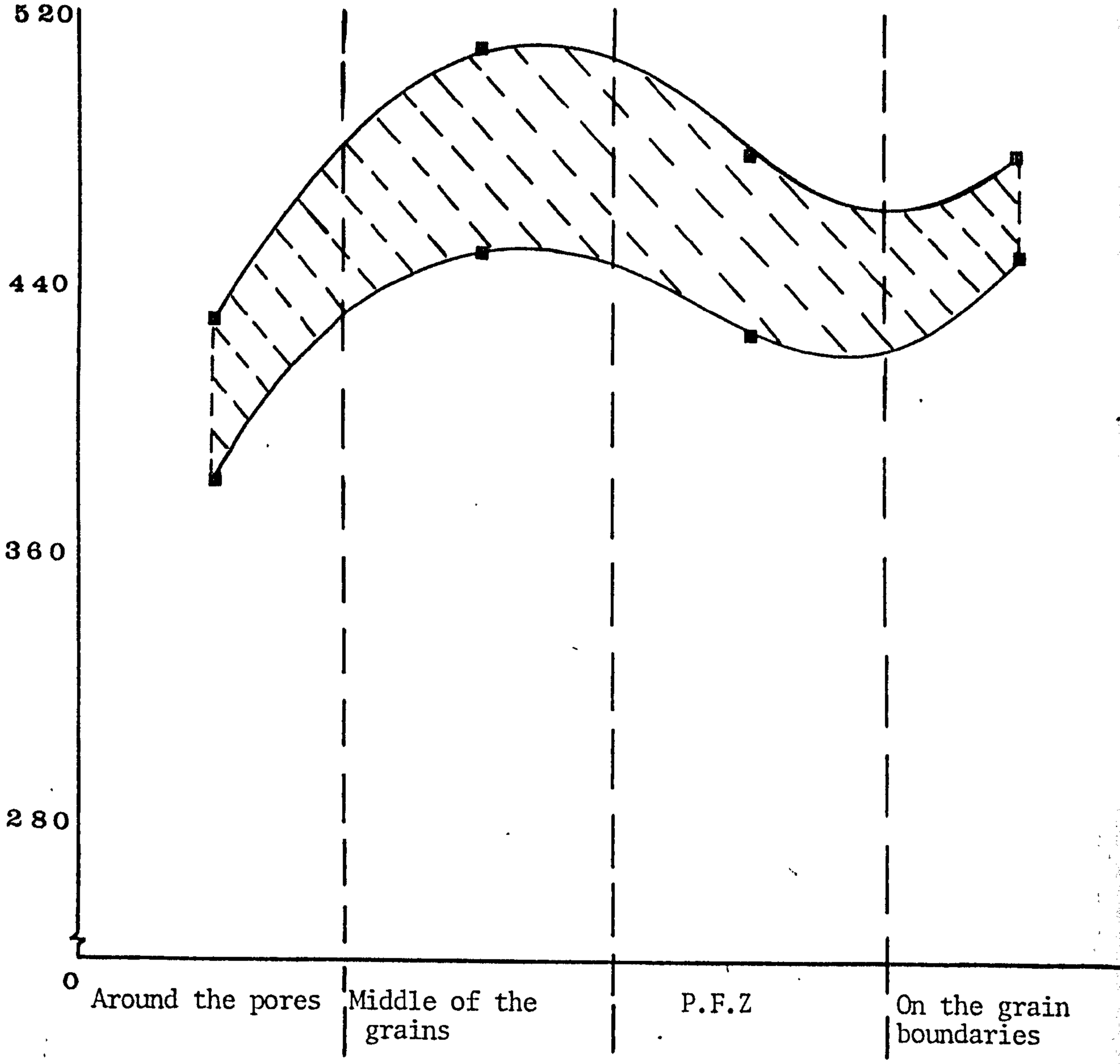

Fig. 55. Micro-hardness of Fe + 4% cu alloy at peak hardness in density $6.8^{g}/_{cc}$.

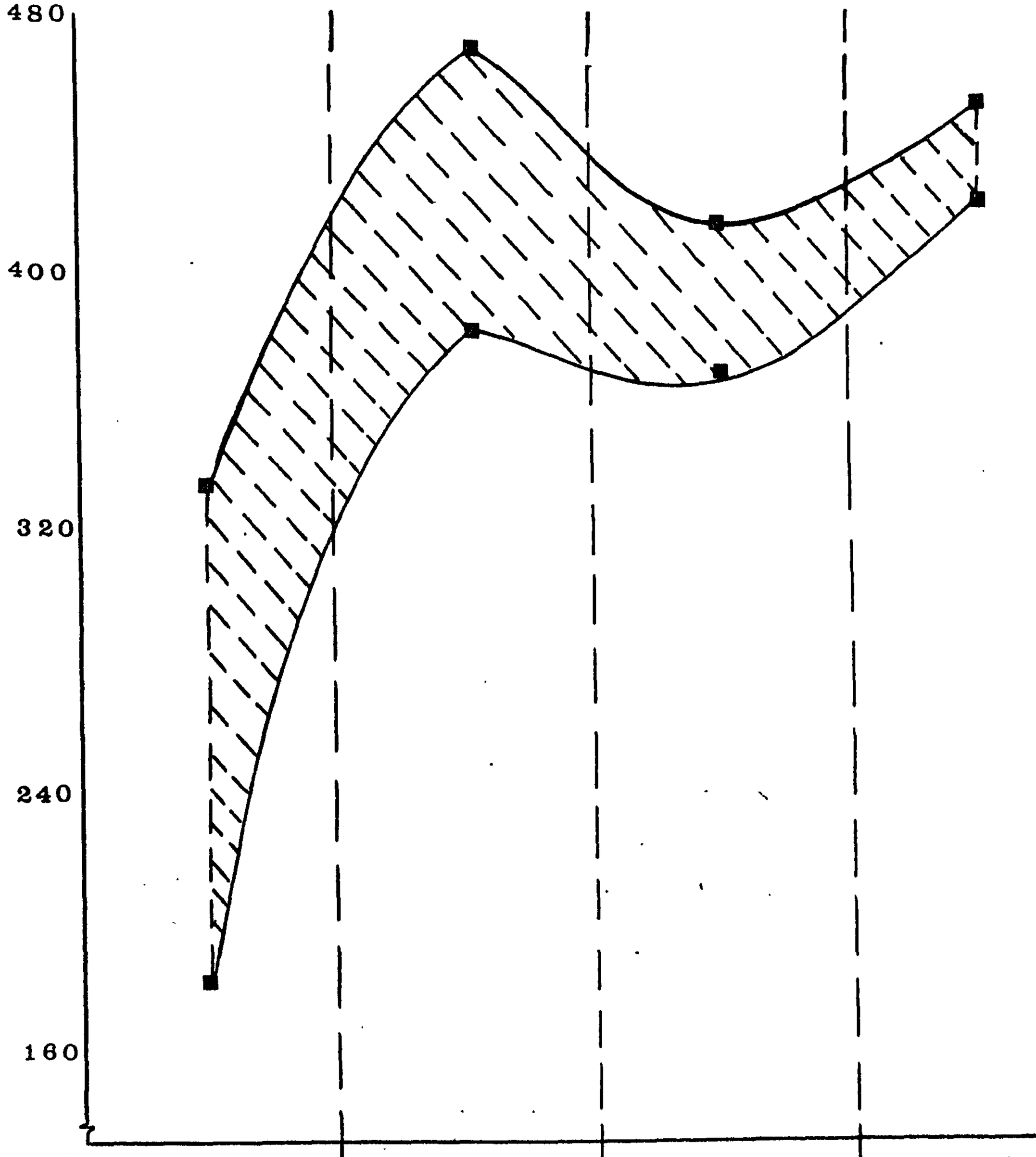

Fig. 56.
Micro-hardness of Fe + 4% Cu alloy at peak hardness in density 6.0 $^{g}/_{cc}$

Key for Figs. 57 and 58

● ●	Fe
○ ○	Aged (steam)
△ △	Aged (Inert gas)

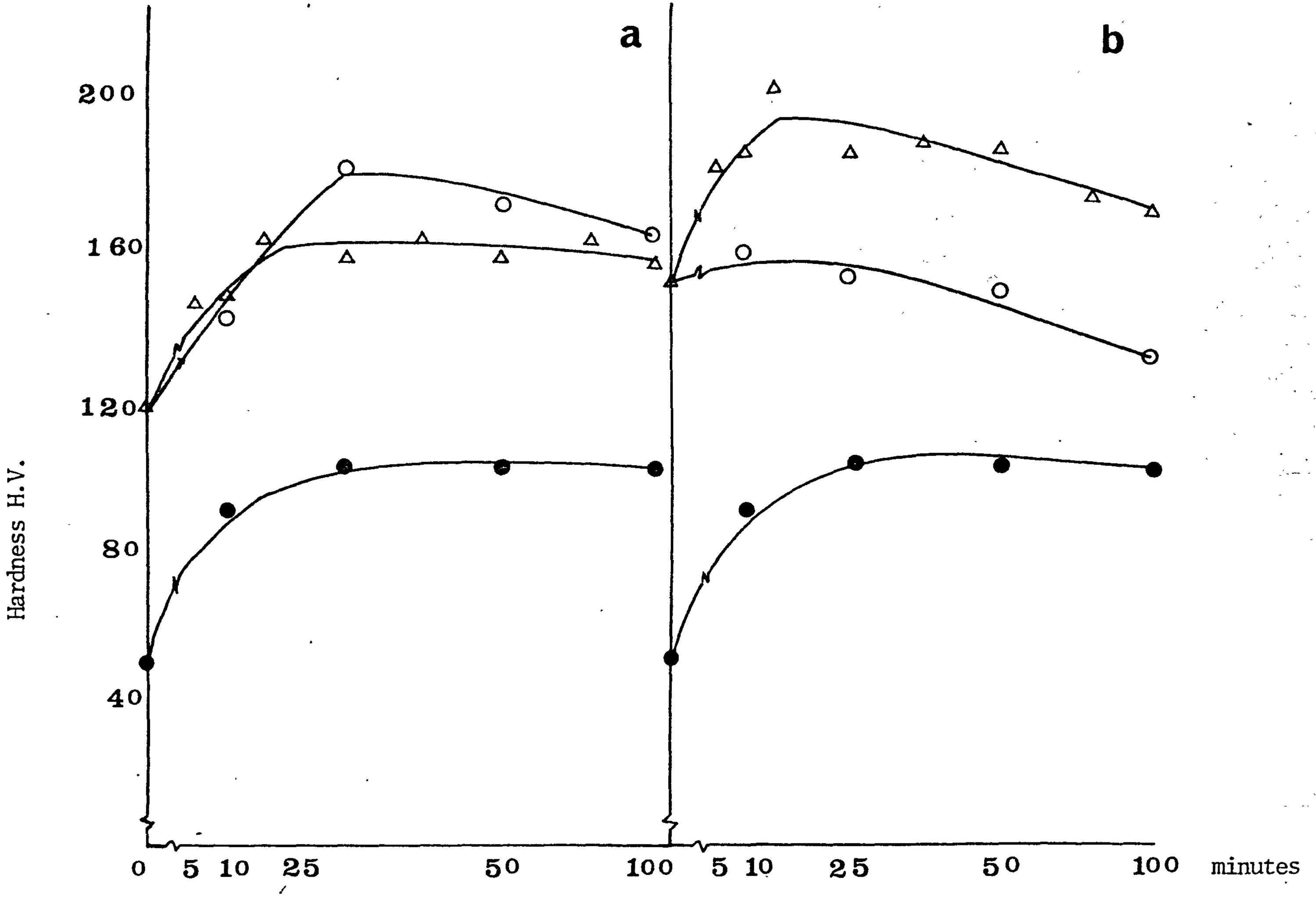

Fig. 57. Vickers hardness as a function of treatment time by steam and inert gas.

a) Fe + 2% Cu b) Fe + 4% Cu

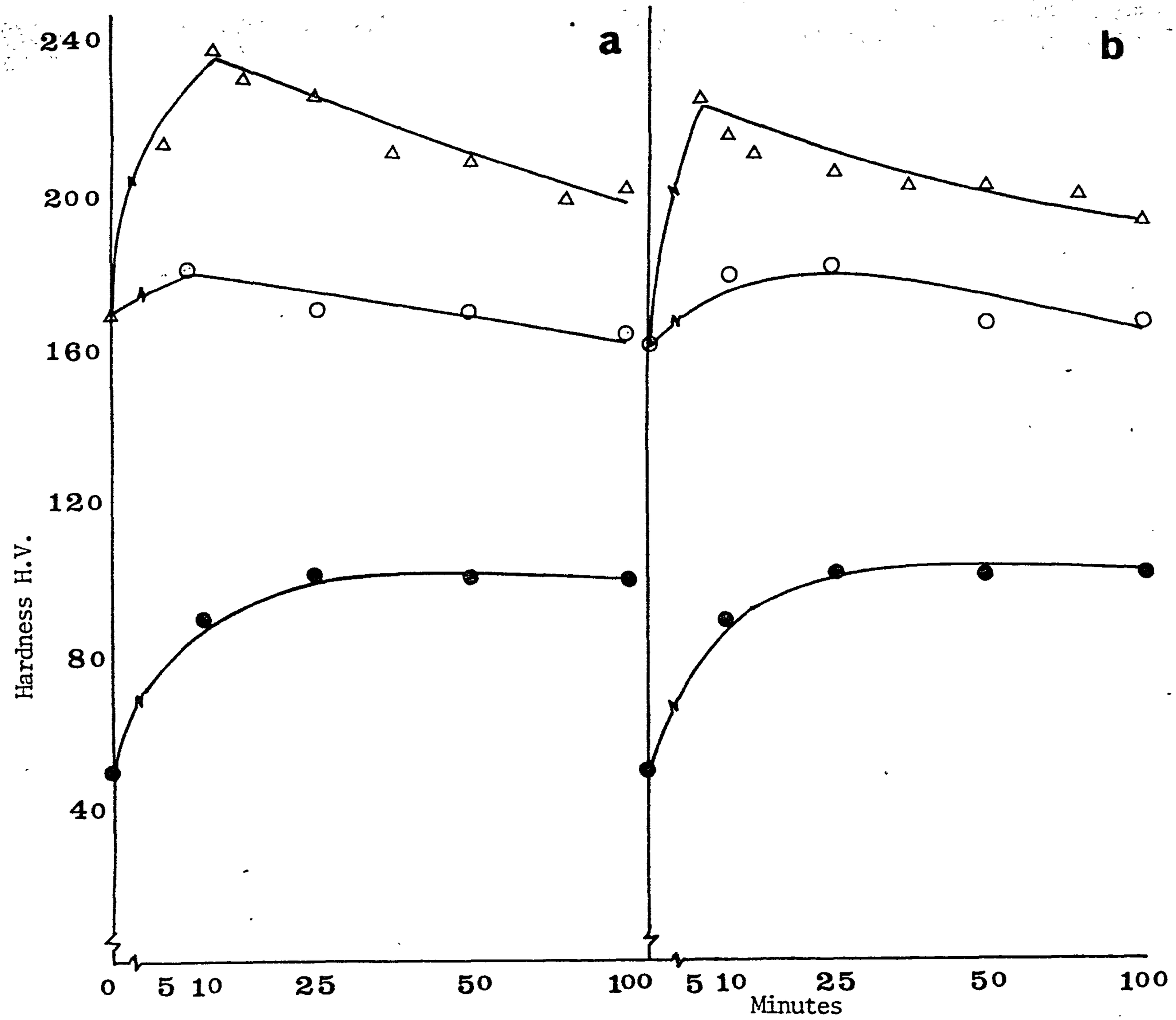

Fig. 58. Vickers hardness as a function of treatment time by steam and inert gas
a) Fe + 6% Cu b) Fe + 8% Cu

Fig. 59. Comparison of Vickers hardness of solution treated and peak hardness (steam and inert gas) condition for the four alloys.

Fig. 60. Vickers hardness as a function of percentage of weight gain for pure iron.

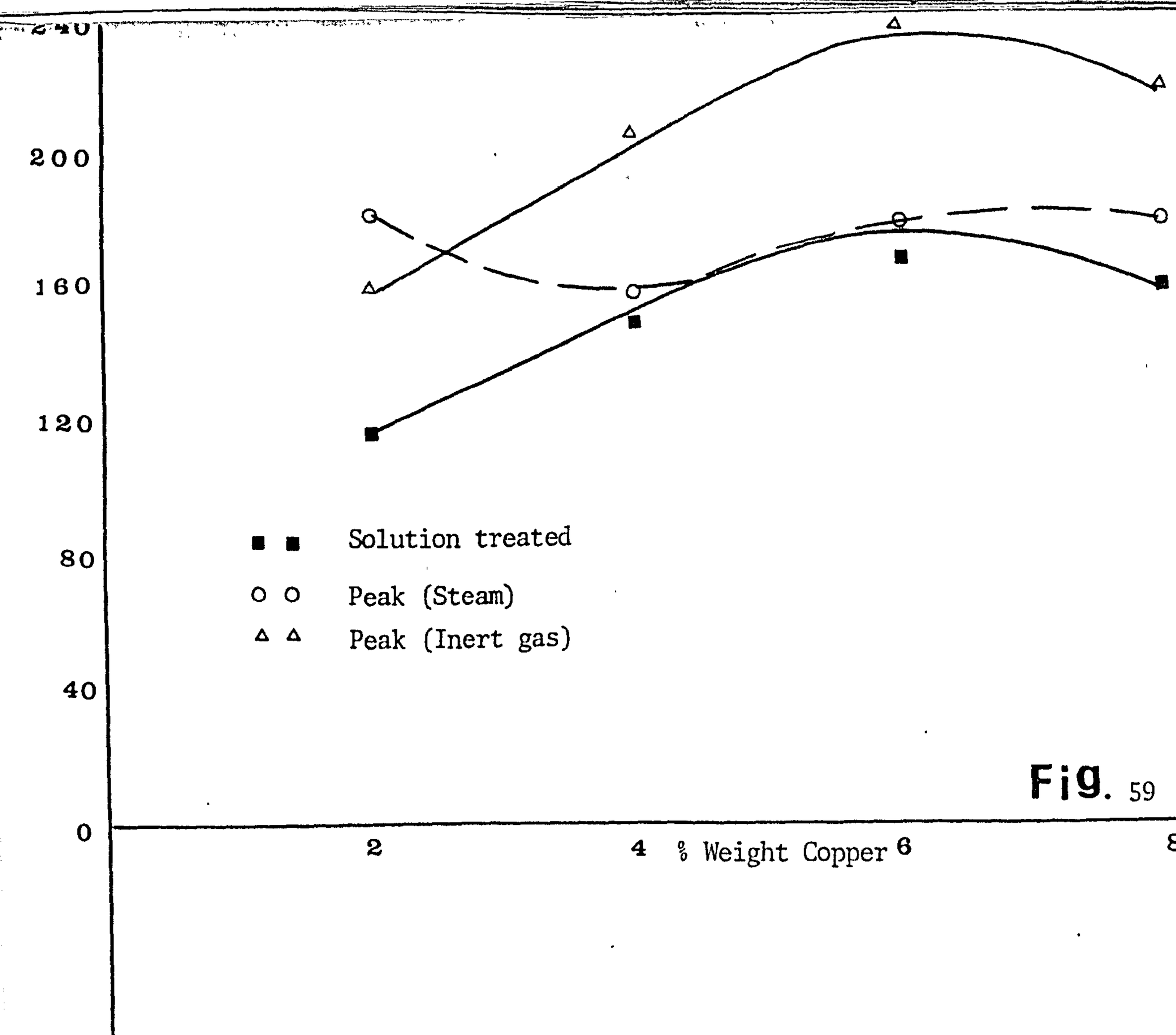
240
200
160
120
80
40
0
2
4
% Weight Copper
6
8
■ ■ Solution treated
○ ○ Peak (Steam)
△ △ Peak (Inert gas)

Fig. 59

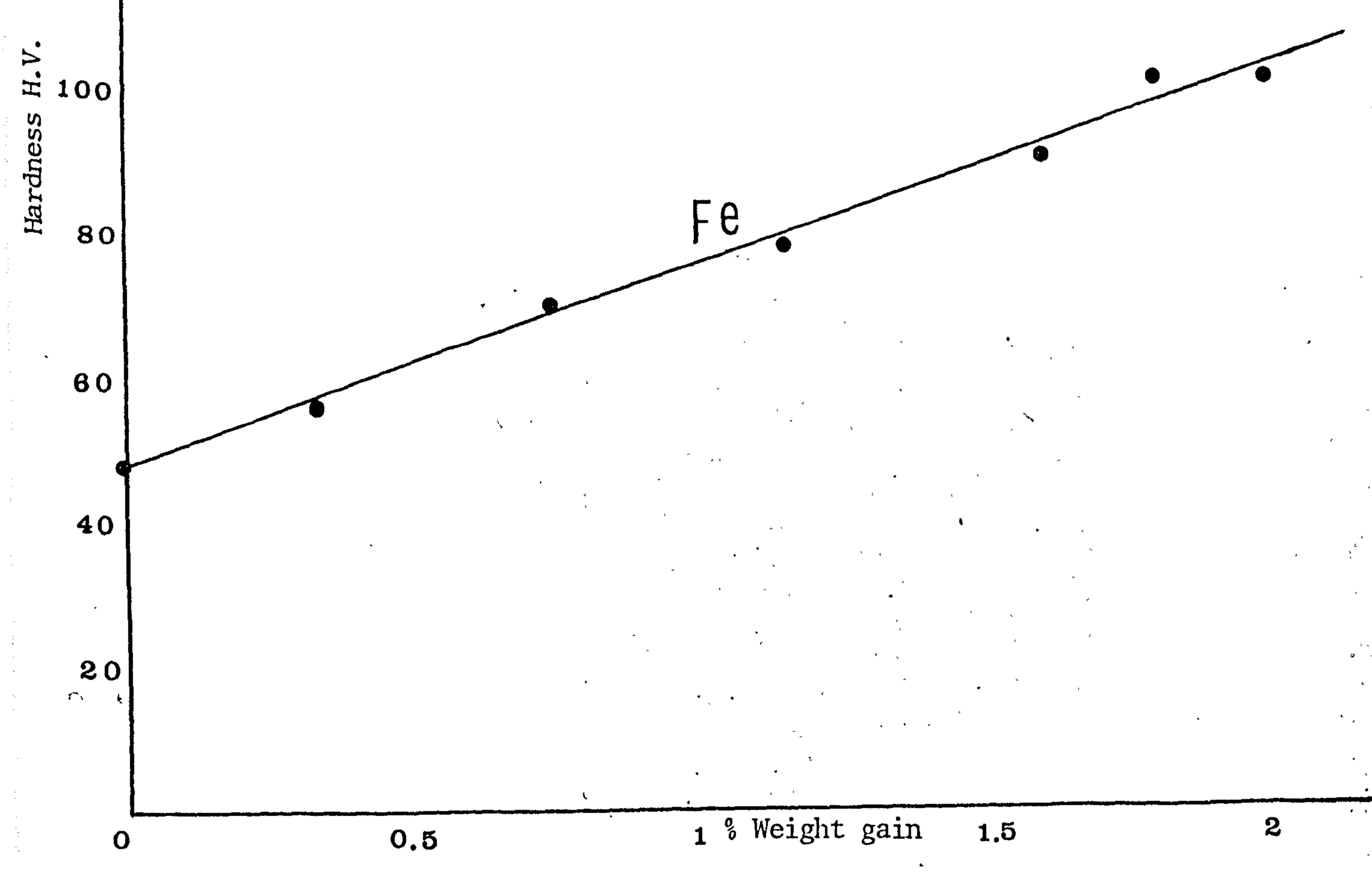
Hardness H.V.
100
80
60
40
20
0
Fe
0
0.5
1
% Weight gain
1.5
2

Fig. 60

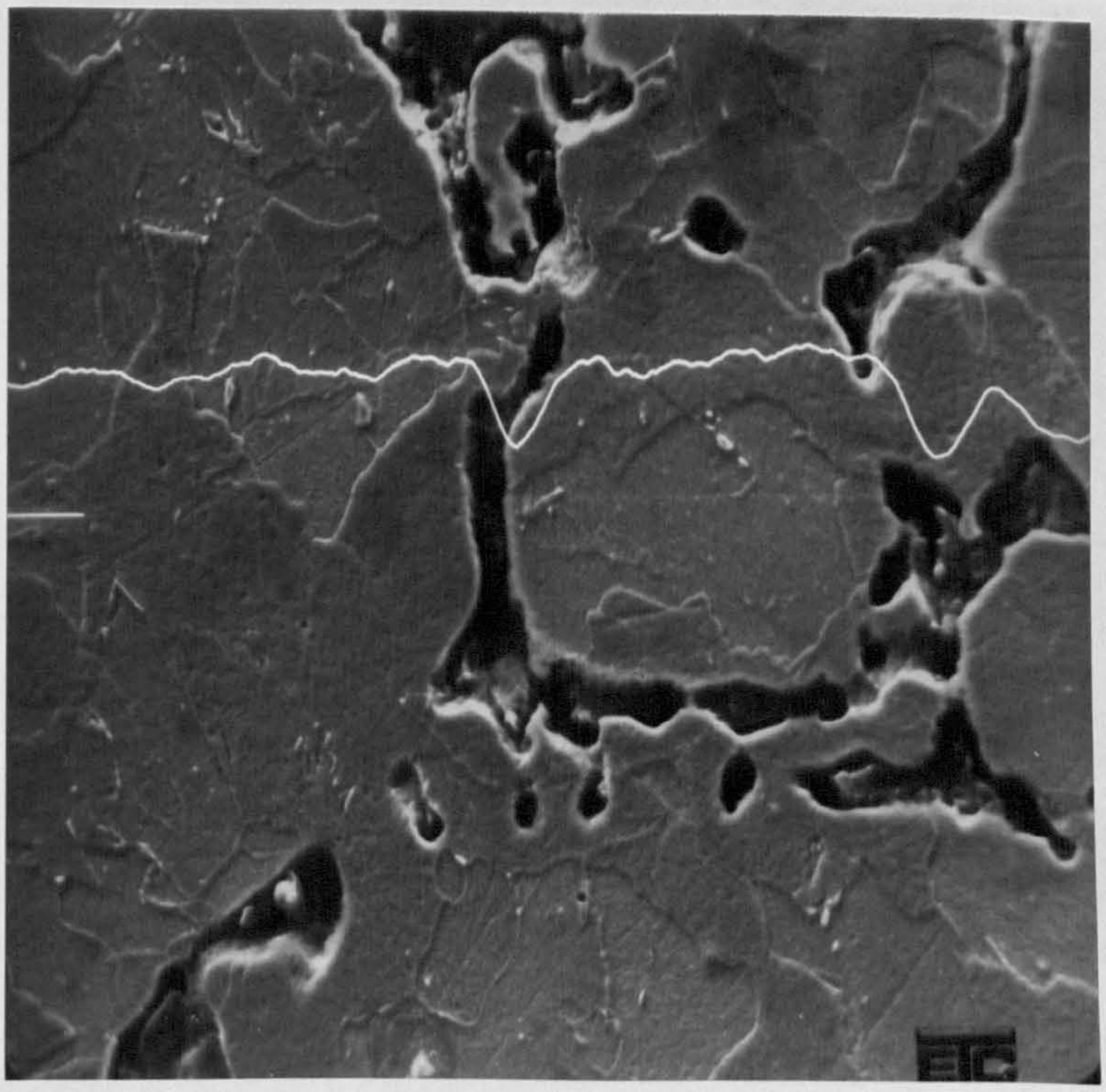

Fig. 61a. - 100# Pre-alloyed (Fe + 2% Cu) D = 6.8 $^{g}/_{cc}$
(W.Q.) Aged (100 minutes
(525° C x 1K

Cu Line Probe

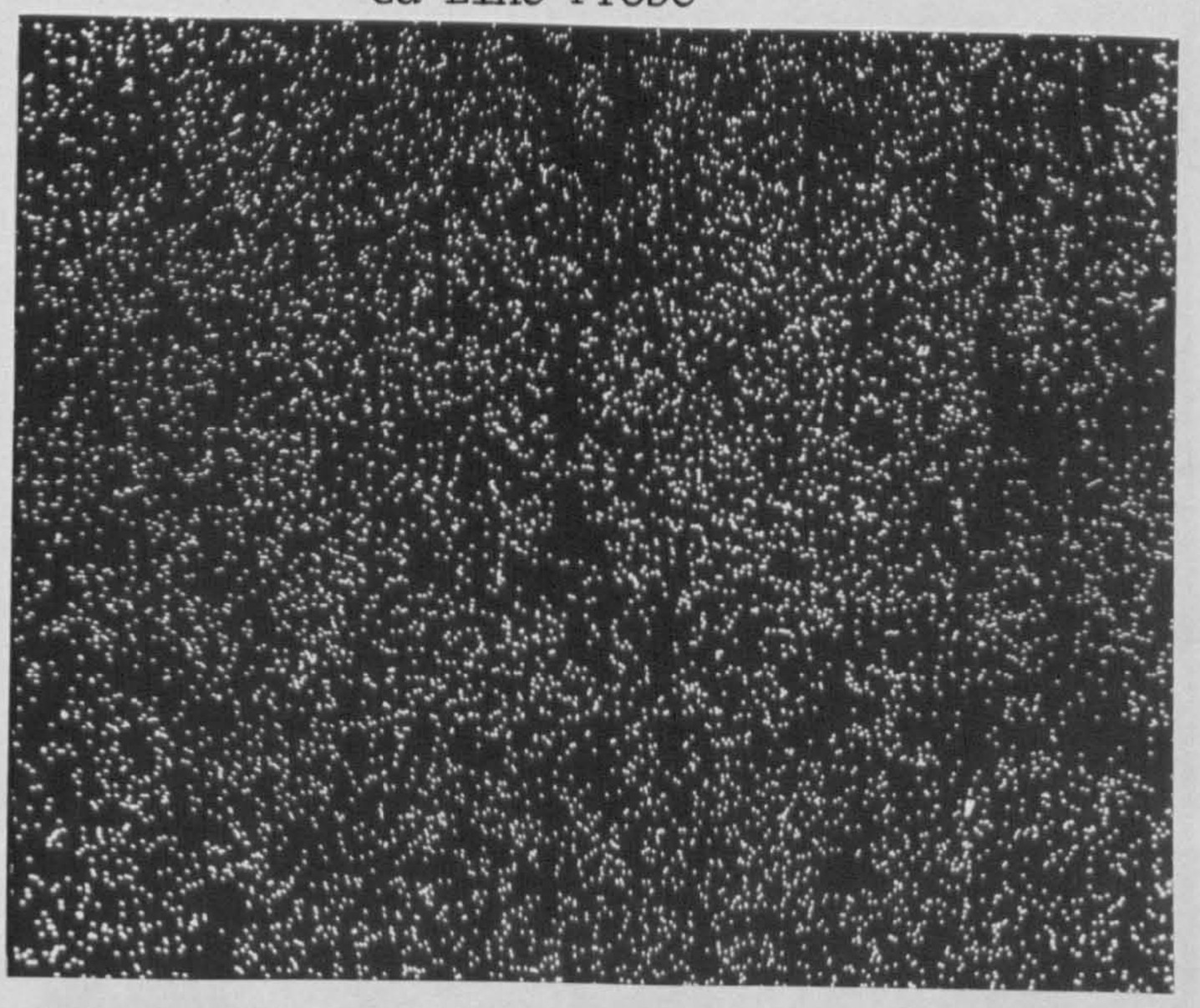

Fig. 61b. Above sample Cu X-ray probe x 1K

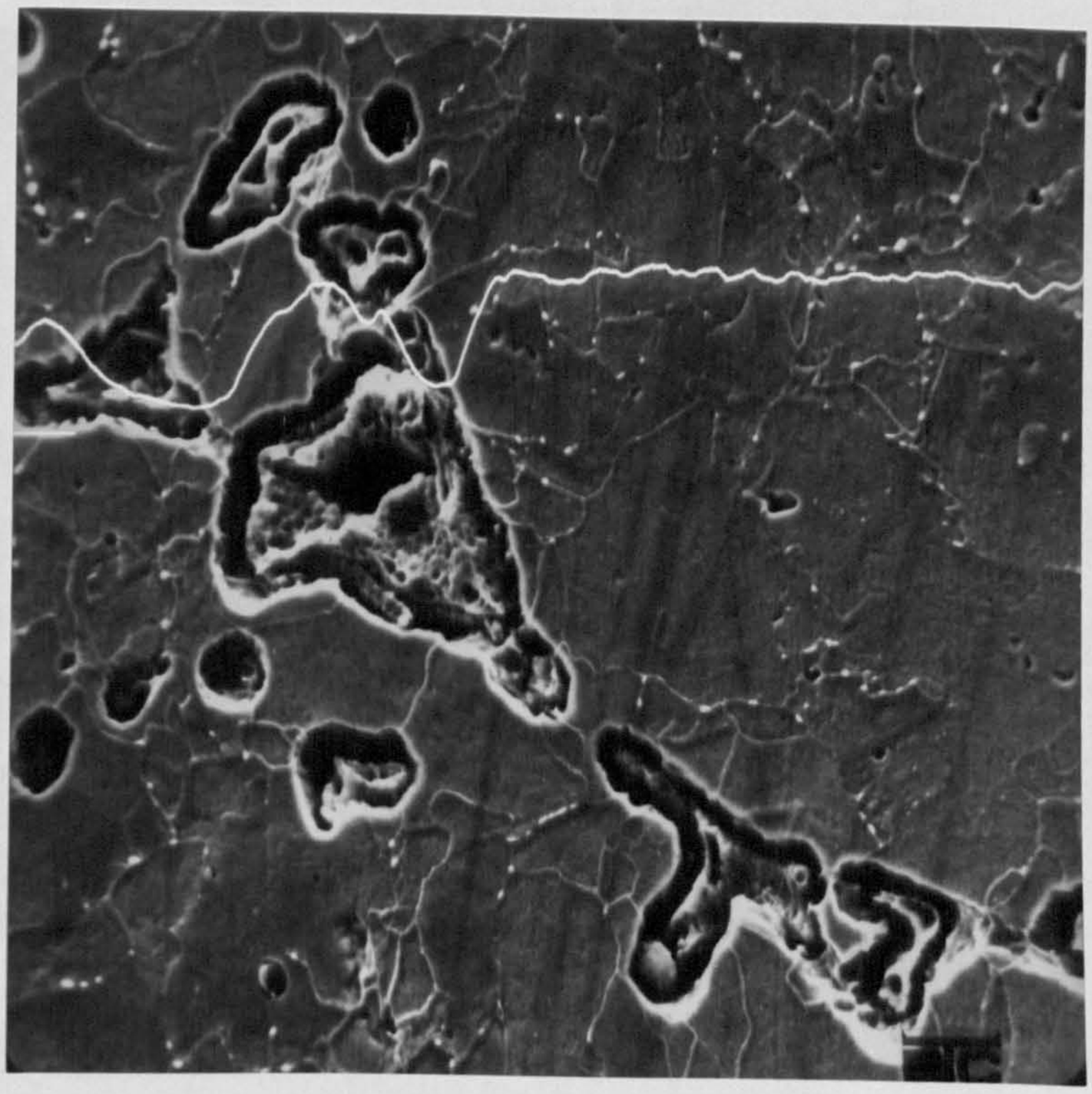

Fig. 62a. - 100# Pre-alloyed (Fe + 2% Cu) D = 6.8 $^{g}/_{cc}$
(W.Q.) Steam treated (100 minutes (525° C x 1K

Cu Line Probe

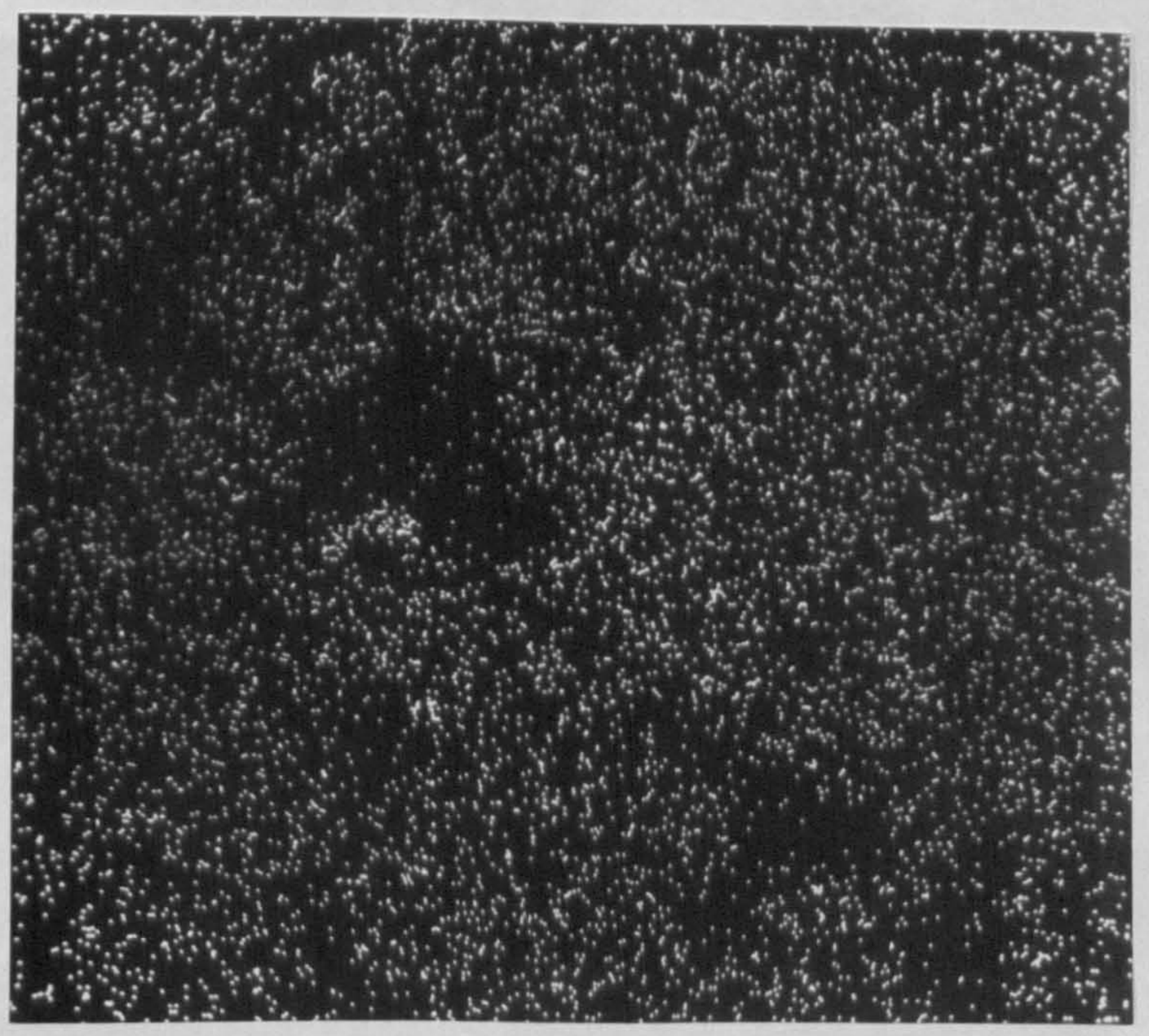

Fig. 62b. Above sample Cu X-ray probe x 1K

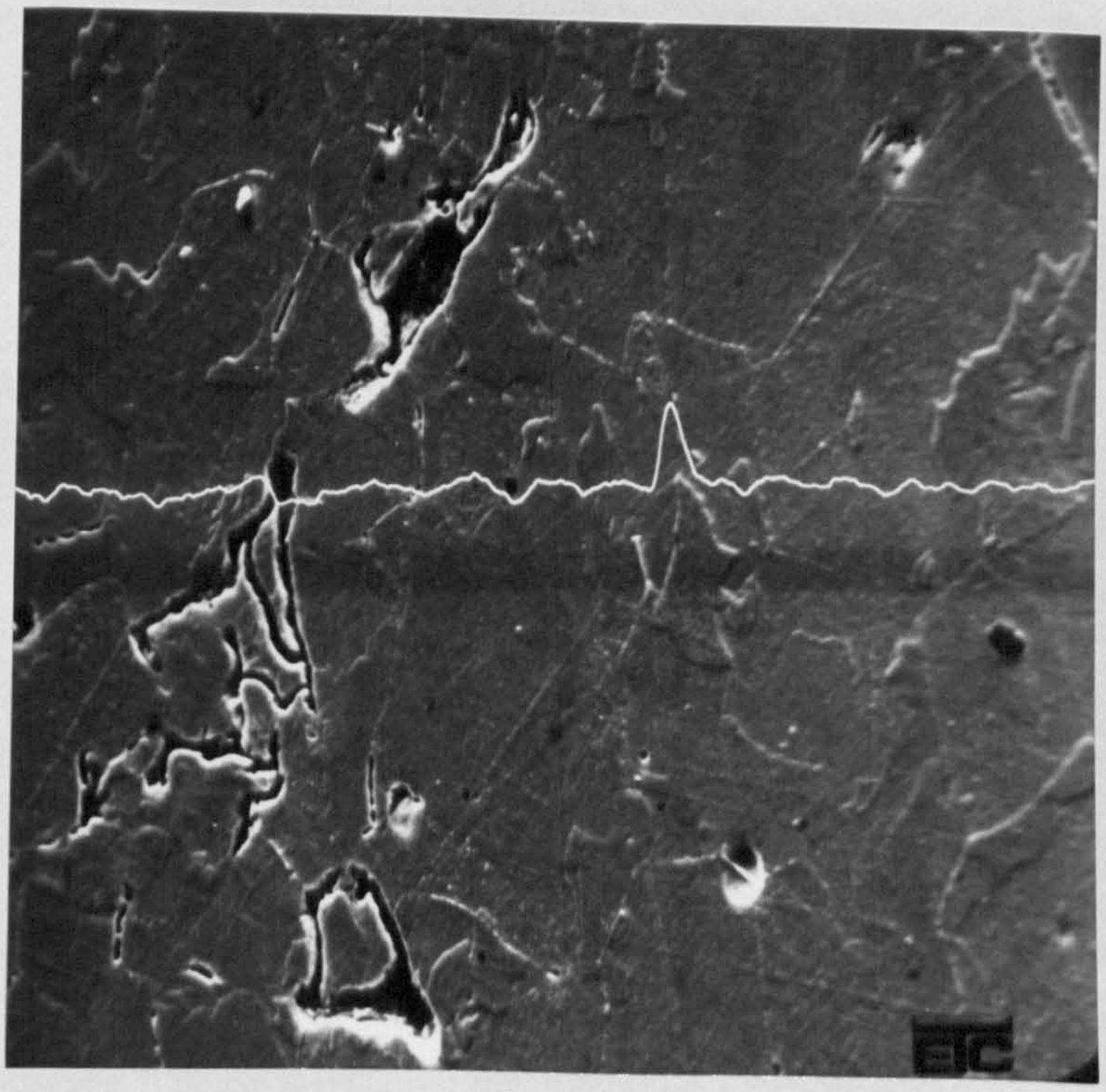

Fig. 63a. - 100# Pre-alloyed (Fe + 8% Cu) D = 6.8 g/cc

(W.Q.) Aged (100 minutes
(525° C

x 1K

Cu Line Probe

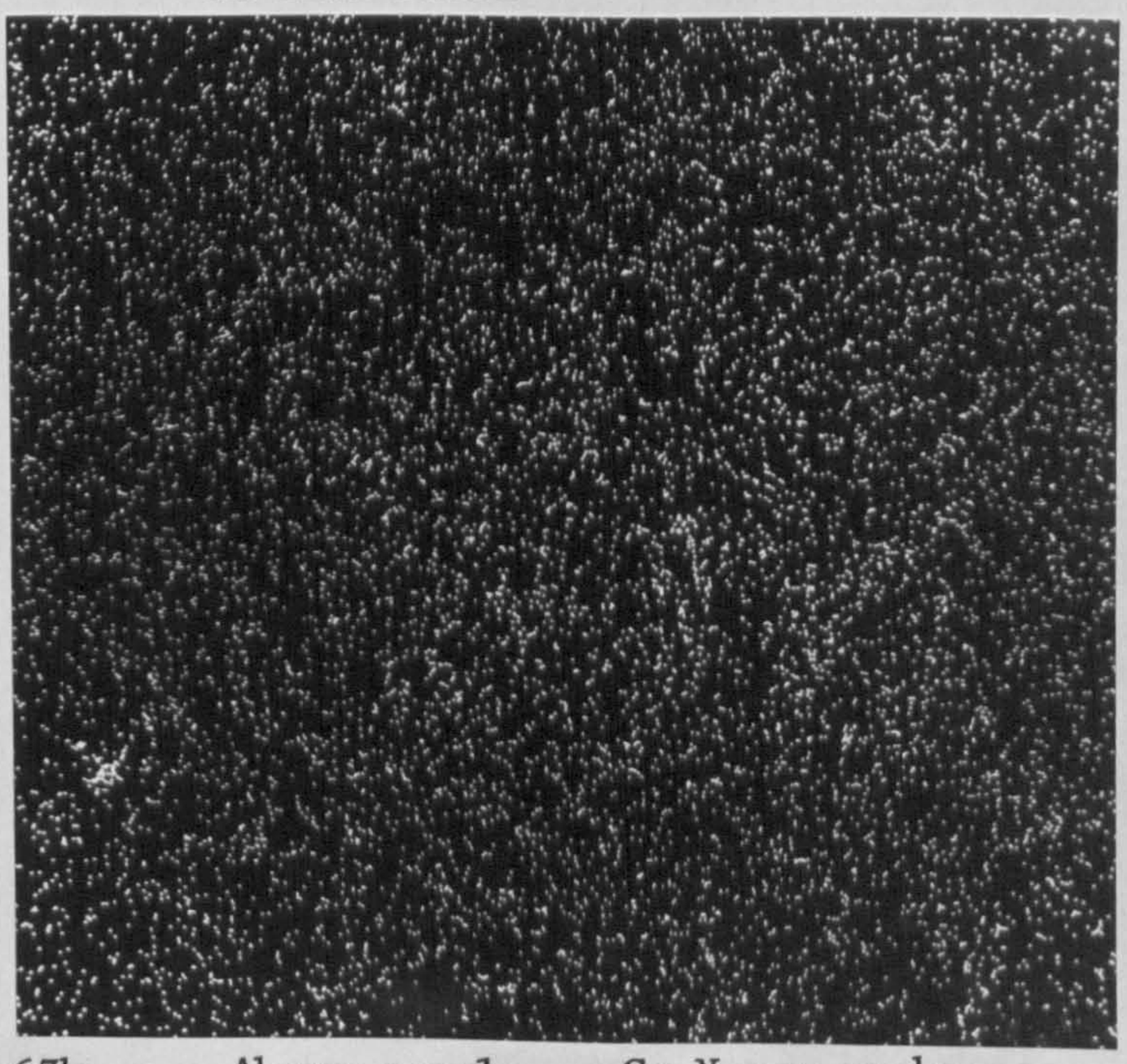

Fig. 63b. Above sample Cu X-ray probe x 1K

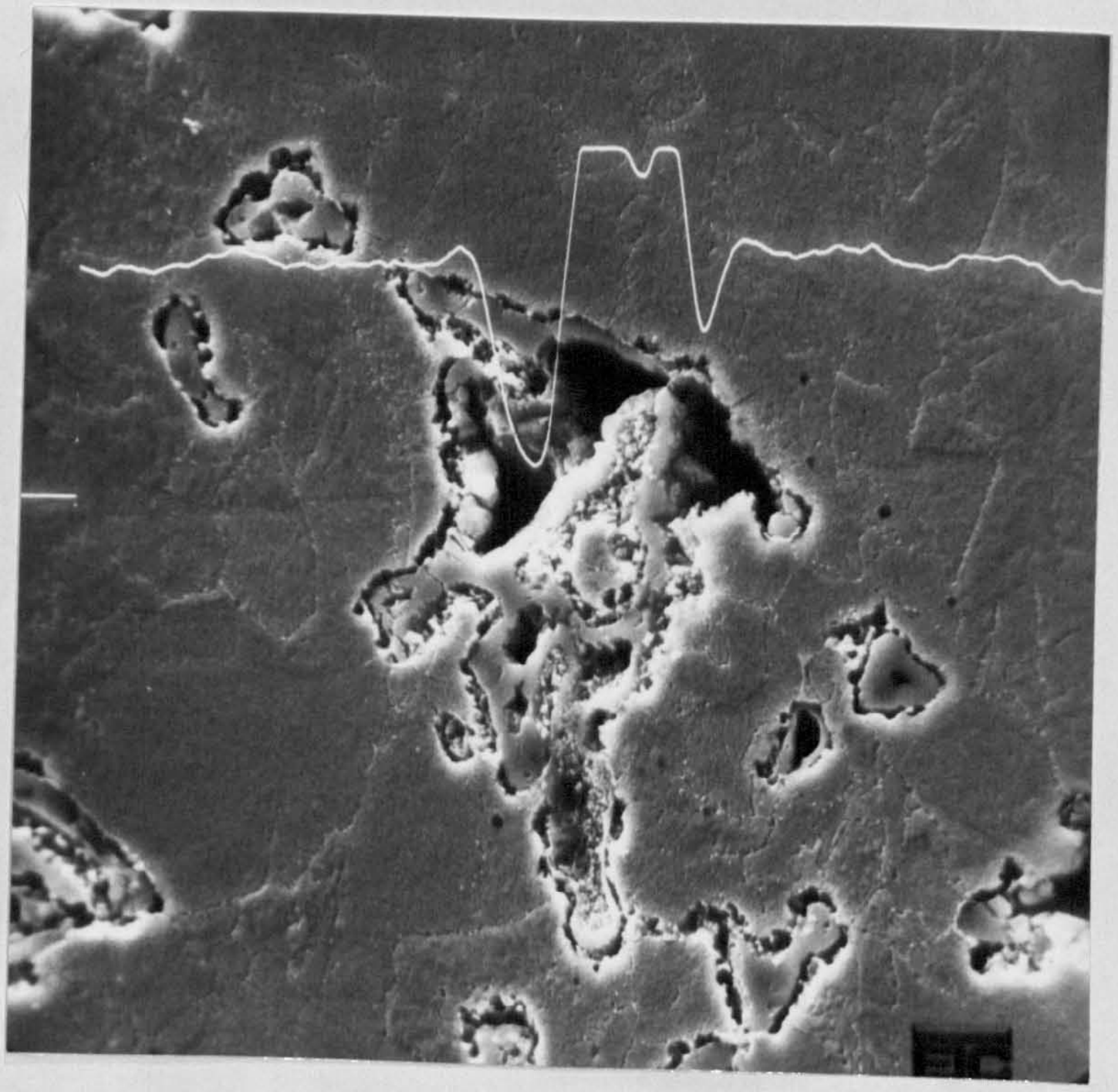

Fig. 64a. - 100# Pre-alloyed (Fe + 8% Cu) D = 6.8 g/cc
(W.Q.) Steam treated (100 minutes (525° C x 1K

Cu Line Probe

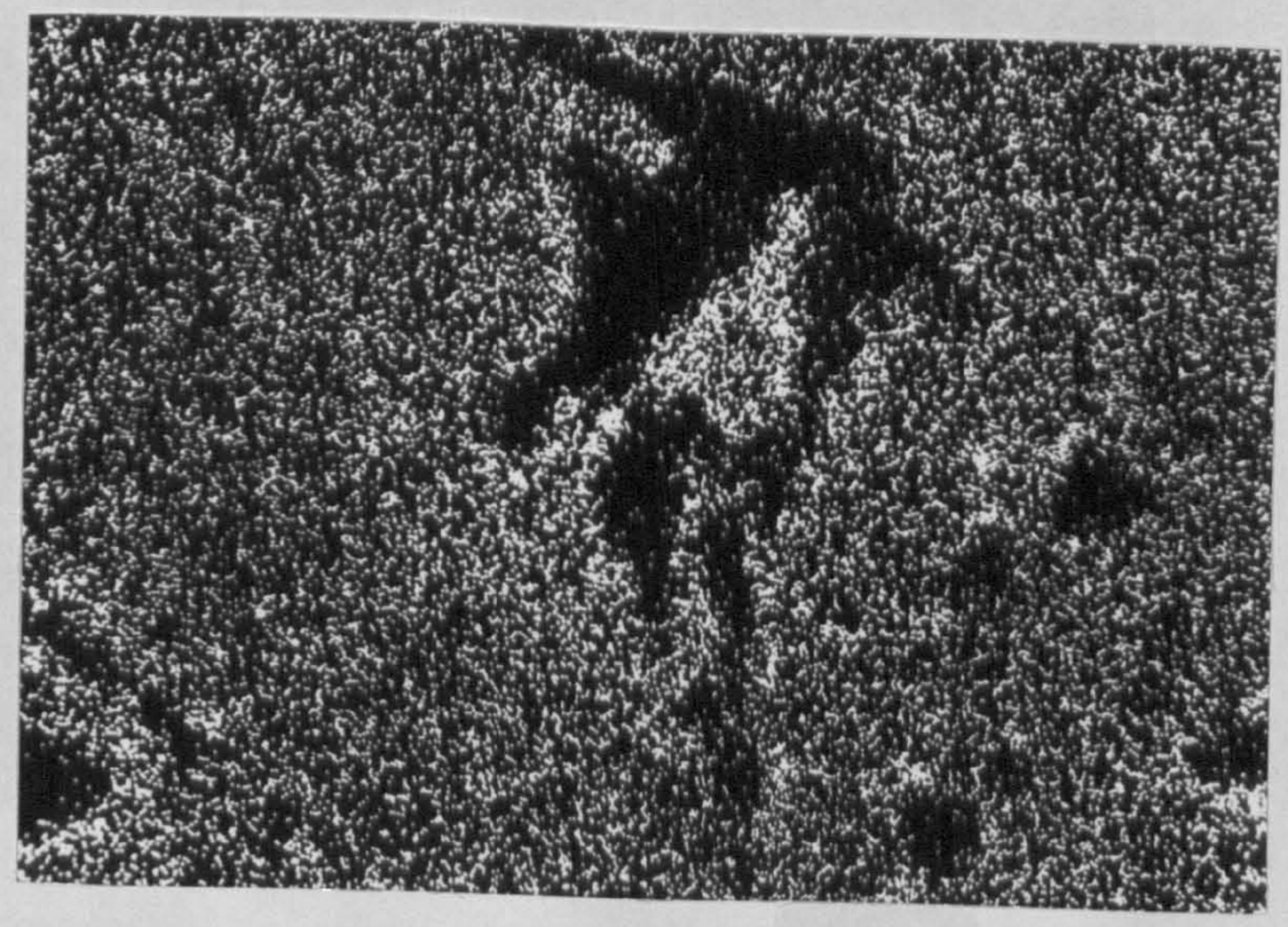

Fig. 64b. Above sample Cu X-ray probe x 1K

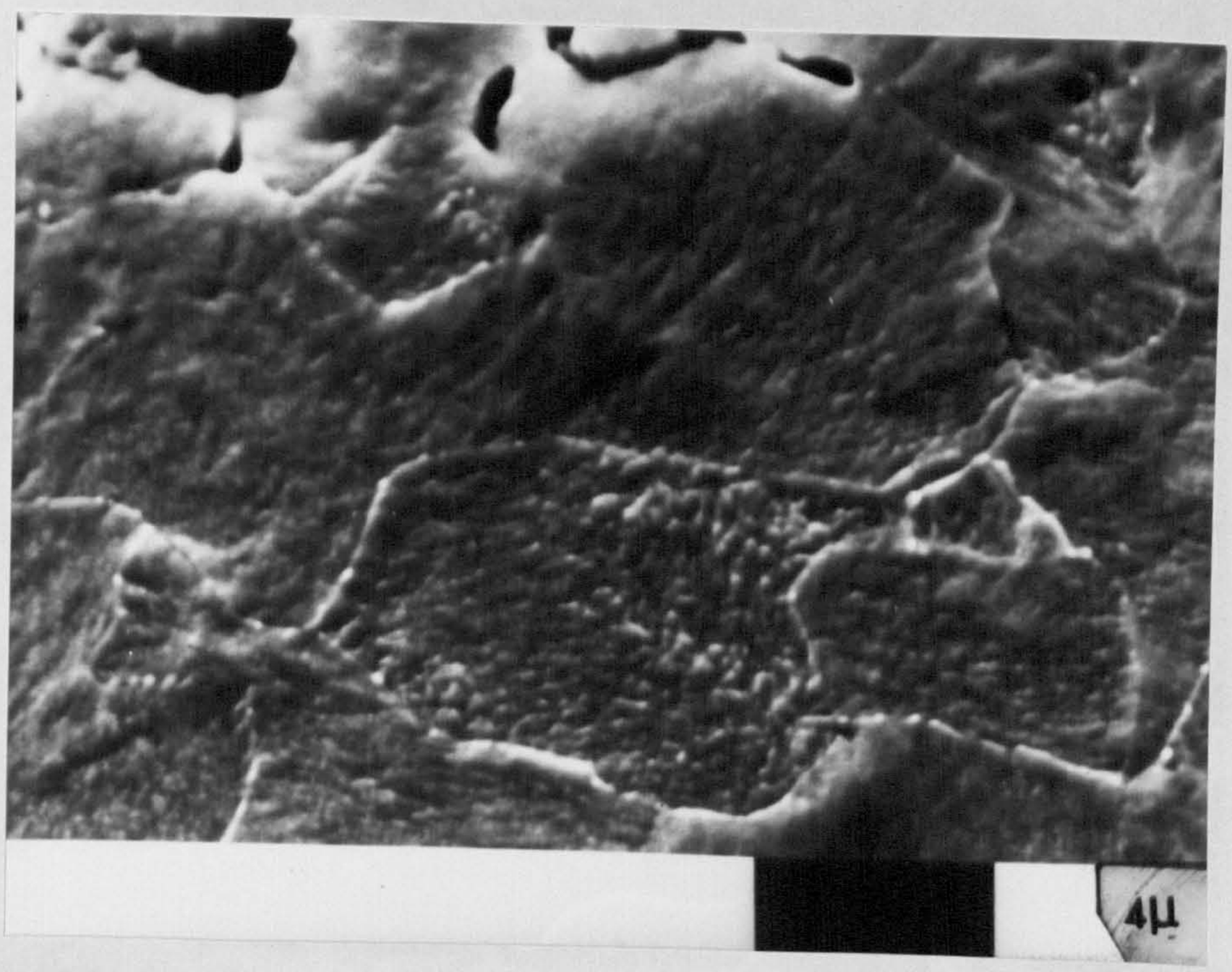

Fig. 65. - 100# Pre-alloyed (Fe + 6% Cu) D = 6.8 $^{g}/_{cc}$
(W.Q.) Steam treated (75 minutes (525° C + Aged (498.75 hours (525° C
x 5K

Fig. 66. - 100# Pre-alloyed (Fe + 8% Cu) D = 6.8 $^{g}/_{cc}$
(W.Q.) Steam treated (75 minutes (525° C + Aged (498.75 hours (525° C
x 5K

Fig. 67. - 100# Pre-alloyed (Fe + 4% Cu) D = 6.0 g/cc
(W.Q.) Steam treated (100 minutes
(525° C x 2K
Cu Line Probe

Fig. 68. - 100# Pre-alloyed (Fe + 6% Cu) D = 6.0 g/cc
(W.Q.) Steam treated (100 minutes
(525° C x 5K
Cu Line Probe

Key for Figs. 69, 70, 71 and 72

● ●	Density 6.8 $^{g}/_{cc}$
○ ○	Density 6.4 $^{g}/_{cc}$
△ △	Density 6.0 $^{g}/_{cc}$

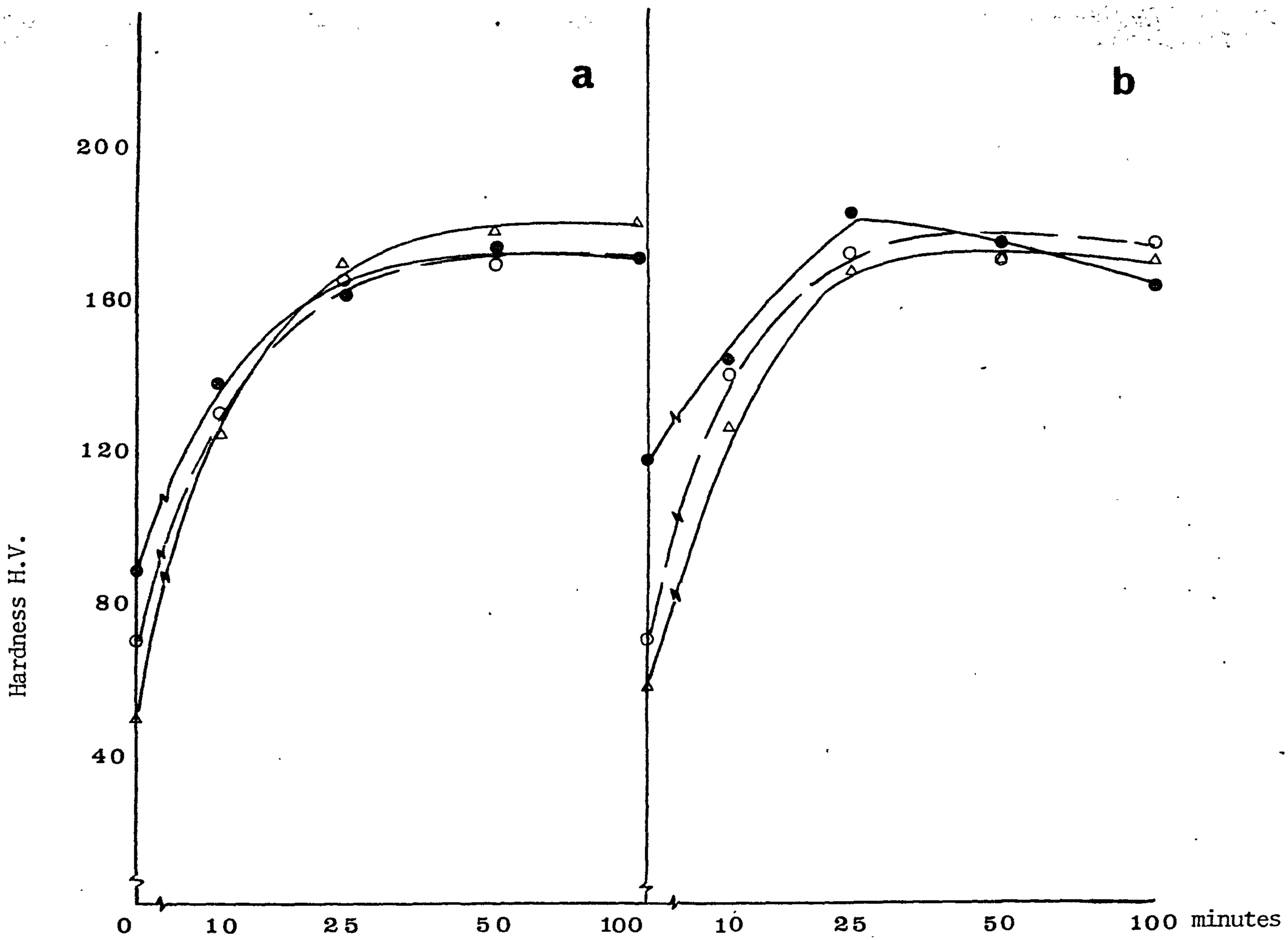

Fig. 69. Vickers hardness as a function of steam treatment time for Fe + 2% Cu alloy.
a) Furnace cooled samples b) Water quenched samples

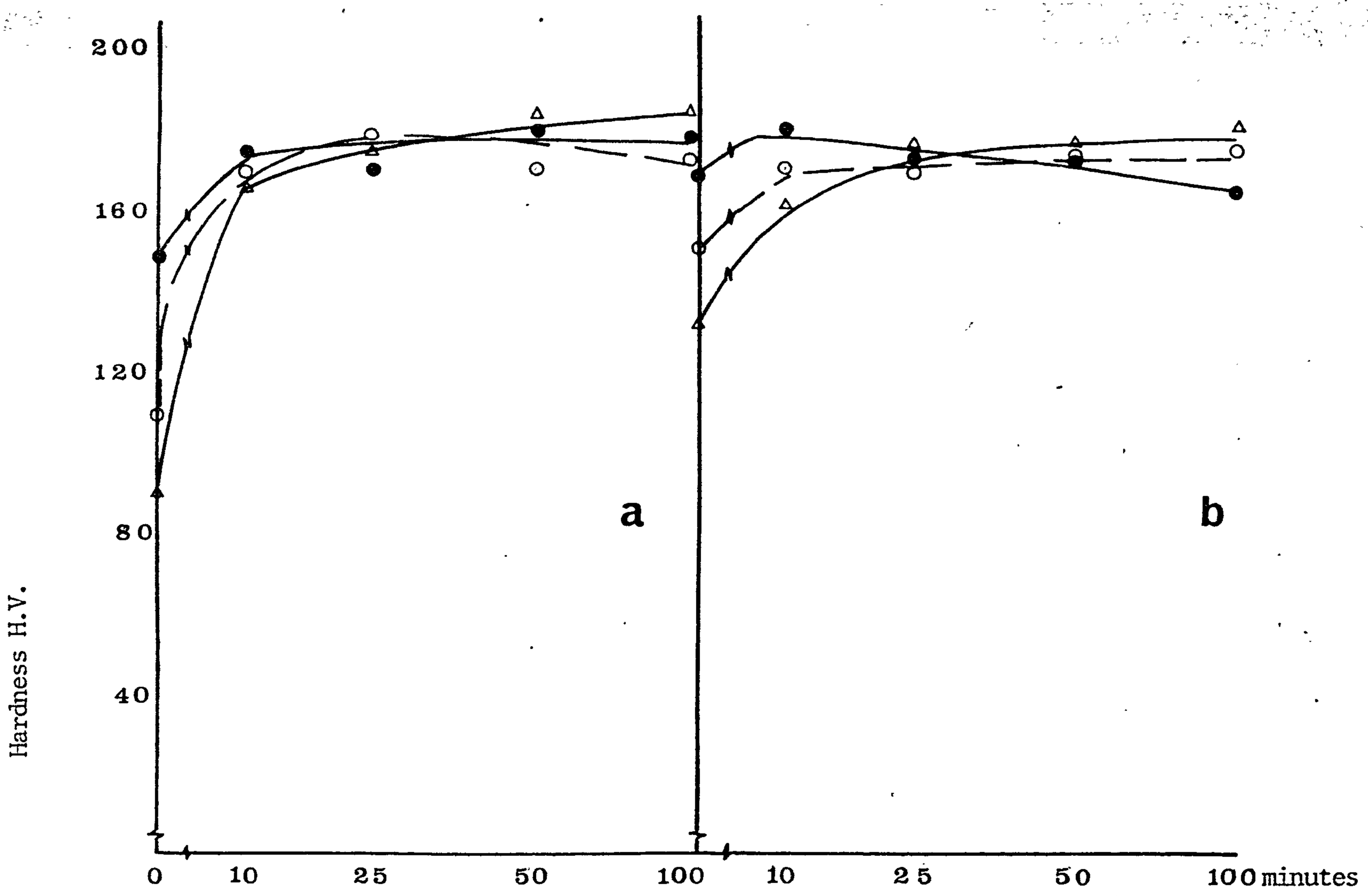

Fig. 70. Vickers hardness as a function of steam treatment time for Fe + 4% Cu alloy
a) Furnace cooled samples b) Water quenched samples

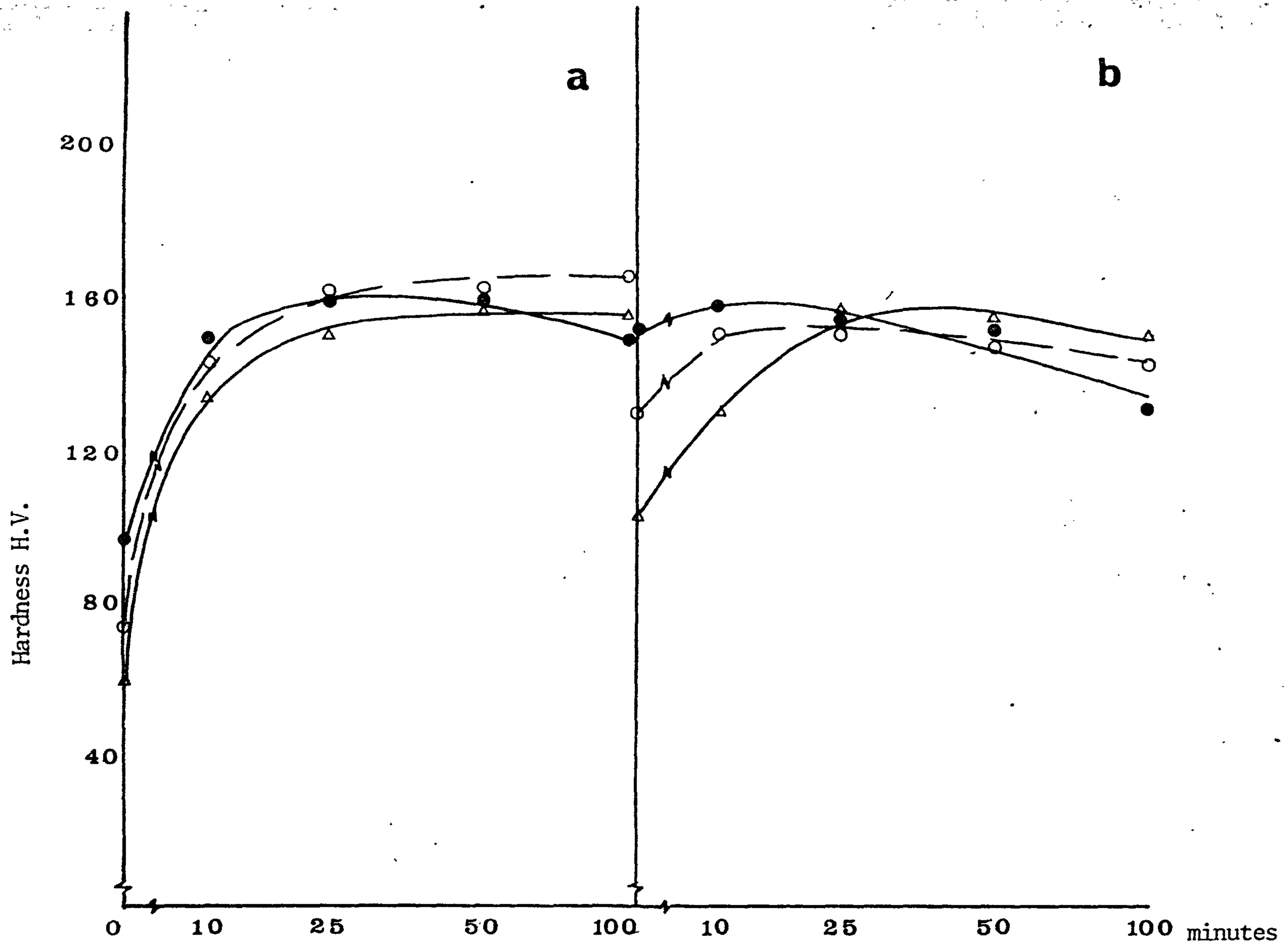

Fig. 71. Vickers hardness as a function of steam treatment time for Fe + 6% Cu alloy.
a) Furnace cooled samples b) Water quenched samples

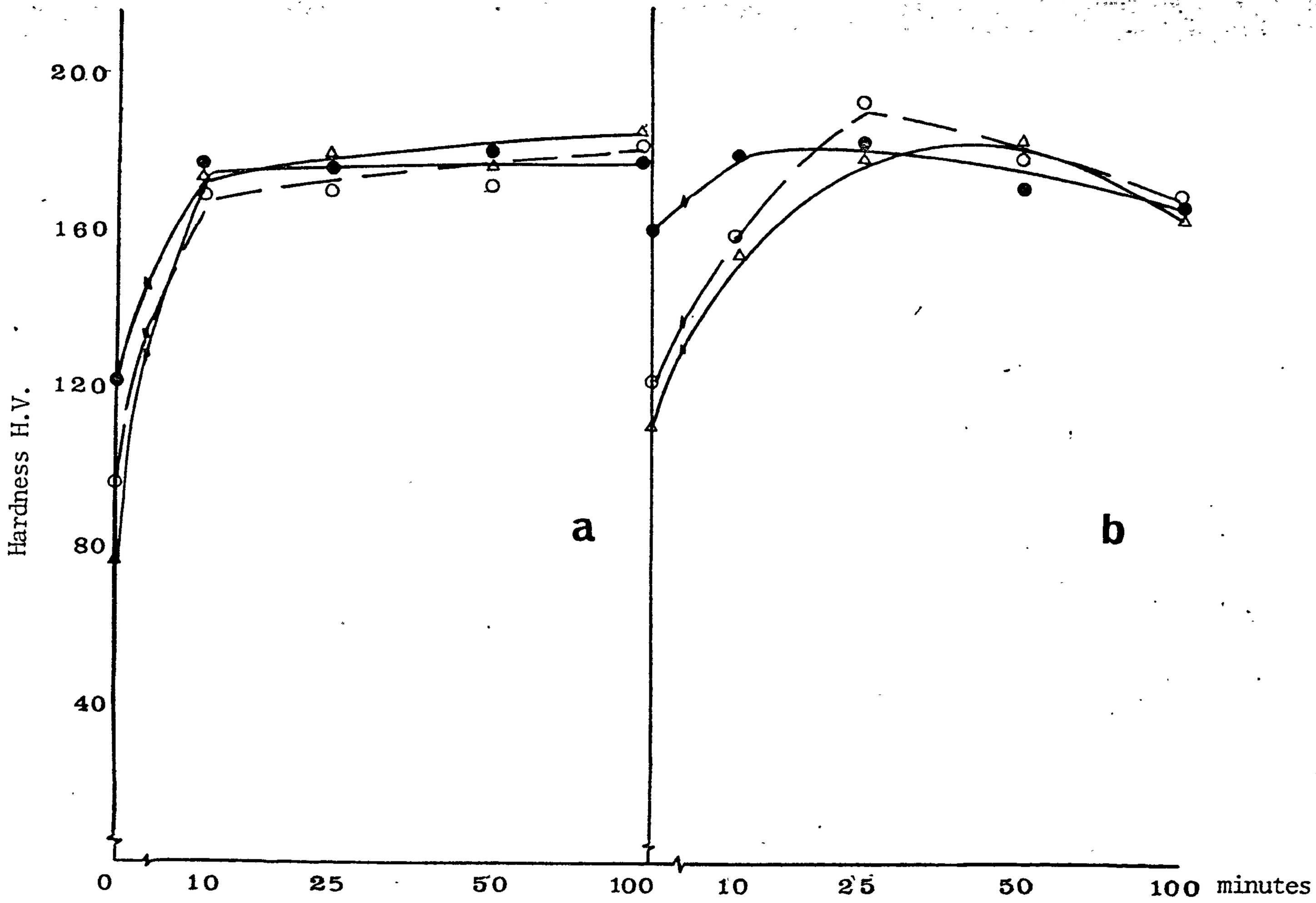

Fig. 72. Vickers hardness as a function of steam treatment time for Fe + 8% Cu alloy.
a) Furnace cooled samples b) Water quenched samples.

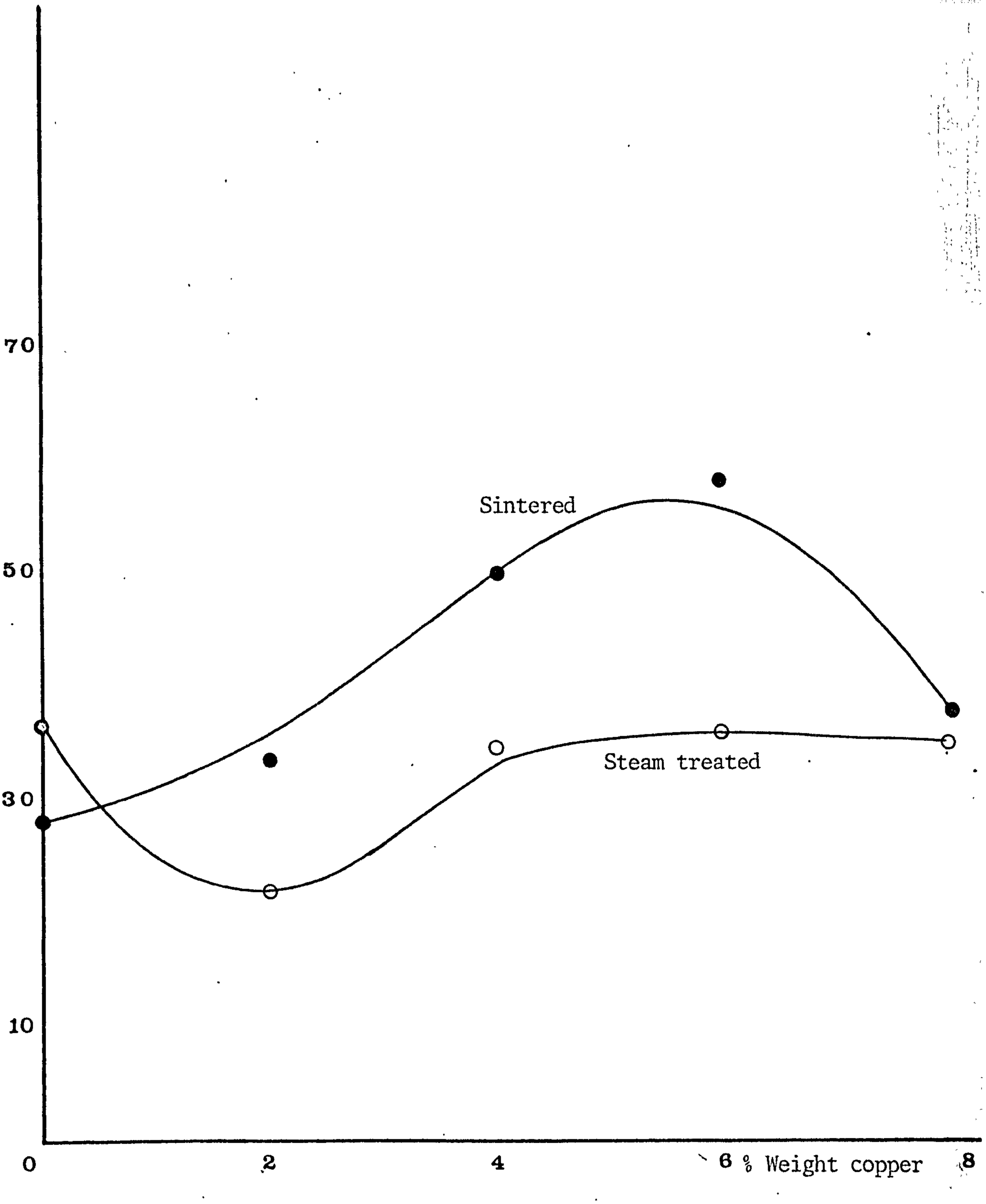

Fig. 73. Radial crushing strength as a function of copper content in density 6.4 $^{g}/_{cc}$.

Key for Figs. 74, 75, 76, 77 and 78.

□ □ 1 Kg Load

■ ■ 3 Kgs Load

△ △ 5 Kgs Load

Fig. 74. Scar width as a function of sliding distance for pure iron.

a) Sintered samples b) Steam treated samples

Fig. 75. Scar width as a function of sliding distance for Fe + 2% Cu alloy.

a) Sintered samples b) Steam treated samples

Fig. 76. Scar width as a function of sliding distance for Fe + 4% Cu alloy.

a) Sintered samples b) Steam treated samples

Fig. 77. Scar width as a function of sliding distance for Fe + 6% Cu alloy.

a) Sintered samples b) Steam treated samples

Fig. 78. Scar width as a function of sliding distance for Fe + 8% Cu alloy.

a) Sintered samples b) Steam treated samples

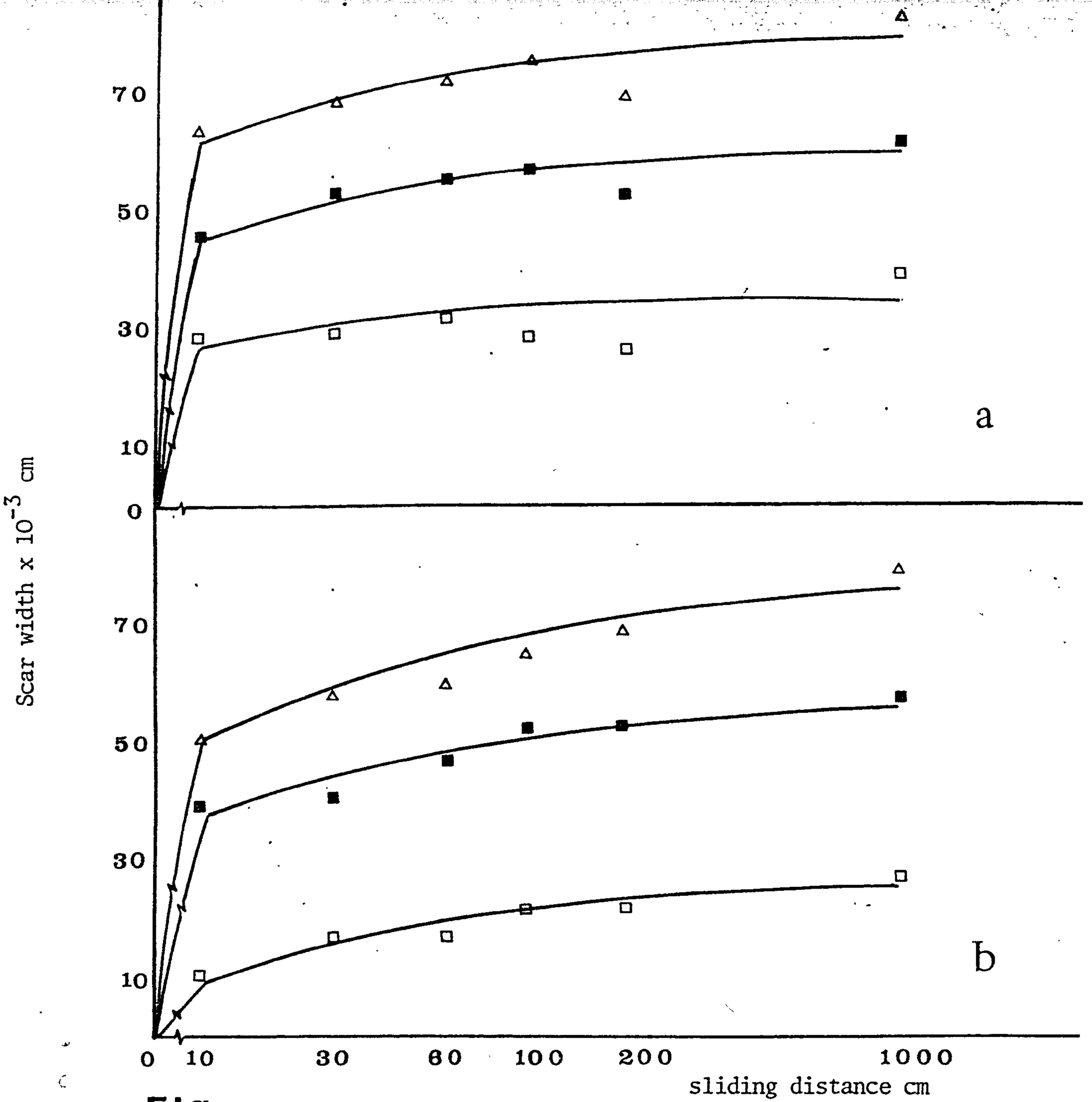
Scar width x 10^{-3} cm
70
50
30
10
0
a
70
50
30
10
0
10
30
60
100
200
1000
sliding distance cm
b

Fig. 74

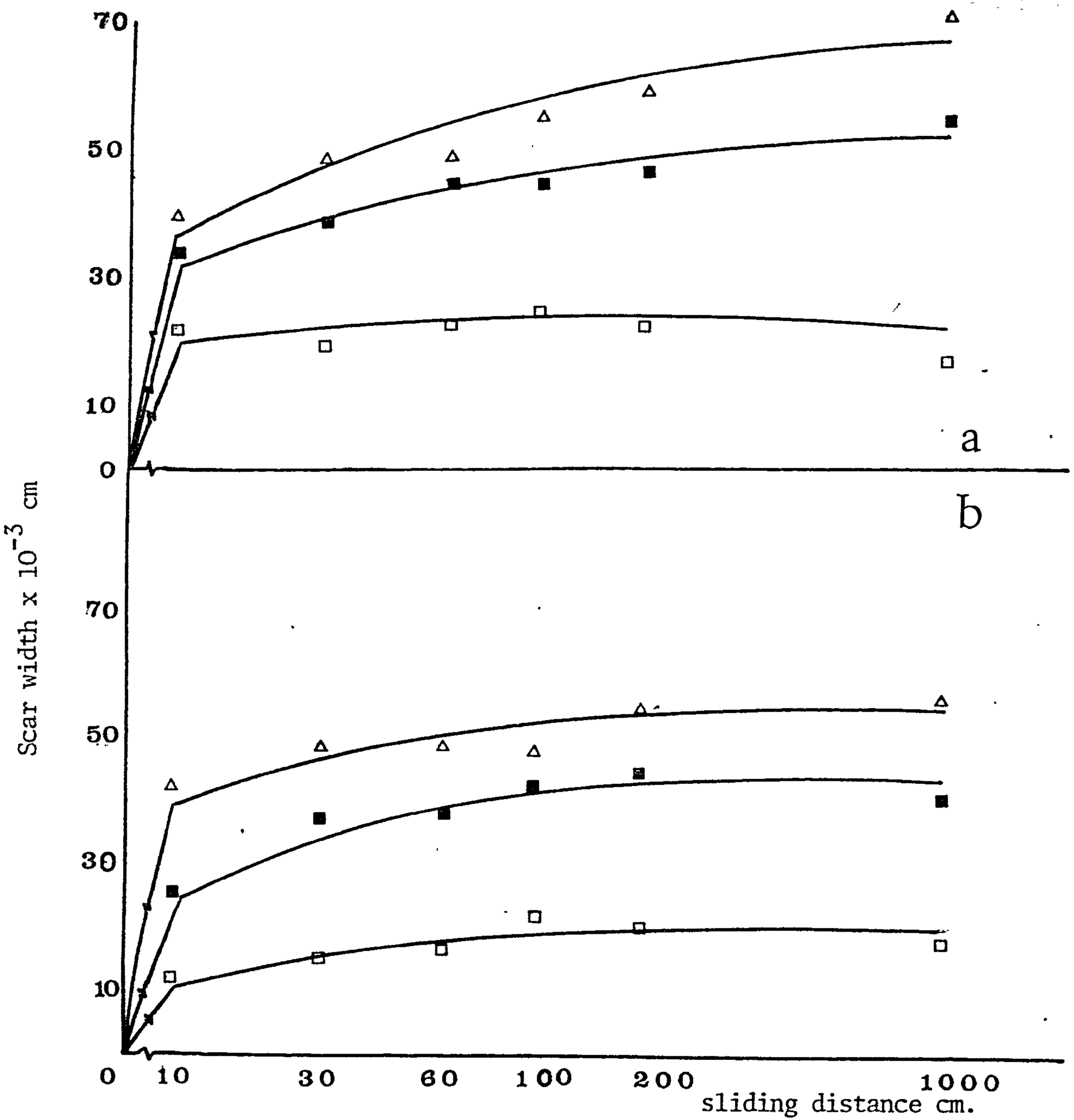
70
50
30
10
0
70
50
30
10
0
10
30
60
100
200
1000
a
b
Scar width x 10⁻³ cm
sliding distance cm.

Fig. 75.

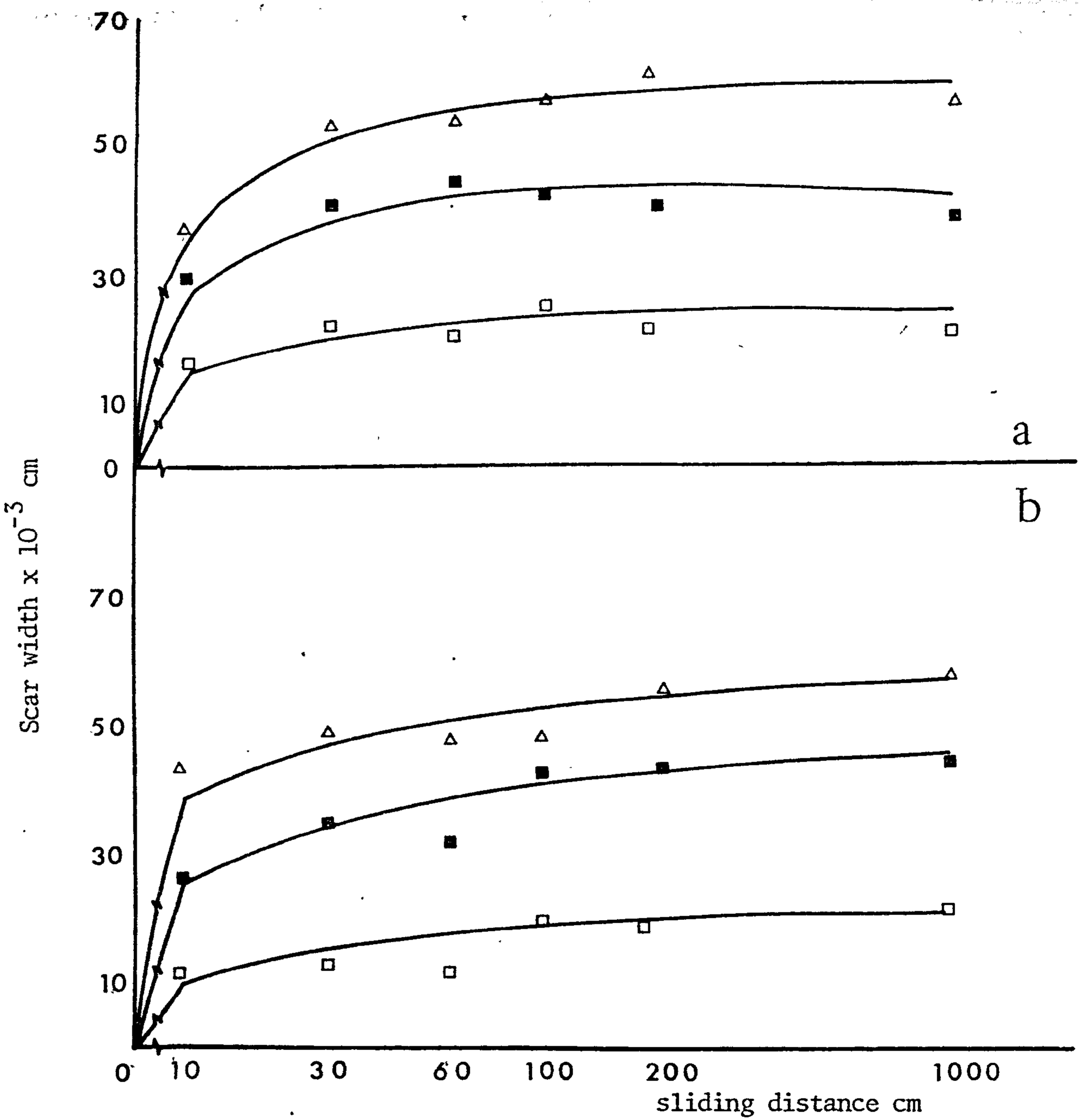
70
50
30
10
0
70
50
30
10
a
b
Scar width x 10^{-3} cm
0
10
30
60
100
200
1000
sliding distance cm

Fig. 76

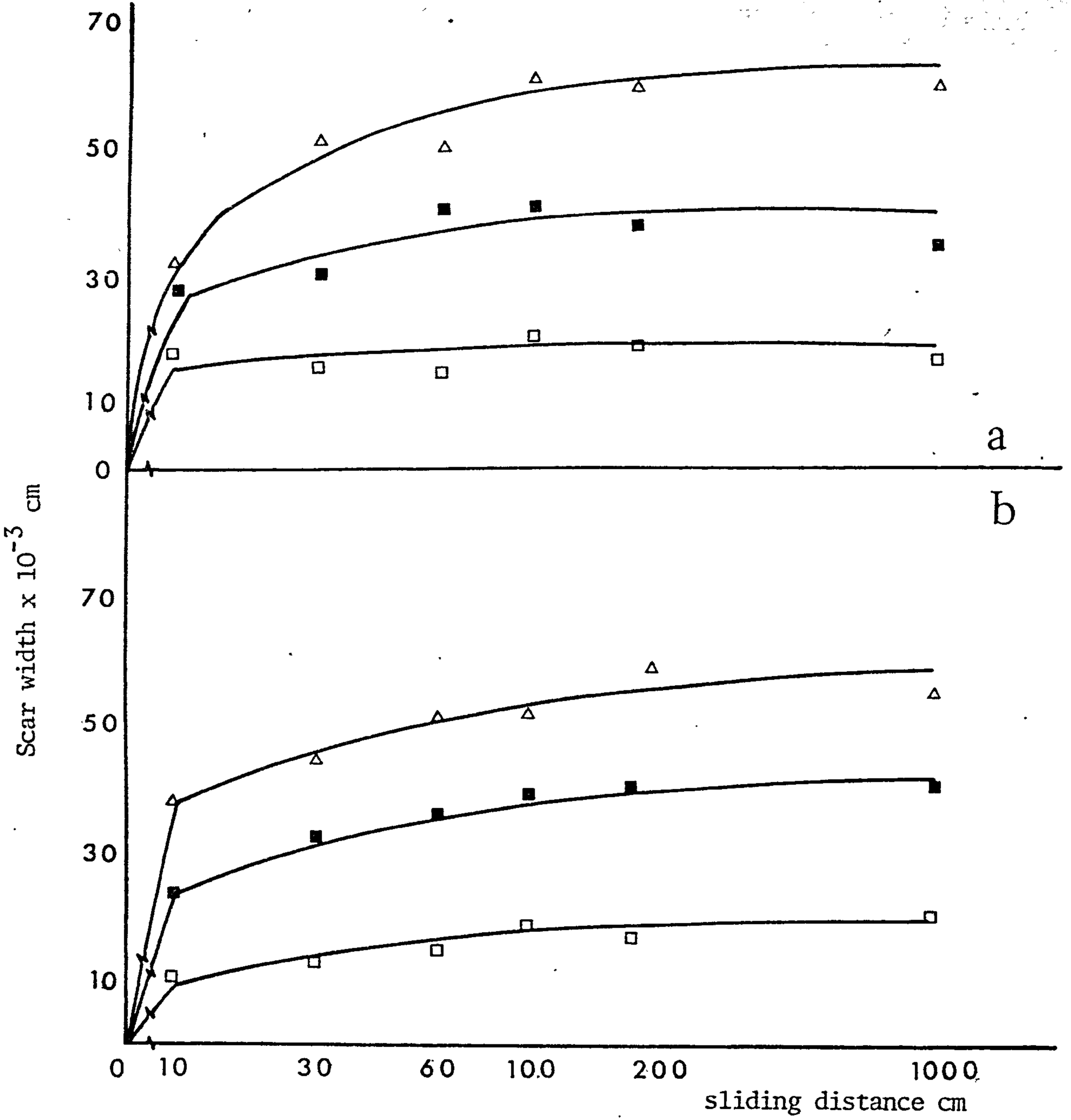
70
50
30
10
0
70
50
30
10
a
b
Scar width x 10^{-3} cm
0
10
30
60
100
200
1000
sliding distance cm

Fig. 77

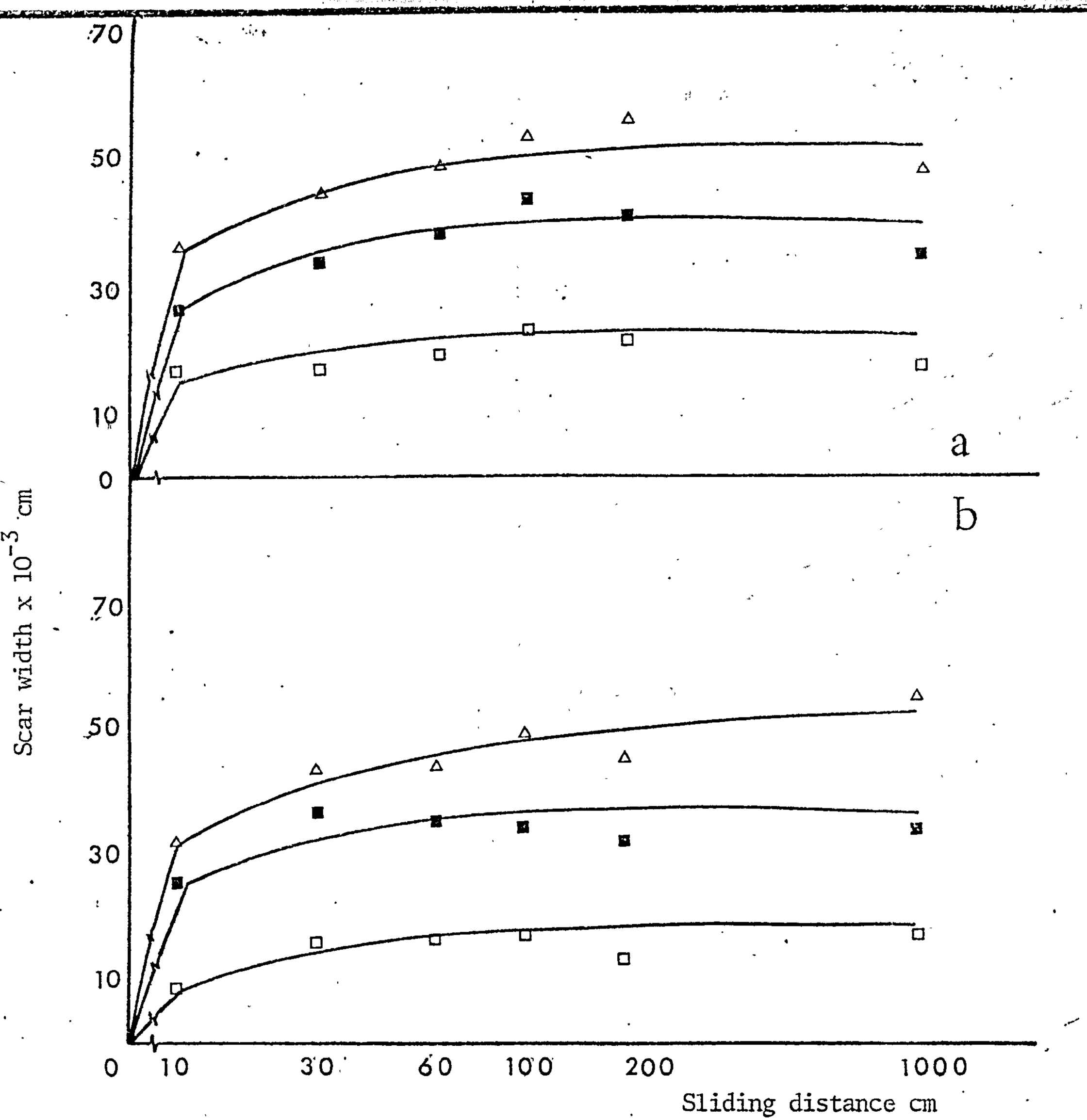
70
50
30
10
0
70
50
30
10
0
10
30
60
100
200
1000
a
b
Scar width x 10^{-3} cm
Sliding distance cm

Fig. 78.

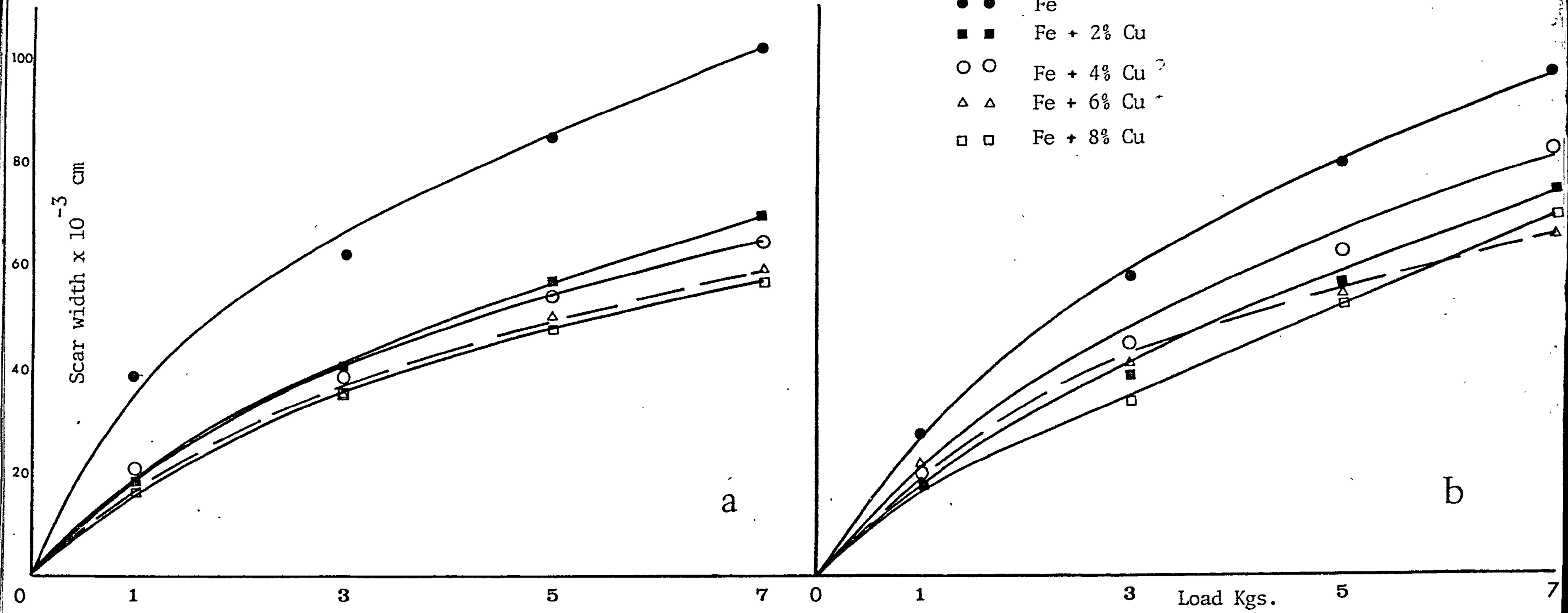

Fig. 79. Scar width as a function of load after 1000 cm sliding distance.

a) Sintered samples.

b) steam teated samples

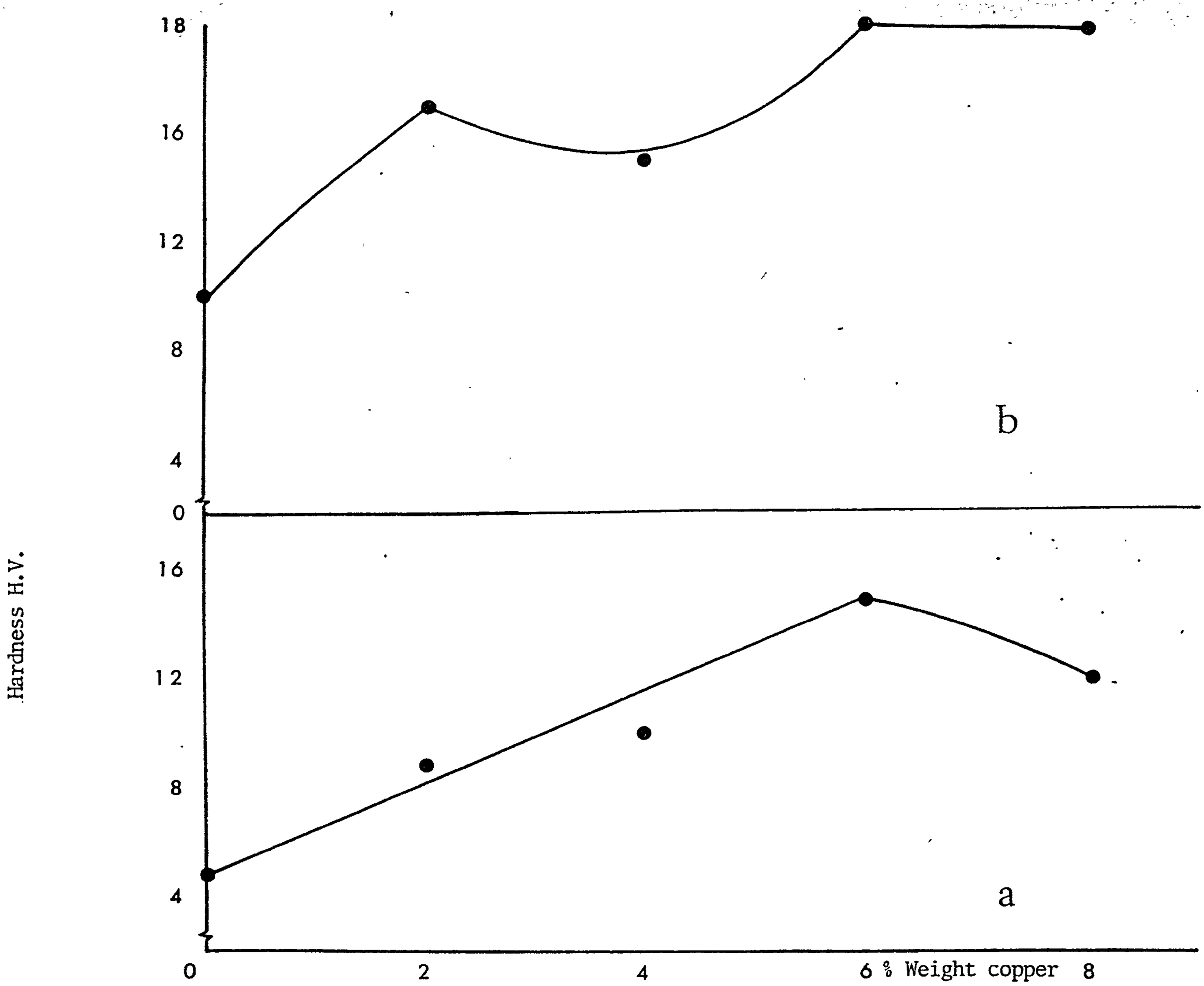

Fig. 80. Vickers hardness as a function of copper content
a) Sintered samples b) steam treated samples

Key for Figs. 81, 82 and 83

● ● Sintered samples

○ ○ Steam treated samples

Key for Figs 84 and 85

● ● Fe

■ ■ Fe + 2% Cu

○ ○ Fe + 4% Cu

□ □ Fe + 6% Cu

△ △ Fe + 8% Cu

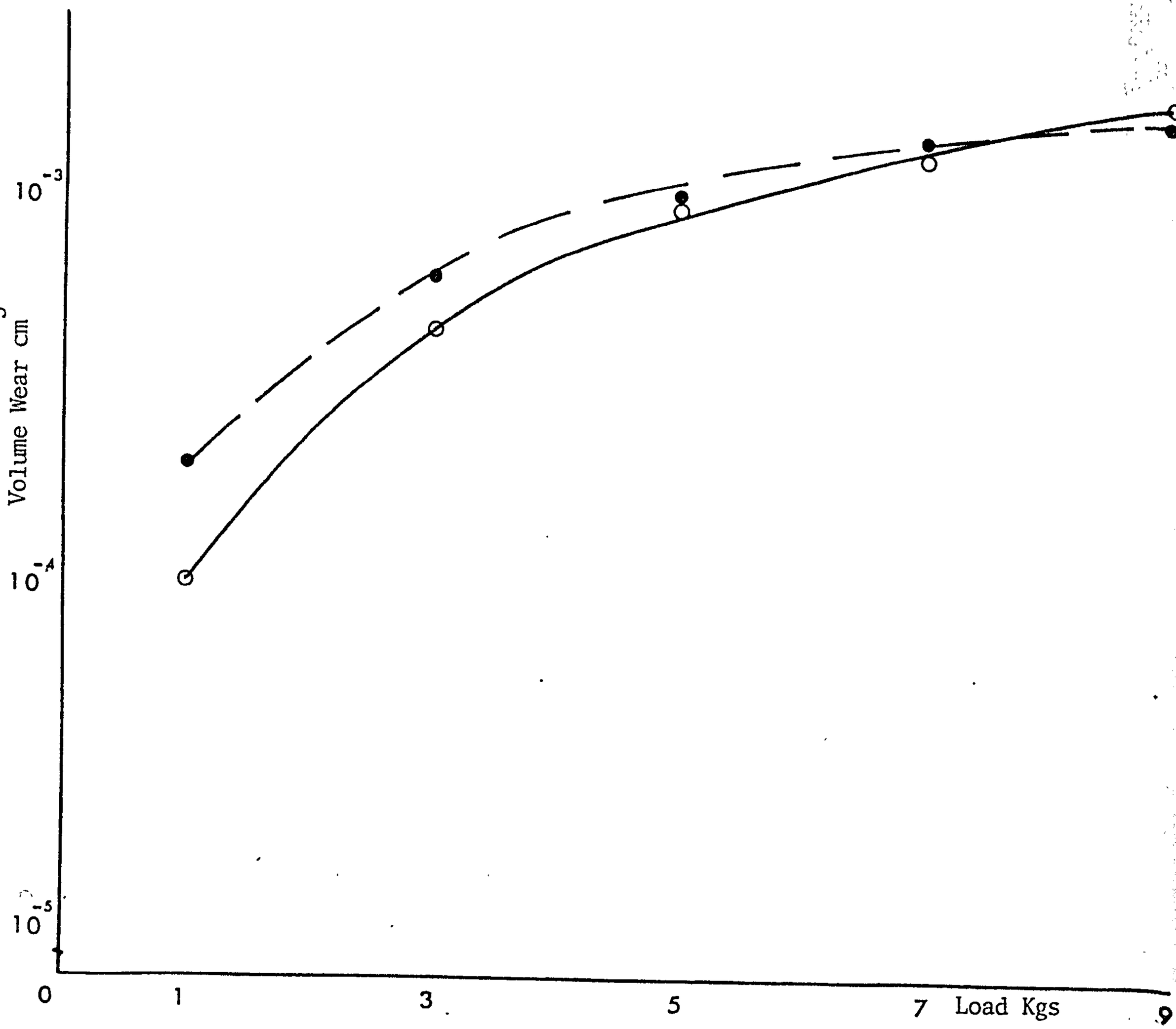

Fig. 81. Volume wear as a function of load after 1000 cm sliding distance for pure iron.

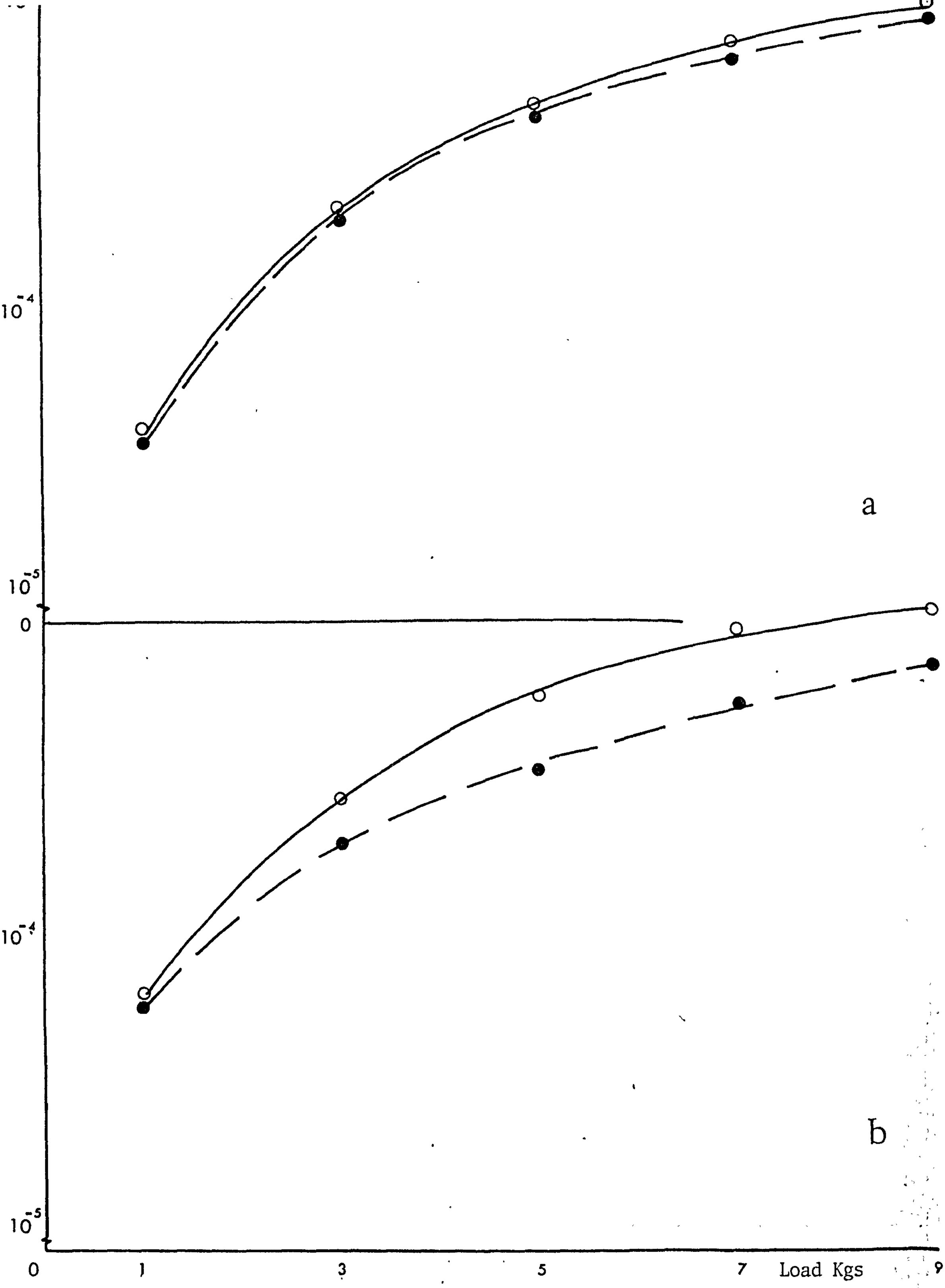

Fig. 82. Volume wear as a function of load after 1000 cm sliding distance.

a) Fe + 2% Cu b) Fe + 4% Cu

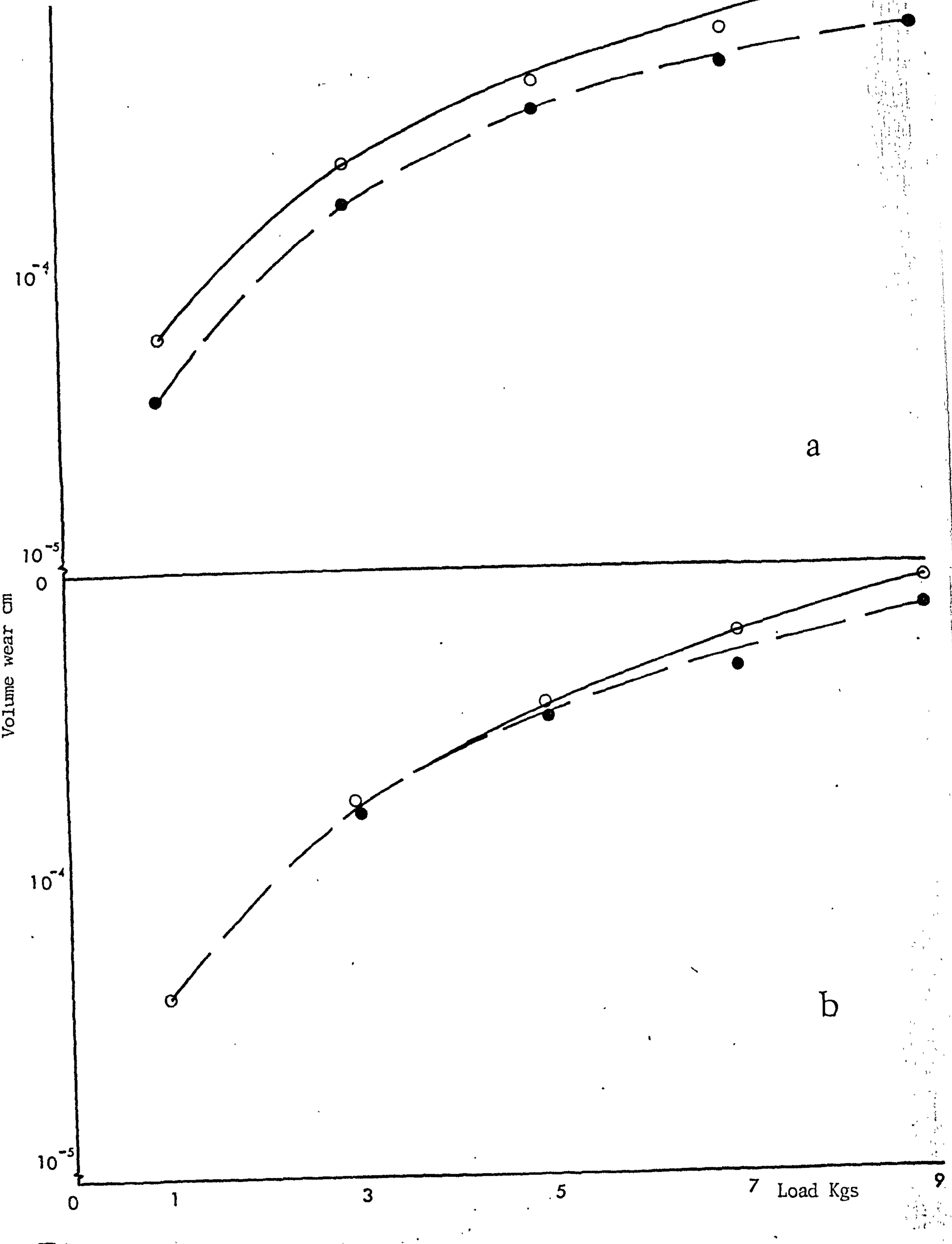

Fig. 83. Volume wear as a function of load after 1000 cm sliding distance.
a) Fe + 6% Cu' b) Fe + 8% Cu

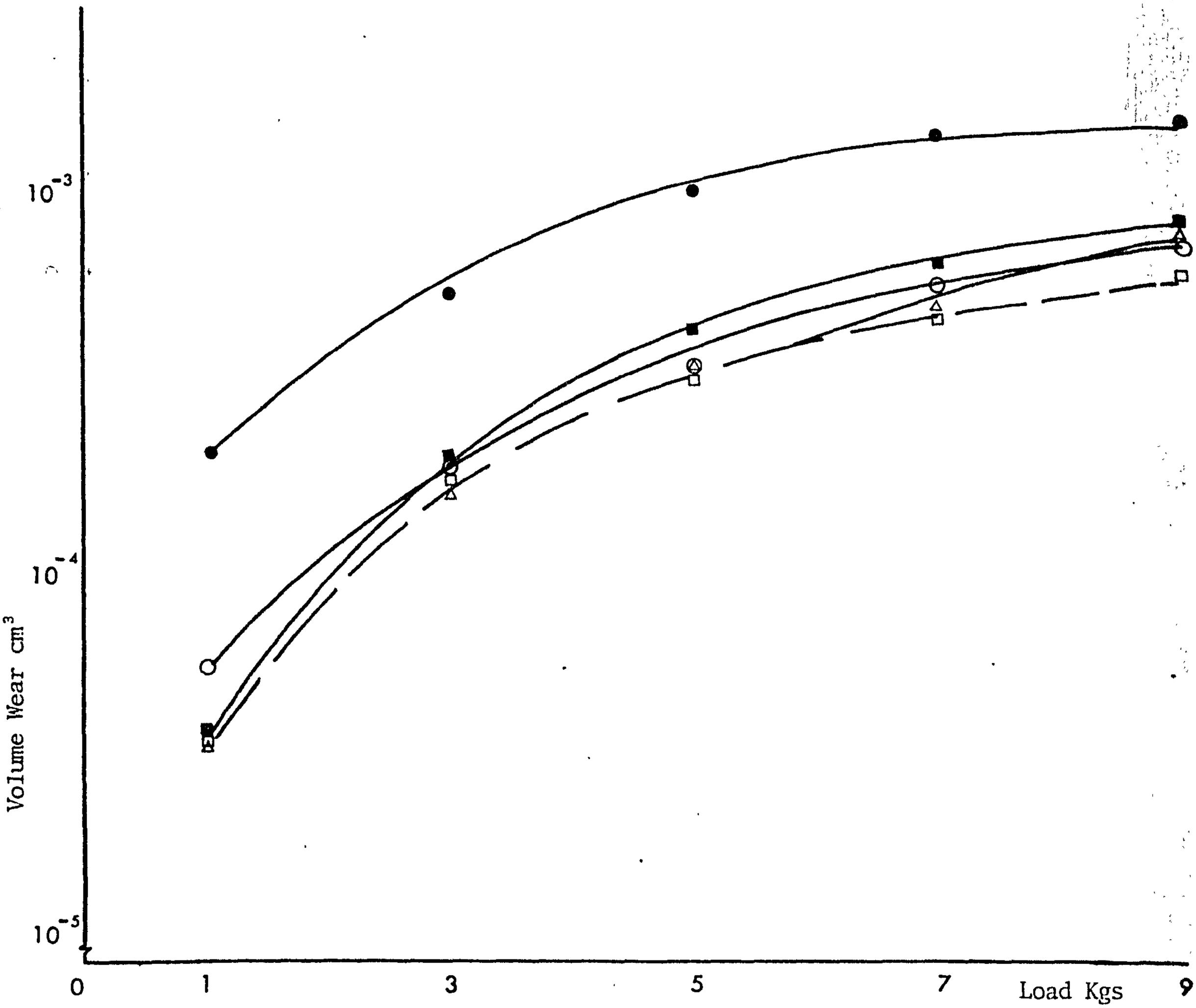

Fig. 84 Volume wear as a function of load after 1000 cm sliding distance for sintered samples.

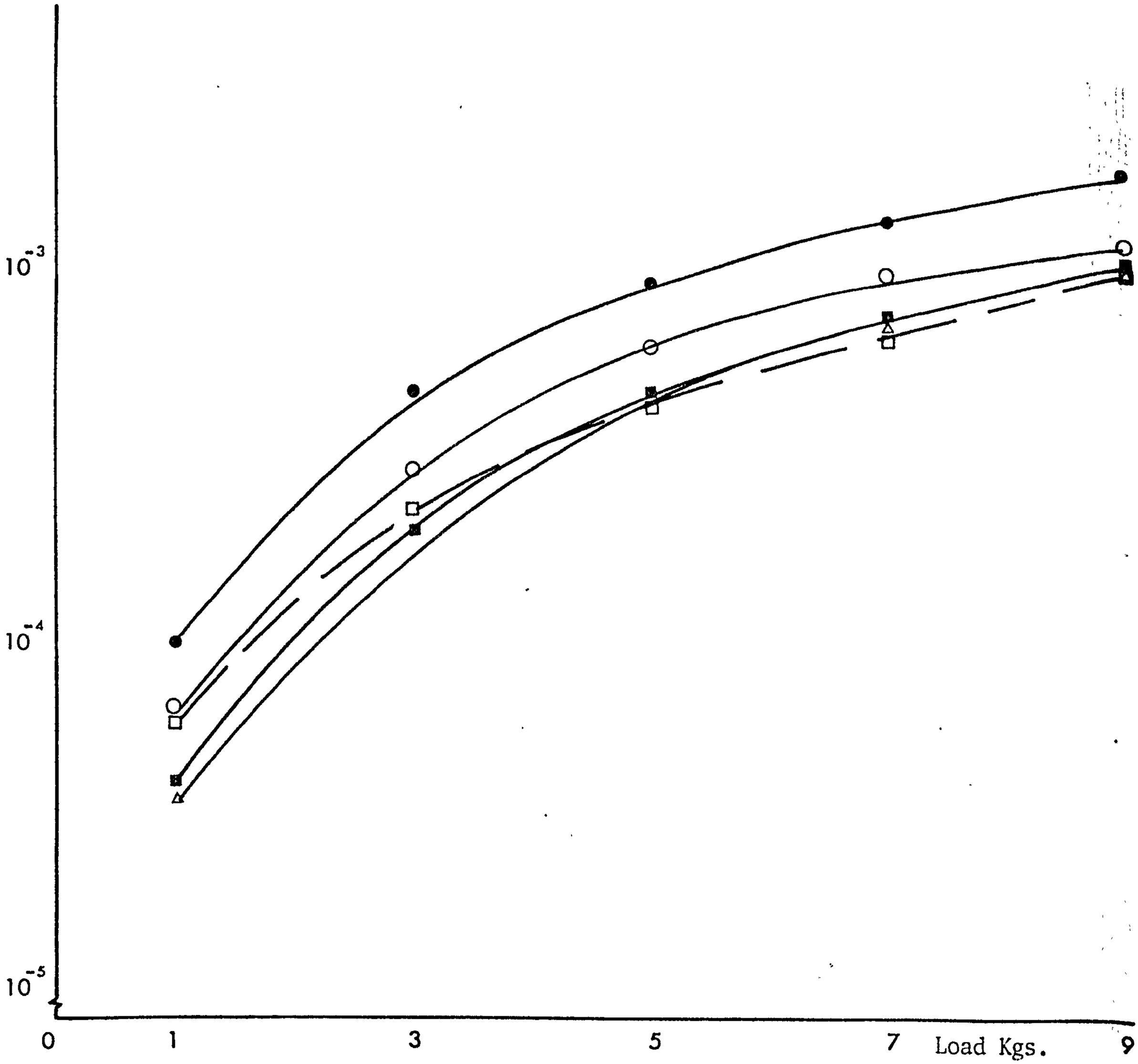

Fig. 85. Volume wear as a function of load after 1000 cm sliding distance for steam treated samples.

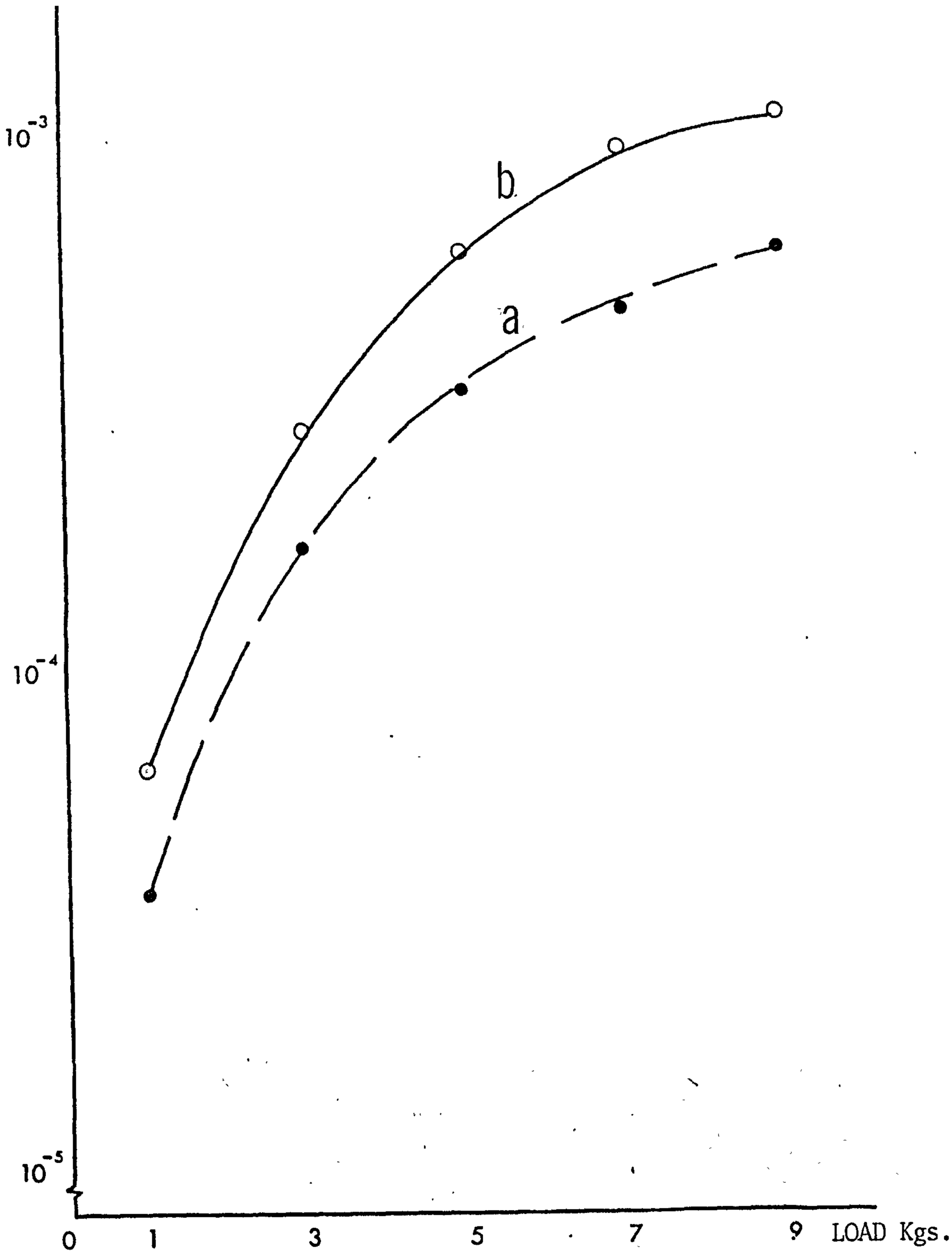

Fig. 86. Volume wear as a function of load after 1000 cm sliding distance.

a) Sintered Fe + 6% Cu alloy b) steam treated Fe + 4% Cu alloy.

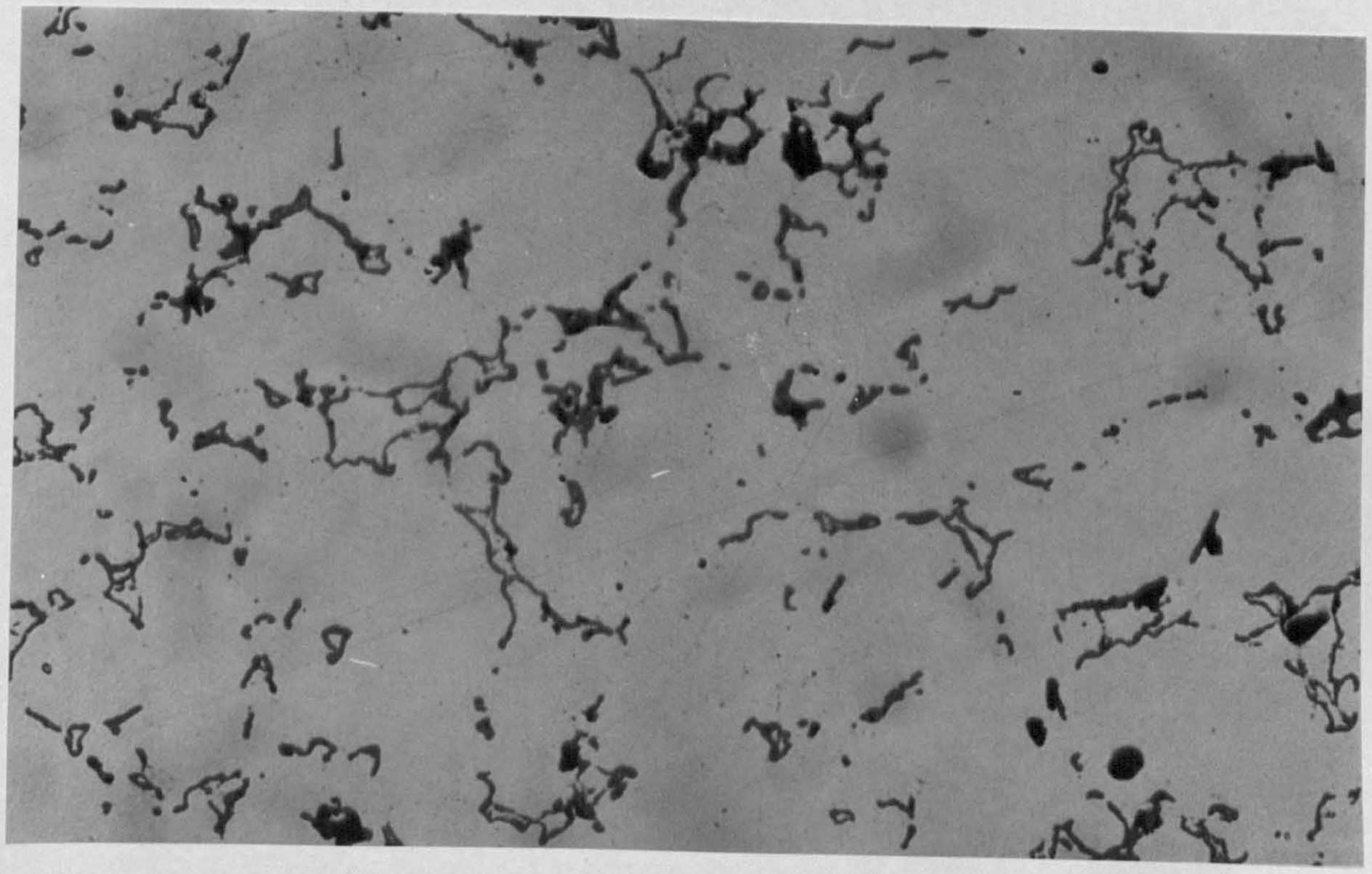

Fig. 87. - 100# A.S.C. (Fe) D = 6.4 g/cc

Machined after sintering and then steam heated for 100 minutes at 525°C. x 200

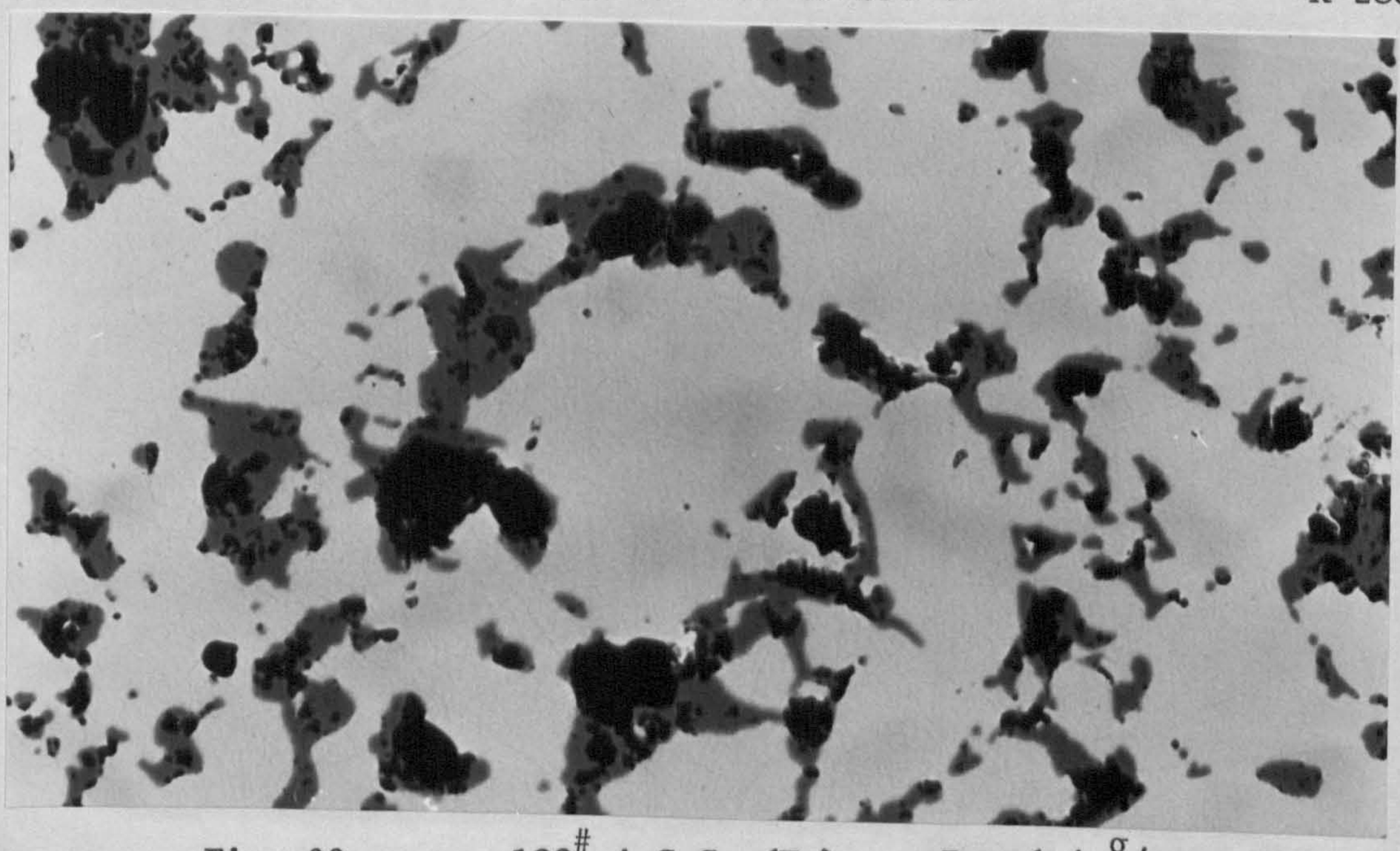

Fig. 88. - 100# A.S.C. (Fe) D = 6.4 g/cc

Steam treated for 100 minutes at 525°C
"Unmachined surface" x 200

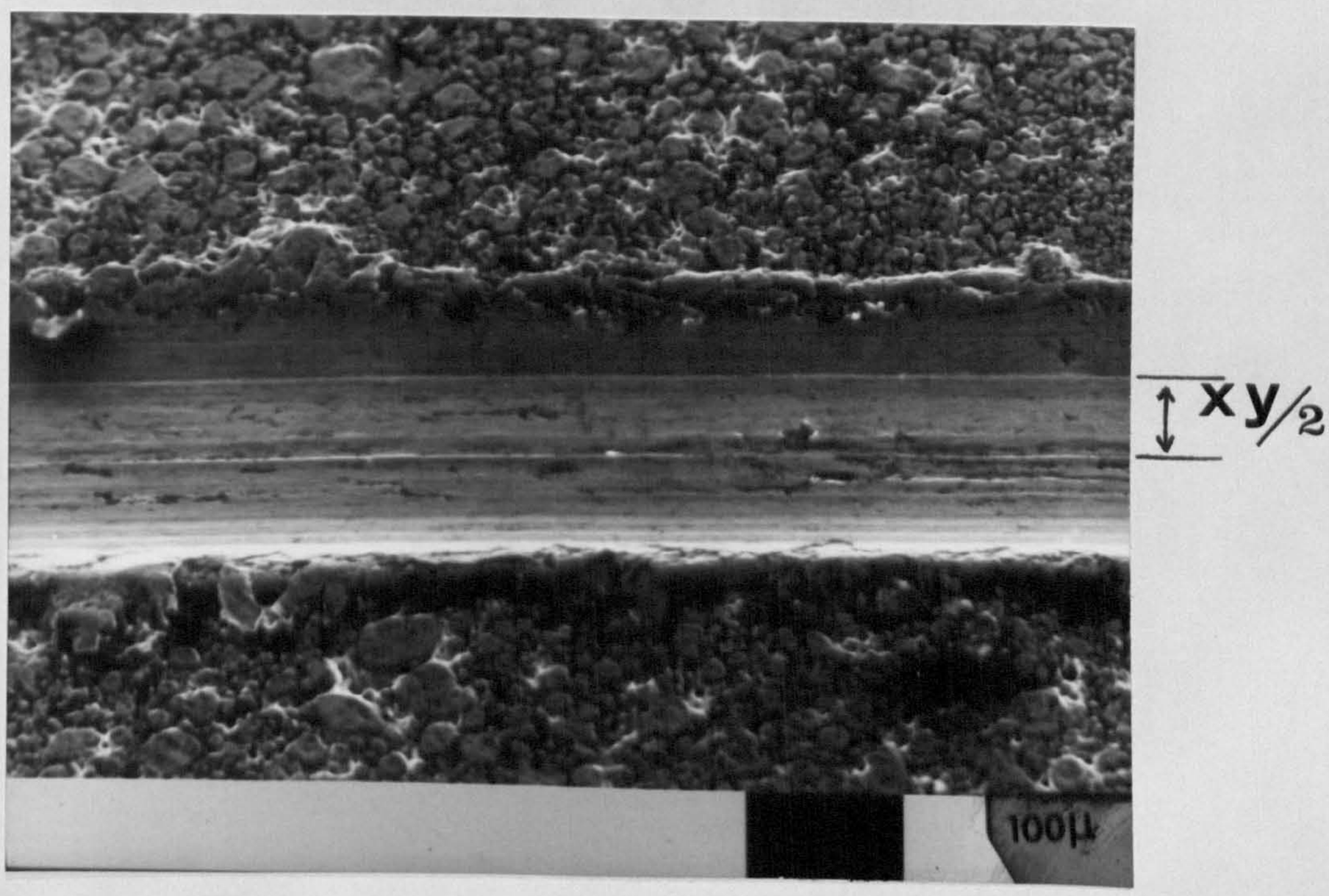

Fig. 89. Track of steam treated (Fe) after 1000 cm sliding distance under 1 Kg load. $D = 6.8\ ^{g}/_{cc}$ x 100

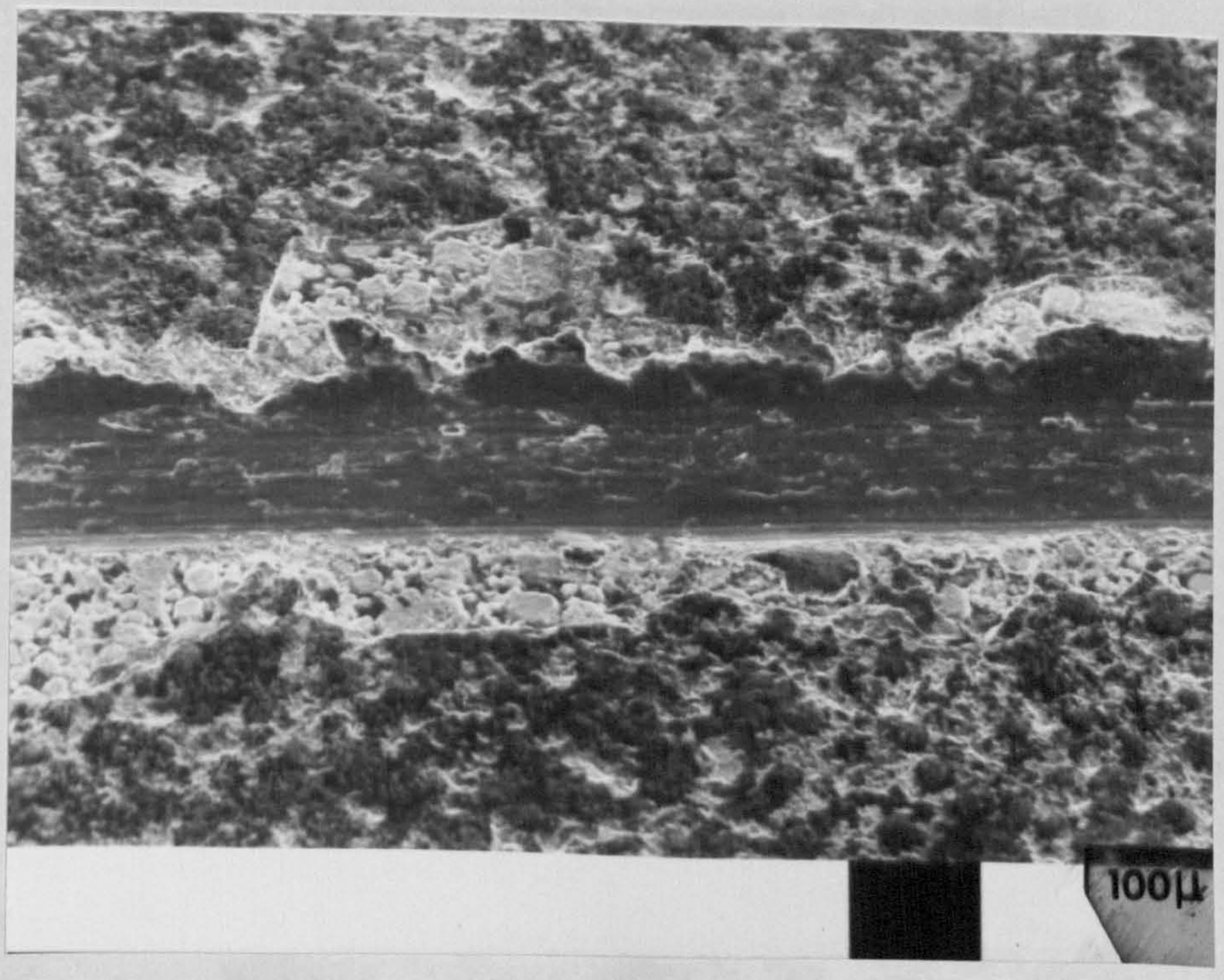

Fig. 90. Track of steam treated (Fe + 8% Cu) after 1000 cm sliding distance under 1 Kg load.

$D = 6.8\ ^{g}/_{cc}$ x 100

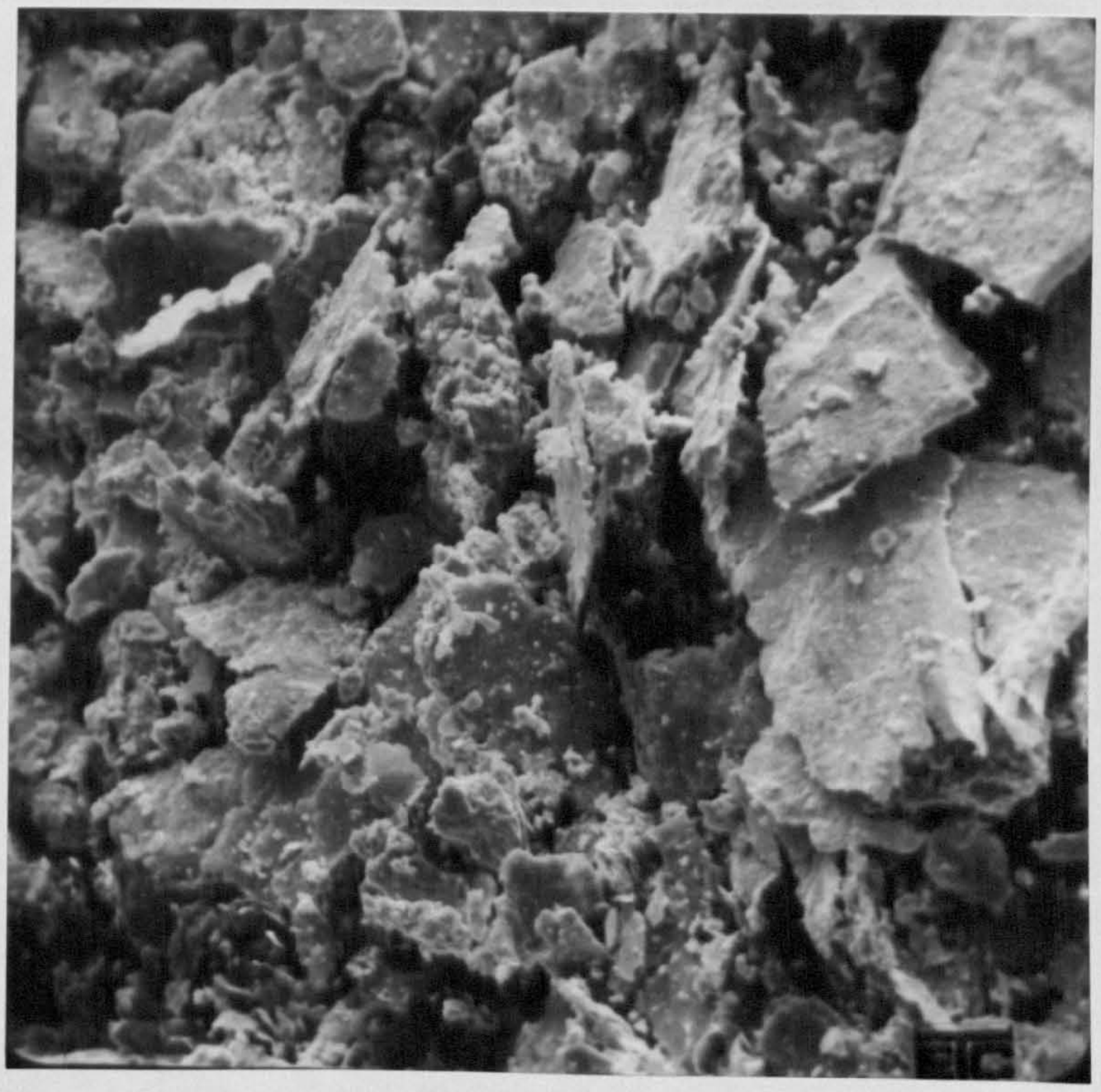

Fig. 91. Debris of steam treated (Fe + 8% Cu) after 1000 cm sliding distance under 9 Kgs load.
$D = 6.8\ ^{g}/_{cc}$ x 500

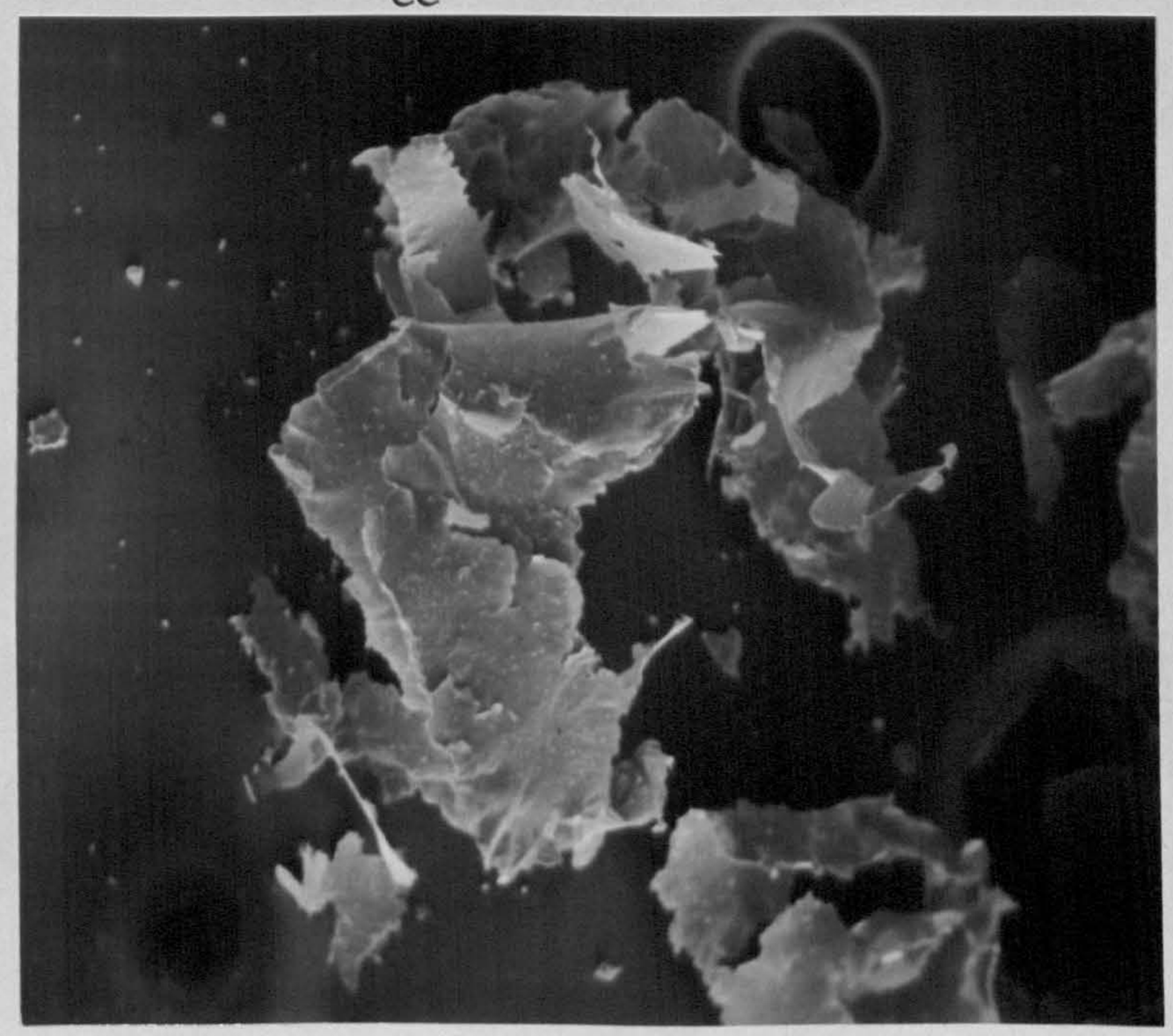

Fig. 92. Debris of sintered (Fe + 8% Cu) after 1000 cm sliding distance under 9 Kgs load.
$D = 6.8\ ^{g}/_{cc}$ x 100

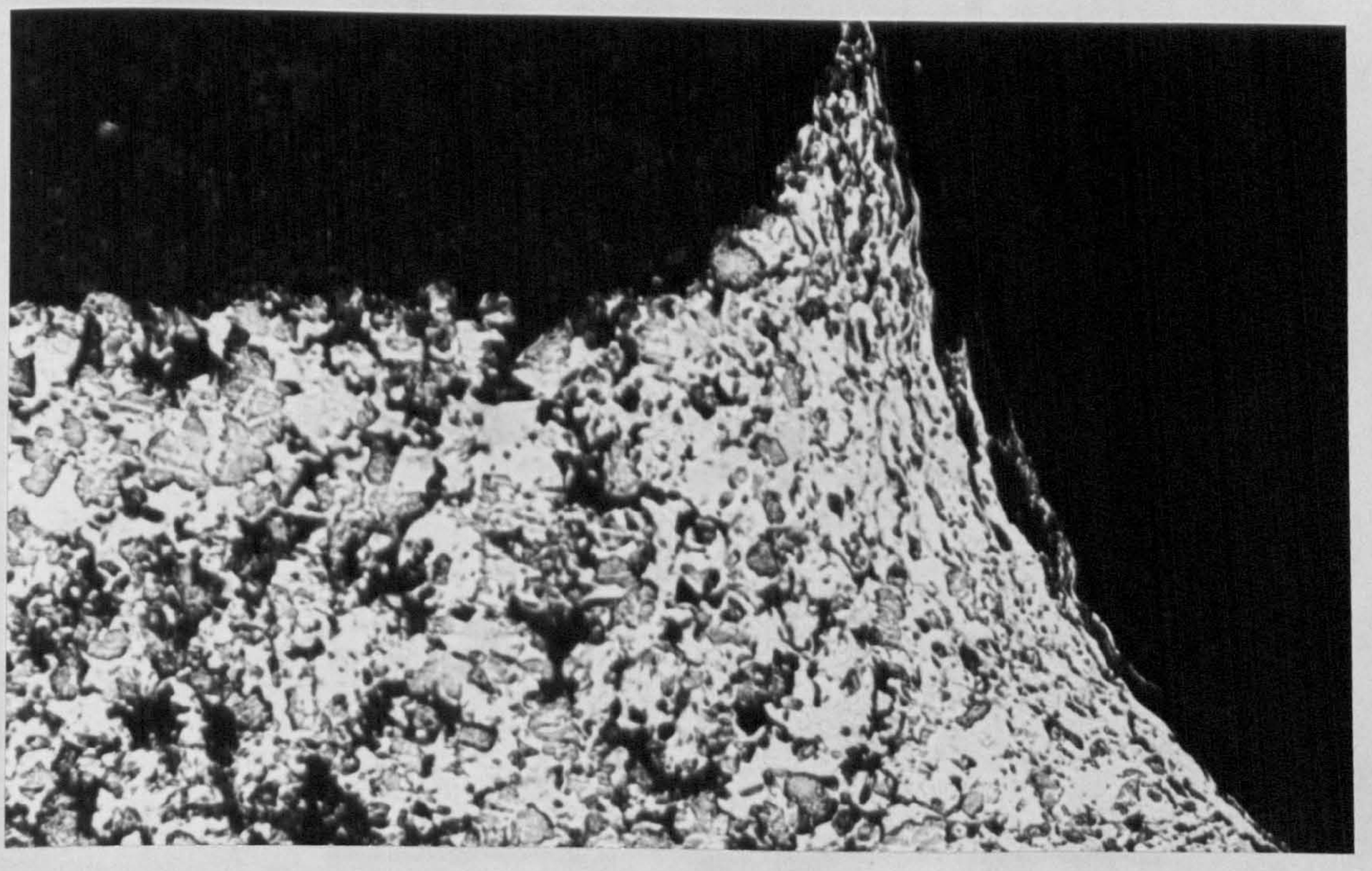

Fig. 93. Taper section of sintered (Fe + 2% Cu) after wear under 7 Kgs load.

$D = 6.8\ ^{g}/_{cc}$ x 200

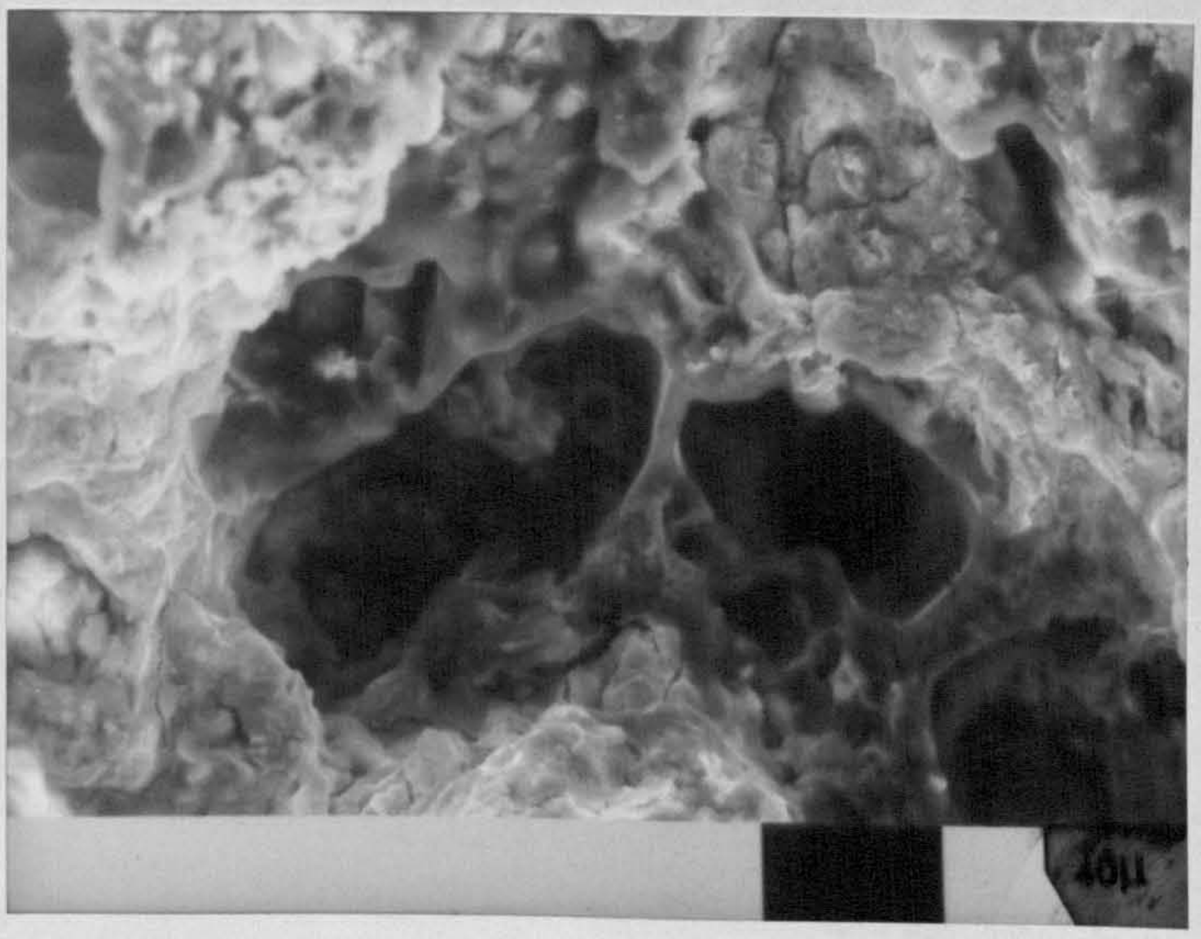

Fig. 94. Porosity network on the surface of sample white areas are porosity network (resin) and empty spaces are dissolved metal. x 500

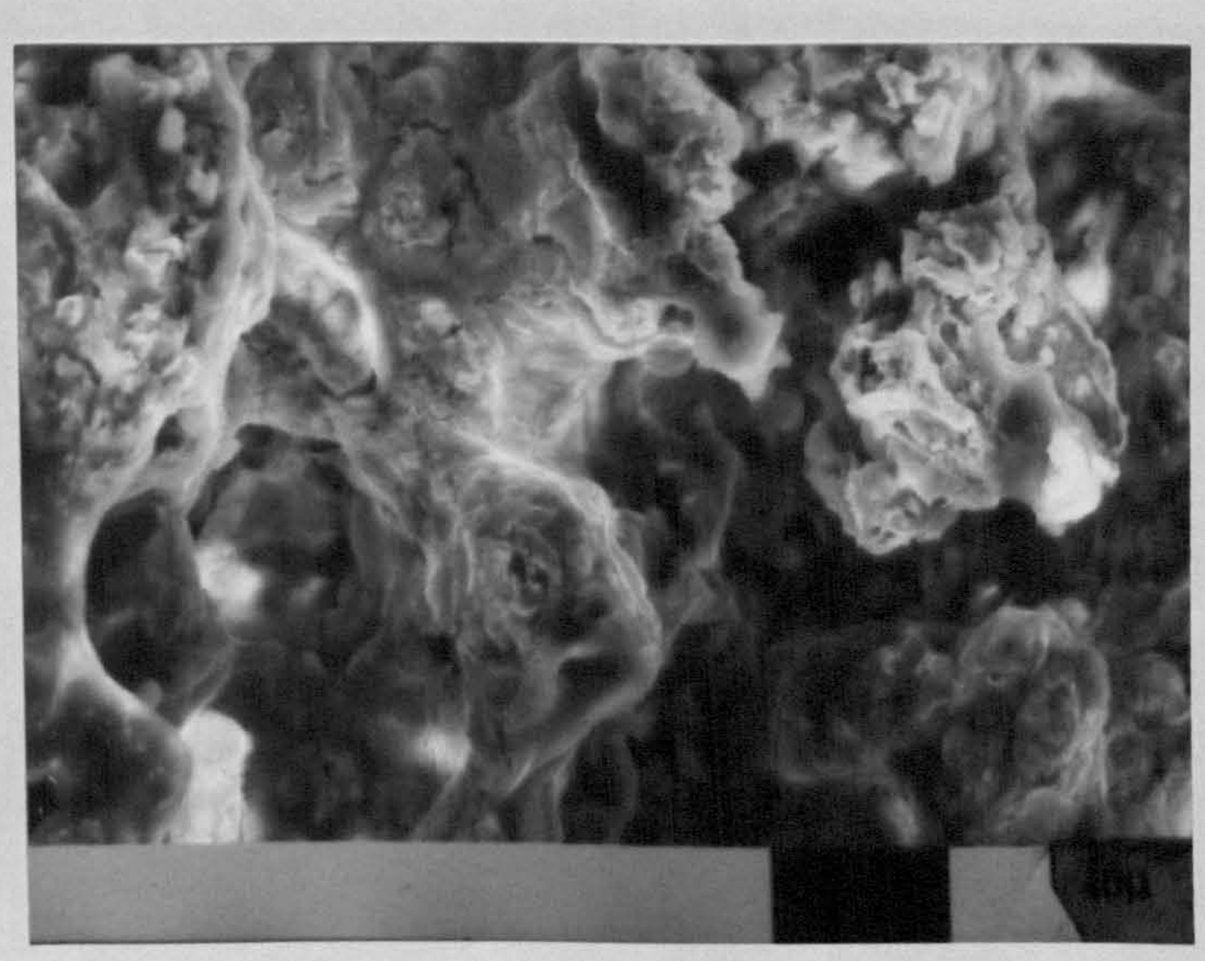

Fig. 95. Porosity network on the wall of specimens "as above". x 500

Fig. 96a. Bottom of track in sintered (Fe + 4% Cu) after 1000 cm sliding distance under 5 Kgs load.

$D = 6.8\ ^{g}/_{cc}$ x 1K

Fig. 96b. Bottom of track in steam treated (Fe + 4% Cu) after 1000 cm sliding distance under 5 Kgs load.

$D = 6.8\ ^{g}/_{cc}$ x 1K

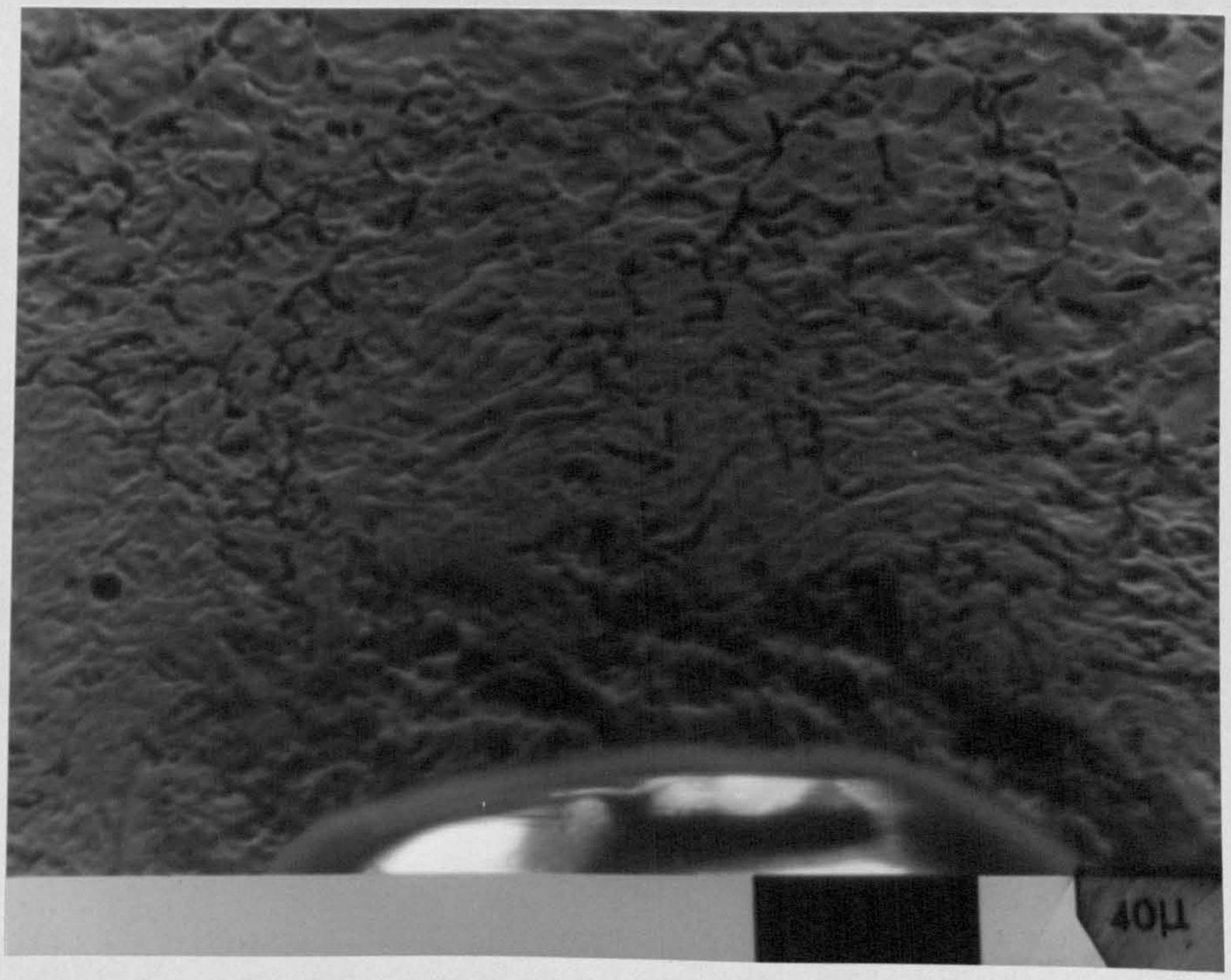

Fig. 97a. Taper section of sintered (Fe + 8% Cu) after 1000 cm sliding distance under 5 Kgs load.

$D = 6.8 \, g/cc$ x 500

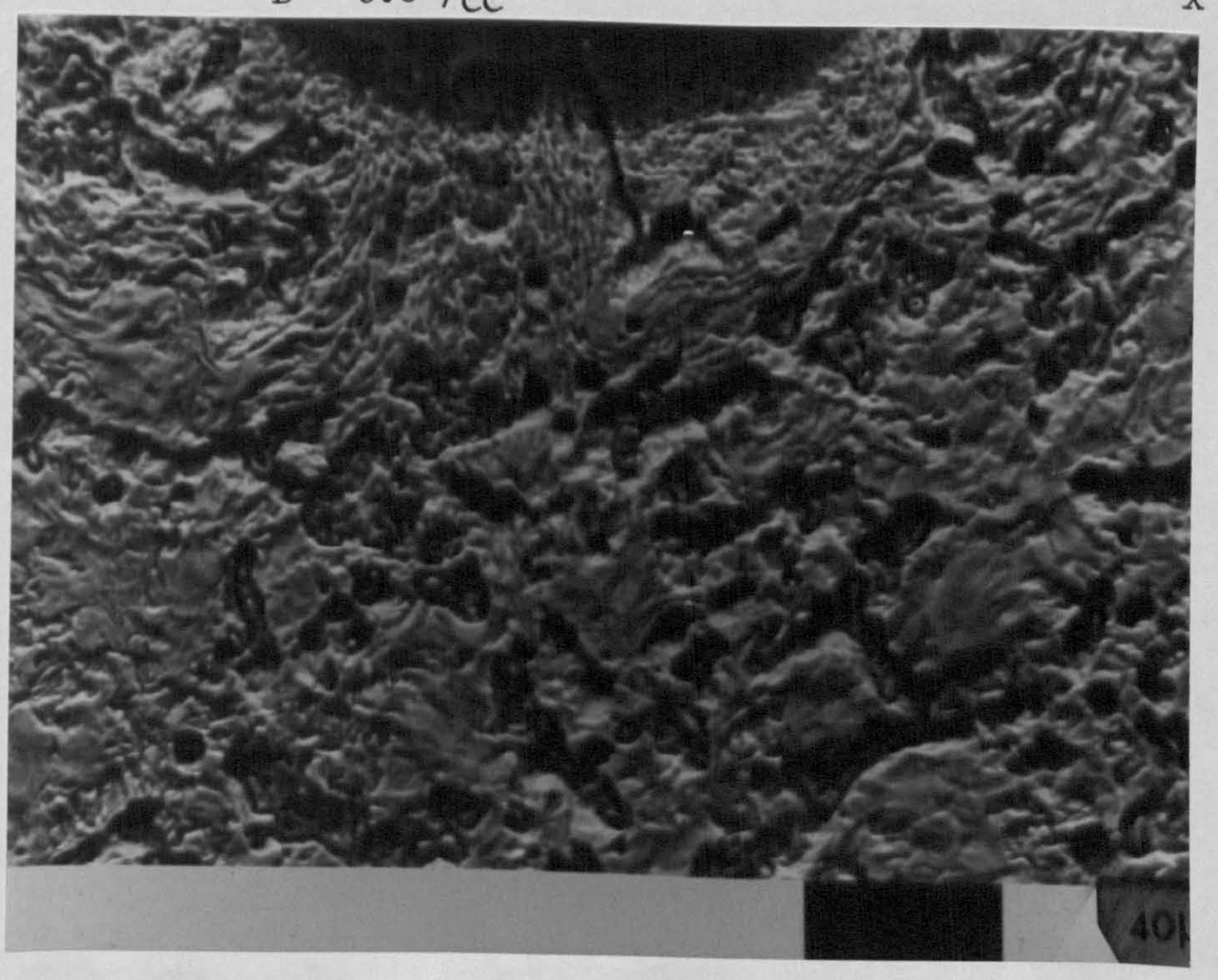

Fig. 97b. Taper section of steam treated (Fe + 8% Cu) after 1000 cm sliding distance under 5 Kgs load.

$D = 6.8 \, g/cc$ x 500

Fig. 98a. Bottom track of sintered (Fe) after 1000 cm sliding distance under 3 Kgs load.

$D = 6.8\ ^{g}/_{cc}$ x 1K

Fig. 98b. Bottom track of steam treated (Fe) after 1000 cm sliding distance under 3 Kgs load.

$D = 6.8\ ^{g}/_{cc}$ x 1K

Fig. 99a. Bottom track of sintered (Fe) after 1000 cm sliding distance under 9 Kgs load.

$D = 6.8\ ^{g}/_{cc}$ x 1K

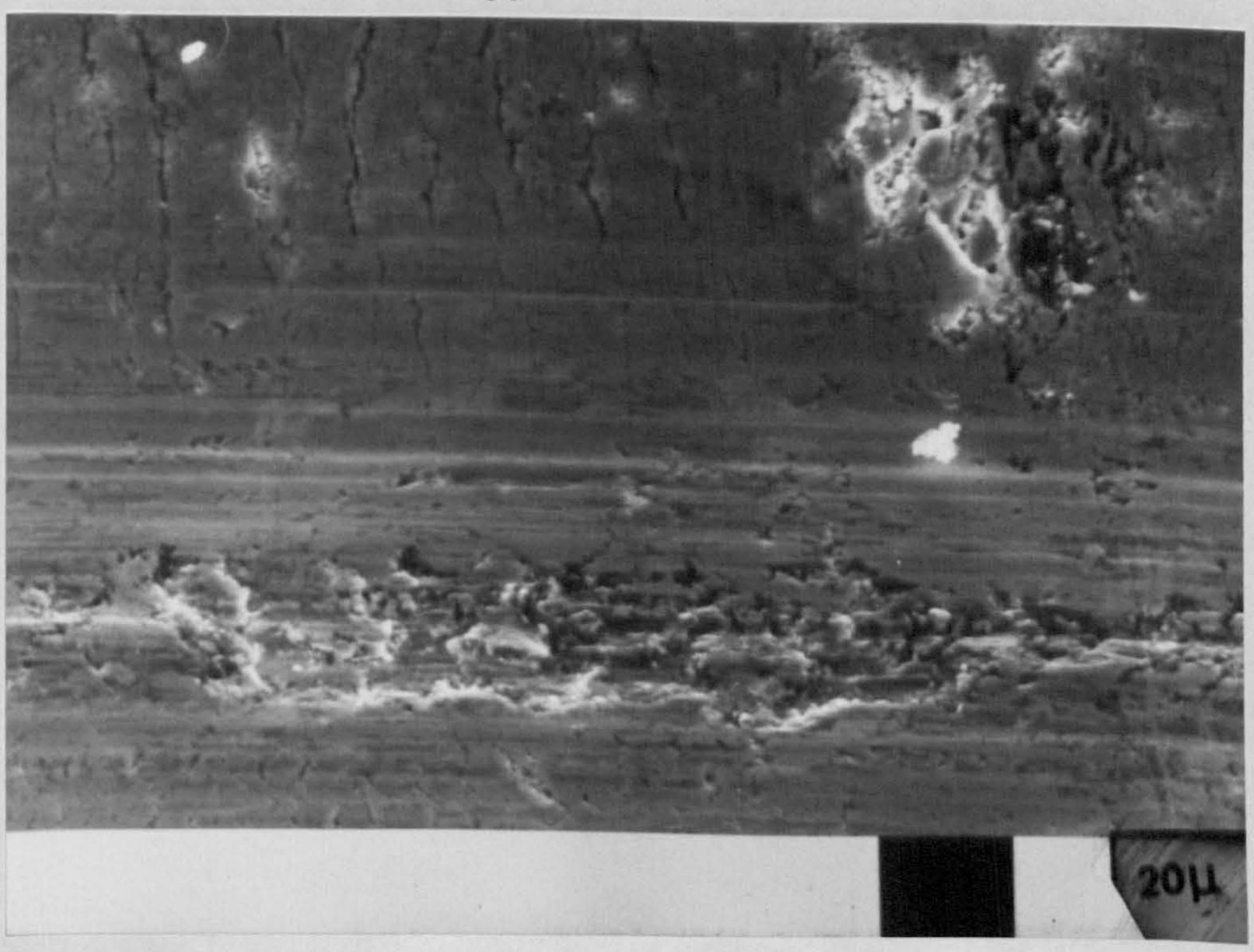

Fig. 99b. Bottom track of steam treated (Fe) after 1000 cm sliding distance under 9 Kgs load.

$D = 6.8\ ^{g}/_{cc}$ x 1K

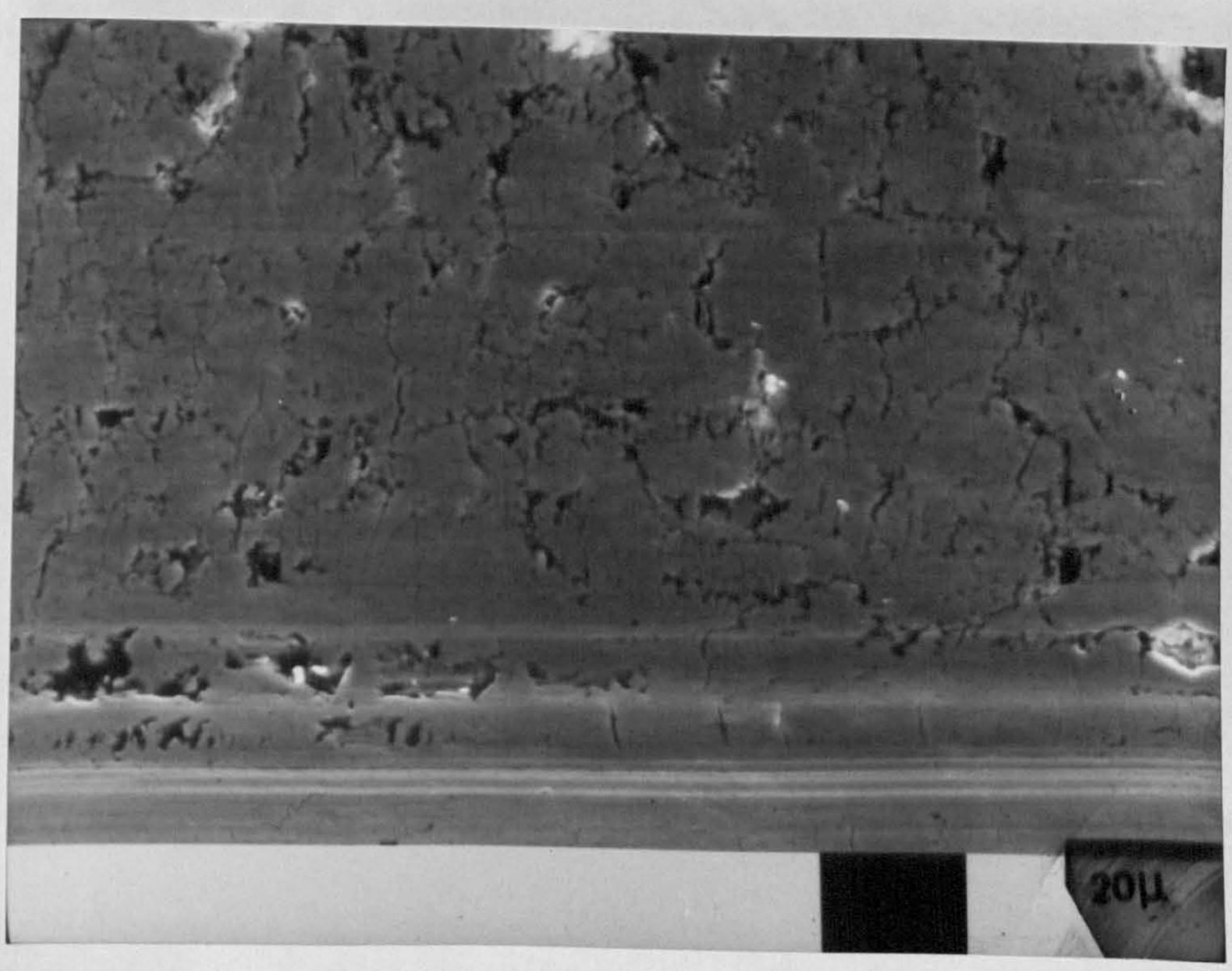

Fig. 100a. Wall of track in sintered (Fe + 6% Cu) after 1000 cm sliding distance under 5 Kgs load.
$D = 6.8\ ^{g}/_{cc}$ x 1K

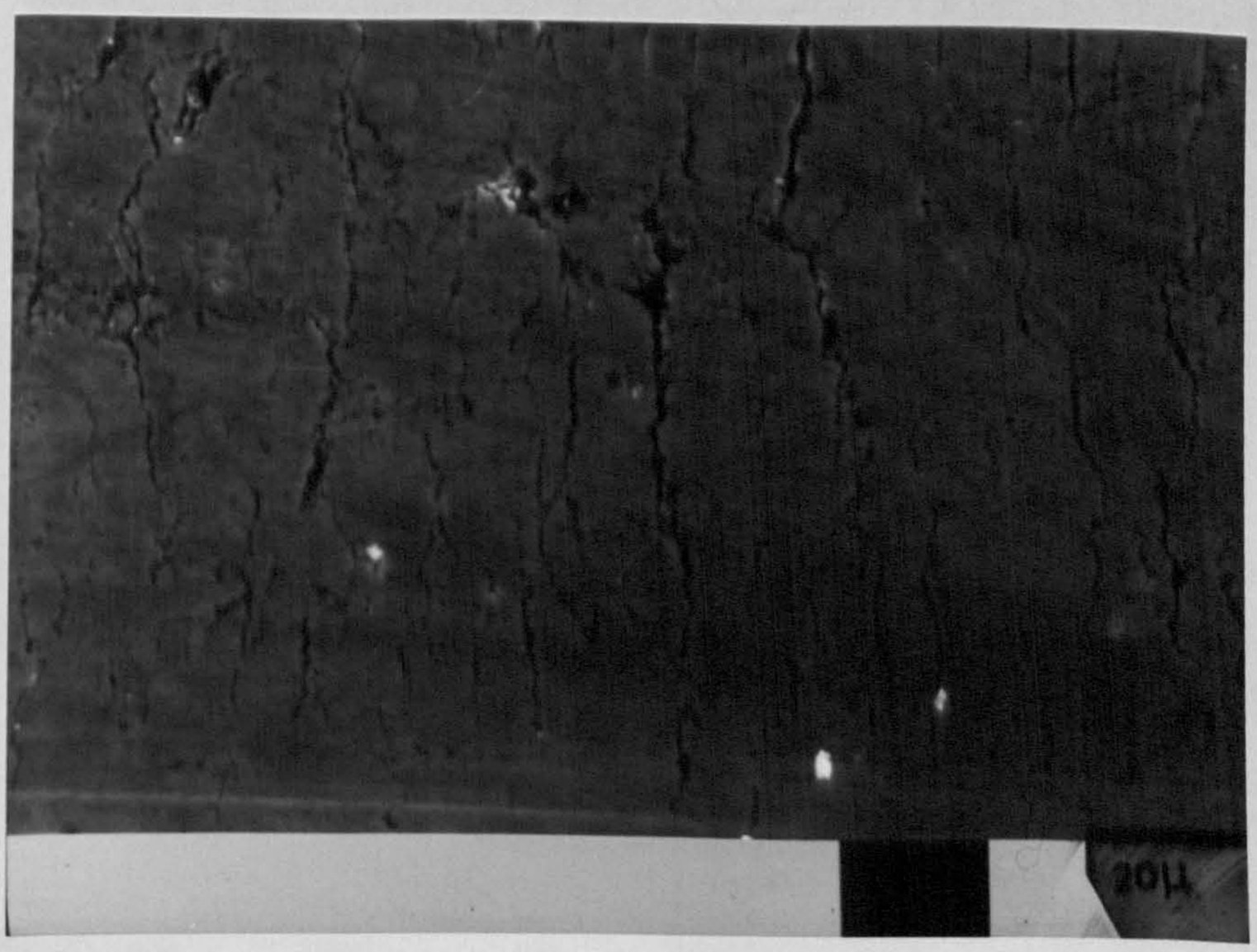

Fig. 100b. Wall of track in steam treated (Fe + 6% Cu) after 1000 cm sliding distance under 5 Kgs load.
$D = 6.8\ ^{g}/_{cc}$ x 1K

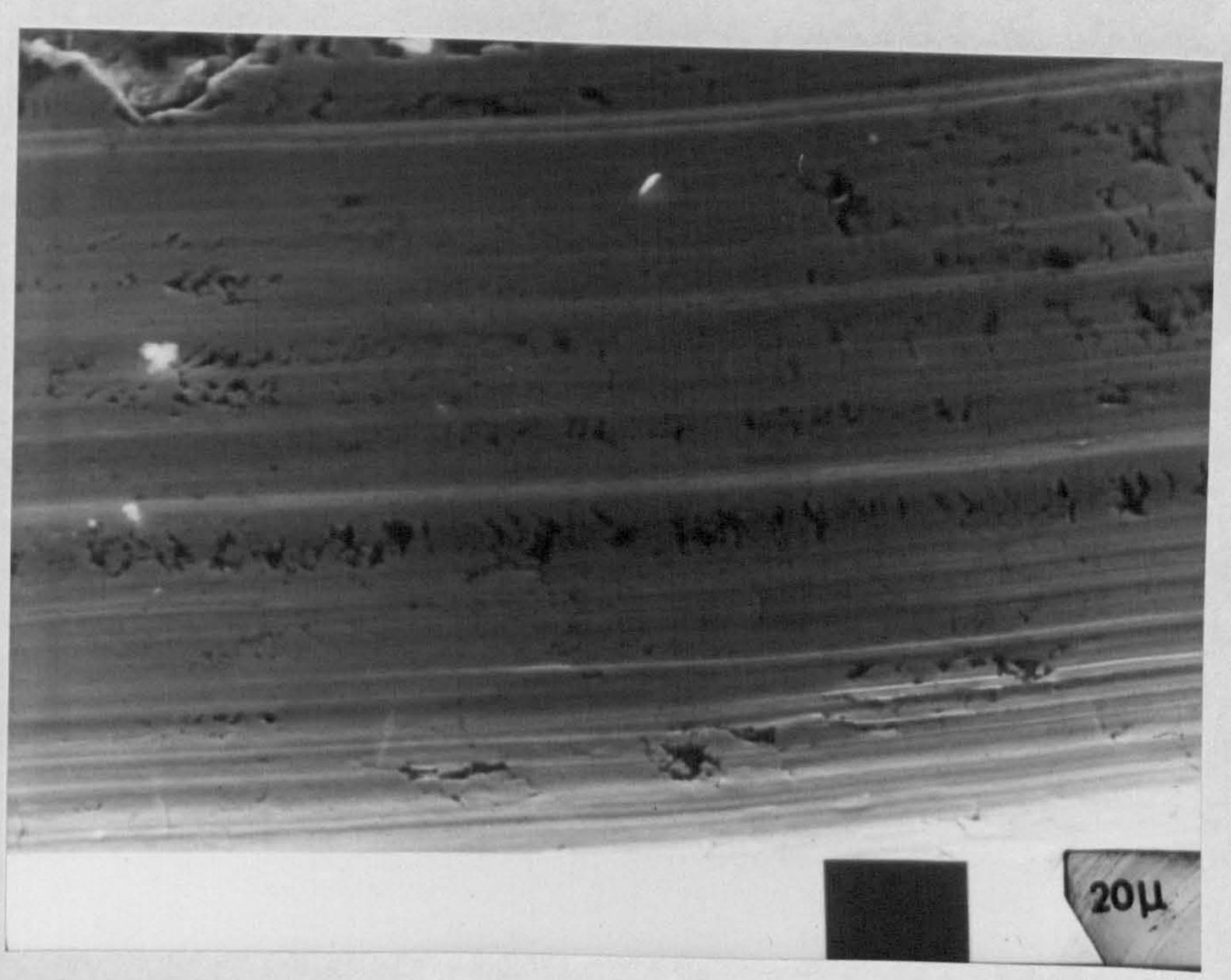

Fig. 101a. Bottom of track in sintered (Fe + 6% Cu) after 1000 cm sliding distance under 5 Kgs load.
$D = 6.8\ ^{g}/_{cc}$ x 1K

Fig. 101b. Bottom of track in steam treated (Fe + 6% Cu) after 1000 cm sliding distance under 5 Kgs load.
$D = 6.8\ ^{g}/_{cc}$ x 1K

Material Type	Modulus of elasticity, N/mm²	Ring Ultimate Tensile Strength, N/mm²	Un-notched Wohler Fatigue Strength, N/mm²	Brinell Hardness	Coefficient of Linear Expansion per degC × 10^{-6}
Cr-alloyed iron	115 000	280 (min.)	~162	230	14·1 (0–200°C) 16·1 (0–500°C)
Cr–Mo alloyed iron	150 000	430 (min.)	265	255	15·1 (0–200°C) 16·8 (0–500°C)

Table 4a[2] Properties of Typical Centri-Cast Piston-Ring Materials

Designation	Composition, wt.-%						
	Tc	Si	Mn	P	Ni	Cr	Mo
Cast Irons Mk.							
2	3·2	2·4	0·8	0·6	—	0·3	—
9	3·0	2·0	0·8	0·45	—	0·9	0·3
11	3·4	2·2	0·7	0·1	0·15	0·3	0·4
12	3·3	2·2	0·8	0·6	—	0·4	—
24	3·2	2·9	0·8	0·7	—	0·7	—
29	3·2	2·5	0·8	0·5	—	0·5	—

Fe-base Sintered Alloys	
FC3/1	0·5% C, 3% Cu
FC3/1	1% C, 3% Cu
FC3/N	As FC3/1 but a harder iron powder is used
FC7	7% Cu
FC10	10% Cu
BM78	10% Cu–Sn + 1% C
SP20	A work-hardening nickel-containing alloy with 0·8% C unless otherwise stated
SP25	Similar to SP20 but containing Mo

Table 4b[2] Designations and Descriptions of Materials Tested

Particle size distr. \ Powders	100# A.S.C. Fe %	- 100# A.S.C. Fe %	- 100# Fe + 2% Cu %	- 100# Fe + 4% Cu %	- 100# Fe + 6% Cu %	- 100# Fe + 8% Cu %
+ 100	5.7	0.0	0.8	0.6	0.6	0.8
- 100 to 200	36.8	27.4	27	22	20.9	21.6
- 200 to 240	15.6	17.6	11.2	11.6	11.4	11.6
- 240 to 270	11.5	13.7	8.4	8.4	8.5	8.8
- 270 to 325	6.3	10.7	6.1	6.4	5.7	5.7
- 325	24.1	30.6	46.5	50.8	52.9	51.5

Table 5. Particle size distribution before annealing

Physical Properties \ Powders	- 100# A.S.C. Fe	- 100# Fe + 2% Cu	- 100# Fe + 4% Cu	- 100# Fe + 6% Cu	- 100# Fe + 8% Cu
A.D. $g/_{cc}$	2.85	2.9	3.0	3.08	3.1
Flow Rate Sec/50 gms	37	34	36	35	32

Table 6. Physical properties of powders before annealing

Powders Particle size distr.	- 100# Fe + 2% Cu %	- 100# Fe + 4% Cu %	- 100# Fe + 6% Cu %	- 100# Fe + 8% Cu %
+ 100	0.2	0.1	0.2	0.2
- 100 to 200	22.9	21.6	18.9	19.9
- 200 to 240	11.1	10.1	9.9	9.5
- 240 to 270	10.8	10.1	10.1	10.2
- 270 to 325	6.6	6.1	6.1	6.4
- 325	48.4	52	54.8	53.8

Table 7. Particle size distribution after annealing

Powders Physical Properties	- 100 # Fe + 2% Cu	- 100 # Fe + 4% Cu	- 100 # Fe + 6% Cu	- 100 # Fe + 8% Cu
A.D. $^{g}/_{cc}$	3.02	3.03	3.09	3.15
Flow Rate Sec/50 gms	None	None	None	None

Table 8. Physical properties of powders after annealing

Code	Powder	Density g/cc
A	- 100# Fe	6.0
B	- 100# Fe	6.4
C	- 100# Fe	6.8
D	- 100# Fe + 2% Cu	6.0
E	- 100# Fe + 2% Cu	6.4
F	- 100# Fe + 2% Cu	6.8
G	- 100# Fe + 4% Cu	6.0
H	- 100# Fe + 4% Cu	6.4
I	- 100# Fe + 4% Cu	6.8
J	- 100# Fe + 6% Cu	6.0
K	- 100# Fe + 6% Cu	6.4
L	- 100# Fe + 6% Cu	6.8
M	- 100# Fe + 8% Cu	6.0
N	- 100# Fe + 8% Cu	6.4
P	- 100# Fe + 8% Cu	6.8

Table 9. Code for different powder and different density.

Sample	Pressure MN/m^2	Green Density g/cc
- 100# Fe	245	6.0
	325	6.4
	450	6.8
- 100# Fe + 2% Cu	430	6.0
	600	6.4
	800	6.8
- 100# Fe + 4% Cu	430	6.0
	585	6.4
	790	6.8
- 100# Fe + 6% Cu	450	6.0
	630	6.4
	830	6.8
- 100# Fe + 8% Cu	400	6.0
	530	6.4
	740	6.8

Table 10a. Relationship between pressure and density in cylindrical samples

Sample	Pressure MN/m^2	Density g/cc
- 100# Fe + 2% Cu	430	6.0

Table 10b. Relationship between pressure and density in Rectangular samples.

Change / Code	In Length %	In Diameter %
A	- 0.2	- 0.1
B	- 0.3	- 0.07
C	- 0.2	- 0.07
D	- 0.9	- 0.8
E	- 0.8	- 0.8
F	- 0.8	- 0.7
G	- 1.0	- 0.7
H	- 0.9	- 0.7
I	- 0.9	- 0.7
J	- 1.0	- 0.7
K	- 0.9	- 0.7
L	- 0.9	- 0.7
M	- 0.7	- 0.4
N	- 0.7	- 0.4
P	- 0.5	- 0.3

Table 11. Dimensional change during sintering

	Sintered Density g/cc	Total Porosity %
Fe + 2% Cu	6.1	24.7
	6.5	18.6
	6.9	12.5
Fe + 4% Cu	6.1	22.3
	6.5	17.3
	6.9	12.2
Fe + 6% Cu	6.1	22.9
	6.5	17.9
	6.9	12.8
Fe + 8% Cu	6.0	24.5
	6.47	19.6
	6.85	14.83

Table 12. Percentage of total porosity after water quenching from solution treatment temperature.

	Powder / Density g/cc	Fe	Fe + 2% Cu		Fe + 4% Cu		Fe + 6% Cu		Fe + 8% Cu	
			F. Cool	W.Q.	F. Cool	W.Q.	F. Cool	W.Q.	F. Cool	W.Q.
Open Porosity %	D = 6.0	23.0	23.3	22.3	21.9	19.58	21.0	19	21.6	21.3
	D = 6.4	18.5	18.03	17.4	17.48	14.72	16.6	13.3	19.1	17.53
	D = 6.8	13.5	12.07	12.09	10.9	9.6	9.03	9.05	14.14	13.5
Hardness Vickers	D = 6.0	29.3	51.4	58.1	59.1	103.4	89	132	77.5	110.6
	D = 6.4	39.1	69.7	70	74.3	129.6	109.1	151.1	97.8	122
	D = 6.8	48.1	88.1	117	98.4	150	149.6	168.3	123.8	159.6

Table 13. Variation in open porosity and hardness after sintering and solution treatment.

	Powder / Density g/cc	Fe	Fe + 2% Cu		Fe + 4% Cu		Fe + 6% Cu		Fe + 8% Cu	
			F. Cool	W.Q.	F. Cool	W.Q.	F. Cool	W.Q.	F. Cool	W.Q.
W.t gain %	D = 6.0	3.1	4.62	2.9	4.2	2.93	4.4	3.0	4.3	3.6
	D = 6.4	2.2	3.11	1.91	3.09	2	2.54	1.98	3.1	2.43
	D = 6.8	1.6	1.72	1.3	1.38	0.8	1.28	0.84	1.76	1.5
Hardness Vickers	D = 6.0	75	124.6	125.6	134.6	129.5	167.1	160.6	174.8	155
	D = 6.4	87.8	130.8	140	144	149.3	170	171.6	171.3	159
	D = 6.8	90.1	138	142	151.5	157.3	178.3	179.5	178.8	178

Table 14. Variation in weight gain and hardness after 10 minutes steam treatment at 525°C

	Powder / Density g/cc	Fe	Fe + 2% Cu		Fe + 4% Cu		Fe + 6% Cu		Fe + 8% Cu	
			F. Cool	W.Q.	F. Cool	W.Q.	F. Cool	W.Q.	F. Cool	W.Q.
W.t gain %	D = 6.0	5.0	6.71	4.45	5.2	3.46	4.31	3.2	4.1	3.9
	D = 6.4	3.17	3.7	3.2	3.5	2.3	2.75	1.8	2.9	2.6
	D = 6.8	1.8	1.8	1.5	1.65	1.02	1.0	0.8	1.79	1.57
Hardness Vickers	D = 6.0	117.5	171.5	169	153	154	178.1	177.1	181.1	178.1
	D = 6.4	109.6	166.5	169.5	162.6	154.8	180.5	171.5	170.5	192
	D = 6.8	101.9	166.3	182.1	159	153.1	170	170.8	176.1	181.6

Table 15. Variation in weight gain and hardness after 25 minutes steam treatment at 525°C

	Powder / Density g/cc	Fe	Fe + 2% Cu		Fe + 4% Cu		Fe + 6% Cu		Fe + 8% Cu	
			F. Cool	W.Q.	F. Cool	W.Q.	F. Cool	W.Q.	F. Cool	W.Q.
W.t gain %	D = 6.0	5.3	6.7	4.7	5	3.7	4.4	3.2	4.1	3.9
	D = 6.4	3.9	4.7	3.35	3.6	2.75	2.88	1.97	3.1	2.5
	D = 6.8	1.99	2	1.75	1.5	1.18	1.4	0.82	1.87	1.46
Harness Vickers	D = 6.0	120	178.8	171.6	158.6	153	183.6	171.5	176.6	183.8
	D = 6.4	114.8	170.3	170.6	160.3	155.3	170.1	172.1	170.6	178
	D = 6.8	101.1	171.6	170.8	160.5	149.5	181.6	172.3	171.1	170

Table 16. Variation in weight gain and hardness after 50 minutes steam treatment at 525°C.

	Powder / Density g/cc	Fe	Fe + 2% Cu		Fe + 4% Cu		Fe + 6% Cu		Fe + 8% Cu	
			F. Cool	W.Q.	F. Cool	W.Q.	F. Cool	W.Q.	F. Cool	W.Q.
W.t gain %	D = 6.0	5.7	6.97	5.5	5.6	3.8	5.0	3.7	4.5	3.9
	D = 6.4	4.15	4.5	3.5	3.2	2.7	3.31	2.05	3.4	2.7
	D = 6.8	1.99	2.3	1.74	1.7	1.2	1.35	1.02	1.99	1.50
Hardness Vickers	D = 6.0	124.6	179	169	155	151.3	187.3	180	187.8	164.3
	D = 6.4	110.8	169	174	167.1	143.3	175.5	170.3	181.5	168.1
	D = 6.8	99.7	168	164.9	148.1	131.5	179.6	165	178.8	165.5

Table 17. Variation in weight gain and hardness after 100 minutes steam treatment at 525°C.

	Alloys / W.t gain / Open Porosity %	Fe	Fe + 2% Cu	Fe + 4% Cu	Fe + 6% Cu	Fe + 8% Cu
Density g/cc	6.0	0.247	0.246	0.194	0.194	0.183
	6.4	0.224	0.201	0.183	0.154	0.154
	6.8	0.147	0.143	0.125	0.112	0.111

Table 18. Variation of % $\frac{\text{W.t gain}}{\text{Open Porosity}}$ in W.Q. samples after 100 minutes steam treatment at 525°C.

Density g/cc	Alloys / W.t gain / Open Porosity %	Fe	Fe + 2% Cu	Fe + 4% Cu	Fe + 6% Cu	Fe + 8% Cu
	6.0	0.247	0.299	0.255	0.238	0.208
	6.4	0.224	0.249	0.183	0.198	0.178
	6.8	0.147	0.19	0.155	0.149	0.14

Table 19. Variations of % $\frac{\text{W.t gain}}{\text{Open Porosity}}$ in F. Cool samples after 100 minutes steam streatment at 525°C.

% W.t gain / Time	Lenel [96] At 575°C	Franklin [98] At 520°C	Franklin [98] At 650°C	Razavizadeh [99] At 525°C	Razavizadeh [99] At 600°C	Present Work At 525°C
10	3.9	2.5	3.4	3.07	4.5	3.1
30	6.7	3.5	3.8	4.7	6.4	5.0
60	7.8	5.3	5.1	5.4	6.7	5.7

Table 20. Comparison of results from previous investigations at D = 6.0 $^{g}/_{cc}$

% W.t gain / Density g/cc	Kanopicky [97] At 600°C	Razavizadeh [99] At 600°C	Razavizadeh [99] At 525°C	Present Work At 525°C
6.0	4	6.7	5.4	5.7
6.4	1.8	4.1	4.0	4.0
6.8	0.8	2.0	2.5	2

Table 21. Comparison of results from previous investigations after 60 minutes steam treatment.

θ	Composition / d	Fe + 2% Cu	Fe + 4% Cu	Fe + 6% Cu	Fe + 8% Cu	Phase
17.05	3.003	"	-	-	-	Fe_3O_4
21.02	2.5004	"	"	"	"	αFe_2O_3
2 4.5	2.1621	"	"	"	"	αFe_2O_3
25.25	2.1012	"	"	"	"	Fe_3O_4
26.15	2.0344	"	"	"	"	αFe
29.7	1.8083	-	-	"	"	Cu
35.9	1.5264	"	"	"	"	αFe_2O_3
38.5	1.4381	"	"	"	"	αFe
43.45	1.3020	"	"	"	"	αFe_2O_3
44.25	1.2833	-	-	"	"	Cu
45.8	1.2493	"	"	"	"	αFe_2O_3
49.7	1.1738	"	"	"	"	αFe
55	1.0921	"	"	"	"	Fe_3O_4
56.1	1.0777	"	"	"	"	FeO
61.75	1.0164	"	"	"	"	αFe
64.8	0.9894	"	"	"	"	Fe_3O_4
68.15	0.9639	"	"	"	"	FeO

(("') This sign means there is this phase
((-) This sign means there is not this phase.

Table 22. Variations of phases in (W.Q.) samples after 100 minutes steam treatment at 525°C (X-ray Diffraction)

θ	Composition / d	Fe + 2% Cu	Fe + 4% Cu	Fe + 6% Cu	Fe + 8% Cu	Phase
17.05	3.003	-	-	-	-	Fe_3O_4
21.02	2.5004	"	"	"	"	αFe_2O_3
24.5	2.1621	"	"	"	"	αFe_2O_3
25.25	2.1012	"	"	"	"	Fe_3O_4
26.15	2.0344	"	"	"	"	αFe
29.7	1.8083	-	-	"	"	Cu
35.9	1.5264	"	"	"	"	αFe_2O_3
38.5	1.4381	"	"	"	"	αFe
43.45	1.3020	"	"	"	"	αFe_2O_3
44.25	1.2833	-	-	"	"	Cu
45.8	1.2493	"	-	-	-	αFe_2O_3
49.7	1.1738	"	"	"	"	αFe
55	1.0921	-	-	"	"	Fe_3O_4
56.1	1.0777	-	-	-	-	FeO
61.75	1.0164	"	"	"	"	αFe
64.8	0.9894	-	-	-	-	Fe_3O_4
68.15	0.9639	-	-	-	-	FeO

Table 23. Variations of phases in (F. Cool) samples after 100 minutes steam treatment at 525°C (X-ray Diffraction)

θ	d	Phase
42.23	1.1458	Cu
37.1	1.2786	Cu
31.46	1.4779	Cu
25.36	1.8014	Cu
21.81	2.078	Cu
21.72	2.081	Cu
17.67	2.5412	Cu

Table 24. Pure copper after 100 minutes steam treatment at 525° C.

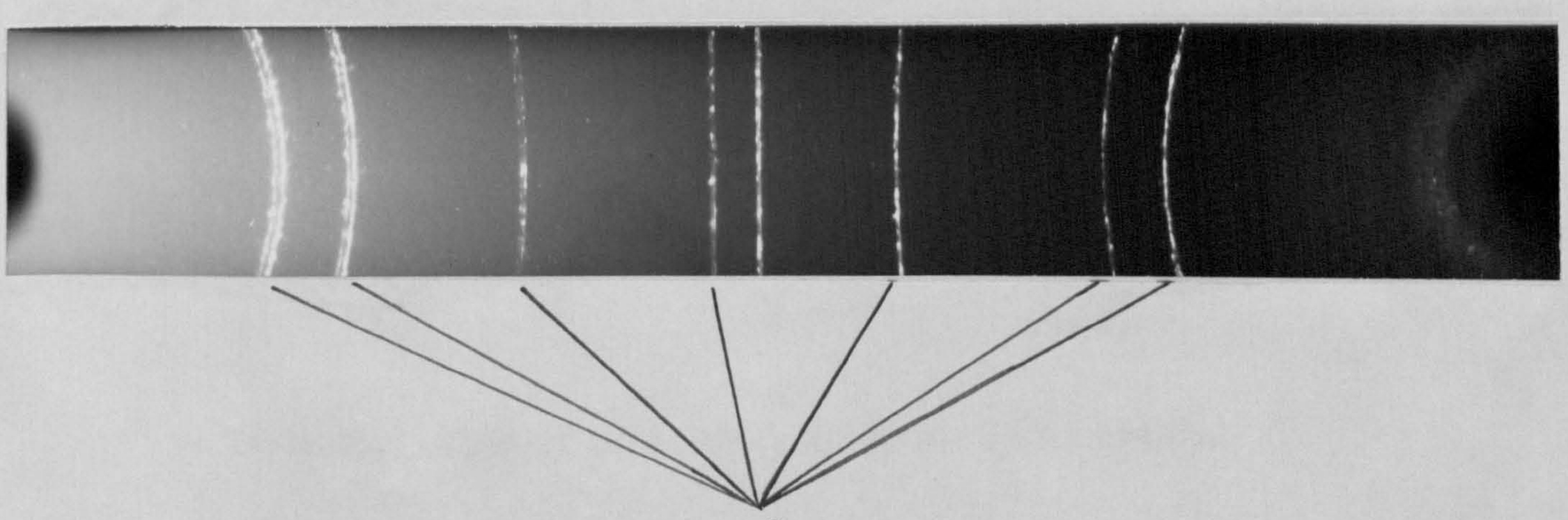

R_1	R_2	D	$D/4 = \theta$	Sin θ	d
316.6	167.7	148.9	37.2	0.60	1.479
309.6	174.7	134.9	33.7	0.55	1.612
292.9	191.5	101.3	25.3	0.42	2.09
283.8	200.5	82.2	20.5	0.35	2.54
277.5	206.9	70.6	17.6	0.30	2.95

Table 25. Type of oxide for pure Fe at 525°C: Fe_3O_4

R_1	R_2	D	$D/4 = \theta$	Sin θ	d
300.6	184	116.5	29.1	0.48	1.838
281.1	203.2	77.9	19.4	0.33	2.68

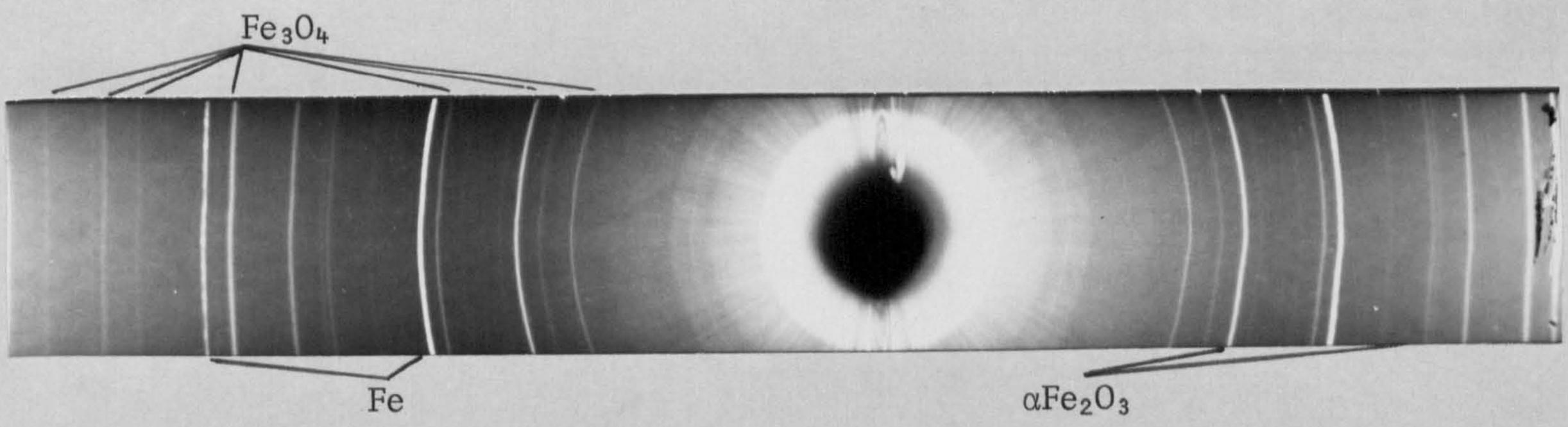

Table 26. Type of oxide for pure Fe at 525°C: αFe_2O_3.

		Time Mins / Density g/cc	5	10	15	25	35	50	75	100
HARDNESS - VICKERS	Fe + 2% Cu	6.0	93	100	99	97	100	93	99	89
		6.4	119	117	133	130	130	128	128	124
		6.8	145	146	162	155	161	153	163	154
	Fe + 4% Cu	6.0	112	122	117	126	120	117	114	109
		6.4	135	139	140	140	140	140	132	135
		6.8	180	185	207	185	190	184	174	170
	Fe + 6% Cu	6.0	140	147	139	135	129	138	123	128
		6.4	160	170	166	165	165	154	151	151
		6.8	214	240	230	226	208	208	198	202
	Fe + 8% Cu	6.0	135	135	133	136	127	130	120	118
		6.4	160	173	159	155	150	140	140	140
		6.8	224	214	212	205	203	203	198	190

Table 27. Variation in hardness for Fe + 2%, 4%, 6% and 8% Cu after ageing at 525°C.

Sample		Resistance R ohm	Area cm^2	ρ ohm cm	Average ρ
X	1	136×10^{-6}	5024×10^{-4}	219381×10^{-10}	226503×10^{-10}
	2	134×10^{-6}	5078×10^{-4}	226817×10^{-10}	
	3	137×10^{-6}	5109×10^{-4}	233311×10^{-10}	
Z	4	141×10^{-6}	5024×10^{-4}	236128×10^{-10}	238270×10^{-10}
	5	141×10^{-6}	5019×10^{-4}	237566×10^{-10}	
	6	142×10^{-6}	5094×10^{-4}	241116×10^{-10}	

Table 28. Difference between Resistivity in F. Cooled and W. Quenched samples of Fe + 2% Cu

X = means samples were sintered for 1 hour at 1120°C and then F. cooled.

Z = means F. cooled samples were solution treated for 1 hour at 1000° C and then W. Quenched.

Area	Around the Pores	Middle of the grains	P.F.Z.	on the grains
H.V.N. D = 6.0	333	472	417	453
	290	453	410	440
	239	434	400	434
	185	417	380	430
	180	386	371	425
H.V.N. D = 6.8	429	509	479	479
	418	495	460	468
	402	479	451	460
	390	460	442	458
	381	451	429	451

Table 29. Variations of micro-hardness in Fe + 4% Cu alloy at Peak hardness (after 25 minutes ageing at 525^{o}C)

Alloys	Fe	Fe + 2% Cu	Fe + 4% Cu	Fe + 6% Cu	Fe + 8% Cu
Radial Crushing Stress Nm^{-2}	28×10^7	33×10^7	50×10^7	58×10^7	37×10^7

Table 30. Radial crushing strength in sintered samples

(D = 6.4 $g/_{cc}$, F. Cooled)

Alloys	Fe	Fe + 2% Cu	Fe + 4% Cu	Fe + 6% Cu	Fe + 8% Cu
Radial Crushing Stress Nm^{-2}	37×10^7	22×10^7	35×10^7	36×10^7	35×10^7

Table 31. Radial crushing strength after 50 minutes steam treatment at $525^{o}C$ (D = 6.4 $g/_{cc}$, F. Cooled)

Load Kg / Sample	Scar Width cm x 10^{-3}		
	1 Kg	3 Kgs	5 Kgs
- 100# Fe A.S.C.	29	46	64
- 100# Fe + 2% Cu	22	35	40
- 100# Fe + 4% Cu	17	30	37
- 100# Fe + 6% Cu	18	26	32
- 100# Fe + 8% Cu	17	26	35

Table 32. Scar width variations in sintered samples after 10 passes.

Load Kg / Sample	Scar Width cm x 10^{-3}		
	1 Kg	3 Kgs	5 Kgs
- 100# Fe A.S.C.	11	39	50
- 100# Fe + 2% Cu	12	25	42
- 100# Fe + 4% Cu	12	27	44
- 100# Fe + 6% Cu	11	23	38
- 100# Fe + 8% Cu	9	25	30

Table 33. Scar width variations in steam treated samples after 10 passes.

	Scar Width cm x 10^{-3}		
Load Kg / Sample	1 Kg	3 Kgs	5 Kgs
- 100# Fe A.S.C.	29	53	60
- 100# Fe + 2% Cu	20	39	49
- 100# Fe + 4% Cu	22	41	53
- 100# Fe + 6% Cu	16	30	52
- 100# Fe + 8% Cu	17	34	45

Table 34. Scar width variations in sintered samples after 30 passes.

	Scar Width cm x 10^{-3}		
Load Kg / Sample	1 Kg	3 Kgs	5 Kgs
- 100# Fe A.S.C.	17	41	68
- 100# Fe + 2% Cu	15	37	48
- 100# Fe + 4% Cu	13	35	49
- 100# Fe + 6% Cu	14	33	45
- 100# Fe + 8% Cu	16	37	44

Table 35. Scar width variations in steam treated samples after 30 passes.

	Scar Width cm x 10^{-3}		
Load Kg / Sample	1 Kg	3 Kgs	5 Kgs
- 100 # Fe A.S.C.	32	60	73
- 100# Fe + 2% Cu	23	45	48
- 100# Fe + 4% Cu	20	45	53
- 100# Fe + 6% Cu	15	41	50
- 100# Fe + 8% Cu	19	38	49

Table 36. Scar width variations in sintered samples after 60 passes.

	Scar Width cm x 10^{-3}		
Load Kg / Sample	1 Kg	3 Kgs	5 Kgs
- 100# Fe A.S.C.	17	47	60
- 100# Fe + 2% Cu	16	38	47
- 100# Fe + 4% Cu	12	32	48
- 100# Fe + 6% Cu	15	36	52
- 100# Fe + 8% Cu	16	35	44

Table 37. Scar width variations in steam treated samples after 60 passes.

Load Kg / Sample	Scar Width cm x 10^{-3}		
	1 Kg	3 Kgs	5 Kgs
- 100# Fe A.S.C.	28	57	75
- 100# Fe + 2% Cu	25	45	55
- 100# Fe + 4% Cu	25	42	57
- 100# Fe + 6% Cu	21	42	62
- 100# Fe + 8% Cu	23	44	54

Table 38. Scar width variations in sintered samples after 100 passes

Load Kg / Sample	Scar Width cm x 10^{-3}		
	1 Kg	3 Kgs	5 Kgs
- 100# Fe A.S.C.	22	53	65
- 100# Fe + 2% Cu	22	42	48
- 100# Fe + 4% Cu	20	43	47
- 100# Fe + 6% Cu	19	40	53
- 100# Fe + 8% Cu	17	34	50

Table 39. Scar width variations in steam treated samples after 100 passes.

	Scar Width cm x 10^{-3}		
Load Kg / Sample	1 Kg	3 Kgs	5 Kgs
- 100# Fe A.S.C.	26	53	69
- 100# Fe + 2% Cu	23	47	59
- 100# Fe + 4% Cu	21	39	61
- 100# Fe + 6% Cu	19	38	60
- 100# Fe + 8% Cu	21	41	57

Table 40. Scar width variations in sintered samples after 180 passes.

	Scar Width cm x 10^{-3}		
Load Kg / Sample	1 Kg	3 Kgs	5 Kgs
- 100# Fe A.S.C.	22	53	68
- 100# Fe + 2% Cu	20	44	55
- 100# Fe + 4% Cu	19	44	57
- 100# Fe + 6% Cu	17	41	60
- 100# Fe + 8% Cu	13	32	45

Table 41. Scar width variations in steam treated samples after 180 passes.

Load Kg / Sample	Scar Width cm x 10^{-3}				
	1 Kg	3 Kgs	5 Kgs	7 Kgs	9 Kgs
- 100 Fe A.S.C.	39	62	85	101	106
- 100 Fe + 2% Cu	17	40	56	69	79
- 100 Fe + 4% Cu	21	38	55	64	72
- 100 Fe + 6% Cu	17	35	49	58	66
- 100 Fe + 8% Cu	17	35	48	58	74

Table 42. Scar width variations in sintered samples after 1000 passes.

Load Kg / Sample	Scar Width cm x 10^{-3}				
	1 Kg	3 Kgs	5 Kgs	7 Kgs	9 Kgs
- 100 Fe A.S.C.	27	58	80	97	113
- 100 Fe + 2% Cu	18	39	56	74	86
- 100 Fe + 4% Cu	22	45	60	83	89
- 100 Fe + 6% Cu	21	41	55	66	85
- 100 Fe + 8% Cu	17	34	56	66	82

Table 43. Scar width variations in steam treated samples after 1000 passes.

Load Kg / Sample	Volume Wear cm^3				
	1 Kg	3 Kgs	5 Kgs	7 Kgs	9 Kgs
- 100# Fe A.S.C.	2.1×10^{-4}	5.4×10^{-4}	1.01×10^{-3}	1.4×10^{-3}	1.6×10^{-3}
- 100# Fe + 2% Cu	3.8×10^{-5}	2.17×10^{-4}	4.3×10^{-4}	6.7×10^{-4}	8.8×10^{-4}
- 100# Fe + 4% Cu	6.0×10^{-5}	2.0×10^{-4}	3.4×10^{-4}	5.7×10^{-4}	7.2×10^{-4}
- 100# Fe + 6% Cu	3.8×10^{-5}	1.7×10^{-4}	3.3×10^{-4}	4.7×10^{-4}	6.2×10^{-4}
- 100# Fe + 8% Cu	3.8×10^{-5}	1.7×10^{-4}	3.2×10^{-4}	4.7×10^{-4}	7.8×10^{-4}

Table 44. Volume wear of sintered samples after 1000 passes.

Load Kg / Sample	Volume Wear cm^3				
	1 Kg	3 Kgs	5 Kgs	7 Kgs	9 Kgs
- 100# Fe A.S.C.	1.03×10^{-4}	4.77×10^{-4}	9.0×10^{-4}	1.33×10^{-3}	1.8×10^{-3}
- 100# Fe + 2% Cu	4.3×10^{-5}	2.1×10^{-4}	4.4×10^{-4}	7.7×10^{-4}	1.0×10^{-3}
- 100# Fe + 4% Cu	6.6×10^{-5}	2.8×10^{-4}	6.0×10^{-4}	9.8×10^{-4}	1.1×10^{-3}
- 100# Fe + 6% Cu	6.0×10^{-5}	2.3×10^{-4}	4.2×10^{-4}	6.1×10^{-4}	1.0×10^{-3}
- 100# Fe + 8% Cu	3.8×10^{-5}	1.6×10^{-4}	4.4×10^{-4}	6.17×10^{-4}	9.55×10^{-4}

Table 45. Volume wear of steam treated samples after 1000 passes.

No. of Passes	30 Passes	180 Passes	1000 Passes	Sample Hardness
Sintered	130	160	178	124
Steam Treated	200	210	229	178

Table 46. Sub-surface hardness (H_V) after 30, 180 and 1000 passes for Fe + 8% Cu alloy under a load of 5 Kgs.